MOLECULAR BIOMARKERS IN ANIMAL REPRODUCTION

EDITED BY: Jordi Roca, Isabel Barranco and Cristina Alicia Martinez
PUBLISHED IN: Frontiers in Veterinary Science

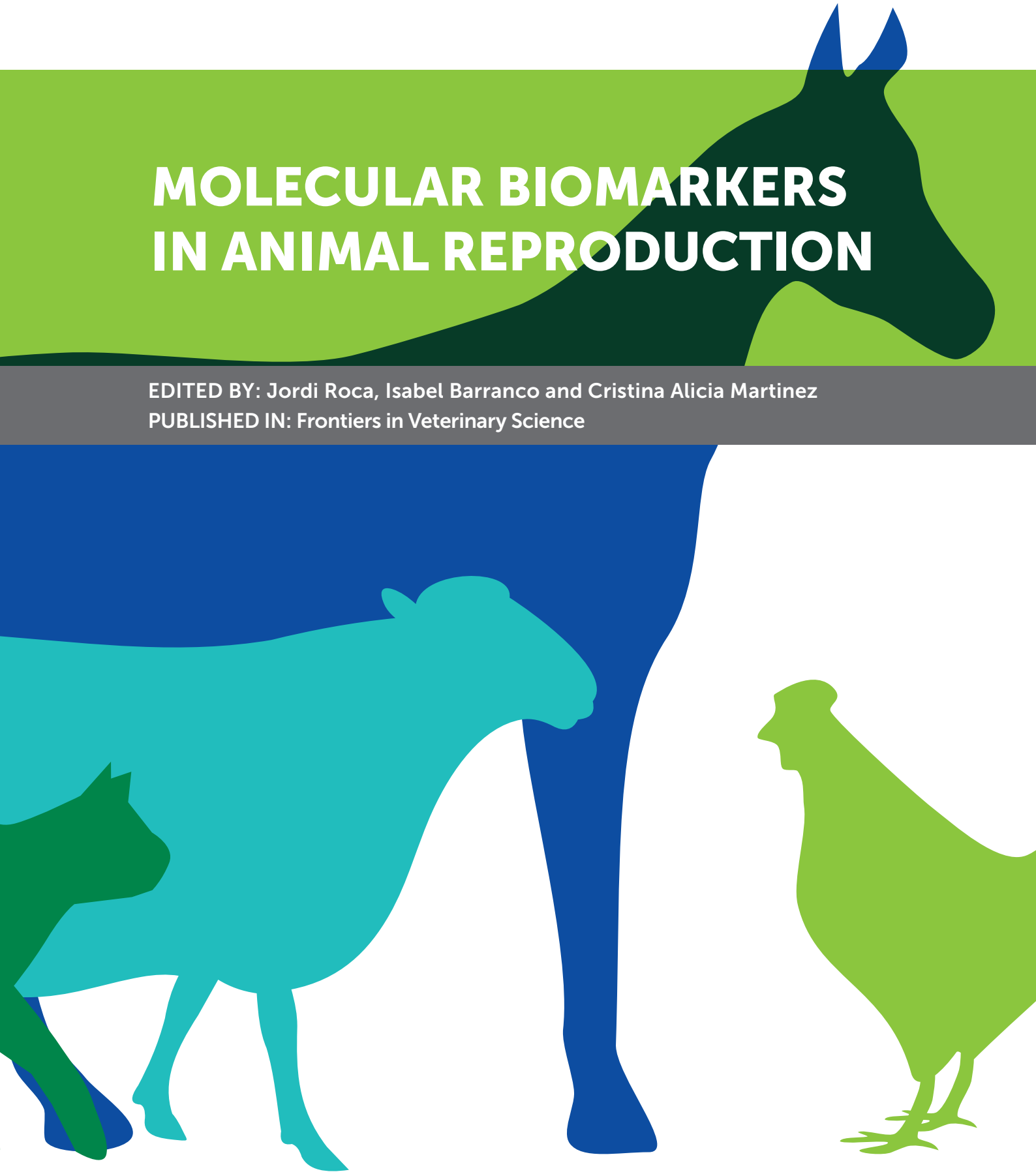

frontiers Research Topics

ISSN 1664-8714
ISBN 978-2-88974-103-8
DOI 10.3389/978-2-88974-103-8

About Frontiers

Frontiers is more than just an open-access publisher of scholarly articles: it is a pioneering approach to the world of academia, radically improving the way scholarly research is managed. The grand vision of Frontiers is a world where all people have an equal opportunity to seek, share and generate knowledge. Frontiers provides immediate and permanent online open access to all its publications, but this alone is not enough to realize our grand goals.

Frontiers Journal Series

The Frontiers Journal Series is a multi-tier and interdisciplinary set of open-access, online journals, promising a paradigm shift from the current review, selection and dissemination processes in academic publishing. All Frontiers journals are driven by researchers for researchers; therefore, they constitute a service to the scholarly community. At the same time, the Frontiers Journal Series operates on a revolutionary invention, the tiered publishing system, initially addressing specific communities of scholars, and gradually climbing up to broader public understanding, thus serving the interests of the lay society, too.

Dedication to Quality

Each Frontiers article is a landmark of the highest quality, thanks to genuinely collaborative interactions between authors and review editors, who include some of the world's best academicians. Research must be certified by peers before entering a stream of knowledge that may eventually reach the public - and shape society; therefore, Frontiers only applies the most rigorous and unbiased reviews.
Frontiers revolutionizes research publishing by freely delivering the most outstanding research, evaluated with no bias from both the academic and social point of view. By applying the most advanced information technologies, Frontiers is catapulting scholarly publishing into a new generation.

What are Frontiers Research Topics?

Frontiers Research Topics are very popular trademarks of the Frontiers Journals Series: they are collections of at least ten articles, all centered on a particular subject. With their unique mix of varied contributions from Original Research to Review Articles, Frontiers Research Topics unify the most influential researchers, the latest key findings and historical advances in a hot research area! Find out more on how to host your own Frontiers Research Topic or contribute to one as an author by contacting the Frontiers Editorial Office: frontiersin.org/about/contact

MOLECULAR BIOMARKERS IN ANIMAL REPRODUCTION

Topic Editors:
Jordi Roca, University of Murcia, Spain
Isabel Barranco, University of Bologna, Italy
Cristina Alicia Martinez, Linköping University, Sweden

Citation: Roca, J., Barranco, I., Martinez, C. A., eds. (2022). Molecular Biomarkers in Animal Reproduction. Lausanne: Frontiers Media SA.
doi: 10.3389/978-2-88974-103-8

Table of Contents

frontiers in Veterinary Science

EDITORIAL
published: 01 December 2021
doi: 10.3389/fvets.2021.802187

Editorial: Molecular Biomarkers in Animal Reproduction

Cristina Alicia Martínez[1], *Jordi Roca*[2]* *and Isabel Barranco*[3]

[1] *Department of Biomedical and Clinical Sciences, Faculty of Medicine and Health Sciences, Institutionen för biomedicinska och kliniska vetenskaper (BKV), BKH/Obstetrics and Gynaecology, Linköping University, Linköping, Sweden,* [2] *Department of Medicine and Animal Surgery, Faculty of Veterinary Medicine, International Excellence Campus for Higher Education and Research "Campus Mare Nostrum", University of Murcia, Murcia, Spain,* [3] *Department of Veterinary Medical Sciences, University of Bologna, Bologna, Italy*

Keywords: omics, biomarker, reproduction, fertility, livestock species

Editorial of the Research Topic

Molecular Biomarkers in Animal Reproduction

Improving the reproductive efficiency of livestock species remains challenging the scientific community. Emerging 'omics technologies, such as genomics, transcriptomics, proteomics, and metabolomics, are helping to overcome this challenge (1, 2). These high-throughput technologies make it possible to identify the set of molecules and regulatory networks which are directly or indirectly involved in reproductive processes, and to recognize molecules that play a key role in major reproductive events (3). In this context, one of the purposes of this special issue was to highlight the increasing applicability of 'omics to identify key molecules involved in modulating main reproductive events of animal species of economic interest. Seven out of nine research papers included in this special issue used 'omics-tools, five of them using transcriptomics and the other two using metabolomics and proteomics.

It was not surprising that five out of seven papers involved transcriptomics to study reproductive processes. A large body of research is currently aimed to unravel the transcriptome of gametes and embryos of livestock species, to both explain the roles of RNAs in regulating gene pathways and to unveil RNA markers of key functional events (4). Two of these five transcriptomics-based studies explored the sperm transcriptome for two completely different purposes, one addressing the analytical procedure and the other the practical application. The research conducted by Lian et al. focused on the performance of RNA sequencing (RNA-Seq) in spermatozoa, a method that uses deep sequencing technologies to profile and quantify cellular RNAs (5). Specifically, the research evaluated the impact of the density gradient centrifugation cell purification step recommended in the protocol on the transcriptome profile of pig spermatozoa. Results demonstrated that the purification step influenced RNA abundance in a small number of genes related to translation, transcription, and metabolic processes which, associated to the purification step for removal of expected non-sperm cells as well as immature and non-functional spermatozoa, showing it compromises the soundness of the results. The research conducted by Turri et al. focused on evaluating the value of sperm micro-RNA (miRNA) profiling in predicting the fertile ability of bulls used in artificial insemination (AI) programs. They concluded that integrating sperm miRNA profiling into the battery of advanced sperm functional assessments improved our predictive capacity. The other three transcriptomic-based papers investigated female functional reproductive events. The research conducted by Pan et al. focused on decoding the complete transcriptome of granulosa cells of Chinese Buffalo ovarian follicles. Granulosa cells play a key role in the regulation of oocyte maturation and follicular atresia, the latter being one of the main factors limiting female reproductive performance in livestock species, yet involving unclear molecular mechanisms (6). The results highlighted several messenger RNAs (mRNAs), miRNAs and long non-coding RNAs

OPEN ACCESS

Edited and reviewed by:
Arumugam Kumaresan, National Dairy Research Institute (ICAR), India

***Correspondence:**
Jordi Roca
roca@um.es

Specialty section:
This article was submitted to Animal Reproduction - Theriogenology, a section of the journal Frontiers in Veterinary Science

Received: *26 October 2021*
Accepted: *11 November 2021*
Published: *01 December 2021*

Citation:
Martínez CA, Roca J and Barranco I (2021) Editorial: Molecular Biomarkers in Animal Reproduction. Front. Vet. Sci. 8:802187. doi: 10.3389/fvets.2021.802187

(lncRNAs) with regulatory roles that were differentially expressed between granulosa cells of healthy and atretic follicles, possibly involved in critical developmental and atresia events of buffalo ovarian follicles. Del Rio and Madan explored the existence of miRNAs in media used during *in vitro* culture of bovine preimplantation embryos and identified a total of 111 miRNAs, which would regulate genes involved in early bovine embryo development. The latest transcriptomic-based work was performed by Hebbar et al. also in female buffaloes. They explored circulating miRNAs in urine to identify potential non-invasive biomarkers of estrus and highlighted the miRNA bta-mir-99a-5p, which was less abundant during estrus than during diestrus.

The other two omics-based studies used metabolomics and proteomics approaches. Metabolomics is the newest of the 'omics used to search for molecular markers of reproductive (dys)functionality displaying some advantages over the other 'omics, such as faster throughput and the ability to measure the end products of regulatory processes (7). Using a liquid chromatography-mass spectrometry-based non-targeted metabolomic approach, Mo et al. decoded the metabolic profile of atretic ovarian follicles in sows and identified 18 metabolites involved in lipid and amino acid metabolism presumably involved in follicular atresia. The last 'omic study was conducted by Fernández-Hernández et al. decoding the proteome profile of equine oviductal fluid collected before and after ovulation attempting identification of fertilization-related proteins. They identified a total of 1,173 proteins, 691 of which were included in the *Equus caballus* taxonomy and, using an iTRAQ approach, highlighted several proteins that were differentially expressed between pre- and post-ovulatory stages, some of them having a clear role in sperm-oviduct interactions and fertilization.

The special issue was also open to research or review papers exploring molecules with potential predictive value for reproductive events in livestock species and the remaining three articles served this purpose. The research conducted by Gautam et al. studied the anti-Müllerian hormone (AMH), a glycoprotein member of the transforming growth factor beta family involved in ovarian functionality (8) and considered as a reliable marker of reproductive output in dairy cattle breeds (9). The research sequenced the entire coding region of the AMH gene in water buffalo and goat females and suggested that the AMH gene has a similar and critical physiological reproductive function in both species. The research conducted by Ribas-Maynou et al. focused on sperm nuclear DNA. Early identification and removal of male breeders showing high percentages of ejaculated sperm with damaged nuclear DNA is a priority for swine AI centers to improve the fertility efficiency of AI programs (10). Despite this conclusive evidence, there is still no standardized measurement method for practical use in the porcine AI laboratories. The aim of the study conducted by Ribas-Maynou et al. was to evaluate the practical suitability of some of the most used methods. They tested eight methods, namely the direct measurement methods TUNEL, TUNEL with decondensation, the alkaline and neutral Comet assays, and chromomycin A3 (CMA3); and the indirect methods sperm chromatin structure assay (SCSA), and the alkaline and neutral sperm chromatin dispersion (SCD) assays. Based on the ability to measure the degree of chromatin damage, the study concluded that direct methods are more suitable than indirect methods. Finally, Pérez-Gómez et al. provided a timely and comprehensive review summarizing the events that take place during preimplantation embryo development in ungulates in order to identify genes regulating lineage differentiation. The review also discusses studies reporting altered lineage development in embryos produced *in vitro* and, finally, provides a general view of molecular markers of lineage differentiation. In this regard, they emphasize that transcriptomics is a powerful tool for discovering molecular markers of embryo quality.

Taken together, these papers demonstrate that omics are powerful tools to provide a more in depth understanding of reproductive events and to identify molecular markers to select best breeders or improve reproductive performance of livestock species.

AUTHOR CONTRIBUTIONS

All authors have contributed to the writing of this editorial and have approved it for publication.

FUNDING

CM and IB were financially supported by the European Union's Horizon 2020 research and innovation program (grants H2020-MSCA-IF-2019-891663 and H2020- MSCA-IF-2019-891382).

REFERENCES

1. Özbek M, Hitit M, Kaya A, Jousan FD, Memili E. Sperm functional genome associated with bull fertility. *Front Vet Sci.* (2021) 8:610888. doi: 10.3389/fvets.2021.610888
2. Long JA. The 'omics' revolution: use of genomic, transcriptomic, proteomic and metabolomic tools to predict male reproductive traits that impact fertility in livestock and poultry. *Anim Reprod Sci.* (2020) 220:106354. doi: 10.1016/j.anireprosci.2020.106354
3. Soler L, Uzbekova S, Blesbois E, Druart X, Labas V. Intact cell MALDI-TOF mass spectrometry, a promising proteomic profiling method in farm animal clinical and reproduction research. *Theriogenology.* (2020) 150:113–21. doi: 10.1016/j.theriogenology.2020.02.037
4. Gebremedhn S, Ali A, Hossain M, Hoelker M, Salilew-Wondim D, Anthony RV, et al. MicroRNA-mediated gene regulatory mechanisms in mammalian female reproductive health. *Int J Mol Sci.* (2021) 22:938. doi: 10.3390/ijms22020938
5. Hrdlickova R, Toloue M, Tian B. RNA-Seq methods for transcriptome analysis. *Wiley Interdiscip Rev RNA.* (2017) 8. doi: 10.1002/wrna.1364
6. Worku T, Rehman ZU, Talpur HS, Bhattarai D, Ullah F, Malobi N, et al. MicroRNAs: new insight in modulating follicular atresia: a review. *Int J Mol Sci.* (2017) 18:333. doi: 10.3390/ijms18020333
7. Bracewell-Milnes T, Saso S, Abdalla H, Nikolau D, Norman-Taylor J, Johnson M, et al. Metabolomics as a tool to identify biomarkers to predict and improve outcomes in reproductive medicine: a systematic review. *Hum Reprod Update.* (2017) 23:723–36. doi: 10.1093/humupd/dmx023

8. Moolhuijsen LME, Visser JA. Anti-Müllerian hormone and ovarian reserve: update on assessing ovarian function. *J Clin Endocrinol Metab.* (2020) 105:3361–73. doi: 10.1210/clinem/dgaa513
9. Alward KJ, Bohlen JF. Overview of Anti-Müllerian hormone (AMH) and association with fertility in female cattle. *Reprod Domest Anim.* (2020) 55:3–10. doi: 10.1111/rda.13583
10. Roca J, Broekhuijse ML, Parrilla I, Rodriguez-Martinez H, Martinez EA, Bolarin A. Boar differences in artificial insemination outcomes: can they be minimized? *Reprod Domest Anim.* (2015) 50 (Suppl. 2):48–55. doi: 10.1111/rda.12530

Conflict of Interest: The authors declare that the research was conducted in the absence of any commercial or financial relationships that could be construed as a potential conflict of interest.

Publisher's Note: All claims expressed in this article are solely those of the authors and do not necessarily represent those of their affiliated organizations, or those of the publisher, the editors and the reviewers. Any product that may be evaluated in this article, or claim that may be made by its manufacturer, is not guaranteed or endorsed by the publisher.

frontiers in Veterinary Science

ORIGINAL RESEARCH
published: 08 March 2021
doi: 10.3389/fvets.2021.627094

Characterization of Anti-Müllerian Hormone (AMH) Gene in Buffaloes and Goats

Devika Gautam[1], *Ashutosh Vats*[1], *Prasanna Pal*[2], *Avijit Haldar*[3] *and Sachinandan De*[1]*

[1] *Animal Genomics Lab, Animal Biotechnology Centre, ICAR-National Dairy Research Institute (NDRI), Karnal, India,* [2] *Animal Physiology Division, ICAR-National Dairy Research Institute (NDRI), Karnal, India,* [3] *ICAR-Agricultural Technology Application Research Institute (ATARI), Indian Council of Agricultural Research, Kolkata, India*

The Anti-Müllerian Hormone (AMH) is a member of the transforming growth factor beta (TGF-β) superfamily, playing a significant role in cell proliferation, differentiation and apoptosis. In females, AMH is secreted throughout their reproductive life span from ovaries, whereas in males it is secreted by gonadal cells at a very early stage of testicular development. AMH is a promising marker of ovarian reserve in women and can be used to measure the female reproductive lifespan. In the present study, we cloned and sequenced the GC rich *AMH* gene from Indian riverine buffalo (*Bubalus bubalis)* and goat (*Capra hircus*). Obtained sequences were compared to the AMH sequences of other mammals, and corresponding amino acid sequences revealed that the caprine and bovine AMH sequences are more closely related to each other than to those of other mammals. Furthermore, we analyzed the chromosomal localization of *AMH* genes in mammalian species to understand potential syntenic relationship. The *AMH* gene is localized between the sequences for the *SF3A* and *JSRP1* genes and maintains this precise location in relation to other nearby genes. The dN/dS ratio of *AMH* gene did not indicate any pressure for either positive or negative selection; thus, the physiological function of the *AMH* gene in the reproduction of these two ruminant species remains very vital. Similar to other mammals, the *AMH* gene may be an important indicator for regulating female reproductive biology function in bovine, cetacean, caprine, and camelidae.

Keywords: Anti-Müllerian hormone, phylogenetic tree, syntenic analysis, Indian water buffalo, goat, reproduction, fertility

OPEN ACCESS

Edited by:
Cristina Alicia Martinez, Linköping University, Sweden

Reviewed by:
Gregorio Miguel Ferreira De Camargo, Federal University of Bahia, Brazil
Sankarganesh Devaraj, Kalasalingam University, India

***Correspondence:**
Sachinandan De
sachinandan@gmail.com

Specialty section:
This article was submitted to Animal Reproduction - Theriogenology, a section of the journal Frontiers in Veterinary Science

Received: *08 November 2020*
Accepted: *16 February 2021*
Published: *08 March 2021*

Citation:
Gautam D, Vats A, Pal P, Haldar A and De S (2021) Characterization of Anti-Müllerian Hormone (AMH) Gene in Buffaloes and Goats. Front. Vet. Sci. 8:627094. doi: 10.3389/fvets.2021.627094

INTRODUCTION

Anti-Müllerian hormone (AMH), also known as Müllerian-Inhibiting Substance (MIS), is a well-studied regulatory molecule impacting on reproductive function, and has specifically studied in male sexual differentiation during early embryonic development. AMH is synthesized by fetal Sertoli cells at the time of testicular differentiation and induces regression of the Mullerian ducts that form the base for the development of the oviducts, uterus and upper part of the vagina in males (1). In the absence of AMH, the Mullerian ducts develop into the oviducts, the uterus and the upper part of the vagina (2). Postnatally, serum AMH concentration increases significantly until puberty, followed by a slow decline throughout the rest of life (3). This decline has been attempted to be modeled by a variety of approaches, with a cubic model resulting in the best fit model that delineates the change of plasma AMH level with the advancement of age in cattle and goats (4–6). The gradual decline of serum AMH concentration runs in

parallel with the depletion of the number of growing ovarian follicles (7), making this hormone an ideal prognostic biomarker of the ovarian follicular reserve (8, 9), and thus for fertility and herd longevity in cattle farm (10). In addition, AMH may also be used as a diagnostic marker for ovarian functional disorders in domestic animals. Indeed, AMH levels are increased in women with polycystic ovary syndrome (PCOS) (11, 12); however, this question, with particular reference to anestrus and repeat breeding, has not yet been studied in farm animals.

AMH has a molecular weight of 140 kDa, corresponding to 553–575 amino acids and belonging to the transforming growth factor-beta (TGF-β) superfamily (11). It is a dimeric glycoprotein consisting of two identical subunits linked by sulfide bridges and characterized by the N-terminal dimer (pro-region) and C-terminal dimer (TGF-β domain). The AMH protein is encoded by the *AMH* gene that spans over 2.75 Kbp and contains five exons. The gene is located in chromosome 7 in cattle, horses and goats; chromosome 5 in sheep; chromosome 9 in buffalo; and chromosome 2 in pig (12, 13). In Nelore cattle, the three synonymous mutations (rs527023314, rs722016629, and rs134387246) were found in exon 5 of AMH, which may be associated with early pregnancy occurrence and age at first calving in this cattle breed (14). In ovaries, AMH is produced by the granulosa cells of early growing follicles and is proportional to the antral follicle count, which is a significant determinant of the age-related decline in female fertility due to decrease in ovarian reserve (15). AMH expression reaches its peak level in primordial, primary, and secondary follicles and AMH expression is strongest in granulosa cells of preantral and small antral follicles, whereas it decreases once the dominant follicle is selected and is absent in atretic follicles. This dynamic expression was firstly reported in rabbits (16), and then in the rat (17), human (18), cattle (19), chicken (20), sheep (21), mares (22), buffalo (23), goats (24), and pigs (25). These observations strongly suggest that AMH is a dominant regulator of early follicular growth. AMH hormone levels and antral follicle populations can be used as a marker to genetically improve fertility rates in Nelore cattle and to screen for better oocyte donors (26). The *AMH* gene has not been characterized in many domestic animals, specifically large as well as small ruminant species. In India, riverine buffalo are representative of large domestic ruminant, whereas goats are the major small ruminant, and both play an economically important role. Therefore, the objective of the present study was to clone and sequence the *AMH* gene in Indian riverine buffalo and goat. The deduced amino acid sequence of Indian riverine buffalo and goat AMH as well as sixteen other mammalian AMH amino acid sequences was used to understand the phylogenetic relationships to assess potential changes in reproductive processes.

MATERIALS AND METHODS

Ethics Statement

The study was approved (IAEC/41/14) by the Institutional Animal Ethics Committee (IACE), ICAR-NDRI, Karnal.

Experimental Design

Ovaries of Indian riverine buffalo (*Bubalus bulalis)* and goat (*Capra hircus*) were used to isolate RNA which was subsequently used to amplify the *AHM* cDNA. The resulting fragments were cloned and sequenced. The deduced AMH sequences were used to construct the phylogenetic tree of the *AMH* gene.

Sample Collection

The *AMH* gene is expressed only in the ovarian granulosa cells and male fetal testis. Hence, 150 ovaries from 75 Indian riverine buffaloes and 30 ovaries from 15 goats of unknown history, parity and cyclic condition were collected from the slaughterhouse at Gazipur, New Delhi and Municipal Corporation (Karnal, Haryana), respectively. The ovaries were washed with 0.9% normal saline supplemented with 100 μg/ml streptomycin. The samples were brought to the laboratory within three to four hours in RNA*later* (AM7021, Thermo Scientific) at 4°C. Small follicles were searched and aspirated with the help of a sterile syringe and a needle. Ovaries with a cyst like growth and damaged ones were not used.

Total RNA Isolation and cDNA Construction

Small follicles from healthy ovaries of Indian riverine buffaloes and goats were aspirated as described (25, 26), and the pooled fluid containing granulosa cells were centrifuged at 500×*g* for 5 min followed by washing twice with 1x PBS. RNA was isolated according to the manufactures protocol using TRI reagent (T9424, Sigma Aldrich, Merck, Darmstadt, Germany). The quality and quantity of RNA was checked through 1.5% agarose gel electrophoresis and spectrophotometrically through NanoDrop 2000 (Thermo Scientific, Delaware, USA). First strand cDNA was synthesized from 1 to 2 μg of total RNA using SuperScript® III First-Strand Synthesis System (18080051, Invitrogen, USA) for RT-PCR.

Amplification and Cloning of *AMH* Coding Sequence

The PCR primers were designed based on bovine AMH sequence available at NCBI, USA (Accession No: M13151.1 and NM_173890.1). The primer pair [Forward: 5'AGGATGCCCGGTCCATCTCTCTCT 3' (24bp) and Reverse: 5' ACCGGCAGCCGCATTCGGTGG 3' (21bp)] was used to amplify the 1728bp *AMH* coding sequence of Indian riverine buffalo and goat *AMH* by polymerase chain reaction (PCR) using cDNA as a template. The PCR reaction was carried out with 25 μl a master mix containing 2 μl of cDNA, 10 pmol each of forward and reverse primers, 1x Taq assay buffer, 200 μM of deoxynucleotide triphosphates (dNTPs), 2.5 μl of GC enhancer and 0.75 units Taq DNA polymerase (Bangalore Genei Pvt. Ltd., Bangalore, India). The PCR reaction was performed in a Veriti Thermal Cycler (Applied Biosystem, Thermo Fisher Scientific, USA) by programming the cycling parameters consisting of an initial denaturation at 95°C for 3 min followed by amplification for 35 cycles (each consisting of denaturation at 95°C for 30 s, annealing at 55°C for 30 s and extension at 72°C for 2 min). Final extension of 7 min was at 72°C. The PCR amplified DNA fragments were resolved by electrophoresis on 1.5% agarose gel stained with ethidium bromide in 1x tris acetate EDTA

(TAE) buffer and visualized in Gel Documentation system (Gel Doc-XR, BioRad, USA) against 1 Kbp DNA ladder (SM0311, Thermo Scientific™). The band corresponding to 1728 bp was carefully excised and DNA was extracted using a NucleoSpin gel extraction Kit according to manufacturer's instruction (740609.250, Macherey-Nagel, Germany). The amplified Indian riverine buffalo and goat *AMH* gene fragments were cloned into a linearized vector (pTZ57R/T) using InsTAclone PCR cloning kit (K1214, Thermo Scientific, USA), which was subsequently used to transform *E. coli* XL-1Blue chemically competent cells using ampicillin (50 mg/ml) as a selection marker for multiplication of the insert. Six to eight recombinant colonies containing a plasmid with insert were enriched on Luria Bertani (LB) broth. The plasmid DNA was extracted by the alkaline lysis method (27) with slight modifications. The positive clones for *AMH* gene were screened with vector-specific primers and sequenced by sanger dideoxy method through capillary sequencing.

Sequence Acquisition, Multiple Sequence Alignment, and Phylogenetic Tree Construction

Extracted plasmids containing the appropriate inserts were sequenced using universal sequencing primers [M13 (-20)] Forward and [M13 (-20)] Reverse. The chromatogram was analyzed for read quality assessment and vector contamination using VecScreen (http://www.ncbi.nlm.nih.gov). The multiple sequence alignments were performed using the MAFFT tool (for multiple alignment using fast Fourier transform, version:7) (28). The coding regions were translated through the Expasy translate tool (https://web.expasy.org/translate/). The forward and reverse sequences along with the reference sequences were aligned using MAFFT and the assembled entire coding sequences were submitted to GenBank, NCBI. A phylogenetic tree was generated to establish the molecular evolutionary relationship of AMH amino acid sequences of Indian riverine buffalo and goat and with fourteen other mammalian species. The evolutionary history was inferred using the Neighbor-Joining method and the optimal tree with the sum of branch length = 0.89 is shown. The phylogenetic inference was further validated with the bootstrapping (1000 replicates). The passion correction method was used to compute the evolutionary distances and was in the number of amino acid substitutions per site. All ambiguous positions were removed for each sequence pair (pairwise deletion option). There was a total of 623 positions in the final dataset. Evolutionary analyses were conducted in Molecular Evolutionary Genetics Analysis (MEGA X) (29).

Selection Pressure Analysis

Selection pressure on protein coding gene of mammalian *AMH* was analyzed in Mega-Datamonkey server based on single likelihood ancestor counting (SLAC) method (30). The selection pressures were calculated by comparing the rate of substitutions at silent sites (dS), which were presumed neutral, to the rate of substitutions at non-silent sites (dN). The dN/dS is measured across the whole protein coding sequence between two divergent species for selection. If the ratio = 1, then the whole coding sequence evolved neutrally, then all nucleotide in a sequence is equally likely to change, when $0<dN/dS<1$, it would be under constraint > 1, it would be under positive selection.

RESULTS

Amplification of High GC Containing *AMH* Coding Sequence

The *AMH* gene corresponding to 1728 base pairs was amplified from cDNA of Indian riverine buffalo and goat granulosa cells. The amplified product was checked on 1.5% agarose gel as shown in **Figure 1**, then followed by sequencing. The total GC content in the complete coding sequence of the *AMH* gene is 72%. The exon wise GC content were 69, 69, 73, 71, and 74%, respectively in exon I-V. The 595 amino acid residues of AMH protein consists of 24 residue signal peptides and 551 amino acid residues of the mature protein. The TGF-β domain is composed of 99 amino acids from the mature peptide. Indian riverine buffalo and goat AMH protein comprised 12 conserved cysteine residues. The highest occurring amino acids are leucine and proline accounting to 16 and 12%, respectively in the polypeptide chain. The least occurring amino acids are Met, Try, Lys, and Ile. The peptide sequences of both the animals contain two N-glycosylation sites (78-NGSR and 344-NLSD). The AMH proteins are more conserved in the C-terminal than N-terminal.

Genetic and Syntenic Analysis of AMH

A phylogenetic tree of the relation of the domestic animals' AMH amino acid sequences with that of dolphin, whale and primate is presented (**Figure 2**). Phylogenetic analysis of AMH peptide of around 401–575 amino acid residues across the mammalian species distinctly represents two major clades, one representing Bovidae, Cetacea, Camelidae, and the other comprising the Primates and Equidae. The topology found is according to the phylogenetic grouping of cloven-hoofed, cetaceans and primates. The cloven-hoofed, ruminant vertebrates covering cattle, Indian riverine buffalo, sheep and goat are highly similar based on AMH amino acid sequence data. Cetaceans diverging from its even-toed ungulates ancestors are close to cloven-hoofed, ruminant vertebrates in phylogenetic trees. The odd-toed mammals; rhinoceros and three-toed equids are located near to each other in the phylogenetic tree and are closer to the primates. Alpaca and dromedary camels are closely related to pigs which diverged from primates and ruminant vertebrates. The molecular phylogenetic analysis of the *AMH* gene provides us with accurate descriptions of patterns of relatedness and evolutionary relationships among animal species being studied (**Figure 2**). The physical co-localization of *AMH* gene is in between *SF3A2* (Splicing factor 3A subunit 2) and *JSRP1* (Junctional sarcoplasmic reticulum protein 1) genes. The gene order of *SF3A2, AMH*, and *JSRP1* are highly conserved among mammalian species included in the present study. Gene encoding *AMH* and *JSRP1* in all these mammals are oriented facing each other, while gene encoding *SAF3A2* is either oriented toward *AMH* in the case of cattle, pig, monkey, horse, deer, sheep, and human or oriented opposite to AMH in the case of Indian riverine buffalo, goat, whale, dolphin, camel, and donkey (**Figure 2**). Around 2.1 Kbp of *AMH* consists of five exons and four introns of varying length with 72% GC content

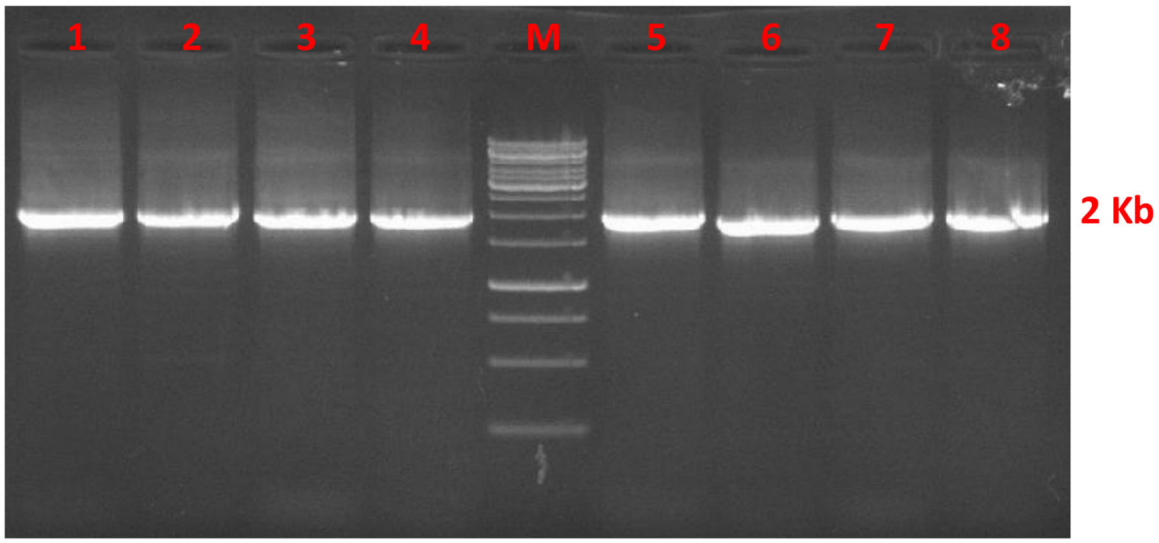

FIGURE 1 | Agarose gel stained with ethidium bromide represents *AMH* gene fragment of 1728 bp from cDNA of buffalo (lane 1–4) and goat (lane 5–8) granulosa cell. Lane M is 1 Kbp DNA marker.

across exons and introns. The fifth exon comprises 800–900 bp making it the largest followed by exon one, four, two and three. Among mammals, the numbers of nucleotides in each exon are consistent. Higher conservation around the species is found among exon 2 and 3 regions. The matured AMH peptide consists of 575 amino acid residues with the N-terminal pro-region and the C-terminal region (TGF-β) in cattle. The signal peptide comprising of 24 amino acid residues is located in the first exon, rest part of exon one, two, three, four and some part of exon five makes N-terminal AMH and the TGF-β domain part is located at the end part of exon five (25).

TGF-β Domain in AMH Is Conserved Across the Mammalian Species

The TGF-β domain in the *AMH* gene across species is conserved with nine amino acid variations across these mammalian spices. TGF-β domain comprises 99 amino acids (from 477 to 575 in cattle, goat and sheep; 323 to 421 in yak and 462 to 560 in human), and 77 amino acids in Alpaca (from 342 to 418) amino acids. In cattle, buffalo, goat, sheep and deer the only amino acid residue located at 533 is changed from Threonine to Alanine, this change is conserved across the other species. Similarly, primates have another amino acid substitution at 505 (Alanine to Valine) and 544 (Threonine to Alanine). Cetaceans have Glycine instead of Alanine at 478, equine and camels have Arginine in place of Serine at 482. The highly conserved amino acid sequence of AMH-TGF-β domain among the mammalian type maybe for the maintained functions (**Figure 3B**). The positions of critical amino acids such as Methionine, Cysteine and Proline are unchanged in all the species compared for the TGF-β domain region (**Figure 3B**).

Selective Pressure Analysis on *AMH* (dN/dS Ratio)

The evolutionary pressure on AMH protein is quantified by the substitution rates at non-synonymous and synonymous sites. The dN/dS ratio of this gene did not show either positive or negative selection pressure, and it therefore can be assumed that the function of AMH across species was retained (31). AMH is possibly required for the stable physiological function in reproduction of cattle, buffalo, sheep, goat, and deer. Most of the AMH codon sites are under adverse selection; the function is maintained though some sites are positively selected for a change (**Figure 4**).

DISCUSSION

AMH plays a vital role in mammalian female reproduction, especially in follicular growth and differentiation; its expression is restricted to granulosa cells of adult ovaries. The increase in follicular size increases the AMH level. The dynamic expression pattern marks an AMH to be a potential endocrine marker to the size of ovarian pool, to improve reproduction rates and for the selection of better oocyte donor (9, 13, 21, 26). In our present study, we report for the first time the complete coding sequence of *AMH* in Indian riverine buffalos and goats.

The limited AMH sequence information in ruminant available so far may be due to technical problems in cloning and sequencing a GC-rich sequence (32, 33). Before our study, several unsuccessful attempts were made to amplify the coding sequence in Indian riverine buffalo and goat. All sequences obtained in the present study were deposited in NCBI (MH479929.2 and MH479928.2). We have compared our AMH DNA and protein sequences (MH479929.2; QBZ68774 and MH479928.2; QBZ68773) with the sequences of buffalo and goat present in the

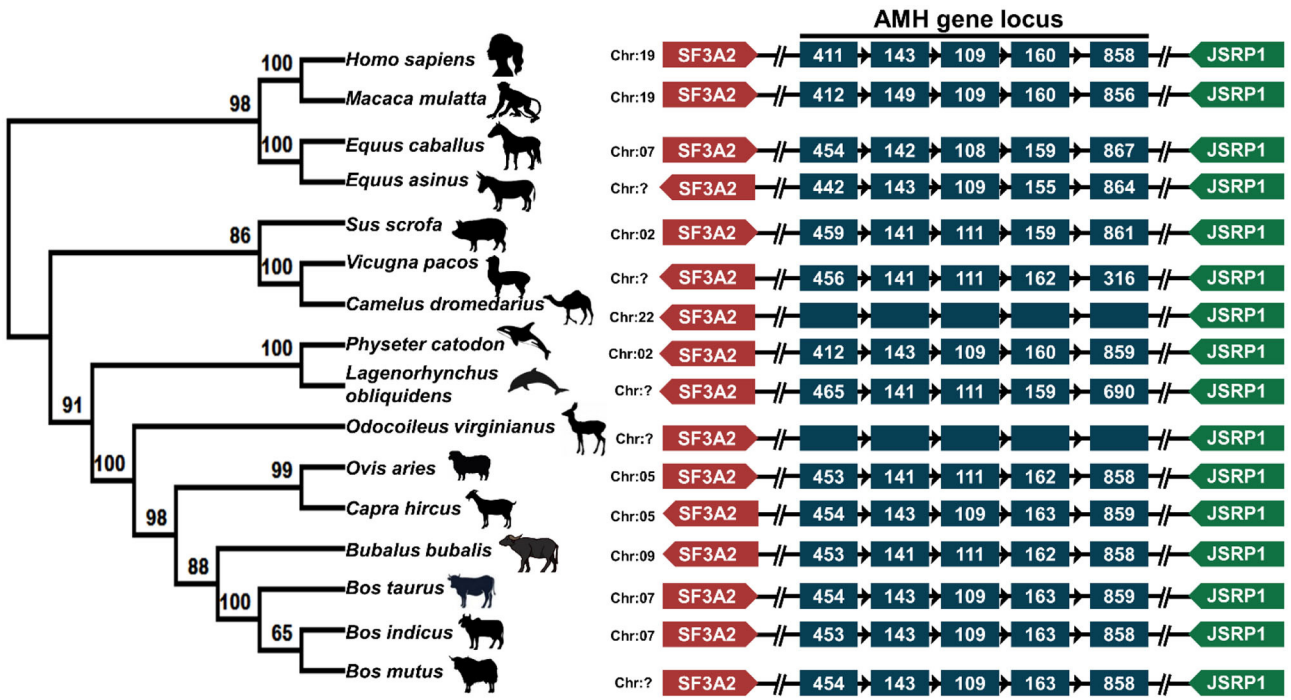

FIGURE 2 | Phylogenetic and syntenic analysis of AMH: the left panel depicts the phylogenetic analysis of AMH amino acids of sixteen mammalian species performed in MegaX. The rooted phylogenetic tree is constructed from Neighbor-Joining method with bootstrap value of 1,000. The middle panel is showing the chromosomal location of *AMH* gene in respective animals. The right panel shows the syntenic analysis of the *AMH* gene of these animals. The neighboring genes *SF3A2* on the right side and *JSRP1* gene on the left side of *AMH* are represented in different colors. The arrow head represents the orientation of the genes. *AMH* gene in the middle is shown in blue color where each box representing the exon. The amino acid accession numbers for phylogenetic and syntenic analysis are: NP_000470.3 (*Homo sapiens*); NP_999475.2 (*Sus scrofa*); XP_014977898.2 (*Macaca mulatta*); NP_776315.1 (*Bos taurus*); NP_001304192.1 (*Equus caballus*); XP_014701194.1 (*Equus asinus*); XP_019820099.1 (*Bos indicus*); XP_005888453.1 (*Bos mutus*); NP_001295528.1 (*Ovis aries*); XP_020761609.1 (*Odocoileus virginianus*); XP_023990190.1 (*Physeter catodon*); QBZ68774.1 (*Bubalus bubalis*); QBZ68773 (*Capra hircus*); XP_026941471.1 (*Lagenorhynchus obliquidens*); XP_006206642.1 (*Vicugna pacos*) and XP_031293953.1 (*Camelus dromedarius*).

database (buffalo sequence: XP_006047877 and AFH66811, and goat sequence: XP_017906255 (isoform 2) and XP_017906254 (isoform1) obtained from whole genome shotgun sequence. Our buffalo AMH protein shared 99 and 96% identity, respectively with the database sequence XP_006047877 and AFH66811. Our goat AMH protein (QBZ68773) shared 99% identities with predicted isoform 2 (XP_017906255) and 95% identities with isoform 1 (XP_017906254). An additional twenty-eight amino acids (RCAQARTWGCGECGRRSLAPSRPPTLLS) located between position 289 and 319 of the matured protein of goat isoform 1 was not detected in any of our sequences nor in goat isoform 2 and other buffalo sequences (**Figure 5**). Overall, the AMH protein of buffalo and goat show a higher degree of homology in the C-terminal region compared to the N-terminal region, potentially due to the presence of the conserved TGF-β domain in the C-terminus. The presence of critical amino acids (Cys and Pro), highest and lowest occurring amino acid residue and the glycosylation sites in buffalo and goat AMH proteins were found to be similar compared to human and bovine sequences (34). The coding sequence of *AMH* in both animals contain five repeats of CCGCCC, and the same repeat sequences were also found in the promoter regions of other GC rich genes such as *c-myc*, *EGF* receptor and *AMH* where *sp1* transcription factor may regulate such genes containing this repeat (34). The fragile X syndrome (*FMR1*) gene exerts independent function on follicle recruitment and ovarian reserve (35). Approximately 29–30 CGG repeats on the *FMR1* gene appear reflective of usual ovarian reserve. The higher and lower CGG repeats on the *FMR1* gene denote similar risks toward premature ovarian senescence and female infertility (35). Interestingly, AMH also represents a significant association with a number of CGG repeats, a similar pattern is observed in our buffalo and goat nucleotide sequence where 46 CGG repeats are found. In the phylogenetic tree, the ruminant vertebrates covering cattle, buffalo, sheep, and goat diverging from human, primates, rhinoceros, camel, horse, and donkey may be a cause of differences in amino acid sequence composition. In Mice, AMH confined both pre-antral and early antral stages of the follicular maturation, while in primates AMH inhibitory actions are effective during antral follicle development. In non-human primate pre-antral follicles respond differently to AMH. These observations suggest the species-specific AMH behavior on follicular development and selection of dominant follicle (36, 37). In mare and women, hormonal and cyclic changes are related as they age, reproductive aging in both the species is observed with rise in FSH. The oocytes of these species are maintained in meiotic arrest for ages (38). In contrast to

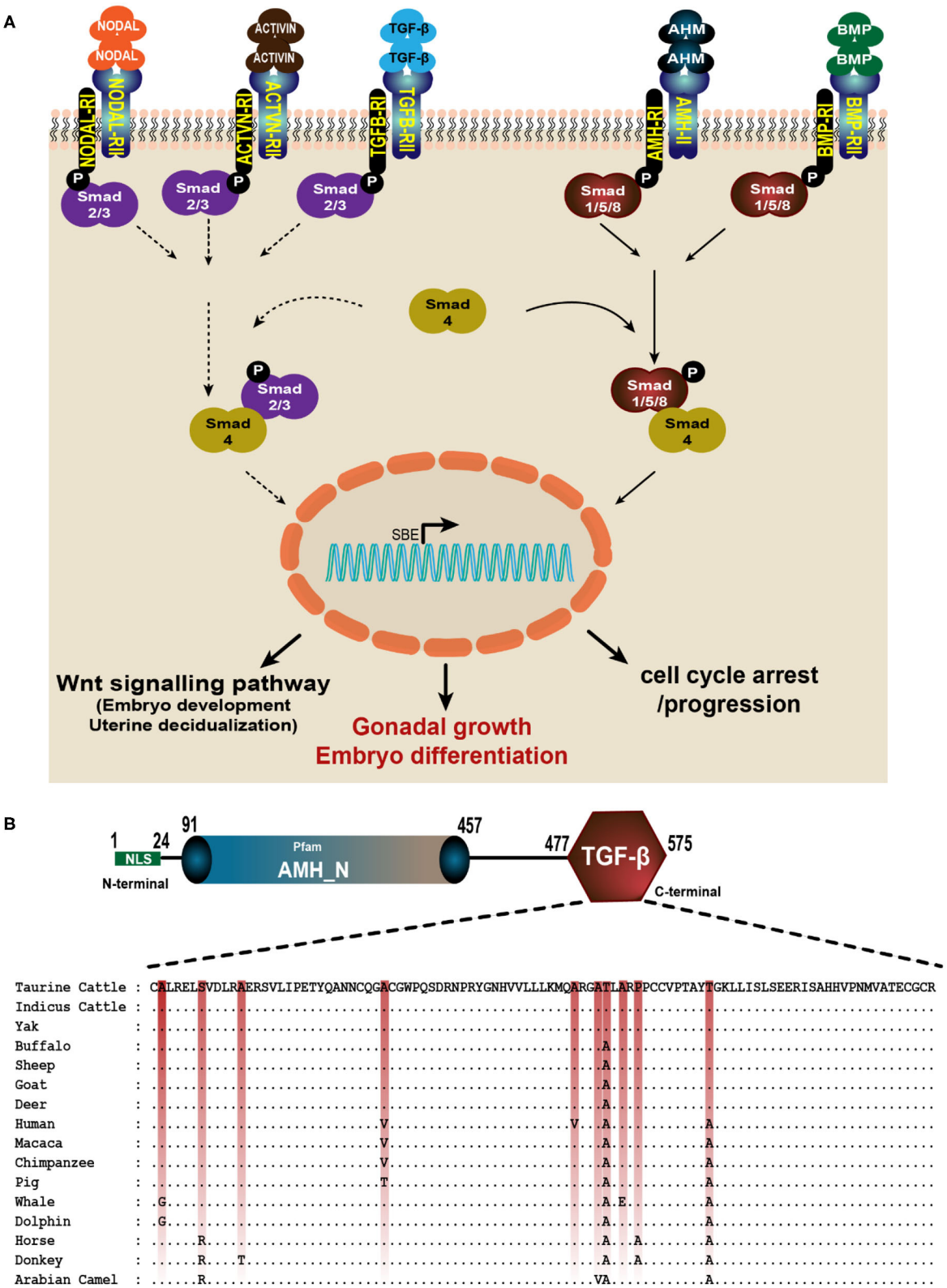

FIGURE 3 | AMH is a member of TGF-β superfamily. **(A)** AMH signals through its own dedicated type II receptor (AMHRII) like other members of TGF-βs. They phosphorylate their type I receptor (AMHRI) and R-Smads (Smad1, 5, and 8). The active R-Smads then interact with co-Smad4 which translocate to the nucleus and

(Continued)

FIGURE 3 | induce various effective roles such as cell growth and differentiation, proliferation and apoptosis. **(B)** The multiple alignment of TGF-β domain in AMH gene consisting 99 amino acids is done using GeneDoc software. The amino acid accession numbers are: NP_000470.3 (Human); NP_999475.2 (Pig); XP_014977898.2 (Macaca); NP_776315.1 (Taurine Cattle); NP_001304192.1 (Horse); XP_014701194.1 (Donkey); XP_019820099.1 (Indicus Cattle); XP_005888453.1 (Yak); NP_001295528.1 (Sheep); XP_020761609.1 (Deer); XP_023990190.1 (Sperm whale); QBZ68774.1 (Buffalo); QBZ68773 (Goat); XP_026941471.1 (Dolphin) and XP_031293953.1 (Arabian Camel).

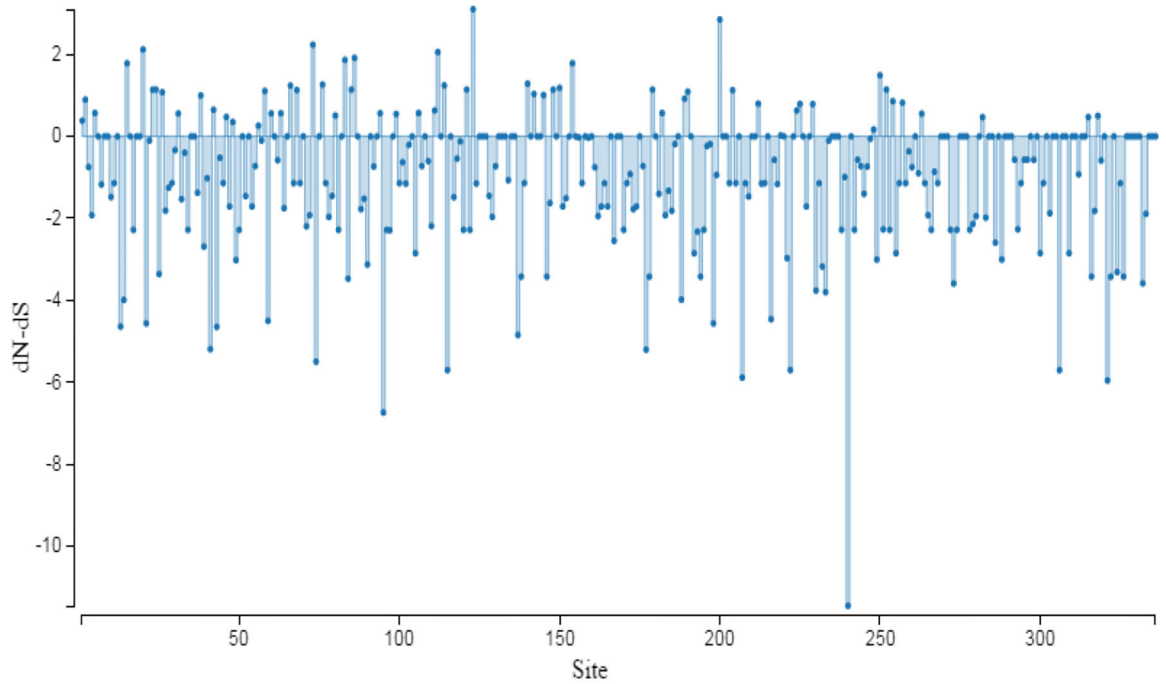

FIGURE 4 | Graphic representation of dN/dS ratio for selective pressure on evolution of protein. The sites under selection are studied through SLAC method of Datamonkey server. The coding region of *AMH* gene used for analysis has the following accession numbers: NM_000479.5 (*Homo sapiens*); NM_214310.3 (*Sus scrofa*); XM_015122412 (*Macaca mulatta*); XM_016934640 (*Pan troglodytes*); NM_173890 (*Bos taurus*); NM_001317263 (*Equus caballus*); XM_014845708 (*Equus asinus*); XM_019964540 (*Bos indicus*); XM_005888391 (*Bos mutus*); NM_001308599 (*Ovis aries*); XM_020905950 (*Odocoileus virginianus*); XM_006206580 (*Vicugna pacos*); XM_024134422 (*Physeter catodon*); XM_027085670 (*Lagenorhynchus obliquidens*); XM_004441423 (*Ceratotherium simum simum*); XM_031438093 (*Camelus dromedarius*); MH479929 (*Bubalus bubalis*) and MH479928 (*Capra hircus*).

cattle, which only develops one or two anovulatory waves while, both mare and women develop major ovulatory as well as major and minor anovulatory waves (39). The similarities in follicle development and oocyte qualities in mare and women might be the reason that equids are closer to primates according to AMH phylogenetic studies herein. In women, AMH and AFC (Antral Follicle count) have been associated with fertility in both assisted reproduction settings as well as natural fertility in the general population (15, 40). Similarly, association between peripheral AMH concentrations and fertility of mares has been reported recently (41). The closer relationship between the equids and the primates in the phylogenetic tree might be a new finding and to our knowledge, this is the first report of associations of AMH gene between the equids and the primates. Being a member of the TGF-β family which has a vital role in cellular growth, differentiation and immunosuppression, the *AMH* gene among mammalian species has maintained its sequence integrity and their physical co-localization so, not allowing any major changes, hence are not under selection pressures.

There is a classical view of a finite primordial follicle pool in the ovaries called ovarian reserve to understand ovarian aging process better (42). During the aging process, both the number and quality of the oocytes in the ovaries decrease and reach a point beyond that, no more viable offspring may be produced and the associated cyclic endocrinological activities cease, entering the menopause in females. However, menopause like stage has not been coined in farm animal species. The ovarian reserve declines progressively with increasing chronological age within expected ranges of plasma AMH concentrations (8). Plasma AMH concentration has been demonstrated to have a high degree of correlation with ovarian antral follicle count in cattle and buffaloes (43).

The TGF-β superfamily is composed of many genes including TGF-βs, the growth and differentiation factor (GDF) subfamily, bone morphogenetic protein (BMP) subfamily, activin, inhibin, AMH and follistatin (FS) (13). Being a member of the TGF-β family, AMH exerts its biological actions by interacting with its specific anti-Müllerian hormone receptor type I (AMHRI) and anti-Müllerian hormone receptor type II (AMHRII) (44). The human *AMHRII* gene is expressed in granulosa and theca cells, and also present in other tissues such as the brain, breast and endometrium although their functional role remains elusive (11,

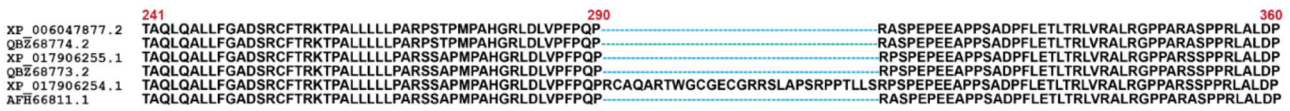

FIGURE 5 | Alignment of buffalo and goat AMH proteins (QBZ68774 and QBZ68773) with reference AMH proteins (XP_006047877, XP_017906255, XP_017906254 and AFH66811). Goat AMH isoform 1 (XP_017906254.1) with additional 28 amino acids are shown.

45). AMH signals by binding to transmembrane AMHRII and results in the phosphorylation and activation of type I receptor kinase by the constitutively active kinase domain of the type II receptor (46). The activated type I receptor then phosphorylates the cytoplasmic regulatory Smad proteins (R-Smads: 1, 5, or 8) which migrate into the nucleus, interact with co-Smad protein (Smad4) and, in concert with other transcription factors, regulate responsive genes (11). Activation of Smad4 leads to downstream signaling of various pathways like cell differentiation, apoptosis, neurogenesis, etc. (**Figure 3A**). The type II receptor for AMH (AMHRII) is one of five type II receptors in the TGF-β family. AMH and AMHRII are mutually specific (47). AMH involved in reproductive development, must be cleaved to bind its type II receptor (AMHRII), but dissociation of the pro-region from the mature C-terminal dimer is not required for this initial interaction (48). It was shown recently that AMH engages AMHRII at a similar interface compared to activin and BMP class ligands bind the type II receptor (AMHRII), ACVR2B; however, there are significant molecular differences at the ligand interface of these two receptors, where ACVR2B is mostly hydrophobic, and AMHRII is predominately charged. Although the location of ligand binding on the receptor is similar to ACVR2A, ACVR2B, and BMPR2; AMHRII uses unique ligand-receptor interactions to impart specificity for AMH (49).

Peripheral AMH concentrations are increasingly been used as biomarker of ovarian dysfunction in human reproduction and fertility. In patients with premature ovarian failure, AMH is undetectable or greatly reduced depending on the number of antral follicles in the ovaries (50). In contrast, AMH levels are increased in women with PCOS (18, 51). In women with PCOS, an accumulation of primary follicle was observed resulting in numbers higher than that of secondary follicles (52). However, AMH data in case of anestrus and repeat breeding has not yet been published in farm animals. Buffaloes with pubertal anestrus have been shown to have AMH deficient plasma concentration (0.53 ± 0.12 ng/ ml), while plasma AMH concentrations were found to be ≤ 2 ng/ ml in anestrus and repeat breeding cases (Unpublished data). Knowledge of *AMH* gene characterization and peripheral AMH levels in certain conditions (such as cystic ovarian syndrome, anestrus, repeat breeding condition etc.) may provide more insight into the possible cause or the effect of altered function of AMH in economic livestock animals.

CONCLUSION

The entire coding region of the *AMH* gene has been sequenced for the first time from cDNA of Indian riverine buffalo and goat. Phylogenetic and syntenic analysis of *AMH* gene shows that the cloven-hoofed, ruminant vertebrates like cattle, buffalo, sheep, and goat are closely related and may be correlated with evolutionary changes in the biological process of interest; however, diverged from primates, human, camel, horse, and donkey. The *AMH* gene is positioned between *SF3A2* and *JSRP1* gene in all these mammals. The dN/dS ratio of *AMH* gene shows no positive selection pressure suggesting the similar and crucial physiological function of *AMH* gene in reproduction of these animals covering the family of Bovidae, Cetacea and Camelidae remain the same.

DATA AVAILABILITY STATEMENT

The datasets presented in this study can be found in online repositories. The names of the repository/repositories and accession number(s) can be found here: https://www.ncbi.nlm.nih.gov/, MH479929.2 and https://www.ncbi.nlm.nih.gov/, MH479928.2.

ETHICS STATEMENT

The animal study was reviewed and approved by the Institutional Animal Ethics Committee (IACE), ICAR-NDRI, Karnal Approval no: IAEC/41/14.

AUTHOR CONTRIBUTIONS

DG and AV collected the samples and performed the laboratory work and analyzed the data. SD designed and supervised the research work and drafted the manuscript. AH participated in planning the research program and edited the manuscript. All the authors evaluated the manuscript.

FUNDING

The authors gratefully acknowledged the Department of Biotechnology, Ministry of Science and Technology, Govt. of India, New Delhi, India for funding the project (Grant number: BT/179/NE/TBP/2011).

ACKNOWLEDGMENTS

We would like to express our gratitude to Prof. Dirk Werling for proofreading the manuscript and to the Director, ICAR-National Dairy Research Institute, Karnal - 132001, Haryana, India for the necessary support and assistance during the study.

REFERENCES

1. Josso N, Racine C, Di Clemente N, Rodolfo Rey, Xavier F. The role of anti-Mullerian hormone in gonadal development. *Mol Cell Endocrinol.* 5:3–7. doi: 10.1016/S0303-7207(98)00186-5
2. Munsterberg A, Lovell-Badge R. Expression of the mouse anti-Mullerian hormone gene suggests a role in both male and female sexual differentiation. *Development.* (1991) 113:613–24.
3. Zec I, Tislaric-Medenjak D, Bukovec Megla Z, Kucak I. Anti-Müllerian hormone: a unique biochemical marker of gonadal development and fertility in humans. *Biochem Medica.* (2011) 21:219–30. doi: 10.11613/bm.2011.031
4. Haldar A. Age-specific peripheral anti-müllerian hormone concentration in buffaloes. *J Anim Res.* (2020) 10:725–32. doi: 10.30954/2277-940x.05.2020.8
5. Haldar A, De S, Singh V, Datta M, Pal P, Prakash BS. Age-specific peripheral anti-müllerian hormone concentrations in goats (Capra hircus). *Indian J Anim Res.* (2019) 53:599–603. doi: 10.18805/ijar.B-3569
6. Haldar A, De S, Gautam D, Chakraborty D, Dey S, Pal P. Age-specific peripheral anti-mullerian hormone (AMH) concentration: a candidate endocrine marker for fertility assessment in cattle. *Int J Livest Res.* (2019) 1:1612. doi: 10.5455/ijlr.20190704071612
7. De Vet A, Laven JSE, De Jong FH, Themmen APN, Fauser BCJM. Antimüllerian hormone serum levels: a putative marker for ovarian aging. *Fertil Steril.* (2002) 77:357–62. doi: 10.1016/S0015-0282(01)02993-4
8. Visser JA, de Jong FH, Laven JSE, Themmen APN. Anti-Müllerian hormone: a new marker for ovarian function. *Reproduction.* (2006) 131:1–9. doi: 10.1530/rep.1.00529
9. Rico C, Médigue C, Fabre S, Jarrier P, Bontoux M, Clément F, et al. Regulation of anti-Müllerian hormone production in the cow: a multiscale study at endocrine, ovarian, follicular, and granulosa cell levels. *Biol Reprod.* (2011) 84:560–71. doi: 10.1095/biolreprod.110.088187
10. Mossa F, Jimenez-Krassel F, Scheetz D, Weber-Nielsen M, Evans ACO, Ireland JJ. Anti-Müllerian Hormone (AMH) and fertility management in agricultural species. *Reproduction.* (2017) 154:R1–R1. doi: 10.1530/REP-17-0104
11. Josso N, Di Clemente N. Transduction pathway of anti-Müllerian hormone, a sex-specific member of the TGF-β family. *Trends Endocrinol Metab.* (2003) 14:91–7. doi: 10.1016/S1043-2760(03)00005-5
12. Gao Q, Womack JE. A genetic map of bovine chromosome 7 with an interspecific hybrid backcross panel. *Mamm Genome.* (1997) 8:258–61. doi: 10.1007/s003359900405
13. Umer S, Zhao SJ, Sammad A, Sahlu BW, Yunwei P, Zhu H. AMH: could it be used as a biomarker for fertility and superovulation in domestic animals? *Genes (Basel).* (2019) 10:9. doi: 10.3390/genes10121009
14. Pierucci JC, Tonhati H, De Albuquerque LG, Cardoso DF, De Abreu Dos Santos DJ, Freitas AC, et al. Amh Polymorphisms and their association with traits indicative of sexual precocity in nelore heifers. *Semin Agrar.* (2019) 40:1489–99. doi: 10.5433/1679-0359.2019v40n4p1489
15. Van Rooij IAJ, Broekmans FJM, Scheffer GJ, Looman CWN, Habbema JDF, De Jong FH, et al. Serum antimüllerian hormone levels best reflect the reproductive decline with age in normal women with proven fertility: a longitudinal study. *Fertil Steril.* (2005) 83:979–87. doi: 10.1016/j.fertnstert.2004.11.029
16. Ueno S, Kuroda T, Maclaughlin DT, Ragin RC, Manganaro TF, Donahoe PK. Mullerian inhibiting substance in the adult rat ovary during various stages of the estrous cycle. *Endocrinology.* (1989) 125:1060–6. doi: 10.1210/endo-125-2-1060
17. Baarends WM, Uilenbroek JTJ, Kramer P, Hoogerbrugge JW, Van Leeuwen ECM, Themmen APN, et al. Anti-müllerian hormone and anti-müllerian hormone type ii receptor messenger ribonucleic acid expression in rat ovaries during postnatal development, the estrous cycle, and gonadotropin-induced follicle growth. *Endocrinology.* (1995) 136:4951–62. doi: 10.1210/endo.136.11.7588229
18. Weenen C, Laven JSE, von Bergh ARM, Cranfield M, Groome NP, Visser JA, et al. Anti-Müllerian hormone expression pattern in the human ovary: potential implications for initial and cyclic follicle recruitment. *Mol Hum Reprod.* (2004) 10:77–83. doi: 10.1093/molehr/gah015
19. Monniaux D, Di Clemente N, Touzé JL, Belville C, Rico C, Bontoux M, et al. Intrafollicular steroids and anti-Müllerian hormone during normal and cystic ovarian follicular development in the cow. *Biol Reprod.* (2008) 79:387–96. doi: 10.1095/biolreprod.107.065847
20. Johnson PA, Kent TR, Urick ME, Trevino LS, Giles JR. Expression of anti-Mullerian hormone in hens selected for different ovulation rates. *Reproduction.* (2009) 137:857–63. doi: 10.1530/REP-08-0406
21. Veiga-Lopez A, Ye W, Padmanabhan V. Developmental programming: prenatal testosterone excess disrupts anti-Müllerian hormone expression in preantral and antral follicles. *Fertil Steril.* (2012) 97:748–56. doi: 10.1016/j.fertnstert.2011.12.028
22. Claes A, Ball BA, Troedsson MHT, Curry TE, Squires EL, Scoggin KE. Molecular changes in the equine follicle in relation to variations in antral follicle count and anti-Müllerian hormone concentrations. *Equine Vet J.* (2016) 48:741–8. doi: 10.1111/evj.12514
23. Liang A, Salzano A, D'Esposito M, Comin A, Montillo M, Yang L, et al. Anti-Mullerian hormone (AMH) concentration in follicular fluid and mRNA expression of AMH receptor type II and LH receptor in granulosa cells as predictive markers of good buffalo (Bubalus bubalis) donors. *Theriogenology.* (2016) 86:963–70. doi: 10.1016/j.theriogenology.2016.03.020
24. Rocha RMP, Lima LF, Carvalho AA, Chaves RN, Bernuci MP, Rosa-e-Silva ACJS, et al. Immunolocalization of the Anti-Müllerian Hormone (AMH) in caprine follicles and the effects of amh on in vitro culture of caprine pre-antral follicles enclosed in ovarian tissue. *Reprod Domest Anim.* (2016) 51:212–9. doi: 10.1111/rda.12668
25. Almeida FRCL, Costermans NGJ, Soede NM, Bunschoten A, Keijer J, Kemp B, et al. Presence of anti-Müllerian hormone (AMH) during follicular development in the porcine ovary. *PLoS ONE.* (2018) 13:1–8. doi: 10.1371/journal.pone.0197894
26. Grigoletto L, Santana MHA, Bressan FF, Eler JP, Nogueira MFG, Kadarmideen HN, et al. Genetic parameters and genome-wide association studies for anti-müllerian hormone levels and antral follicle populations measured after estrus synchronization in nellore cattle. *Animals.* (2020) 10:1–15. doi: 10.3390/ani10071185
27. Bimboim HC, Doly J. A rapid alkaline extraction procedure for screening recombinant plasmid DNA. *Nucleic Acids Res.* (1979) 7:1513–23. doi: 10.1093/nar/7.6.1513
28. Katoh K, Rozewicki J, Yamada KD. MAFFT online service: multiple sequence alignment, interactive sequence choice and visualization. *Brief Bioinform.* (2018) 20:1160–6. doi: 10.1093/bib/bbx108
29. Kumar S, Stecher G, Li M, Knyaz C, Tamura K. MEGA X: molecular evolutionary genetics analysis across computing platforms. *Mol Biol Evol.* (2018) 35:1547–9. doi: 10.1093/molbev/msy096
30. Weaver S, Shank SD, Spielman SJ, Li M, Muse SV, Kosakovsky Pond SL. Datamonkey 2.0: a modern web application for characterizing selective and other evolutionary processes. *Mol Biol Evol.* (2018) 35:773–7. doi: 10.1093/molbev/msx335
31. Kryazhimskiy S, Plotkin JB. The population genetics of dN/dS. *PLoS Genet.* (2008) 4:e1000304 doi: 10.1371/journal.pgen.1000304
32. Imbeaud S, Carré-eusèbe D, Rey R, Belville C, Josso N, Picard JY. Molecular genetics of the persistent müllerian duct syndrome: a study of 19 families. *Hum Mol Genet.* (1994) 3:125–31. doi: 10.1093/hmg/3.1.125
33. McDowell DG, Burns NA, Parkes HC. Localised sequence regions possessing high melting temperatures prevent the amplification of a DNA mimic in competitive PCR. *Nucleic Acids Res.* (1998) 26:3340–7. doi: 10.1093/nar/26.14.3340
34. Cate RL, Mattaliano RJ, Hession C, Tizard R, Farber NM, Cheung A, et al. Isolation of the bovine and human genes for müllerian inhibiting substance and expression of the human gene in animal cells. *Cell.* (1986) 45:685–98. doi: 10.1016/0092-8674(86)90783-X
35. Gleicher N, Weghofer A, Oktay K, Barad D. Relevance of triple CGG repeats in the FMR1 gene to ovarian reserve. *Reprod Biomed Online.* (2009) 19:385–90. doi: 10.1016/s1472-6483(10)60173-3
36. Silva MSB, Giacobini P. New insights into anti-Müllerian hormone role in the hypothalamic–pituitary–gonadal axis and neuroendocrine development. *Cell Mol Life Sci.* (2020) 78:1–6. doi: 10.1007/s00018-020-03576-x
37. Xu J, Bishop C V, Lawson MS, Park BS, Xu F. Anti-Mü llerian hormone promotes pre-antral follicle growth, but inhibits antral follicle maturation and dominant follicle selection in primates. *Hum Reprod.* (2016) 31:1522–30. doi: 10.1093/humrep/dew100

38. Carnevale EM. The mare model for follicular maturation and reproductive aging in the woman. *Theriogenology*. (2008) 69:23–30. doi: 10.1016/j.theriogenology.2007.09.011
39. Ginther OJ. The mare: A 1000-pound guinea pig for study of the ovulatory follicular wave in women. *Theriogenology*. (2012) 77:818–28. doi: 10.1016/j.theriogenology.2011.09.025
40. Hansen KR, Hodnett GM, Knowlton N, Craig LB. Correlation of ovarian reserve tests with histologically determined primordial follicle number. *Fertil Steril*. (2011) 95:170–5. doi: 10.1016/j.fertnstert.2010.04.006
41. Ball BA, El-Sheikh Ali H, Scoggin KE, Riddle WT, Schnobrich M, Bradekamp E, et al. Relationship between anti-Müllerian hormone and fertility in the mare. *Theriogenology*. (2019) 125:335–41. doi: 10.1016/j.theriogenology.2018.11.005
42. Broekmans FJ, Soules MR, Fauser BC. Ovarian aging: mechanisms and clinical consequences. *Endocr Rev*. (2009) 30:465–93. doi: 10.1210/er.2009-0006
43. Baldrighi J, Sá Filho MF, Batista EOS, Lopes RNVR, Visintin JA, Baruselli PS, et al. Anti-Mullerian hormone concentration and antral ovarian follicle population in Murrah heifers compared to Holstein and Gyr kept under the same management. *Reprod Domest Anim*. (2014) 49:1015–20. doi: 10.1111/rda.12430
44. Durlinger ALL, Visser JA, Themmen APN. Regulation of ovarian function: the role of anti-Müllerian hormone. *Reproduction*. (2002) 124:601–9. doi: 10.1530/rep.0.1240601
45. Broer SL, Broekmans FJM, Laven JSE, Fauser BCJM. Anti-Müllerian hormone: ovarian reserve testing and its potential clinical implications. *Hum Reprod Update*. (2014) 20:688–701. doi: 10.1093/humupd/dmu020
46. Shi Y, Massagué J. Mechanisms of TGF-β signaling from cell membrane to the nucleus. *Cell*. (2003) 113:685–700. doi: 10.1016/S0092-8674(03)00432-X
47. Mishina Y, Rey R, Finegold MJ, Matzuk MM, Josso N, Cate RL, et al. Genetic analysis of the Mullerian-inhibiting substance signal transduction pathway in mammalian sexual differentiation. *Genes Dev*. (1996) 10:2577–87. doi: 10.1101/gad.10.20.2577
48. Di Clemente N, Jamin SP, Lugovskoy A, Carmillo P, Ehrenfels C, Picard JY, et al. Processing of anti-müllerian hormone regulates receptor activation by a mechanism distinct from TGF-β. *Mol Endocrinol*. (2010) 24:2193–206. doi: 10.1210/me.2010-0273
49. Hart KN, Pépin D, Czepnik M, Donahoe PK, Thompson TB. Mutational analysis of the putative Anti-Müllerian hormone (AMH) binding interface on its type II receptor, AMHR2. *Endocrinol (United States)*. (2020) 161:66. doi: 10.1210/endocr/bqaa066
50. Méduri G, Massin N, Guibourdenche J, Bachelot A, Fiori O, Kuttenn F, et al. Serum anti-Müllerian hormone expression in women with premature ovarian failure. *Hum Reprod*. (2007) 22:117–23. doi: 10.1093/humrep/del346
51. Wachs DS, Coffler MS, Malcom PJ, Chang RJ. Serum anti-Mullerian hormone concentrations are not altered by acute administration of follicle stimulating hormone in polycystic ovary syndrome and normal women. *J Clin Endocrinol Metab*. (2007) 92:1871–4. doi: 10.1210/jc.2006-2425
52. Maciel GAR, Baracat EC, Benda JA, Markham SM, Hensinger K, Chang RJ, et al. Stockpiling of transitional and classic primary follicles in ovaries of women with polycystic ovary syndrome. *J Clin Endocrinol Metab*. (2004) 89:5321–7. doi: 10.1210/jc.2004-0643

Conflict of Interest: The authors declare that the research was conducted in the absence of any commercial or financial relationships that could be construed as a potential conflict of interest.

frontiers in Veterinary Science

ORIGINAL RESEARCH
published: 08 April 2021
doi: 10.3389/fvets.2021.658968

Does miRNA Expression in the Spent Media Change During Early Embryo Development?

*Paul Del Rio and Pavneesh Madan**

Biomedical Sciences, Ontario Veterinary College, University of Guelph, Guelph, ON, Canada

Distinct miRNA populations have been detected in the spent media of *in-vitro* culture systems. However, profiling has been limited to media conditioned with blastocyst-stage embryos. Therefore, the aim of the study was to profile extracellular miRNAs throughout the pre-implantation period in bovine embryos. To achieve this, cumulus oocyte complexes were aspirated from ovaries, *in-vitro* matured, fertilized, and cultured under standard laboratory procedures to the 2-cell, 8-cell, or blastocyst stage of development. At each developmental stage, 25 μl of spent *in-vitro* culture media was collected, pooled to 300 μl, and processed for total RNA extraction. *In-vitro* culture media, which never came in contact with any embryos, were additionally processed for total RNA extraction to serve as a negative control. Following hybridization on a GeneChip miRNA 4.0 array, comparative analysis was conducted between spent media and control samples. In total, 111 miRNAs were detected in the spent media samples, with 56 miRNAs identified in blastocyst spent media, 14 miRNAs shared between 8-cell and blastocyst spent media, 7 miRNAs shared between all 3 conditions, and 6 miRNAs exclusive to 2-cell spent media. miRNA-mRNA target prediction analysis revealed that the majority of genes predicted to be regulated by the miRNAs identified in the study have roles in cellular process, metabolic process, and biological regulation. Overall, the study suggest that miRNAs can be detected in the spent media of *in-vitro* culture system throughout the pre-implantation period and the detected miRNAs may influence genes impacting early embryo development.

Keywords: miRNA, culture media, IVF, early embryo health, bovine

OPEN ACCESS

Edited by:
Cristina Alicia Martinez, Linköping University, Sweden

Reviewed by:
Deqiang Miao, Washington State University, United States
Luiz S. A. Camargo, Brazilian Agricultural Research Corporation (EMBRAPA), Brazil

***Correspondence:**
Pavneesh Madan
pmadan@uoguelph.ca

Specialty section:
This article was submitted to Animal Reproduction Theriogenology, a section of the journal Frontiers in Veterinary Science

Received: *26 January 2021*
Accepted: *11 March 2021*
Published: *08 April 2021*

Citation:
Rio PD and Madan P (2021) Does miRNA Expression in the Spent Media Change During Early Embryo Development? Front. Vet. Sci. 8:658968. doi: 10.3389/fvets.2021.658968

INTRODUCTION

Declining cattle fertility is a widely recognized problem resulting in economic losses and culling of cattle (1). Although a multitude of factors contribute to declines in reproductive fitness, early embryonic mortality remains a major cause of infertility (2). It is estimated that 75–80% of fetal losses following successful AI occurs within this period and is more frequently observed in repeat service cattle (3). With declining successes with traditional AI, the industry has looked toward the use of IVF systems, as an alternative means of attaining embryos for transfer. According to the International Embryo Transfer Society (IETS), the period of 2013–2017 has seen consistent increases in embryos being produced, with 2017 seeing almost one million embryos produced *in-vitro* (4–8). Although IVF systems allow for the selection of potentially genetically superior gametes and embryos, its uses within the industry have been limited. With pregnancy and calving rates remaining similar to natural breeding or AI, combined with costly materials and skilled labor

requirements, the mainstream use of IVF systems in the industry is yet to be seen (9). A limitation in the IVF system that needs to be addressed for its mainstream application in the industry is the methodologies used for assessing embryo viability. Currently, the industry standard is morphological assessment, which involves the embryologist to score embryos on parameters based on appearance such as cleavage rate, blastomere size, blastomere symmetry, number of blastomeres, homology of cytoplasm, and zona pellucida thickness, as outlined by the IETS (10). Although studies have shown that morphological assessment do correlate with better implantation and calving rates, the subjective nature of scoring by the embryologist makes the process inconsistent (11). Studies have shown that morphologically high-quality embryos may possess aneuploidies that can alter an embryo's overall developmental potential (1). Efforts have been made toward developing other non-invasive forms of assessment such as the characterization of miRNAs in spent media (SM) conditioned with embryos. miRNAs are small non-coding RNAs (18–22 nt) involved in post-transcriptional regulation of gene expression causing either the translational repression or controlled degradation of the mRNA (12). Binding in the 3′untranslated region is not completely complementary, therefore allowing miRNAs to have multiple gene targets across an organism (12). These gene targets have been associated to have influences in all biological systems, such as apoptosis, growth, proliferation, reproduction, and development, with expression occurring in a spatially and temporally specific manner (13).

In embryos, multiple studies have been conducted showing that miRNAs play a significant role in coordinating gene expression throughout this crucial developmental period. It has been determined that certain miRNAs are required at key stages of the pre-implantation developmental period, defined as from day 0 to day 8, with miR-25 and miR-181 being identified as being expressed in the early and late stages, respectively (14). It is also noted that a host of miRNAs may play a role in regulating genes that facilitate the processes involved in maternal to embryonic transition, often seen as one of the greatest developmental milestone in early embryonic development (14).

In light of new research, it has also been implicated that these temporal changes in miRNA expression may also be reflected in the SM. Multiple studies have shown that miRNAs can be released into the extracellular environment via containment in exosomes, apoptotic bodies, or bound to proteins. In embryos, studies conducted by Kropp et al. (15), Rosenbluth et al. (16), and Kropp et al. (17), showed that miRNAs can be detected in the SM of bovine and human IVF systems (15–17). These studies showed that there are significant differences in the miRNAs detected in the SM of degenerate embryos and embryos that successfully formed into blastocyst. This suggest that miRNAs in the SM may be used as biomarkers of early embryonic health as changes in intra-cellular miRNA expression may be reflected in the extra-cellular milieu, and that these changes may reflect the overall health or quality of the embryo.

To the best of our knowledge, profiling of miRNAs in the SM have been limited to either a few candidate miRNAs, or only examined the blastocyst stage of development. Preliminary studies conducted in our lab using previously cited candidate miRNAs suggest that miRNAs can be detected in the SM of cleavage-staged embryos. Therefore, the objective of this study is to globally profile the miRNAs present in the SM throughout the pre-implantation developmental period using a microarray approach. This method will allow for the discovery of miRNAs detected at earlier stages of embryo development, as well as discovery of miRNAs that are shared between or throughout the pre-implantation developmental period.

MATERIALS AND METHODS

Chemicals

All chemicals were attained from Sigma-Aldrich, Oakville, ON, Canada, unless stated otherwise.

Oocyte Collection and *in-vitro* Production of Bovine Embryos

Bovine ovaries were collected from a local abattoir (Cargill Canada, Guelph, Ontario) and transported to the laboratory in a thermo flask under phosphate buffered saline (NaCl, 136.9 mM; Na2HPO4, 8.1 mM; KCL, 1.47 mM; KH2PO4, 1.19 mM; MgCl2.6H2O, 0.49 mM) at a temperature of 35–36°C. Follicles ranging from 4 to 8 mm were aspirated using an 18G vacutainer needle and was suspended in HEPES-buffered Hams F-10 supplemented with 2% donor calf serum (PAA Laboratories Inc., ON, Canada). Cumulus oocytes complexes (COCs) were washed twice with 3 mL synthetic *in-vitro* maturation (S-IVM) media (TCM-199 plus 2% donor calf serum, Sigma-Aldrich) and washed once with 3 mL S-IVM supplemented with 0.5 g/ml of follicle stimulating hormone, 1 g/ml of luteinizing hormone and 1 g/ml of estradiol. Approximately, groups of 15–20 COCs with homogenous cytoplasm and 4–5 layers of granulosa cells were matured in 80 μl drops of S-IVM under a layer of silicone oil for 22–24 h at 38.5°C in an atmosphere of 5% CO_2 with 100% humidity. After maturation, the COCs were washed twice with 3 ml HEPES buffered Tyrode's albumin-lactate-pyruvate medium (HEPES/Sperm TALP) supplemented with 15% BSA (0.0084 mg/ml final; fatty acid free) and washed twice with 3 mL IVF-TALP (IVF-TALP consisting of Tyrode's solution, supplemented with 15% BSA and 2 mg/ml heparin). Approximately 20 COCs were placed in 80 μl drops of IVF-TALP under a layer of silicone oil. Frozen thawed bovine sperm was prepared using swim-up technique. Thawed sperm was placed in HEPES/Sperm TALP and incubated for 45 min at 38.5°C in an atmosphere of 5% CO_2 with 100% humidity prior to centrifugation at 200 g for 7 min. The COCs and sperm were co-incubated at a final concentration of 1.0×10^6 at 38.5°C in 5% CO_2 with maximum humidity. At 18 h post fertilization (hpf), the presumptive zygotes were denuded by gentle vortexing for 90 s, followed by washing twice with 3 ml HEPES/Sperm TALP, and once with *in-vitro* culture (IVC) media [$CaCl_2 \cdot 2H_2O$, 1.17 mM; KCL, 7.16 mM; KH_2PO_4, 1.19 mM; $MgCl_2 \cdot 6H_2O$, 0.49 mM; NaCl, 107.7 mM; $NaHCO_3$, 25.07 mM, Na lactate (60% syrup), 3.3 mM; ChemiconMillipore, Billerica, MA, USA] supplemented with 50 μL of 100× non-essential amino acids (glycine, L-alanine, L-asparagine, L-aspartic acid, L-glutamic acid, L-proline, L-serine; all 0.2 mM final), 100 μL

TABLE 1 | Spent media collection schedule at various stages [adapted from Van Soom et al. (Van 18), Perkel and Madan (18)].

Cell stage	Hour-Post fertilization (HPF)
2-cell	18–30
8-cell	60–80
Blastocyst	168–192

50x essential amino acids (L-arginine hydrochloride, 0.6 mM final; L-cysteine, 0.1 mM final; L-histidine hydrochlorideH_2O, 0.2 mM final; L-isoleucine, 0.4 mM final; L-leucine, 0.4 mM final; L-lysine hydrochloride, 0.4 mM final; L-methionine, 0.1 mM final; L-phenylalanine, 0.2 mM final; L-threonine, 0.4 mM final; L-tyrosine, 0.2 mM final; L-tryptophan, 0.05 mM final; L-valine, 0.4 mM final), 25 μL of sodium pyruvate (0.00886 mg/ml final), 2.5 μL of gentamicin (25 mg/ml final; all from Invitrogen, Burlington, ON, Canada), and 280 μl of 15% bovine serum albumin (0.0084 mg/ml final). Approximately 30 presumptive zygotes (PZ) with homogenous cytoplasm were cultured in 30 μl of IVC media under silicone oil at 38.5°C in an atmosphere of 5% CO_2, 5% O_2, 90% N_2 and cohorts of embryos were cultured to the 2-cell, 8-cell, and/or blastocyst stage of development and SM was collected at specific HPF after each desired time stage was reached (**Table 1**).

Collection of Spent *in-vitro* Culture Media

Prior to collection of SM at each developmental stage, developmental rates for 2-cell, 8-cell, and blastocyst formation was recorded to ensure that culture conditions were representative of average IVP production rates as reported by Van Soom et al. (19). Following this, the embryos were removed from the IVC drops, washed 5 times in PBS, and flash frozen in liquid nitrogen and stored at −80°C for future downstream gene analysis. Approximately 25 μL of SM was collected from each drop, and samples were pooled together in 1.5 mL Eppendorf tubes for each of the developmental stage analyzed. The pooled samples were flash frozen in liquid nitrogen and stored at −80°C until RNA processing. In total, 3,000 μL, 3,300 μL, and 1,250 μL of SM was collected from 2-cell, 8-cell, and blastocyst staged embryos, respectively. In addition, 1,050 μL of unconditioned media, which did not contact any embryos, was collected to serve as a negative control.

miRNA Extraction

miRNA extraction was isolated from SM and plain media using a RNeasy mini kit (Qiagen, Hilden, Germany), as downstream array analysis required total RNA sample input. Briefly, 350 μL of SM and plain media was aliquoted to a 2.5 mL Eppendorf tube and equal volumes of QIAzol lysis reagent was added, vortexed for 20 s, and placed on the benchtop at room temperature for 10 min. This was followed by the addition of 350 μL of chloroform and incubated for 2 min at room temperature, prior to centrifugation at 12 g (15,000 RPM) at 4°C for 15 min. After, the supernatant was placed into the RNeasy min elute spin column for total RNA separation. Once all the supernatant was processed, washing steps using buffer RWT, buffer RPE, and 80% ethanol, was performed as per manufacturer protocol. The RNA was eluted using 30 μL of RNAse-free water and immediately stored in −80°C prior to microarray analysis. In total, 3 biological replicates of pooled SM from each timed stage of development and plain media was processed and prepared for microarray analysis.

miRNA Microarray Hybridization

Microarray processing was all conducted by our colleagues at Genome Quebec (McGill University, Montreal, Quebec). Briefly, microarray profiling was conducted using the Affymetrix GeneChip miRNA 4.0 array (Affymetrix, Santa Clara, CA, USA), according to manufacturer's instructions and as described previously by Reza et al. (20). Briefly, each sample of RNA was labeled using the FlashTag Biotin RNA Labeling Kit (Genisphere, Hatfield, PA, USA), quantified, fractionated, and hybridized to the miRNA microarray. The protocol is as follows: labeled RNA is heated to 99°C for 5 min, then heated at 45°C for 5 min, prior to hybridization via constant agitation at 60 rpm for 16 h at 48°C on an Affymetrix 450 Fluidics Station. The microarray chip is washed and stained with Genechip Fluidics Station 450, prior to being scanned with the use of an Affymetrix GCS 3,000 scanner and computed using the Affymetrix Genechip command console software.

Statistical Analysis

For Genechip microarray analysis, CEL files were imported in the Affymetrix Transcriptome Analysis Console® 4.0.2.15 (TAC) software in RMA+DMG (all organisms) mode. Comparative analysis was carried out between SM samples (2-cell, 8-cell, and blastocyst) and control (plain media) using fold-change and independent *T*-test, in which the null hypothesis was that no difference exist between the 2 groups. Probes were differentially expressed at a fold-change of ≤ -2 or ≥ 2 ($p < 0.05$), where probe-sets were considered expressed if ≥50% of samples have a detectable above background (DABG) values below DABG threshold of <0.05 and a false discovery rate (FDR) of <0.05. All statistical test and visualization of differentially expressed genes were done using TAC software (https://www.thermofisher.com/ca/en/home/global/forms/life-science/download-tac-software.html).

Target Pathway Prediction of Differentially Expressed miRNAs

Functional analysis of differentially expressed miRNAs (DEM) detected at 3 SM conditions was performed using TargetScan Human 7.2 (http://www.targetscan.org/vert_71/) under Cow annotation, to construct a gene-list from the DEM. Genes with a cumulative context score of <-0.75 was included in the list. From the gene-list, gene-set enrichment analysis (GSEA) was conducted using PANTHER (http://pantherdb.org/) with Bos Taurus selected for the organism option and functional classification, under gene-ontology: Biological Processes,

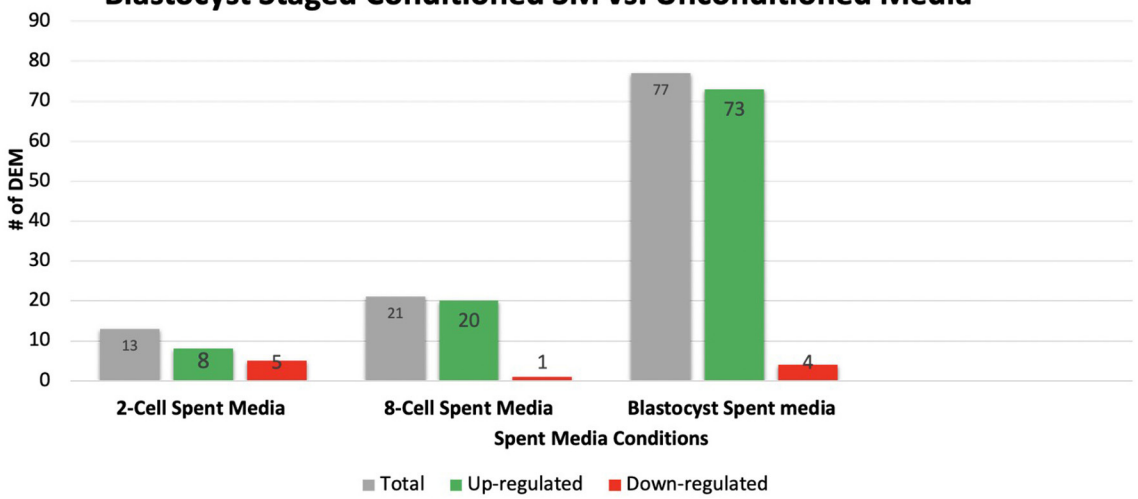

FIGURE 1 | A total of 111 miRNAs were differentially expressed in 2-cell, 8-cell, and blastocyst spent media. Expression of miRNAs in spent media increased throughout the 3 conditions examined, with 13, 21, and 77 miRNAs being detected in 2-cell, 8-cell, and blastocyst spent media, respectively. The majority of miRNAs detected in spent media were blastocyst derived.

was conducted. Pathways with a $p < 0.05$ was considered significantly enriched.

RESULTS

Differentially Expressed miRNAs in 2-Cell, 8-Cell, and Blastocyst SM

Overall, a total of 111 miRNAs were differentially expressed in the SM conditioned with 2-cell, 8-cell, and/or blastocyst embryos, when compared to plain media. Thirteen miRNAs were detected in the 2-cell SM, 21 miRNAs were detected in 8-cell SM, and 77 miRNAs were detected in blastocyst SM (**Figure 1**). Overlapping the miRNA list from each SM condition allowed for the identification of condition-specific miRNAs and miRNAs shared between 2 or more conditions (**Figure 2**). Six miRNAs were solely detected in 2-cell SM, in which 2 were upregulated (bta-miR-2421 and bta-miR-2297) and 4 were downregulated in the SM (bta-miR-296-5p, bta-miR-106b, bta-miR-122, and bta-miR-760-5p) (**Figure 3**). All the miRNAs detected in the 8-cell SM were shared between one or more SM conditions and no miRNAs were unique to 8-cell SM. Of the 77 miRNAs identified in blastocyst SM, 56 miRNAs were exclusive to the SM condition. Fifty-three miRNAs were upregulated (**Supplementary Table 1**) and 3 miRNAs were downregulated in the media (**Figure 4**). The remaining detected miRNAs were shared between 2 or more SM conditions.

Differentially Expressed miRNAs Shared Between 2 or More SM Conditions

Overlapping of the gene-list identified miRNAs that were co-detected in 8-cell and blastocyst SM and all 3 SM conditions.

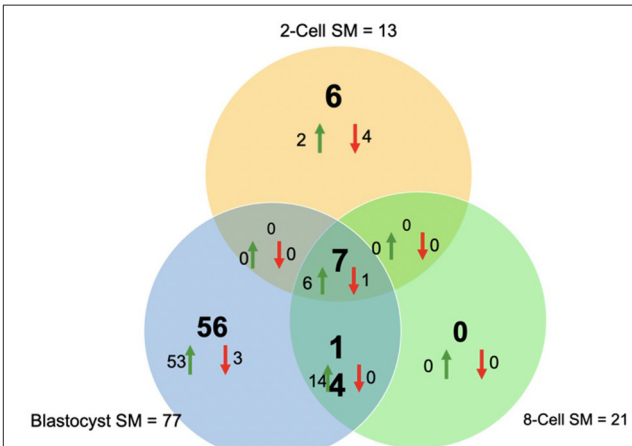

FIGURE 2 | Venn diagram of differentially expressed miRNAs from 2-cell (yellow), 8-cell (green), and blastocyst SM (blue). Overlapping results showed differentially expressed miRNAs shared between 2 or more groups (14 miRNAs between 8-cell and blastocyst spent media; 7 miRNAs between all 3 spent media conditions).

Fourteen miRNAs (bta-miR-296-3p, bta-miR-3141, bta-miR-1584-5p, bta-miR-2888, bta-miR-2374, bta-miR-2893, bta-miR-2899, bta-miR-1343-5p, bta-miR-2328-3p, bta-miR-2887, bta-miR-2487, bta-miR-92a, bta-miR-149-3p, and bta-miR-1246) were co-detected in 8-cell and blastocyst SM (**Figure 5**). All 14 miRNAs were upregulated in comparison to 2 cell SM and unconditioned media. Interestingly, the degree of upregulation increased between 8-cell and blastocyst SM. Seven miRNAs were co-detected in all 3 SM conditions.

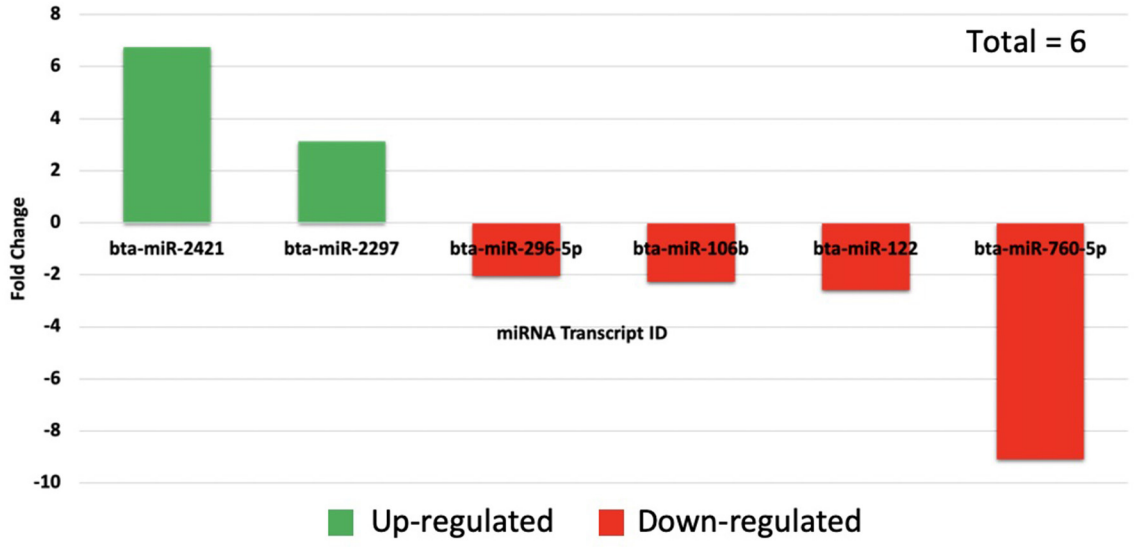

FIGURE 3 | A total of 6 miRNAs were significantly expressed in 2-cell spent media. Two miRNAs were up-regulated, while 4 miRNAs were down-regulated in 2-cell spent media.

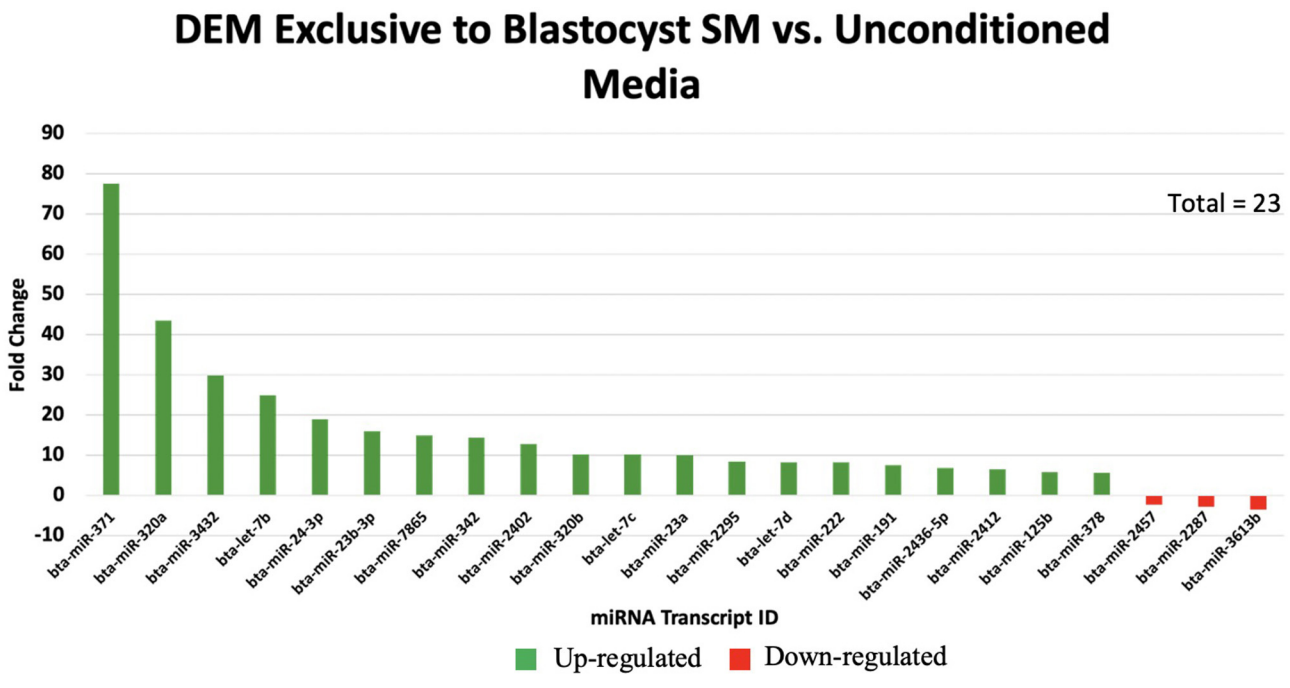

FIGURE 4 | The top 20 of 53 significantly up-regulated miRNAs are graphed with the 3 significantly down-regulated miRNAs exclusive to blastocyst spent media.

Six miRNAs were upregulated (bta-miR-2281, bta-miR-2900, bta-miR-2885, bta-miR-1777a, bta-miR-2305, and bta-miR-1777b) (**Figure 6**) in comparison to unconditioned media and the degree of upregulation increased from one condition to another. One miRNA was consistently downregulated (bta-miR-450b) in comparison to unconditioned media and the degree of downregulation was consistent across all 3 conditions.

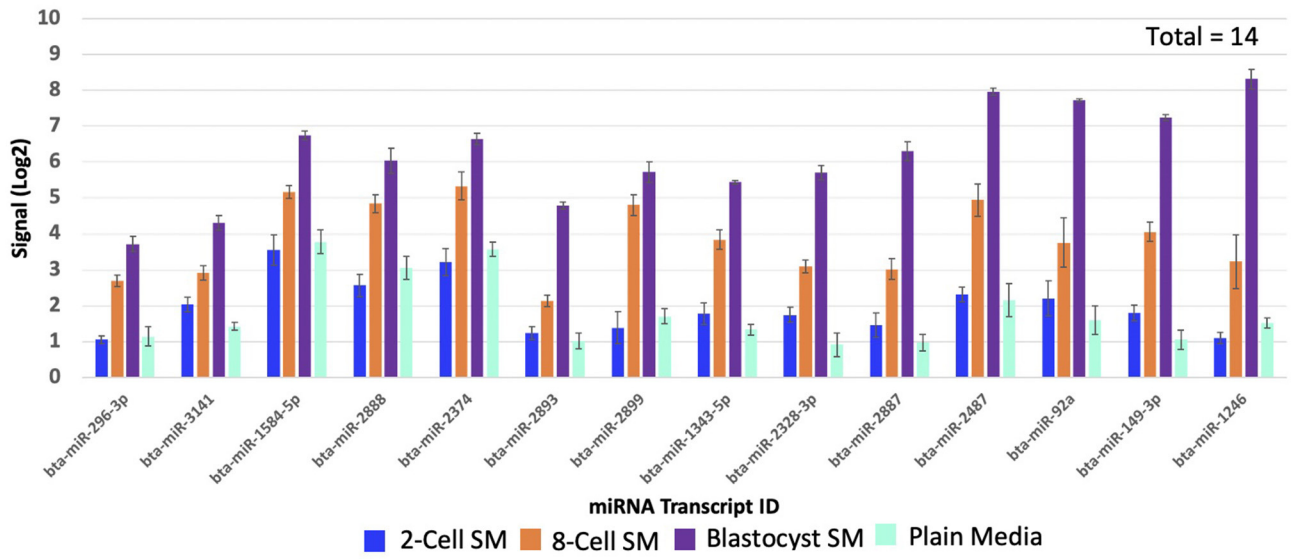

FIGURE 5 | Fourteen miRNAs were significantly shared between 8-cell and blastocyst spent media. All miRNAs increased in levels of up-regulation from the 8-cell to the blastocyst spent media.

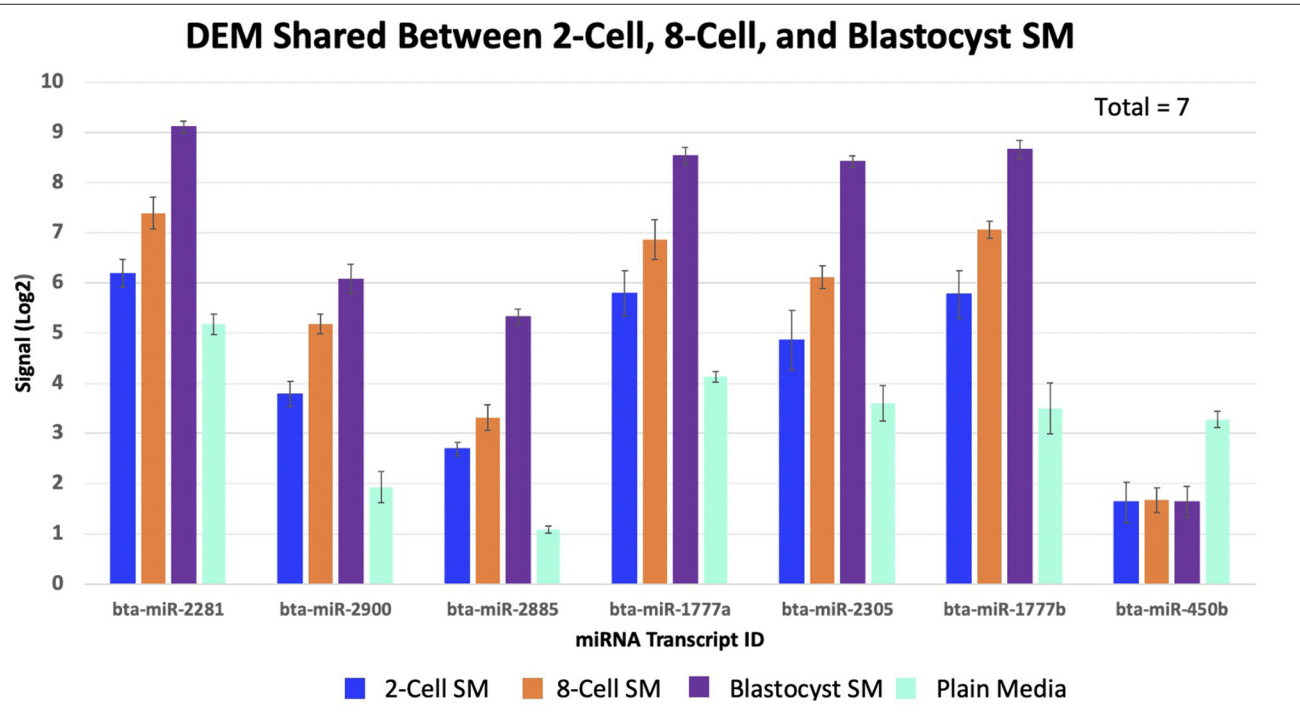

FIGURE 6 | Seven miRNAs were significantly shared between all three spent media conditions. 6 miRNAs increased in levels of up-regulation, while 1 miRNA remained consistently down-regulated (bta-miR-450b).

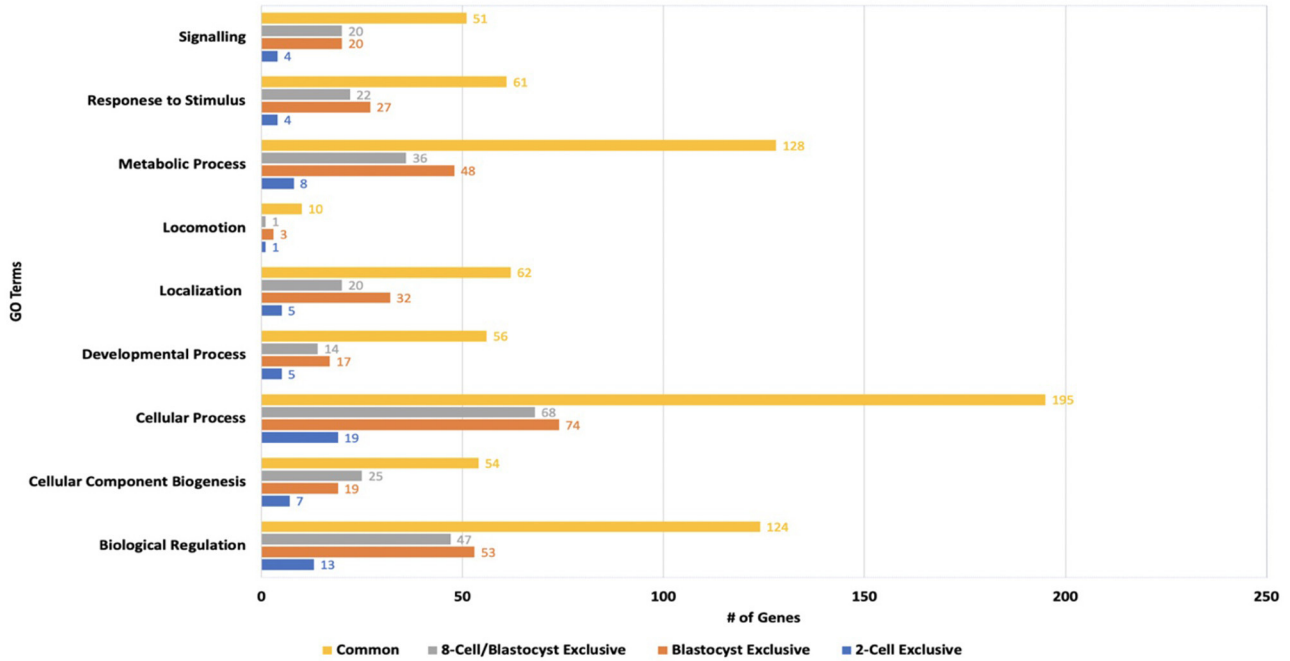

FIGURE 7 | Results of gene-set enrichment analysis of mRNA targets predicted for differentially expressed miRNAs in 2-cell spent media, blastocyst spent media, shared in 8-cell and blastocyst spent media, and common to all 3 spent media conditions. The majority of predicted genes clustered under biological processes involved in cellular process, biological regulation, and metabolic process.

Predictions of miRNA-mRNA Targets for Stage-Specific and Shared Differentially Expressed miRNAs

2-Cell SM

miRNA-mRNA target prediction identified 44 mRNAs as potential targets for the 6 miRNAs identified exclusively to 2-cell SM (**Supplementary Table 2**). When inputted into PANTHER, 42 genes were associated with the 44 predicted mRNAs, with the majority of genes clustering under cellular process (GO:0009987), biological regulation (GO:0065007), and metabolic process (GO:0008152) (**Figure 7**). The highly enriched genes were predicted targets of bta-miR-2421 (**Table 2**).

Blastocyst SM

Due to the high numbers of miRNAs detected in blastocyst SM, only the top 20 upregulated and 3 downregulated miRNAs were considered for miRNA-mRNA target prediction. Of the top 20 upregulated miRNAs, 5 miRNAs (bta-miR-320a, bta-miR-3432, bta-let-7c, bta-miR-191, and bta-miR-378) were excluded from analysis due to predicted genes not meeting the cumulative context score of <-0.75 cutoff or not being found on the TargetScan database. From the remaining 18 miRNAs, a total of 218 mRNAs were identified as possible targets for blastocyst-specific miRNAs (**Supplementary Table 3**). When inputted into PANTHER, 186 genes were associated with the 218 predicted mRNAs, with the majority of genes clustering under cellular process (GO:0009987), biological regulation (GO:0065007), and metabolic process (GO:0008152) (**Figure 7**). The highly enriched genes were predicted targets of bta-miR-7865, bta-miR-2295, and bta-miR-3613b (**Table 2**).

8-Cell and Blastocyst Shared miRNAs

Bta-miR-296-3p and bta-miR-2487 did not meet the cutoff criteria and was not found in the TargetScan database, respectively, thus was excluded from the analysis. Of the remaining 12 miRNAs, a total of 194 mRNAs were identified as potential targets (**Supplementary Table 4**). When inputted into PANTHER, 168 genes were associated with the 194 predicted mRNAs, with the majority of genes clustering under cellular process (GO:0009987), biological regulation (GO:0065007), and metabolic process (GO:0008152) (**Figure 7**) The highly enriched genes were predicted targets of bta-miR-1343-5p and bta-miR-2899 (**Table 2**).

miRNAs Common to 2-Cell, 8-Cell, and Blastocyst SM

Bta-miR-2881 was not found in the database, thus was excluded from the overall analysis. Of the remaining 6 miRNAs co-detected in all 3 SM condition, a total of 527 miRNAs were identified as potential targets (**Supplementary Table 5**). When inputted into PANTHER, 445 genes were associated with the 527 predicted mRNAs, with the majority of genes clustering under cellular process (GO:0009987), biological regulation

TABLE 2 | miRNA-mRNA targets predicted to have roles in the top 3 biological pathways represented in gene-set enrichment analysis.

Highly represented miRNAs		Genes represented in cellular process, biological regulation, and metabolic process
2-Cell spent media	bta-miR-2421	TCF4, POU6F2, RUNX1T1, TNRC6C, ONECUT2, TNRC6B, THRB
Blastocyst spent media	bta-miR-7865	MZB1, FOSB, LAMTOR1, WDTC1, THRA
	bta-miR-2295	MAPK8IP2, H1FX, SCRT1, MTA3, EOMES
	bta-miR-3613b	SIK2, USP42, CDK12, GLE1, IKZF4
Shared in 8-cell and blastocyst spent media	bta-miR-1343-5p	TFCP2L1, KCTD17, SIX5, PRX, SERPINE3
	bta-miR-2899	DLX1, MTA1, TBC1D14, HEYL, HCFC1
Common to 2-cell, 8-cell, and blastocyst spent media	bta-miR-2305	PLA2G2F, SMARCC2, SPRY4, CX3CL1, TEAD2, LMX1B, RUNX3, ERF, TBX6, ELK1, SOX15, SPRED2, DAGLA, HNF4A, COMMD7, ZFHX2, RNF144A, KMT2B, MAPK12, FEV, TIMP2, IKZF4, CSDC2, DERL3, CIC, RNPS1, SAMD4B
	bta-miR-2900	FOXJ2, DDA1, PTK2B, HOXA3, CNOT3, MAPK1, SRRM4, NRBP1, PPARD, TRAF3, NODAL, PRKCG, PIAS4, TCF7L2
	bta-miR-1777a	MSI1, CACNG7, TBX5, BRSK1, CRTC1, ZC3H4, TBX10, IGF1R, LEMD2, CTIF, HIF3A, DUSP16, SOX12

(GO:0065007), and metabolic process (GO:0008152) (**Figure 7**). The highly enriched genes were predicted targets of bta-miR-2305, bta-miR-2900, and bta-miR-1777a (**Table 2**).

Overall, GSEA analysis revealed that the majority of the miRNAs detected in the 4 conditions (2-cell SM, 8-cell SM, 8-cell/blastocyst SM, and common in all 3 SM) had predicted mRNA targets involved in cellular process, biological regulation, and metabolic process. For 2-cell SM, bta-miR-2421 and bta-miR-760-5p mRNA targets were over-represented after enrichment. In blastocyst SM, bta-miR-7865, bta-miR-2295, and bta-miR-3613b mRNA targets were highlighted most during GSEA analysis. For miRNA shared between two or more SM conditions, bta-miR-1343-5p, bta-miR-2899, bta-miR-2888, bta-miR-2305, bta-miR-2900, and bta-miR-1777a mRNA targets were highly represented in the 3 biological processes highlighted in PANTHER.

Annotated Roles of Differentially Expressed miRNAs in Literature

From the 111 miRNAs identified across 3 SM conditions, 32 miRNAs have been previously annotated in literature. 18 miRNAs have been identified in embryo related studies, 14 miRNAs in cancer-related studies, and 5 miRNAs in both embryo and cancer related studies. miRNAs (**Table 3**). It is important to note that all previously annotated miRNAs were exclusively detected in blastocyst SM.

TABLE 3 | List of miRNAs detected in all 3 spent media conditions previously annotated in literature.

Study-Type		miRNA
Embryo-Related	Spent media profiling	miR-24-3p, miR-191, miR-2887
	Role in implantation	miR-320a*, let-7b, miR-23b-3p*, miR-23a, miR-3141, miR-92a*, miR-1246
	Role in differentiation	miR-371, miR-296-5p/3p*, miR-106b*, miR-125b
	Found in germ cells	miR-3432, miR-2487, miR-2885, miR-1777b
Cancer-Related	Onco-genic	miR-106b*, miR-760-5p, miR-371, let-7d, miR-222, miR-378, miR-1343-5p, miR-92a*
	Tumor-suppressive	miR-296-5p/3p*, miR-320a*, miR-320b, miR-23b-3p*, miR-342, let-7c, let-7d, miR-191, miR-149-3p, miR-1246, miR-450b

*The majority (18 miRNAs) have been profiled in embryo-based studies, while 14 miRNAs were explored in cancer-related studies. 5 miRNAs were cited in both embryo and cancer related studies. *Found in both embryo and cancer relate studies.*

DISCUSSION

To the best of our knowledge, this study was the first to characterize miRNAs in the SM throughout the pre-implantation period. We were able to identify miRNAs in the SM at early, mid, and late stages of development. The most diverse expression of miRNAs was detected in blastocyst SM. This finding is consistent with the works of other researchers (15–17, 21) and is largely attributable to the genetic, molecular, and cellular changes occurring during this stage of embryo development. An embryo during this stage rapidly proliferates and differentiates to form the ICM and trophectoderm. Differentiation is a highly choreograph events that requires strict modulation of gene expression. Potentially, miRNAs play a role in synchronizing the events necessary for normal blastocyst development. Therefore, miRNA expression may increase during this stage of development, which is reflected in the SM.

Another explanation to the high numbers of miRNAs detected in blastocyst SM is due to the high cell numbers present at this stage of development. Prior to compaction and blastocyst formation, a growing embryo is made up of relatively few cells, enough to be distinguishable under stereomicroscope. With such few cells prior to compaction, it is believed that miRNA concentrations are far too low to be detected with current assays. In a recent study, it was determined that the majority of miRNAs detected in blastocyst SM was trophectoderm derived (22). Thus, this may contribute to the low numbers of miRNAs

detected in earlier stages as the trophectoderm only forms at later stages of embryo development. Interestingly, the authors also postulated that the blastocyst secretes miRNAs as a method of paracrine communication with the endometrium (22). The diverse population of miRNAs secreted by trophectoderm cells may be up taken by endometrial cells. Once inside, the miRNAs may modulate gene expression to either favor or prevent the implantation of a blastocyst. Therefore, the diverse expression of miRNAs in blastocyst SM may serve a functional role in implantation and/or be a direct by-product of the high cell numbers present at this stage of development.

One finding that was unique in this study was the detection of miRNAs in cleavage stage embryos. Specifically, we were able to detect 6 miRNAs exclusive to 2-cell SM. Moreover, 2-cell SM was the only condition examined that had more miRNAs down-regulated (4 miRNAs) than up-regulated (2 miRNAs). These findings are interesting because this is the first report of miRNAs being detected in 2-cell SM. The wide coverage of miRNAs available on the microarray may have allowed for the detection of miRNAs. The genechip miRNA 4.0 array used for this study had over 46,228 probes comprising of 7,815 probe sets from 71 different species. Since the majority of the miRNAs identified in 2-cell SM and 8-cell SM are ones not previously annotated in embryo-related work, it is possible that the assays previous researchers used did not contain the probes present in our study. Most studies either examined a select few candidate miRNAs using qPCR or a wider population with qPCR array. Although both methods allow for higher sensitivity, lower sample input, and lower false detection rates, both approaches have fewer probe sets than the ones used in this study.

In addition to having more probe-sets, group culturing of embryo may have impacted miRNA detection. Prior studies examining miRNAs throughout the pre-implantation period performed either single-embryo culture or had a lower ratio of embryos to culture media volume. These culturing conditions allowed researchers to discern the miRNAs in the SM to specific embryos. However, as mentioned before, low cell numbers contribute to the lack of miRNAs detected in media. Therefore, previous researcher was only able to detect miRNAs from blastocyst conditioned media, whereby cell numbers are higher. In this study, embryos were cultured in groups of 30 in 30 μl of IVC media. The higher concentration of embryos in the media may have compensated for the few cells available to secrete and/or uptake miRNAs in the media. Therefore, the diversity in the probe-sets present in the array used, in conjunction with higher embryos concentrations may have allowed for the detection of miRNAs in SM cultured with cleavage staged embryos. To this regard, collecting SM from group cultured embryos does not allow for the detection of embryo-specific miRNAs. Therefore, assays such as digital drop PCR, may be used in future SM profiling experiments as its low sample input volume and high sensitivity may suffice in detecting miRNAs in single embryo culture (23).

Another interesting result from the miRNAs detected in 2-cell SM is that it is the only condition where more down-regulated miRNAs were detected in comparison to upregulated miRNAs. This indicates that the 2-cell embryo may be capable of up-taking miRNAs from the extracellular environment. Although undocumented in cleavage stage embryos, previous research has demonstrated that morula-stage embryos are capable of up-taking miRNAs, with subsequent effects on gene expression affecting blastocyst development. Our findings suggest that embryos may be able to up take miRNAs throughout the preimplantation period. This highlights a potential area for the development of therapeutics, whereby certain miRNAs can be supplemented into culture media to modulate gene expression that favors normal embryo development.

Conversely, our findings also highlight the gap in knowledge regarding the native miRNA population found in commercially available culture media. Presently, most culture medias, including ones used for the *in-vitro* maturation, fertilization, and culture of embryos in this study, use serum as a means of improving blastocyst yield. Serum contains various growth factors, adhesion factors, trace hormones, lipids, and minerals essential for the *in-vitro* culture of embryos. Since miRNAs can be found in a wide array of biofluids, it can be postulated that the serum used in culture media contain miRNAs. Currently, the miRNA profile of culture medias are not known and/or disclosed, however, research have shown that miRNAs are present in plain culture media. Instead of modulating genes to stimulate growth, miRNAs may work to negatively inhibit growth and development as observed by Kropp et al. (2015). Since our findings suggest that embryos may be capable of up-taking miRNAs as early as the 2-cell stage, a detailed characterization of miRNAs in culture media may serve to improve the efficiency of *in-vitro* production systems. miRNAs known to negatively affect growth may be removed with the subsequent supplementation of miRNAs known to stimulate development. With the widespread availability of commercially available serum free culture medias, the groups examined in this study can also be conducted using serum-free culture systems. Without the presence of endogenous miRNAs in culture systems, this may identify additional miRNAs secreted by embryos and/or determine the true source of miRNAs detected in the SM from this study.

Focusing on our findings in 8-cell SM, it was determined that 21 miRNAs were detected with no miRNAs exclusively found in the media. It is important to note that EGA occurs during the 8-cell stage in bovine embryos. Perhaps that lack of miRNAs exclusive to 8-cell SM may be related to this developmental event. EGA is the period in embryo development when maternally inherited transcripts are degraded, and transcription of embryonic genome begins (24). miRNAs, on the other hand, serve to primarily inhibit gene expression. Tesfaye et al. (14) do report that intracellular miRNA expression in embryos change dynamically. Some miRNAs are highly expressed in early and late stages of development, while being absent during EGA. Therefore, our findings suggest that miRNA expression may temporally dampened during the 8-cell stage to allow for the events of EGA to proceed.

Although no miRNAs were exclusively detected in 8 cell SM, 7 of the 21 miRNAs were shared between across all 3 SM conditions. This is a significant finding as this is the first instance of miRNAs being demonstrated to have

consistent expression in the SM throughout the preimplantation period. Moreover, 6 miRNAs increased, and 1 miRNA stayed consistently downregulated in expression from one condition to another. Therefore, it may indicate that these miRNAs may play a housekeeping role throughout embryonic development. GSEA analysis did reveal that bta-miR-2305, bta-miR-2900, and bta-miR-1777a mRNA targets were overrepresented in pathways pertaining to cellular process, biological regulation, and metabolic process. Regulation of these pathways are all necessary requirements for embryo development. Perhaps, the promiscuous nature of miRNAs may allow certain miRNAs to be expressed throughout development but regulate different genes in a stage specific manner. Due to the detection of these miRNAs in 2-cell SM, it does present a possibility that these 7 shared miRNAs may be of maternal origin. Evidence suggest that the majority miRNAs expressed in early embryo development are oocyte derived. Therefore, future experiments may profile SM conditioned with mature oocytes for miRNAs. Perhaps, the potential housekeeping roles these miRNAs play in early embryo development may be maternally derived, thus strengthening the relationship of oocyte quality and downstream overall embryo quality.

It is important to note that bta-miR-450b was the only miRNA consistently downregulated across all conditions. Aside from stage specific up take of miRNAs highlighted from our 2-cell SM result, this finding indicates that certain miRNAs may be up-taken throughout the preimplantation period. Thus, this reinforces the idea of embryo having the ability to interact with its environment. Expression of bta-miR-450b was higher in plain media in comparison to all SM condition, suggesting that this miRNA is native to the commercial media used in the study. There is little known regarding bta-miR-450b in embryo development, but a predicted mRNA target is CAM2KN1 (calcium/calmodulin-dependent protein kinase II). In previous studies, it has been demonstrated that CAM2KN1 is an oncogene present in prostate cancer tissue (25). When CAM2KN1 expression was reduced, cell proliferation was impaired and apoptosis was increased (25). Therefore, it is possible that up take of bta-miR-450b in embryos may cause a subsequent decrease in expression of CAM2KN1 or other oncogenes, thereby impairing cell proliferation. Although this has not been explored, it once again highlights the need to profile the miRNA expression across commercially available medias.

Aside from the 7 miRNAs expressed across all 3 SM conditions, our study also detected 14 miRNAs that increased in expression in the SM from the 8-cell-to the blastocyst stage of development. It is known that specific miRNAs are expressed in the embryo from the period of EGA to blastocyst formation, however, no study have been able to demonstrate these changes in the extracellular environment. Therefore, the 14 miRNAs that we identified may play a role in initiating and facilitating an embryos development post EGA. Although none of the miRNAs co-detected in 8-cell and blastocyst SM have been annotated in previous SM and embryo studies, GSEA revealed that predicted mRNA targets impact pathways regulating proliferation, differentiation, and metabolism.

From a broad perspective, the vast majority of miRNAs detected in this study have not been previously annotated in literature, thus their functions are widely unknown. However, literature search did reveal that 32 of the 56 miRNAs detected in blastocyst SM have been previously explored in research. miR-24-3p, miR-191, and miR-2887 have been detected in SM cultured with embryos that failed to progress to the blastocyst stage of development (17). Moreover, miR-320a, let-7b, miR-23b-3p, miR-23a, miR-3141, miR-92a, miR-1246 have been profiled in SM conditioned with embryos that failed to implant (22). Although our study did not separate embryos based on blastocyst outcome and implantation, it appears that the miRNAs detected in blastocyst SM may be derived from poor quality blastocyst and/or ones that arrested. It has been observed that poorer quality embryos have a more dynamic expression of proteins and metabolites (26). Potentially, this dynamic expression may also translate with miRNAs in SM.

It should also be noted that a cohort of blastocyst exclusive miRNAs have been previously annotated in cancer-related studies. Specifically, some blastocyst specific miRNAs have been cited to have either an oncogenic and/or tumor suppressive role in various tissues such as kidney, liver, prostate, and ovary. It is well-established that parallels exist in the biological pathways used in embryogenesis and tumorigenesis. Molecular cues to govern morphological change, differentiation, proliferation, and invasion are all used by the pre-implantation embryo to establish pregnancy. These same processes are used by tumor cells to enhance growth, recruit cells, and coordinate spread to distant tissues. Therefore, connecting the findings of oncogenic studies may be invaluable in unlocking the roles of miRNAs in embryogenesis.

Overall, this study was able to detect miRNAs in the SM across the pre-implantation period. Cross-referencing of miRNAs from each condition allowed for the identification of stage-specific miRNAs and those shared across 2 or more SM conditions. All of the miRNAs identified have gene targets relating to pathways regulating cellular processes, biological regulation, and metabolism. Although the roles of the miRNAs identified are mostly unknown, those that have been identified suggest that miRNAs are indicative of intrinsic embryonic physiology. Future research should focus on qualitatively validating characterized miRNAs within the SM and intracellularly. From these findings, miRNA-mRNA target knockdowns can be performed to elucidate the roles miRNAs play in early embryo development.

DATA AVAILABILITY STATEMENT

The datasets presented in this study can be found in online repositories. The names of the repository/repositories and accession number(s) can be found at: https://www.ncbi.nlm.nih.gov/geo/query/acc.cgi?acc=GSE168551.

AUTHOR CONTRIBUTIONS

PD and PM conceived, developed, and planned the experiments. PD performed all the experiments and including sample preparation and data analysis. The manuscript was written by PD with the support and guidance of PM. PM supervised the project.

FUNDING

This work was supported by the Natural Sciences and Engineering Research Council of Canada (400735) and the Ontario Veterinary College.

SUPPLEMENTARY MATERIAL

The Supplementary Material for this article can be found online at: https://www.frontiersin.org/articles/10.3389/fvets.2021.658968/full#supplementary-material

REFERENCES

1. Khatib H, Huang W, Wang X, Tran AH, Bindrim AB, Schutzkus V, et al. Single gene and gene interaction effects on fertilization and embryonic survival rates in cattle. *J Dairy Sci*. (2009) 92:2238–47. doi: 10.3168/jds.2008-1767
2. Santos JEP, Thatcher WW, Chebel RC, Cerri RLA, Galvao KN. The effect of embryonic death rates in cattle on the efficacy of estrus synchronization programs. *Anim Reprod Sci*. (2004) 82:513–35. doi: 10.1016/j.anireprosci.2004.04.015
3. Perkel KJ, Tscherner A, Merrill C, Lamarre J, Madan P. The ART of selecting the best embryo: a review of early embryonic mortality and bovine embryo viability assessment methods. *Mol Reprod Dev*. (2015) 82:822–38. doi: 10.1002/mrd.22525
4. Perry G. 2013 statistics of embryo collection and transfer in domestic farm animals. *Embryo Transfer Newslet*. (2014) 32:14–24. doi: 10.13140/RG.2.2.22202.59842
5. Perry G. 2014 statistics of embryo collection and transfer in domestic farm animals. *Embryo Transfer Newslet*. (2015) 33:9–18.
6. Perry G. 2015 statistics of embryo collection and transfer in domestic farm animals. *Embryo Transfer Newslet*. (2016). 34:10–24.
7. Perry G. 2016 statistics of embryo collection and transfer in domestic farm animals. *Embryo Transfer Newsl*. (2017) 35:8–23. doi: 10.13140/RG.2.2.24793.42087
8. Viana J. 2018 Statistics of embryo production and transfer in domestic farm animals. *Embryo Technol Newslet*. (2018) 36:8–25.
9. European IVF-monitoring Consortium, European Society of Human Reproduction and Embryology, Calhaz-Jorge C, De Geyter C, Kupka MS, de Mouzon J, et al. Assisted reproductive technology in Europe, 2013: results generated from European registers by ESHRE. *Hum Reprod*. (2017) 32:1957–73. doi: 10.1093/humrep/dex264
10. Mori M, Otoi T, Suzuki T. Correlation between the cell number and diameter in bovine embryos produced *in vitro*. *Reprod Domest Anim*. (2002) 37:181–4. doi: 10.1046/j.1439-0531.2002.00354.x
11. Rocha JC, Passalia F, Matos FD, Maserati Jr MP, Alves MF, De Almeida TG, et al. Methods for assessing the quality of mammalian embryos: how far we are from the gold standard? *JBRA Assist Reprod*. (2016) 20:150. doi: 10.5935/1518-0557.20160033
12. Wahid F, Shehzad A, Khan T, Kim YY. MicroRNAs: synthesis, mechanism, function, and recent clinical trials. *Biochim Biophys Acta Mol Cell Res*. (2010) 1803:1231–43. doi: 10.1016/j.bbamcr.2010.06.013
13. Bartel DP. MicroRNAs: genomics, biogenesis, mechanism, and function. *Cell*. (2004) 116:281–97. doi: 10.1016/S0092-8674(04)00045-5
14. Tesfaye D, Worku D, Rings F, Phatsara C, Tholen E, Schellander K, et al. Identification and expression profiling of microRNAs during bovine oocyte maturation using heterologous approach. *Mol Reprod Dev*. (2009) 76:665–77. doi: 10.1002/mrd.21005
15. Kropp J, Salih SM, Khatib H. Expression of microRNAs in bovine and human pre-implantation embryo culture media. *Front Genet*. (2014) 5:91. doi: 10.3389/fgene.2014.00091
16. Rosenbluth EM, Shelton DN, Wells LM, Sparks AE, Van Voorhis BJ. Human embryos secrete microRNAs into culture media—a potential biomarker for implantation. *Fertil Steril*. (2014) 101:1493–500. doi: 10.1016/j.fertnstert.2014.01.058
17. Kropp J, Khatib H. Characterization of microRNA in bovine *in vitro* culture media associated with embryo quality and development. *J Dairy Sci*. (2015) 98:6552–63. doi: 10.3168/jds.2015-9510
18. Perkel KJ, Madan P. Spent culture medium analysis from individually cultured bovine embryos demonstrates metabolomic differences. *Zygote*. (2017) 25:662–74. doi: 10.1017/S0967199417000417
19. Soom AV, Boerjan ML, Bols PE, Vanroose G, Lein A, Coryn M, et al. Timing of compaction and inner cell allocation in bovine embryos produced *in vivo* after superovulation. *Biol Reprod*. (1997) 57:1041–9. doi: 10.1095/biolreprod57.5.1041
20. Reza AMMT, Cho SK, Choi YJ, Hong K, Kim JH. Microarray profiling of miRNA and mRNA expression in Rag2 knockout and wild-type mouse spleens. *Sci Data*. (2018) 5:1–10. doi: 10.1038/sdata.2018.152
21. Gross N, Kropp J, Khatib H. Sexual dimorphism of miRNAs secreted by bovine *in vitro*-produced embryos. *Front Genet*. (2017) 8:39. doi: 10.3389/fgene.2017.00039
22. Capalbo A, Ubaldi FM, Cimadomo D, Noli L, Khalaf Y, Farcomeni A, et al. MicroRNAs in spent blastocyst culture medium are derived from trophectoderm cells and can be explored for human embryo reproductive competence assessment. *Fertil Steril*. (2016) 105:225–35. doi: 10.1016/j.fertnstert.2015.09.014
23. Gombos KM, Oldal KI, Kalacs K, Godony A, Varnagy J, Bodis GL, et al. "Droplet digital PCR analysis of MiR-191-3p in the spent blastocyst culture media might reflect the reproductive competence of the 3rd day human embryo." *J Clin Invest Lab Med*. (2019) 2:1–5.
24. Graf A, Krebs S, Heininen-Brown M, Zakhartchenko V, Blum H, Wolf E. Genome activation in bovine embryos: review of the literature and new insights from RNA sequencing experiments. *Anim Reprod Sci*. (2014) 149:46–58. doi: 10.1016/j.anireprosci.2014.05.016
25. Wang T, Guo S, Liu Z, Wu L, Li M, Yang J, et al. CAMK2N1 inhibits prostate cancer progression through androgen receptor-dependent signaling. *Oncotarget*. (2014) 5:10293. doi: 10.18632/oncotarget.2511
26. Rødgaard T, Heegaard PM, Callesen H. Non-invasive assessment of *in-vitro* embryo quality to improve transfer success. *Reprod Biomed Online*. (2015) 31:585–92. doi: 10.1016/j.rbmo.2015.08.003

Conflict of Interest: The authors declare that the research was conducted in the absence of any commercial or financial relationships that could be construed as a potential conflict of interest.

frontiers in Veterinary Science

ORIGINAL RESEARCH
published: 17 May 2021
doi: 10.3389/fvets.2021.643910

Urinary Cell-Free miR-99a-5p as a Potential Biomarker for Estrus Detection in Buffalo

*Aparna Hebbar, Rajeev Chandel, Payal Rani, Suneel Kumar Onteru and Dheer Singh**

Animal Biochemistry Division, Molecular Endocrinology, Functional Genomics and Systems Biology Laboratory, Indian Council of Agricultural Research -National Dairy Research Institute, Karnal, India

Accurate estrus detection method is the need of the hour to improve reproductive efficiency of buffaloes in dairy industry, as the currently available estrus detection methods/tools lack high sensitivity and specificity. Recently, circulating miRNAs have been shown as non-invasive biomarkers by various studies. Hence, in order to evaluate their potential as estrus biomarkers, the objective of this study was to identify and compare the levels of 10 hormone-responsive miRNAs in the urine collected at proestrus (PE), estrus (E), and diestrus (DE) phases of buffaloes ($n = 3$) pertaining to a discovery sample. Among 10 urinary miRNAs, the levels of bta-mir-99a-5p (E/PE 0.5-fold, $P < 0.05$; DE/PE 1.9-fold), bta-miR-125b (E/PE 0.5-fold; DE/PE 0.7-fold), bta-mir-145 (E/PE 1.5-fold; DE/PE 0.7-fold), bta-mir-210 (E/PE 1.2-fold, DE/PE 0.7-fold), mir-21 (E/PE 1.5-fold, DE/PE 2-fold), and bta-mir-191 (E/PE 1.3-fold; DE/PE 0.8-fold) were found to be altered during different phases of buffalo estrous cycle. In contrast, bta-mir-126-3p, bta-let-7f, bta-mir-16b, and bta-mir-378 were undetected in buffalo urine. Furthermore, a validation study in an independent group of 25 buffalo heifers showed the increased levels of urinary bta-mir-99a-5p during the DE (3.92-fold; $P < 0.0001$) phase as compared to the E phase. Receiver operating characteristic curve analyses also revealed the ability of urinary miR-99a-5p in distinguishing the E from the DE phase (area under the curve of 0.6464; $P < 0.08$). *In silico* analysis further showed an enrichment of miR-99a-5p putative targets in various ovarian signaling pathways, including androgen/estrogen/progesterone biosynthesis and apoptosis signaling, implicating the role of miR-99a-5p in ovarian physiology. In conclusion, significantly lower levels of bta-mir-99a-5p at the E phase than the DE phase in buffalo urine indicate its biomarker potential, which needs to be further explored in a large cohort in the future studies.

Keywords: estrus, buffalo, bta-miR-99a-5p, urine, cell free miRNA, qRT-PCR

OPEN ACCESS

Edited by:
Cristina Alicia Martinez, Linköping University, Sweden

Reviewed by:
Archunan Govindaraju, Bharathidasan University, India
Mohammad Abdulkader Akbarsha, National College, Tiruchirappalli, India

***Correspondence:**
Dheer Singh
drdheer.singh@gmail.com

Specialty section:
This article was submitted to Animal Reproduction - Theriogenology, a section of the journal Frontiers in Veterinary Science

Received: *19 December 2020*
Accepted: *26 February 2021*
Published: *17 May 2021*

Citation:
Hebbar A, Chandel R, Rani P, Onteru SK and Singh D (2021) Urinary Cell-Free miR-99a-5p as a Potential Biomarker for Estrus Detection in Buffalo. Front. Vet. Sci. 8:643910. doi: 10.3389/fvets.2021.643910

INTRODUCTION

Dairy farming is one of the most significant parts of the agriculture sector in India. Buffaloes are usually found in Southeast Asia and the Mediterranean region (1). They are preferred over other farm animals in India for their higher financial returns *via* milk and meat, better efficiency in utilizing low-quality feed, and resistance to tropical diseases (1, 2). However, poor reproductive efficiency of buffaloes is one of the major limitations hindering their maximum production potential. Several factors lead to poor reproductive performance of buffaloes, including delayed puberty, silent

heat, variation in calving interval, and low conception rate (1, 3), but silent estrus is the major cause of concern (3). In addition, because of lack of an accurate estrus detection method, success of artificial insemination (AI) is limited in buffaloes (4). Generally, estrus is determined by various methods, including hormonal estimation, observation of visual and behavioral signs, gynecoclinical examination, record keeping (5, 6), and various devices (7), but their sensitivity and specificity vary in detecting estrus (8). As per an estimate, ∼50% of ovulations remain unnoticed in dairy industry due to diminished estrus behavior (9). Hence, ineffective estrus detection in dairy animals ultimately creates financial loss to the farmers (7). Thus, an accurate estrus detection in buffaloes is essential for effective reproductive management *via* successful conception, which is usually achieved by carrying out AI generally during ovulation that occurs ∼10–12 h after the end of an estrus (E) phase in cattle and buffaloes (10). Therefore, there is an urgent requirement to develop a highly sensitive and specific estrus detection method for buffaloes to increase the AI success rate.

MiRNAs are small non-coding RNAs that mainly regulate gene expression at posttranscriptional level. Literature survey showed a cyclic expression of miRNAs in bovine ovarian tissues during an estrous cycle (11, 12), suggesting their specific role in different phases of an estrous cycle. Moreover, miRNAs were also reported to be stably present in extracellular environment, either inside extracellular vesicles such as exosomes or as miRNA protein or miRNA lipoprotein complexes (13–15). Evidences showed the presence of tissue-specific miRNAs in circulation at quantifiable levels (16), indicating their use as a biomarker. For example, higher levels of urinary miR-210-3p in cancer patients were significantly reduced in a disease-free stage (17), demonstrating the tumor as their source of origin. Similarly, decreased plasma levels of miR-222, miR-151-5p, and let-7e after thyroidectomy in papillary thyroid cancer patients indicate their secretion in systemic circulation by tumors (18). In this context, biomarker potential of circulating miRNAs was shown for multiple diseases, including reproductive diseases (19, 20).

In contrast to humans, very few research studies showed the biomarker potential of circulating miRNAs in farm animals. miRNAs have been shown to be involved in reproductive physiology in animals, including regulation of follicular and luteal development (21), pregnancy (22), and follicle-to-luteal transition (23). Moreover, it has been reported that the miRNA profile of the reproductive tissues (11, 23, 24) and plasma of bovine varies in different phases of an estrus cycle (9), which could be due to cyclic variation in ovarian hormones, mainly estrogen and progesterone. As the ovary is highly vascularized organ (9), it is reasonable to hypothesize that miRNAs from ovarian tissue may be excreted differentially and/or specifically in circulation, depending on the phase of an estrus cycle, suggesting that circulating miRNAs may mirror ovarian miRNA profile. In addition, some of these systemic miRNAs may get filtered out *via* the kidney and ultimately appear in urine, and hence, they can be used as estrus biomarkers. Thus, circulating miRNAs in bovine urine may convey the specific phase of an estrous cycle.

Although miRNA profile in bovine plasma (9) and ovarian tissues (23, 25–27) gets altered during an estrous cycle, no study has been conducted until now to identify the altered levels of urinary miRNAs during bovine estrous cycle. Therefore, the present study was planned to explore the altered levels of urinary miRNA during estrous cycle considering the buffalo as a model. In this study, we used quantitative reverse transcriptase–polymerase chain reaction (qRT-PCR) to detect the levels of 10 hormone-responsive miRNAs, which were selected on the basis of their implication in ovarian physiology as per the available scientific literature, i.e., miR-125b (28), miR-99a (29), miR-145 (30), miR-21 (31), miR-191 (30), miR-210 (32), let-7f (30), miR-16 (33), miR-378 (30), and miR-126 (34) in buffalo urine and compared their levels across different phases of an estrous cycle. In addition, validation of urinary miR-99a-5p levels was performed in a separate group of 25 buffaloes. At last, *in silico* analysis was done to identify putative targets of miR-99a-5p using miRwalk 2.0 followed by their association analysis with different cellular signaling pathways using Panther, an online tool.

MATERIALS AND METHODS

Experimental Animals

For the discovery phase of the study, three buffalo heifers were managed as per the standard conditions at the Livestock Research Centre, ICAR–National Dairy Research Institute (NDRI), Karnal. In addition, 25 animals, which were presented for AI at the AI center, ICAR-NDRI, were considered for the validation study. The study was approved by the NDRI Institutional Animal Ethics Committee (approval no. 42-IAEC-18-2).

Sample Collection and Processing

Urine and saliva samples were collected in the morning time and in the evening on the day of E (day 0), proestrus (PE) (day −2), and diestrus (DE) (day 10). In case animals did not urinate for 20 min, the animals were stimulated for urination by pouring water on the rump region or by tying the animal or by offering the water to the animal. In brief, midstream urine was collected from healthy buffalo heifers ($n = 3$ for discovery group and $n = 25$ for validation group) in 50 mL centrifuge tubes, transported to the laboratory on ice, and centrifuged at 3,000 *g* for 5 min at 4°C. The supernatant or cell-free urine (CFU) was transferred to another microcentrifuge tube and then either used immediately or stored in −20°C until further use. In case of the discovery group, urine was collected from different phases of three consecutive estrous cycles of each animal, but the samples that belonged to the middle estrous cycle were selected for further analysis. In validation group, urine was collected from buffaloes on day 0 before insemination and again on day 10. Estrus and DE paired samples from animals that showed typical salivary fern pattern of estrus on day 0 and were found to be non-pregnant during 60 days after AI were included in this study.

Detection of an Estrous Cycle Phase

Buffaloes were observed for estrus symptoms twice a day in the morning and the evening for the period of 6 months. E phase was determined by observing various signs such as visual observation (vaginal discharge, hyper salivation, and abnormal posture), gynecoclinical examination (cervical relaxation and

uterine tonicity), and biochemical confirmation (cervical mucus crystallization or salivary fern pattern) and rated as either mild, moderate, or intense as mentioned in **Table 2**. Serum ($n = 3$) was used to estimate the estradiol levels using enzyme-linked immunosorbent assay–based Estradiol Estimation Assay kit (ADI-900-174 by ENZO) as per the manufacturer's protocol.

Saliva Collection and Fern Pattern Analysis

Unstimulated saliva was collected from the lower lip of buffaloes before feeding time in the morning on every alternative day of the estrous cycle, brought to the laboratory on ice and centrifuged at 3,000 *g* for 5 min at 4°C. A 10 μL of cell-free saliva was used for smear preparation on a clean glass slide for observing the salivary fern patterns under an inverted microscope (Nikon Eclipse Ti-S, Japan) to determine the phase of an estrous cycle as per our previous study (2) (**Figure 1**).

Total RNA Isolation

RNA was extracted from CFU using TRIzol LS (Life Technologies, USA) as per the manufacturer's protocol. In brief, 250 μL of CFU was mixed with 750 μL of TRIzol LS and vortexed briefly, and the mixture was kept at room temperature for 5 min. Then, 200 μL of chloroform (Sigma Chemicals Co., catalog no. C2432) was added to the mixture, vortexed for 15 s, and incubated for 15 min at room temperature followed by a centrifugation at 12,000 relative centrifugal force (rcf) for 15 min. Aqueous supernatant was transferred to a fresh Eppendorf tube, 500 μL of isopropanol was added to it, and the mixture was incubated at −20°C for 30 min. Later, it was centrifuged at 12,000 rcf for 10 min. The supernatant was discarded, and the pellet was washed with 70% ethanol. Finally, the RNA pellet was dissolved in 20 μL of nuclease-free water and then either used immediately or stored at −20°C until further use. RNA purity and concentrations were determined by using a Nanodrop spectrophotometer.

cDNA Synthesis

Total RNA was used to prepare cDNA as per the miScript II RT kit (catalog no. 218161, Germany) according to the manufacturer's protocol. In brief, 10 μL of cDNA reaction mixture containing 500 ng of the total RNA, 2 μL of 5X miScript Hispec buffer, 1 μL of RT mix, 1 μL of 10× miScript nucleics mix provided by Qiagen miscript II kit (catalog no. 218161, Germany), and 1 μL of an exogenous spiked-in miRNA control, syn-cel-miR-39-3p (1 μL; miRNeasy Serum/Plasma Spike-In Control, catalog no. 219610, Qiagen Co., Germany) was incubated at 37°C for 60 min and 95°C for 5 min. The prepared cDNA was kept at −20°C until further use.

Real-Time PCR

Urinary levels of miRNAs were determined by qRT-PCR with some modifications using either Light Cycler 480 II (Roche, CA, USA) or Applied Biosystems Fast 7500 Real-Time PCR system (Roche, CA, USA). The primers used for miRNA amplification were designed on the basis of mature miRNA sequences of bovine using miRBase 21 and procured from a commercial firm (**Table 1**) (35). In brief, 12 μL PCR reaction mixture consisting of 5 μL of cDNA (1:20 diluted), 5 μL of 2× Quantilect SYBR Green PCR Master Mix, 1 μL of 5 μM miRNA-specific primer, and 1 μL of 10× miScript Universal Primer (catalog no. 218073, Germany) was incubated at 95°C for 15 min, followed by 40 cycles of 94°C for 15 s, 55°C for 30 s, and 70°C for 30 s. The melt curve analysis was performed at the temperature ranging from 70 to 95°C. Each sample was run in duplicate. qRT-PCR data analysis was done using $2^{-\Delta\Delta Ct}$ method (36) by using cel-miR-39 as an exogeneous spiked-in miRNA for normalization (13).

TABLE 1 | miRNAs primers used in the study.

Gene name	Primer name: sequence (5′ to 3′)	Accession no.
bta-miR-99a-5p	AACCCGTAGATCCGTTCTTGT	MIMAT0003537
bta-mir-145	GTCCAGTTTTCCCAGGAATCCC	MIMAT0003542
bta-mir-125b	TCCCTGAGACCCTAACTTGTGA	MIMAT0003539
bta-mir-126-3p	CGTACCGTGAGTAATAATGCG	MIMAT0003540
bta-miR-21-5p	GCTTATCAGACTGATGTTGAC	MIMAT0003528
bta-let-7f	TGAGGTAGTAGATTGTATAGTT	MIMAT0003519
bta-mir-210	ACTGTGCGTGTGACAGC	MIMAT0003824
bta-mir-378	ACTTGGAGTCAGAAGGC	MIMAT0009305
bta-miR-191	CAACGGAATCCCAAAAG	MIMAT0003819
bta-mir-16b	TAGCAGCACGTAAATATTGG	MIMAT0003525

FIGURE 1 | Typical salivary crystallization of buffalo (air dried, ×200). **(A)** Salivary crystallization during the proestrus phase. **(B)** Typical fern patterns of saliva during the estrus phase. **(C)** Discontinuous and improper crystallization during the diestrus phase.

TABLE 2 | Intensities of overt estrous signs in different buffaloes.

Animal no.	A1	A2	A3
Swollen vulva	+	++	++
Vaginal discharge	++	++	+++
Salivary fern	++	++	+++
Tonicity of uterus	++	++	++

Estrus intensities were determined by visual behaviors and biochemical and gynecoclinical parameter as mild (+), moderate (++), and intense (+ + +).

TABLE 3 | Estradiol levels during different phases of an estrous cycle in buffaloes.

Animal no.	A1	A2	A3	Average	SE
PE	26.9	27.08	34.76	29.58	2.591
E	21.35	16.87	25.96	21.39	2.624
DE	14.39	16.01	18.43	16.28	1.174

Target Gene Prediction and Pathway Analysis for miR-99a-5p

MiRWalk, an online tool, was used to predict putative mRNA targets that might be regulated by miR-99a-5p under a threshold of 3 (37). The resultant predicted targets for miR-99a-5p were run through Protein Analysis Through Evolutionary Relationship (PANTHER) classification system and analysis tools (38) in order to identify their associated biological processes considering the bovine as a genome background.

Statistical Analysis

Statistical analyses were performed either by one-way analysis of variance (ANOVA) followed by *post-hoc* Tukey test or paired *t*-test using GraphPad Prism software 5.1. (GraphPad Software, Inc., San Diego, CA, USA). Results are shown as the mean ± SEM. Receiver operating characteristic (ROC) curve analysis was performed using ΔCt values of the miR-99a-5p in the E and DE phase samples.

RESULTS

Intensity of Estrus Signs

Estrus was determined by various physical indicators such as tonicity of uterus, swelling of vulva, vaginal discharge, and typical salivary fern patterns. Physical indicators were categorized as mild, moderate, and intense as shown in **Table 2**. Among three buffaloes at the E phase, moderate or intense swelling of vulva was recorded in 66.67% of cases together. Similarly, estrus intensity indicators such as vaginal discharge and salivary ferns were observed to be either moderate or intense in all animals (100%). Tonicity of uterus was found to be moderate in 100% of the animals. Serum estradiol levels were further determined at E phase in buffaloes (**Table 3**), which were found to be significantly higher at the PE (29.58 ± 2.591 pg/mL) and E phases (21.39 ± 2.624 pg/mL; $P < 0.05$) as compared to the DE phase (16.28 ± 1.174 pg/mL).

miRNA Urinary Levels

We selected 10 hormone-responsive miRNA candidates identified on the basis of literature (**Table 2**) for qRT-PCR analysis. Unfortunately, the urinary levels of let-7f, mir-126-3p, miR-378, and mir-16b were too low to be detected by qRT-PCR. Of the remaining six miRNAs, mir-145 (1.5-fold E/PE; 0.7-fold DE/PE), mir-21(1.5-fold E/PE; 2-fold DE/PE), miR-210 (1.2-fold E/PE; 0.7-fold DE/PE), mir-191 (1.3-fold E/PE; 0.8-fold DE/PE), and miR-125b (0.5-fold E/PE; 0.7-fold DE/PE) did not significantly change during the E cycle (**Figure 2**). In contrast, miR-99a-5p levels increased at the DE phase (1.9-fold) and decreased at the E phase (0.5-fold $P < 0.05$) compared to the PE phase as shown in **Figure 2**.

Validation of mir-99a-5p Urinary Levels and ROC Curve Analysis

mir-99a-5p levels were analyzed in another group of 25 buffaloes on the day of the E and DE phases during an estrous cycle. mir-99a-5p levels were observed to be significantly increased (3.92-fold; $P < 0.0001$) in the DE phase as compared to the E phase as shown in **Figure 3**. Finally, we determined discriminatory performance of miR-99a-5p using ROC curve analysis as shown in **Figure 4**. E and DE datasets were used to make ROC curve. ROC curve analysis showed that at the 7.962 cutoff value, the sensitivity and specificity of miR-99a-5p in differentiating the E from DE phase were 56 and 60%, respectively; the AUC was 0.6464 (95% confidence interval, 0.4921–0.8007; $P = 0.076$) as shown in **Figure 4**. ROC curve results suggest the potential of miR-99a-5p to distinguish the E and DE phases.

Target Gene Prediction and Pathway Analysis of miR-99a-5p

miRwalk, an online tool, predicted 7,347 target genes for miR-99a-5p (**Supplementary Table 1**). miR-99a-5p target sites were identified in the 5′ UTR, CDs, and 3′ UTR regions of putative targets. Among 7,347 predicted target genes, 3,086 putative target genes having NM_Accession prefixes (**Supplementary Table 2**) were shown to be associated with various cellular pathways (**Supplementary Table 3**) and biological processes (**Supplementary Table 4**) by the PANTHER software. Among the top 15 cellular pathways predicted to be regulated by miR-99a-5p, androgen/estrogen/progesterone biosynthesis and apoptosis signaling pathways have been previously implicated in ovarian physiology (**Figure 5**). Similarly, biological process annotations by PANTHER analysis showed that miR-99a-5p may regulate reproduction and reproductive process (**Figure 6**).

DISCUSSION

Currently, an accurate estrus detection biomarker is the need of the hour for effective reproductive management of buffaloes. Recently, a number of studies reported biomarker potential of circulating miRNAs in biofluids owing to their high stability (39) and good clinical performance (40). Among the various miRNAs evaluated in the present study, we found low levels of miR-99a-5p and bta-mir-125b on the estrus day as compared

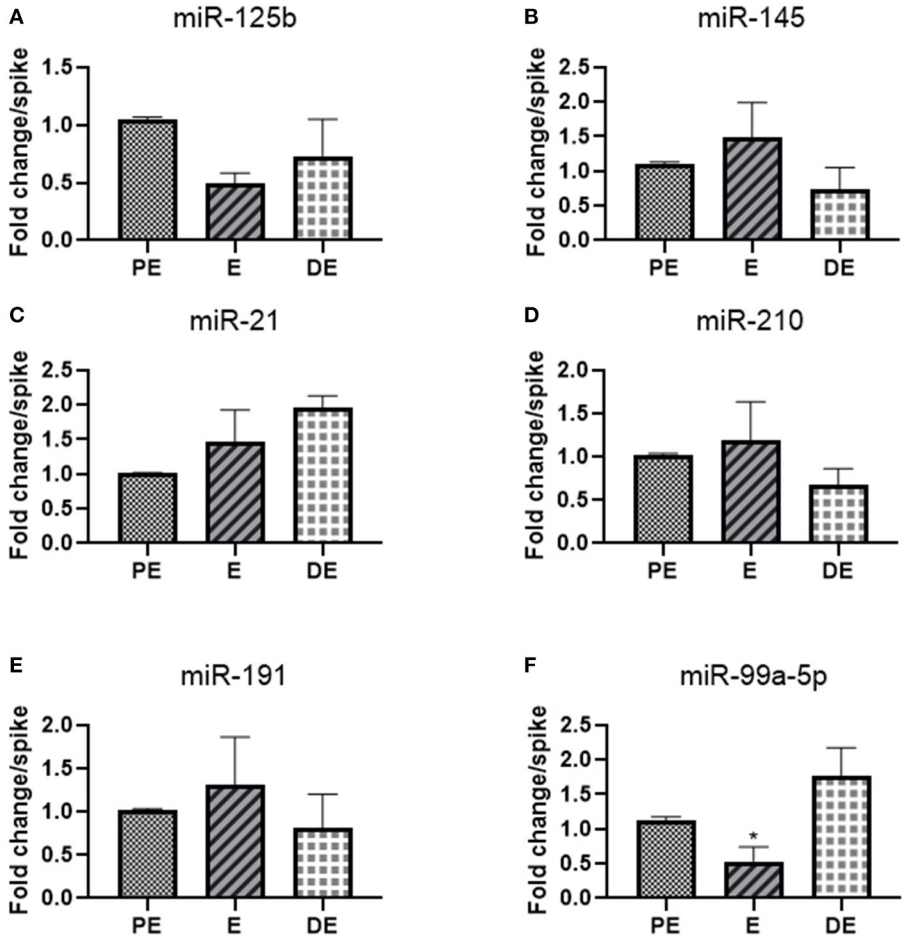

FIGURE 2 | Real-time PCR analysis of miRNAs **(A)** miR-125b, **(B)** miR-145, **(C)** mir-21, **(D)** mir-210, **(E)** miR-191, and **(F)** miR-99a-5p in proestrus (PE), estrus (E), and diestrus (DE) phases. One-way ANOVA test was done followed by *post-hoc* Tukey test for analysis. Each bar in the figure represents the mean ± SE of three independent experiments $^{*}P < 0.05$.

to the PE and DE phases. In contrast, earlier studies showed a higher expression of miR-99a-5p and bta-mir-125b in ovaries during follicular phase and their higher plasma levels during the E phase in cows (9). Another study reported an upregulation of miR-125b expression by androgens, thereby suppressing the follicular atresia *via* targeting a proapoptotic gene (28). Moreover, decreased expression of mir-125b was found in granulosa cells of primordial follicles as compared to primary, secondary, and antral follicles in mouse (41).

In addition, we also found high levels of mir-145, mir-210, and mir-191 on the estrus day as compared to the PE phase. In concordance with our data, higher expression of mir-145 (23, 25) and mir-210 (32) were shown in ovaries during follicular phase, and higher plasma levels of mir-145 were reported during the E phase of cows (9). Furthermore, our study showed a gradual increase of miR-21 levels from the PE to the E phase, followed by its highest levels at the DE phase, which is not in agreement with earlier studies as miR-21 expression in the granulosa cells was found to be lowest on day 14 and at higher levels on day 3 of an estrous cycle (42). Study done by Donadeu et al. (43) reported higher expression of miR-21-5p/-3p in atretic than healthy follicles of cattle. In this context, studies reported the regulation of follicular atresia by miR-21-3p through targeting FGF2 (44) and VEGFA (45) that ultimately inhibits bovine granulosa cell autophagy by repressing AKT/mTOR signaling and PI3K/AKT signaling, respectively. Another study reported the higher expression of bta-miR-21-5p during early CL (1–7 days) as compared to middle CL and late CL (46), suggesting its role in the corpus luteum formation, functionalization, and corpus luteum regression (23). Luteinizing hormone was reported to upregulate antiapoptotic miR-21 in murine granulosa cells, suggesting its role in granulosa cell survival and differentiation (47). Moreover, elevated levels of miR-21, miR-145, and miR-378 in follicular fluid aspirated from dominant follicles during seasonal anovulation as compared to the seasonal ovulation period in mares further suggest their role in follicle maturation (48). Literature survey also showed the higher levels of miR-125b (23, 27) and miR-145 (23, 25) and low

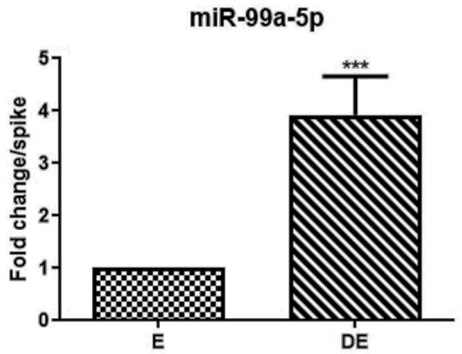

FIGURE 3 | Real-time PCR analysis of mir-99a-5p in the validation population of the animals in estrus (E) and diestrus (DE). The paired *t*-test was used for analysis. Each bar represents the mean ± SEM of 25 independent experiments. ***$P < 0.001$.

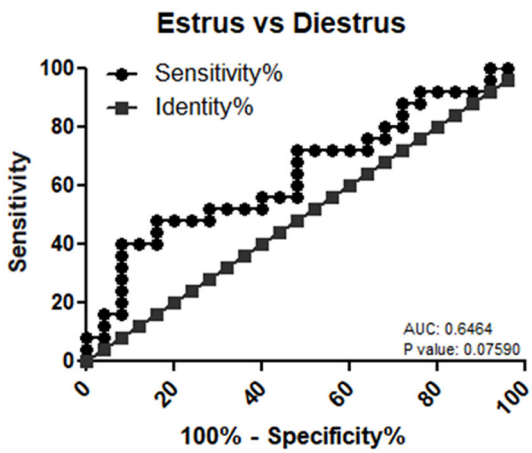

FIGURE 4 | Receiver operating characteristic (ROC) curve of miR-99a-5p as a diagnostic marker for estrus.

levels of miR-21 (23, 26) in follicular tissues as compared to luteal tissues in the ovaries, indicating their role in follicle-to-luteal transition. At last, let-7f, miR-16b, miR-126-3p, and mir-378 were not detected in buffalo urine, suggesting their levels might be below the detection limit of qRT-PCR or completely absent. In this context, Weber et al. (49) reported that urine generally has the lowest amount of miRNAs among 12 different biological fluids.

Hormone plays an important role in estrous cycle regulation. In this context, multiple studies showed a reciprocal relationship between miRNAs expression/levels and hormones. One of the studies suggested partial regulation of circulating miR-125b, miR-99a, miR-145, and miR-378 by hormones in hyperstimulated heifers (50). Hu et al. (51) reported downregulation of miR-125b expression in response to 17α-E2. Reciprocally, miRNAs also regulate ovarian hormone biosynthesis and release. Sirotkin et al. (52) demonstrated the role of miRNAs in the regulation of estradiol (miR-125b and miR-126), testosterone (miR-16, miR-145, miR-125b, miR-21, and miR-126), and progesterone (miR-16, miR-145, miR-125b, and miR-126) release, respectively, in granulosa cells. Zhang et al. (53) reported that decreased expression of miR-125b-5p stimulates testosterone secretion and decreases the estradiol release in mouse preantral follicles *via* regulation of PAK3/ERK1/2 signaling. Hence, it can be concluded that miRNAs and hormonal interplay might be involved in estrous cycle regulation. Moreover, multiple investigations showed the extracellular presence of the miRNAs evaluated in the present study. Naji et al. (54) reported that higher levels of miR-145 in follicular fluid can be used as a predictive biomarker for polycystic ovary syndrome. Singh et al. (55) reported the lower levels of salivary mir-16b in the presence of dominant ovarian follicle. Li et al. (34) reported higher serum levels of miR-126-3p during ovulation and midluteal phase in comparison to early follicular phase. A study conducted with cow plasma demonstrated the significantly increased levels of miR-99a-5p, let-7f, miR-145, and miR-125b in estrus as compared to the other phases during estrous cycle of cows (9). Taken together, the miRNA presence in biofluids further suggests their potential use as a biomarker.

Among the studied miRNAs, miR-99a-5p can be used as an estrus biomarker. Tripurani et al. (56) reported that the higher expression of miR-99a in ovarian tissue suggested its role in basic reproductive activities. Geng et al. (57) reported decreased proliferation and increased apoptosis of granulosa cells by miR-99a *via* targeting insulin like growth factor 1R, suggesting its expression might be low during folliculogenesis, which could partly explain its low urinary levels during estrus in buffaloes. Literature survey also indicated the role of miR-99a in cell cycle (58) and glucose metabolism (59). Noferesti et al. (50) reported hormonal regulation of circulating miR-99a, which further explains its dynamic urinary levels during an estrous cycle due to hormonal cyclicity. The functions of miR-99a-5p have not been reported completely as yet in relation to fertility and physiological functions in the ovary; we herein speculate its possible role by predicting the association of miR-99a-5p targets with different cellular pathways, including those pathways associated with biosynthesis of androgen, estrogen, and progesterone hormones and apoptosis, which ultimately suggests its role in the reproductive process. Hence, *in silico* analysis gives clues regarding the implication of miR-99a-5p in ovarian physiology. Moreover, ROC curve analysis gave a solid support that miR-99a-5p could clearly differentiate between the E and DE phase. At last, its dynamic presence in plasma and urine during the estrous cycle as shown previously further hints toward its definite potential as an estrus biomarker in the near future. Thus, these data explained why miR-99a could serve as a promising biomarker for estrus detection in buffaloes.

In general context, lack of agreement between the present and numerous previous studies might be due to difference in preanalytical and analytical variables used, including sample source, RNA isolation protocols, RNA quality and quantity, cDNA synthesis kits, miRNA quantification techniques, and normalization gene (60, 61). For example, miRNA profile varies according to different body fluids. For example, an miRNA

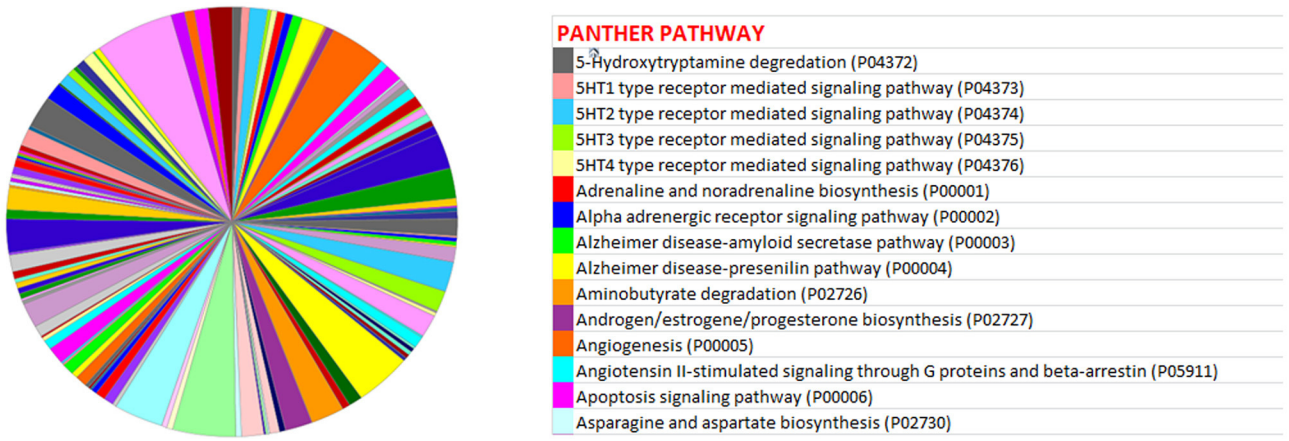

FIGURE 5 | Association of bta-miR-99a-5p target genes with different pathways as shown in the pie chart by PANTHER, an online tool.

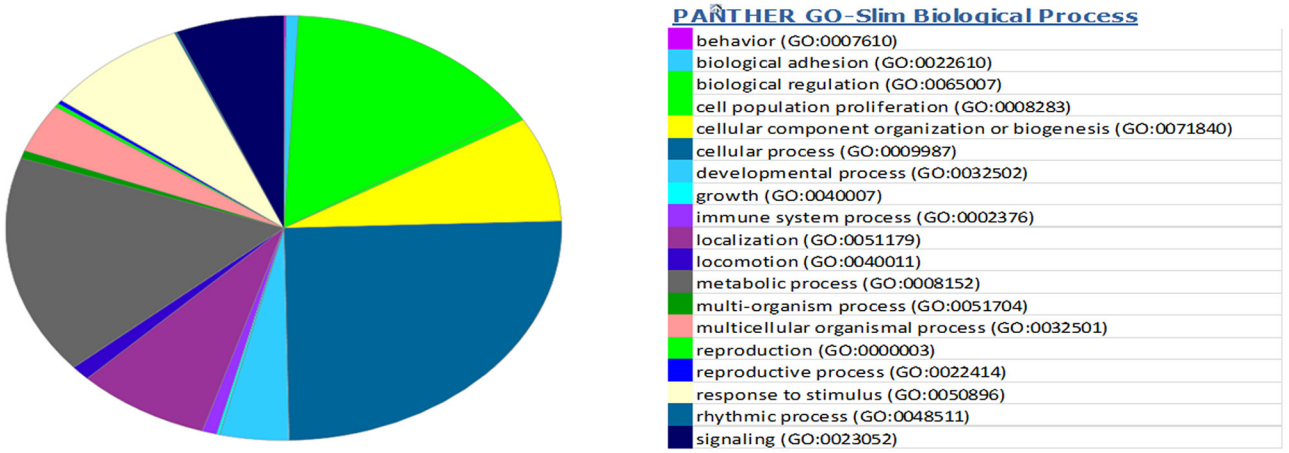

FIGURE 6 | Association of bta-miR-99a-5p target genes with different biological processes as shown in the pie chart by PANTHER, an online tool.

profile in urine and plasma samples from the same animal may vary, as urine being the ultrafiltrate of plasma. In addition, we stored CFU in −20°C, which may affect RNA yield, as urinary Extracellular Vesicles (EVs) or naked miRNAs may get entrapped inside Tamm–Horsfall protein complex present in the urine under low temperature conditions and subsequently get lost during RNA isolation (62). Currently, there is no consensus regarding ideal reference gene that should be used for qRT-PCR data normalization in case of biofluids. In the present study, exogenous cel-mir-39 was used for qRT-PCR data normalization, which may reduce variability caused by differences in reverse transcription efficiency across samples, but it is insufficient to remove technological variability across samples caused by various factors including collection, handling, and storage of samples. At last, cell-free miRNA profile and their levels in urine are dynamic in nature and depend on various factors, including intervariability and intravariability among animals, time point of urine collection, and seasonal variation. Hence, there is always a chance of getting variable miRNA profile from urine taken at the same phase of an estrous cycle.

Our study has a number of limitations. First, our study is not comprehensive in terms of cell-free miRNAs profiling present in buffalo urine, although it showed the biomarker potential of urinary miR-99a-5p for estrus detection. Second, we used a small number of samples during the discovery and validation phase; hence, our finding needs to be verified in a large sample size. Third, our results must be verified in different breeds of buffaloes. Fourth, urinary levels of miR-99a-5p were found to be differentially altered at different phases of estrous cycle in buffalo, but the origin of urinary miR-99a-5p needs to be elucidated in order to draw a significant conclusion regarding its biomarker potential, as it is already reported to be expressed in numerous other tissues (56) apart from the ovary. Hence, the relative contribution of these organs to urinary miR-99a-5p is not known. Similarly, cell-specific expression of miR-99a-5p in ovarian tissue must be determined in order to better estimate its potential

as an estrus biomarker. Fifth, it needs to be deciphered how miR-99a-5p enters the circulation, especially the urine.

In the future, successful clinical use of urinary cell-free miRNAs requires an establishment of guidelines and protocols for urine sampling, processing, storage, and transport; miRNA isolation, normalization, and quantification methods; and miRNA profiling using high-throughput detection techniques. Meanwhile, urinary miRNA diversity and their levels in different phases of an estrous cycle need to be determined for the development of estrus detection biomarker in buffaloes. At last, the biomarker potential of urinary cell-free mir-99a-5p needs to be deciphered in combination with other miRNA panels to increase its sensitivity and specificity for heat detection in the buffalo.

In summary, our study yielded (i) a first insight of hormone-responsive miRNAs levels in buffalo urine using real-time PCR, (ii) a potential of urinary cell-free miR-99a-5p as estrus biomarker in bovine, and (iii) a clue that ovarian-derived miRNAs may get filtered out in buffalo urine. Most importantly, ROC curve analysis showed that urinary levels of miR-99a-5p in buffalo can moderately distinguish the E from DE phases of an estrous cycle, further suggesting its biomarker potential in estrus detection that needs to be further explored in future either alone or in combination with other miRNAs to improve its sensitivity and specificity.

CONCLUSION

The present study reported significantly lower levels of urinary cell-free mir-99a-5p at the E phase as compared to the DE phase in buffalo. This may be helpful for the development of mir-99a-5p–based estrus detection kit in the near future.

DATA AVAILABILITY STATEMENT

The datasets presented in this study can be found in online repositories. The names of the repository/repositories and accession number(s) can be found in the article/**Supplementary Material**.

ETHICS STATEMENT

The animal study was reviewed and approved by IAEC, NDRI, Karnal.

AUTHOR CONTRIBUTIONS

AH and PR: performed the research, methodology, and data analysis. RC: writing—original draft. SO: conceptualization and supervision. DS: conceptualization, supervision, and experimental design. All authors contributed to the article and approved the submitted version.

FUNDING

This work was supported by the Bill & Melinda Gates Foundation [grant number OPP1154401] .

SUPPLEMENTARY MATERIAL

The Supplementary Material for this article can be found online at: https://www.frontiersin.org/articles/10.3389/fvets.2021.643910/full#supplementary-material

REFERENCES

1. Mondal S, Prakash BS, Palta P. Endocrine aspects of oestrous cycle in buffaloes (*Bubalus bubalis*): an overview. *Asian-Australasian J Anim Sci.* (2007) 20:124–31. doi: 10.5713/ajas.2007.124
2. Ravinder R, Kaipa O, Baddela VS, Singhal Sinha E, Singh P, Nayan V, et al. Saliva ferning, an unorthodox estrus detection method in water buffaloes (*Bubalus bubalis*). *Theriogenology*. (2016) 86:1147–55. doi: 10.1016/j.theriogenology.2016.04.004
3. Suthar VS, Dhami AJ. Estrus detection methods in buffalo. *Vet World*. (2010) 3:94–6.
4. De Rensis F, López-Gatius F. Protocols for synchronizing estrus and ovulation in buffalo (*Bubalus bubalis*): a review. *Theriogenology*. (2007) 67:209–16. doi: 10.1016/j.theriogenology.2006.09.039
5. Verma KK, Prasad S, Kumaresan A, Mohanty TK, Layek SS, Patbandha TK, et al. Characterization of physico-chemical properties of cervical mucus in relation to parity and conception rate in Murrah buffaloes. *Vet World*. (2014) 7:467–71. doi: 10.14202/vetworld.2014.467-471
6. Selvam RM, Onteru SK, Nayan V, Sivakumar M, Singh D, Archunan G. Exploration of Luteinizing hormone in murrah buffalo (*Bubalus bubalis*) urine: extended surge window opens door for estrus prediction. *Gen Comp Endocrinol.* (2017) 251:121–6. doi: 10.1016/j.ygcen.2016.12.002
7. Roelofs J, López-Gatius F, Hunter RHF, van Eerdenburg FJCM, Hanzen C. When is a cow in estrus? Clinical and practical aspects. *Theriogenology*. (2010) 74:327–44. doi: 10.1016/j.theriogenology.2010.02.016
8. Selvam RM, Archunan G. A combinatorial model for effective estrus detection in Murrah buffalo. *Vet World.* (2017) 10:209–13. doi: 10.14202/vetworld.2017.209-213
9. Ioannidis J, Donadeu FX. Circulating microRNA profiles during the bovine oestrous cycle. *PLoS ONE*. (2016) 11: e0158160. doi: 10.1371/journal.pone.0158160
10. Rao TKS, Kumar N, Kumar P, Chaurasia S, Patel NB. Heat detection techniques in cattle and buffalo. *Vet World*. (2013) 6:363–9. doi: 10.5455/vetworld.2013.363-369
11. Sontakke SD, Mohammed BT, McNeilly AS, Donadeu FX. Characterization of microRNAs differentially expressed during bovine follicle development. *Reproduction.* (2014) 148:271–83. doi: 10.1530/REP-14-0140
12. Jerome A, Thirumaran SMK, Kala SN. Identification of microRNAs in corpus luteum of pregnancy in buffalo (*Bubalus bubalis*) by deep sequencing. *Iran J Vet Res*. (2017) 18:287–90. doi: 10.14202/vetworld.2017.1129-1134
13. Mitchell PS, Parkin RK, Kroh EM, Fritz BR, Wyman SK, Pogosova-Agadjanyan EL, et al. Circulating microRNAs as stable blood-based markers for cancer detection. *Proc Natl Acad Sci USA*. (2008) 105:10513–8. doi: 10.1073/pnas.0804549105
14. Arroyo JD, Chevillet JR, Kroh EM, Ruf IK, Pritchard CC, Gibson DF, et al. Argonaute2 complexes carry a population of circulating microRNAs

independent of vesicles in human plasma. *Proc Natl Acad Sci USA*. (2011) 108:5003–8. doi: 10.1073/pnas.1019055108
15. Vickers KC, Palmisano BT, Shoucri BM, Shamburek RD, Remaley AT. MicroRNAs are transported in plasma and delivered to recipient cells by high-density lipoproteins. *Nat Cell Biol*. (2011) 13:423–33. doi: 10.1038/ncb2210
16. Williams Z, Ben-Dov IZ, Elias R, Mihailovic A, Brown M, Rosenwaks Z, et al. Comprehensive profiling of circulating microRNA *via* small RNA sequencing of cDNA libraries reveals biomarker potential and limitations. *Proc Natl Acad Sci USA*. (2013) 110:4255–60. doi: 10.1073/pnas.1214046110
17. Petrozza V, Costantini M, Tito C, Giammusso LM, Sorrentino V, Cacciotti J, et al. Emerging role of secreted miR-210-3p as potential biomarker for clear cell Renal Cell Carcinoma metastasis. *Cancer Biomarkers*. (2020) 27:181–8. doi: 10.3233/CBM-190242
18. Yu S, Liu Y, Wang J, Guo Z, Zhang Q, Yu F, et al. Circulating microRNA profiles as potential biomarkers for diagnosis of papillary thyroid carcinoma. *J Clin Endocrinol Metab*. (2012) 97:2084–92. doi: 10.1210/jc.2011-3059
19. Wu L, Zhou H, Lin H, Qi J, Zhu C, Gao Z, et al. Circulating microRNAs are elevated in plasma from severe preeclamptic pregnancies. *Reproduction*. (2012) 143:389–97. doi: 10.1530/REP-11-0304
20. Miura K, Higashijima A, Murakami Y, Tsukamoto O, Hasegawa Y, Abe S, et al. Circulating chromosome 19 miRNA cluster microRNAs in pregnant women with severe pre-eclampsia. *J Obstet Gynaecol Res*. (2015) 41:1526–32. doi: 10.1111/jog.12749
21. Donadeu FX, Schauer SN, Sontakke SD. Involvement of miRNAs in ovarian follicular and luteal development. *J Endocrinol*. (2012) 215:323–34. doi: 10.1530/JOE-12-0252
22. Wessels JM, Edwards AK, Khalaj K, Kridli RT, Bidarimath M, Tayade C. The microRNAome of pregnancy: deciphering miRNA networks at the maternal-fetal interface. *PLoS ONE*. (2013) 8: e72264. doi: 10.1371/journal.pone.0072264
23. McBride D, Carré W, Sontakke SD, Hogg CO, Law A, Donadeu FX, et al. Identification of miRNAs associated with the follicular-luteal transition in the ruminant ovary. *Reproduction*. (2012) 144:221–33. doi: 10.1530/REP-12-0025
24. Salilew-Wondim D, Ahmad I, Gebremedhn S, Sahadevan S, Hossain MM, Rings F, et al. The expression pattern of microRNAs in granulosa cells of subordinate and dominant follicles during the early luteal phase of the bovine estrous cycle. *PLoS ONE*. (2014) 9: e106795. doi: 10.1371/journal.pone.0106795
25. Ling YH, Guo XF, Chen T, Ding JP, Ma YH, Chu MX, et al. Characterization and analysis of differentially expressed microRNAs in hircine ovaries during the follicular and luteal phases. *Anim Reprod Sci*. (2016) 166:47–57. doi: 10.1016/j.anireprosci.2016.01.003
26. Zhu L, Chen T, Sui M, Han C, Fang F, Ma Y, et al. Comparative profiling of differentially expressed microRNAs between the follicular and luteal phases ovaries of goats. *Springerplus*. (2016) 5:1233. doi: 10.1186/s40064-016-2902-1
27. Zhang X, Zhang L, Shang J, Tao Q, Tian M, Ma Y, et al. Combined microRNAome and transcriptome analysis of follicular phase and luteal phase in porcine ovaries. *Reprod Domest Anim*. (2019) 54:1018–25. doi: 10.1111/rda.13457
28. Sen A, Prizant H, Light A, Biswas A, Hayes E, Lee HJ, et al. Androgens regulate ovarian follicular development by increasing follicle stimulating hormone receptor and microRNA-125b expression. *Proc Natl Acad Sci USA*. (2014) 111:3008–13. doi: 10.1073/pnas.1318978111
29. Xie J, Cao Y. Expression of TGF-β1 and miR-99a in serum of patients with early spontaneous abortion and correlation with hormone levels during pregnancy. *Exp Ther Med*. (2019) 17:4593–7. doi: 10.3892/etm.2019.7477
30. Di Leva G, Piovan C, Gasparini P, Ngankeu A, Taccioli C, Briskin D, et al. Estrogen mediated-activation of miR-191/425 cluster modulates tumorigenicity of breast cancer cells depending on estrogen receptor status. *PLoS Genet*. (2013) 9:e1003311. doi: 10.1371/annotation/92dfa670-d431-4d68-b70b-706df1f93e46
31. Wickramasinghe NS, Manavalan TT, Dougherty SM, Riggs KA, Li Y, Klinge CM. Estradiol downregulates miR-21 expression and increases miR-21 target gene expression in MCF-7 breast cancer cells. *Nucleic Acids Res*. (2009) 37:2584–95. doi: 10.1158/0008-5472.SABCS-3051
32. Shukla A, Dahiya S, Onteru SK, Singh D. Differentially expressed miRNA-210 during follicular-luteal transition regulates pre-ovulatory granulosa cell function targeting HRas and EFNA3. *J Cell Biochem*. (2018) 119:7934–43. doi: 10.1002/jcb.26508
33. Yu X, Zhang X, Dhakal IB, Beggs M, Kadlubar S, Luo D. Induction of cell proliferation and survival genes by estradiol-repressed microRNAs in breast cancer cells. *BMC Cancer*. (2012) 12:29. doi: 10.1186/1471-2407-12-29
34. Li P, Wei J, Li X, Cheng Y, Chen W, Cui Y, et al. 17β-estradiol enhances vascular endothelial Ets-1/ MIR-126-3p expression: the possible mechanism for attenuation of atherosclerosis. *J Clin Endocrinol Metab*. (2017) 102:594–603. doi: 10.1210/jc.2016-2974
35. Kozomara A, Griffiths-Jones S. MiRBase: annotating high confidence microRNAs using deep sequencing data. *Nucleic Acids Res*. (2014) 42:gkt1181. doi: 10.1093/nar/gkt1181
36. Livak KJ, Schmittgen TD. Analysis of relative gene expression data using real-time quantitative PCR and the 2-ΔΔCT method. *Methods*. (2001) 25:402–8. doi: 10.1006/meth.2001.1262
37. Dweep H, Gretz N, Sticht C. MiRWalk database for miRNA-target interactions. *Methods Mol Biol*. (2014) 1182:289–305. doi: 10.1007/978-1-4939-1062-5_25
38. Mi H, Huang X, Muruganujan A, Tang H, Mills C, Kang D, et al. PANTHER version 11: expanded annotation data from Gene Ontology and Reactome pathways, and data analysis tool enhancements. *Nucleic Acids Res*. (2017) 45:D183–9. doi: 10.1093/nar/gkw1138
39. Mall C, Rocke DM, Durbin-Johnson B, Weiss RH. Stability of miRNA in human urine supports its biomarker potential. *Biomark Med*. (2013) 7:10.2217/bmm.13.44. doi: 10.2217/bmm.13.44
40. Wang J, Chen J, Sen S. MicroRNA as biomarkers and diagnostics. *J Cell Physiol*. (2016) 231:25–30. doi: 10.1002/jcp.25056
41. Yao N. A network of miRNAs expressed in the ovary are regulated by FSH. *Front Biosci*. (2009) 3239:3447. doi: 10.2741/3447
42. Tian M, Zhang X, Ye P, Tao Q, Zhang L, Ding Y, et al. MicroRNA-21 and microRNA-214 play important role in reproduction regulation during porcine estrous. *Anim Sci J*. (2018) 89:1398–405. doi: 10.1111/asj.13087
43. Donadeu FX, Mohammed BT, Ioannidis J. A miRNA target network putatively involved in follicular atresia. *Domest Anim Endocrinol*. (2017) 58:76–83. doi: 10.1016/j.domaniend.2016.08.002
44. Ma L, Tang X, Guo S, Liang M, Zhang B, Jiang Z. miRNA-21–3p targeting of FGF2 suppresses autophagy of bovine ovarian granulosa cells through AKT/mTOR pathway. *Theriogenology*. (2020) 157:226–37. doi: 10.1016/j.theriogenology.2020.06.021
45. Ma L, Zheng Y, Tang X, Gao H, Liu N, Gao Y, et al. MiR-21-3p inhibits autophagy of bovine granulosa cells by targeting VEGFA *via* PI3K/AKT signaling. *Reproduction*. (2019) 158:441–52. doi: 10.1530/REP-19-0285
46. Gecaj RM, Schanzenbach CI, Kirchner B, Pfaffl MW, Riedmaier I, Tweedie-Cullen RY, et al. The dynamics of microRNA transcriptome in bovine corpus luteum during its formation, function, and regression. *Front Genet*. (2017) 8:213. doi: 10.3389/fgene.2017.00213
47. Carletti MZ, Fiedler SD, Christenson LK. MicroRNA 21 blocks apoptosis in mouse periovulatory granulosa cells. *Biol Reprod*. (2010) 83:286–95. doi: 10.1095/biolreprod.109.081448
48. Donadeu FX, Schauer SN. Differential miRNA expression between equine ovulatory and anovulatory follicles. *Domest Anim Endocrinol*. (2013) 45:122–5. doi: 10.1016/j.domaniend.2013.06.006
49. Weber JA, Baxter DH, Zhang S, Huang DY, Huang KH, Lee MJ, et al. The microRNA spectrum in 12 body fluids. *Clin Chem*. (2010) 56:1733–41. doi: 10.1373/clinchem.2010.147405
50. Noferesti SS, Sohel MMH, Hoelker M, Salilew-Wondim D, Tholen E, Looft C, et al. Controlled ovarian hyperstimulation induced changes in the expression of circulatory miRNA in bovine follicular fluid and blood plasma. *J Ovarian Res*. (2015) 8:81. doi: 10.1186/s13048-015-0208-5
51. Hu Z, Shen WJ, Cortez Y, Tang X, Liu LF, Kraemer FB, et al. Hormonal regulation of microRNA expression in steroid producing cells of the ovary, testis and adrenal gland. *PLoS ONE*. (2013) 8:e78040. doi: 10.1371/journal.pone.0078040
52. Sirotkin AV, Ovcharenko D, Grossmann R, Lauková M, Mlynček M. Identification of microRNAs controlling human ovarian cell steroidogenesis *via* a genome-scale screen. *J Cell Physiol*. (2009) 219:415–20. doi: 10.1002/jcp.21689

53. Zhang X, Xiao H, Zhang XEQ, Gong X, Li T, Han Y, et al. Decreased microRNA-125b-5p disrupts follicle steroidogenesis through targeting PAK3/ERK1/2 signalling in mouse preantral follicles. *Metabolism*. (2020) 107:154241. doi: 10.1016/j.metabol.2020.154241
54. Naji M, Nekoonam S, Aleyasin A, Arefian E, Mahdian R, Azizi E, et al. Expression of miR-15a, miR-145, and miR-182 in granulosa-lutein cells, follicular fluid, and serum of women with polycystic ovary syndrome (PCOS). *Arch Gynecol Obstet*. (2018) 297:221–31. doi: 10.1007/s00404-017-4570-y
55. Singh P, Golla N, Singh P, Baddela VS, Chand S, Baithalu RK, et al. Salivary miR-16, miR-191 and miR-223: intuitive indicators of dominant ovarian follicles in buffaloes. *Mol Genet Genomics*. (2017) 292:935–53. doi: 10.1007/s00438-017-1323-3
56. Tripurani SK, Xiao C, Salem M, Yao J. Cloning and analysis of fetal ovary microRNAs in cattle. *Anim Reprod Sci*. (2010) 120:16–22. doi: 10.1016/j.anireprosci.2010.03.001
57. Geng Y, Sui C, Xun Y, Lai Q, Jin L. MiRNA-99a can regulate proliferation and apoptosis of human granulosa cells *via* targeting IGF-1R in polycystic ovary syndrome. *J Assist Reprod Genet*. (2019) 36:211–21. doi: 10.1007/s10815-018-1335-x
58. Cui L, Zhou H, Zhao H, Zhou Y, Xu R, Xu X, et al. MicroRNA-99a induces G1-phase cell cycle arrest and suppresses tumorigenicity in renal cell carcinoma. *BMC Cancer*. (2012) 12:546. doi: 10.1186/1471-2407-12-546
59. Li W, Wang J, Chen QD, Qian X, Li Q, Yin Y, et al. Insulin promotes glucose consumption *via* regulation of miR-99a/mTOR/PKM2 pathway. *PLoS ONE*. (2013) 8:e64924. doi: 10.1371/journal.pone.0064924
60. Martínez-Fernández M, Paramio JM, Dueñas M. RNA detection in urine: from RNA extraction to good normalizer molecules. *J Mol Diagnostics*. (2016) 18:15–22. doi: 10.1016/j.jmoldx.2015.07.008
61. Armstrong DA, Dessaint JA, Ringelberg CS, Hazlett HF, Howard L, Abdalla MAK, et al. Pre-analytical handling conditions and small RNA recovery from urine for miRNA profiling. *J Mol Diagnostics*. (2018) 20:565–71. doi: 10.1016/j.jmoldx.2018.04.003
62. Wachalska M, Koppers-Lalic D, van Eijndhoven M, Pegtel M, Geldof AA, Lipinska AD, et al. Protein complexes in urine interfere with extracellular vesicle biomarker studies. *J Circ Biomarkers*. (2016) 5:4. doi: 10.5772/62579

Conflict of Interest: The authors declare that the research was conducted in the absence of any commercial or financial relationships that could be construed as a potential conflict of interest.

frontiers in Veterinary Science

SYSTEMATIC REVIEW
published: 15 June 2021
doi: 10.3389/fvets.2021.680539

Lineage Differentiation Markers as a Proxy for Embryo Viability in Farm Ungulates

Alba Pérez-Gómez, Leopoldo González-Brusi, Pablo Bermejo-Álvarez and Priscila Ramos-Ibeas**

Department of Animal Reproduction, National Institute for Agriculture and Food Research and Technology (INIA), Madrid, Spain

Embryonic losses constitute a major burden for reproductive efficiency of farm animals. Pregnancy losses in ungulate species, which include cattle, pigs, sheep and goats, majorly occur during the second week of gestation, when the embryo experiences a series of cell differentiation, proliferation, and migration processes encompassed under the term conceptus elongation. Conceptus elongation takes place following blastocyst hatching and involves a massive proliferation of the extraembryonic membranes trophoblast and hypoblast, and the formation of flat embryonic disc derived from the epiblast, which ultimately gastrulates generating the three germ layers. This process occurs prior to implantation and it is exclusive from ungulates, as embryos from other mammalian species such as rodents or humans implant right after hatching. The critical differences in embryo development between ungulates and mice, the most studied mammalian model, have precluded the identification of the genes governing lineage differentiation in livestock species. Furthermore, conceptus elongation has not been recapitulated *in vitro*, hindering the study of these cellular events. Luckily, recent advances on transcriptomics, genome modification and post-hatching *in vitro* culture are shedding light into this largely unknown developmental window, uncovering possible molecular markers to determine embryo quality. In this review, we summarize the events occurring during ungulate pre-implantation development, highlighting recent findings which reveal that several dogmas in Developmental Biology established by knock-out murine models do not hold true for other mammals, including humans and farm animals. The developmental failures associated to *in vitro* produced embryos in farm animals are also discussed together with Developmental Biology tools to assess embryo quality, including molecular markers to assess proper lineage commitment and a post-hatching *in vitro* culture system able to directly determine developmental potential circumventing the need of experimental animals.

Keywords: embryo quality, embryo transfer, developmental biology, lineage markers, viability, conceptus elongation, assisted reproductive technologies, post-hatching embryo culture

OPEN ACCESS

Edited by:
Cristina Alicia Martinez, Linköping University, Sweden

Reviewed by:
Deqiang Miao, Washington State University, United States
Isabelle Hue, INRAE Centre Jouy-en-Josas, France

****Correspondence:***
Pablo Bermejo-Álvarez
bermejo.pablo@inia.es
Priscila Ramos-Ibeas
ramos.priscila@inia.es

Specialty section:
This article was submitted to Animal Reproduction - Theriogenology, a section of the journal Frontiers in Veterinary Science

Received: *14 March 2021*
Accepted: *24 May 2021*
Published: *15 June 2021*

Citation:
Pérez-Gómez A, González-Brusi L, Bermejo-Álvarez P and Ramos-Ibeas P (2021) Lineage Differentiation Markers as a Proxy for Embryo Viability in Farm Ungulates. Front. Vet. Sci. 8:680539. doi: 10.3389/fvets.2021.680539

INTRODUCTION

Optimal reproductive performance in farm animals relies on the proper accomplishment of the different biological processes leading to delivery. Starting from the ovulation of a competent oocyte, conception requires a successful fertilization to produce a zygote, which marks the onset of preimplantation development. During preimplantation development, complex cell proliferation,

differentiation and migration processes must be finely controlled to ensure embryo viability and subsequent embryo implantation. Following embryo implantation, a fetus will be developed, ultimately resulting in a newborn. When global reproductive failures in farm ungulates are dissected into these steps, preimplantation development (i.e., the period compromised between fertilization and implantation) clearly stands out as the most problematic. For instance, in the case of cattle, embryonic losses prior to day 16 (D16) post-insemination can rise up to 50% in high yielding dairy cows (1), whereas in pigs it has been estimated that one into five embryos dies before implantation (2).

Preimplantation development in ungulates can be divided into two periods. The first period spans from fertilization to blastocyst hatching, i.e., the release of the embryo from a glycoprotein protective shell termed zona pellucida. This pre-hatching period is common to all mammals and constitutes the whole preimplantation period in rodents and humans, where blastocysts implant right after hatching. In contrast, ungulates exhibit a second preimplantation period termed conceptus elongation. During conceptus elongation the ungulate blastocyst must undergo dramatic morphological changes that, in the case of cattle, convert a ∼150 μm D7 blastocyst into a ∼30 cm long D21 conceptus around implantation (3, 4). Reproductive failures occurring during preimplantation development can be originated in any of these periods, but developmental collapse during conceptus elongation is the main responsible for global reproductive failures in ungulates (5). To illustrate the magnitude of this problem in cattle farms, it has been estimated that one third of the viable D6 blastocysts fail to elongate and maintain pregnancy by D28 (6), and embryo mortality during early conceptus elongation (D7–D14) oscillates between 26 and 34% (4). In this perspective, the study of the cell differentiation, proliferation, and migration processes occurring during preimplantation development is crucial to understand conceptus collapse and, thereby, finding suitable markers to assess proper lineages development is key to improve reproductive efficiency in livestock ungulates.

The molecular basis of the developmental processes occurring during the first weeks of pregnancy in ungulates is only partially understood, mainly due to two technical limitations: the lack of an *in vitro* system able to recapitulate conceptus elongation, and the difficulties for performing loss-of-function studies in these species. Luckily, recent advances in *in vitro* culture of post-hatching blastocysts in cattle (7) and sheep (own unpublished data), together with the development of CRISPR-Cas9 technology to perform loss of function studies in livestock species are set to boost our knowledge on molecular markers for assessing proper embryo development.

In this review, we discuss the differences between ungulate embryo development and that of rodents and humans, highlighting the molecular markers involved in the first lineages differentiation events occurring in ungulates. We also revise different studies that have reported impaired lineages development in *in vitro*-produced embryos, and provide insights into the potential of lineages markers and post-hatching embryo culture systems to assess embryo quality in farm animals.

MOLECULAR CONTROL OF THE FIRST CELL LINEAGE DIFFERENTIATIONS

Segregation of the first cell lineages in the embryo is critical for proper pregnancy establishment and fetus development. Unfortunately, comprehensive understanding of this process is only available in mice, which became a classical model in Developmental Biology due to its low maintenance cost, fast life cycle and, particularly, due to the well-developed techniques for genome modification in this species. Although the first stages of early embryo development are broadly conserved in mammals, increasing amount of research using novel technologies such as single cell transcriptomics or generation of knock-out embryos by CRISPR-Cas9 are revealing important differences in gene regulatory networks between rodent and non-rodent species.

The First Decision: Inner Cell Mass vs. Trophectoderm

During the first cell divisions, the embryo relies on maternal transcripts and proteins until the embryonic genome is activated between the 2- (rodents) and 4/8-cell stages (lagomorphs, ungulates, and primates) (8). At these early stages of development, blastomeres are morphologically indistinguishable, but from the 8-cell stage in the mouse, cells located in the outside of the embryo undergo a process of polarization that will influence their fate, biasing outer polar cells toward trophectoderm (TE) and inner apolar cells toward inner cell mass (ICM) (9–11) (**Figure 1**). The formation of an apical domain in the outer cells triggers a transcriptional network involving Hippo/YAP signaling and the activation of *Tead4* in the mouse, which leads to the downregulation of the pluripotency factor *Sox2* and the upregulation of *Cdx2* from the morula stage (12–15). Activation of CDX2 downregulates *Oct4* (14, 16) and activates the expression of other TE markers such as *Gata3*, *Eomes* or *Elf5* (17), allowing the emergence of the first cell lineages during the formation of the blastocyst: TE, which will mediate implantation, and ICM that will form the embryo proper.

These transcription factors exhibit different temporal expression profiles and roles in cell differentiation events in non-rodent mammals (**Table 1**). TE-specific genes *CDX2*, *GATA3*, or *TEAD4* are also expressed in the TE of bovine (18–20), porcine (21, 22), and human (20, 23, 24) blastocysts, but remarkable differences in timing of expression and function have been observed between ungulates and rodents. For instance, CDX2 protein expression before the blastocyst stage is restricted to some scattered cells in pig and cattle, contrasting to the ubiquitous expression in mice (14, 25–27), and both CDX2 and OCT4 are expressed in the TE until late blastocyst stages in humans, pigs and cattle (25, 26, 28, 29), in contrast to the mutually exclusive expression observed in mouse blastocysts (14). In the same line, whereas CDX2 represses *Oct4* expression in the TE of murine blastocysts (16), *CDX2* downregulation does not affect *OCT4* expression in bovine embryos (25, 30), and bovine *OCT4* promoter lacks an essential region -CR4- necessary for repression of OCT4 in mouse TE (25). Recent KO

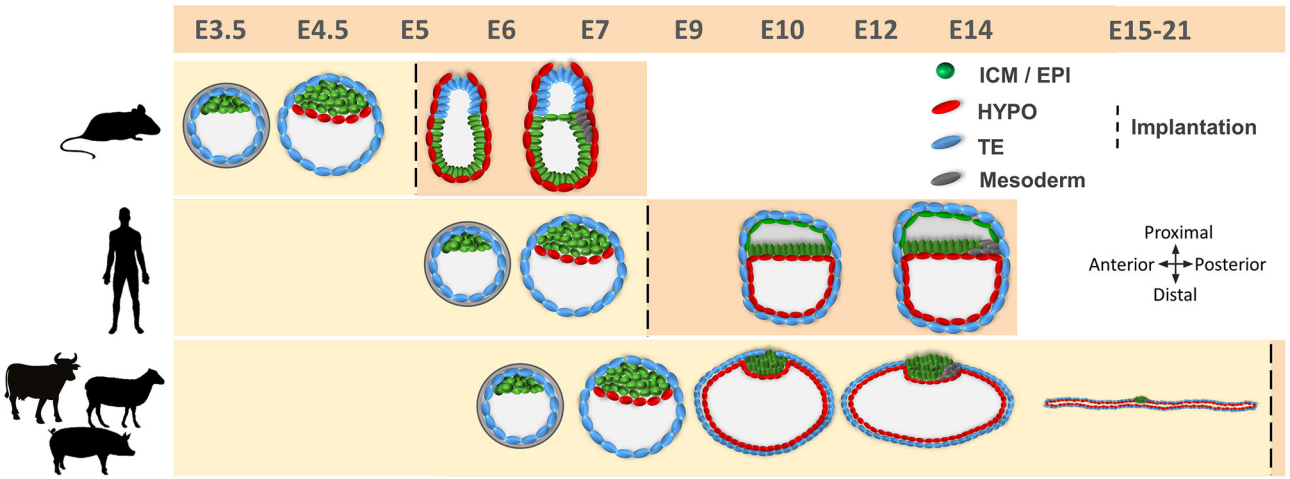

FIGURE 1 | Comparative developmental timeline between mice, humans, and farm ungulates. Different cell lineages are indicated. Embryo development in humans and farm ungulates is delayed compared to mice. Implantation takes place after blastocyst hatching in mice and humans, while in farm ungulates it occurs following conceptus elongation. Mouse epiblast develops in a cup shape after the blastocyst stage, while in humans and farm ungulates it forms a flat embryonic disc. E, embryonic day; ICM, inner cell mass; EPI, epiblast; HYPO, hypoblast; TE, trophectoderm.

experiments have also highlighted a different function of OCT4 in rodents vs. ungulates and humans. *Oct4* KO mouse embryos develop to blastocyst, although hypoblast formation—explained in the next section—is impaired, but the absence of OCT4 protein in *OCT4* KO morulae has been observed to impair blastocyst formation and reduce *CDX2* expression in both cattle (31) and humans (32, 33).

Other transcription factors involved in TE vs. ICM differentiation in mouse also seem to play different roles in ungulate development. TEAD4, the upstream regulator of TE genes such as *CDX2* and *EOMES*, does not appear to be essential for TE specification in ungulates, as its downregulation does not impair blastocyst formation in cattle (34, 35), whereas *Tead4* ablation in mice completely abolishes blastocoel formation (36, 37). Furthermore, transcription factors downstream *TEAD4* such as *EOMES* and *ELF5* are still not expressed at the blastocyst stage in cattle (18, 30, 38), pigs (21) and humans (24). Although gene ablation experiments in ungulates are required to faithfully elucidate the role of these genes, these evidences strongly suggest that the transcriptional network required for TE specification in ungulates is considerably different to that of mice. In this perspective, early TE specification could have emerged as an evolutionary mechanism in rodents to allow implantation at an earlier stage than in other species. Fortunately, recent improvements in genome edition techniques in ungulates (39, 40) currently allow the exploration of the molecular machinery involved in ICM/TE specification in farm animals. Genome editing constitutes also an unvaluable tool to study other reproductive processes (41). For instance, the generation of aromatase-null porcine conceptuses has uncovered that intrinsic estrogen conceptus production is not required for early maternal recognition of pregnancy or implantation in pig, in striking contrast to previous beliefs (42).

The Second Decision: Epiblast vs. Hypoblast

After the differentiation of the TE, the second cell fate decision takes place in the ICM and determines the emergence of the pluripotent epiblast and the extraembryonic hypoblast (**Figure 1**). In mice, hypoblast markers are sequentially expressed, starting with GATA6 at the 8-cell, PDGFRα at the 16-cell, SOX17 at the 32-cell, and GATA4 at the 64-cell stages (43, 44). Later on, the cells forming the early ICM (E3.5) co-express both epiblast (OCT4, SOX2, and NANOG) and hypoblast (GATA6, SOX17, and PDGFRA) proteins, but by E4.5 these cells will show mutually exclusive expression for both markers (43, 45). Although the detailed temporal expression pattern of these markers is not available for most domestic mammals, there are broad similarities in the gene regulatory network controlling the second lineage specification within mammals (46). For example, *PDGFRα* and *SOX17* are also co-expressed with epiblast markers in the bipotent ICM cells and become restricted to hypoblast cells in late blastocysts in human, pig and cattle embryos (18, 21, 24). However, important differences have been also reported between rodent and non-rodent species (**Table 1**). GATA6, together with the epiblast marker NANOG, are expressed in all cells of the mouse morula and their mutual repression in the late ICM is essential for epiblast vs. hypoblast specification (43, 47). However, this might not be a strict requirement in all mammals, since GATA6 is expressed in all cell lineages of the blastocyst in primates, pigs and cattle, only becoming restricted to the hypoblast at later developmental stages (18, 21, 24, 48–50), and NANOG is not expressed in the human, pig and cattle morula (21, 26, 51, 52). Once specified, hypoblast cells reorganize to form an epithelium lying in contact with the blastocoel cavity (43) and migrate to cover the inner embryo surface in primates and ungulates (7) (**Figure 1**).

TABLE 1 | Species-specific differences in the expression of lineage markers.

Marker		Mouse				Human				Cow/pig			
		Early blastocyst		Late blastocyst		Early blastocyst		Late blastocyst		Early blastocyst		Late blastocyst	
		ICM	TE	EPI	HYPO	ICM	TE	EPI	HYPO	ICM	TE	EPI	HYPO	TE
ICM/EPI	OCT4	+	−	+	−	+	+	+	+	+	+	+	+	+
	SOX2	+	−	+	−	+	−	+	−	+	−	+	−	−
	NANOG	+	−	+	−	+	−	+	−	+	−	+	−	−
HYPO	GATA6	+	−	−	+	+	+	−	+	+	+	−	+	−
	SOX17	+	−	−	+	+	−	−	+	+	−	−	+	−
	PDGFRA	+	−	−	+	+	−	−	+	+	−	−	+	−
	GATA4	+	−	−	+	+	−	−	+	+	−	−	+	−
TE	CDX2	−	+	−	−	−	+	−	−	−	+	−	−	+
	GATA3	−	+	−	−	−	+	−	−	−	+	−	−	+
	TEAD4	−	+	−	−	+	+	+	+	+	+	+	+	+
	EOMES	−	+	−	−	−	−	−	−	−	−	−	−	−
	ELF5	−	+	−	−	−	−	−	−	−	−	−	−	−

Green (positive) and red (negative) colors indicate differences in the expression of specific markers between species.

POST-HATCHING DEVELOPMENT IN UNGULATES: CONCEPTUS ELONGATION

A characteristic aspect of ungulate development is TE fate. After blastocyst hatching, the TE can be classified into mural TE, which covers the blastocoel cavity, and polar TE, covering the ICM. While in rodents and primates, the polar TE forms the extraembryonic ectoderm (ExE), contributing to implantation and becoming part of the placenta, in lagomorphs (53) and ungulates (3) this function is accomplished by the mural TE. The polar TE, also known as Rauber's layer (RL), is removed through an apoptotic mechanism (54) around D9–D11 in pigs (55), D10–D12 in horses (56), D11–D12 in sheep (own unpublished observations) and by day 14 in cattle (54), directly exposing the epiblast to the uterine histotroph (**Figure 1**). Shortly after the disappearance of the RL, the extraembryonic membranes (EEMs, composed by mural TE and hypoblast) undergo extensive proliferation. As a consequence of this proliferation, the embryo is termed conceptus (EEMs + embryo proper) and it progresses from spherical through ovoid, tubular and filamentous stages reaching a length of ∼30 cm in cattle (3) and ∼100 cm in pigs (57) by the time of implantation, which starts about D14 in pigs (58), D15 in the sheep (59), and D19 in cattle (60). In other non-ungulate domestic species, such as rabbits and horses, the blastocyst also experiences a massive growth of EEMs before implantation, reaching up to 20 mm in horses and 5 mm in rabbits, but it remains spherical (8).

Besides the massive proliferation of EEMs, major developmental events take place in the epiblast before implantation: an anterioposterior axis is established that will outline the body plan, and the three germ layers become specified, together with the germline (61–63). Before the RL disintegrates, the epiblast forms a small cavity that will be opened once the RL disappears, unfolding the epiblast (64, 65). This contrasts with murine and human development, where the epiblast cavitates to form the amniotic cavity (66–68) (**Figure 1**). Roughly concomitant to RL disintegration, the ungulate epiblast develops into a clearly identifiable circular light structure: the embryonic disc (ED), where epiblast cells develop tight junctions and form a basal lamina toward the hypoblast (63). When the ED is fully formed, expression of core pluripotency markers SOX2, OCT4, and NANOG is restricted to the epiblast (21, 25, 69). During the next days, the ED will acquire an oval shape and a higher density at the posterior edge, associated with the ingression of the first cells into the primitive streak and the beginning of gastrulation. Some cells at the posterior part of the epiblast start to express the mesoderm marker *BRACHYURY* (T) and to downregulate *SOX2* before the primitive streak is morphologically visible (59, 69–72). These T-positive cells will be the first cells to egress into the space between the epiblast and the hypoblast and will form the mesoderm, which quickly migrates to cover the whole embryonic disc. At the same time, more epiblast cells continue to egress through the primitive streak to form the endoderm, which lies on the dorsal hypoblast, while the mesoderm forms a mesenchyme between the epiblast and the endoderm. Epiblast cells that do not pass through the streak will form the ectoderm (73, 74). The primitive streak will

be extended in an anterior direction, being the anterioposterior axis of the embryo proper aligned with the proliferation of the extra-embryonic membranes (i.e., conceptus elongation axis) (75).

Our knowledge of the genes and signaling pathways controlling gastrulation in mammals is mainly derived from the mouse embryo, in which gastrulation occurs following implantation. Key genes involved in gastrulation such as *BRACHYURY*, *EOMES*, *BMP4*, *NODAL*, *CER1*, or *FOXA2* seem to play conserved roles in ungulates, although with some differences in their location and temporal expression (3, 59, 63, 65, 71, 76, 77).

EPIBLAST DEVELOPMENT CONSTITUTES THE MAJOR OBSTACLE FOR EMBRYO SURVIVAL

The developmental defects ultimately leading to embryo mortality during conceptus elongation have been difficult to explore, given the challenges for obtaining elongating embryos *in vivo*. However, several *in vitro* evidences and *in vivo* observations point to the development of the epiblast as the most vulnerable process. *In vitro* evidences show that the requirements for trophectoderm and hypoblast development are less restrictive than those required for epiblast survival. Primary bovine trophectoderm cell cultures can be established using relatively simple media supplemented with 10 % serum (78, 79), whereas conditions required for truly pluripotent epiblast cell culture in farm animals remain to be captured (80). In the same line, early *in vitro* culture systems designed for the development of post-hatching ungulate embryos were successful in achieving trophectoderm proliferation and some degree of hypoblast migration, but the epiblast degenerated (81–83). To attain epiblast survival *in vitro*, we required a way more complex medium (termed N2B27) containing aminoacids, lipids, vitamins, hormones, and growth factors not present in previous systems (7). Yet, under our system epiblast survival is observed in 55–60% of the *in vitro* produced embryos, whereas trophoblast and hypoblast proliferation is found in all surviving structures.

Failure in epiblast development has been also observed *in vivo*. Embryo transfer of *in vitro* produced (IVP) embryos often results in lower pregnancy rates compared to their *in vivo* counterparts, as it will be discussed below, and failures in epiblast development seem to be the main responsible for such developmental arrest. IVP-derived bovine conceptuses have been reported to exhibit smaller EDs than their *in vivo* counterparts (84), and multiple studies have reported a remarkably high percentage (23–65%) of IVP-derived conceptuses lacking EDs (4, 85–90), as reviewed by Ealy et al. (91). Impaired ED development has also been observed in ovine and bovine embryos produced by somatic cell nuclear transfer (SCNT), a technology that induces pleiotropic effects over different lineages (92, 93). Interestingly, embryos lacking an ED were also observed after SCNT at a very high rate, ranging from 20 to 58% (**Table 2**) (89, 94, 96–99), and failures in a mechanism that populates inner cells based on asymmetric divisions of outer cells have been proposed to be responsible for developmental arrest in SCNT rabbit embryos (95). Moreover, transcriptional alterations in embryonic lineages of SCNT embryos were 10–20-fold more abundant in the epiblast than in extraembryonic lineages, both in cattle and mice (89, 98, 101, 102). Accordingly, some authors have observed that normal elongation in SCNT cattle embryos was more frequent (46/50 embryos) than normal ED formation and gastrulation (38/50) (98).

TABLE 2 | Embryonic disc development in embryos produced by assisted reproductive technologies.

Species	ART	Embryo transfer	Embryo recovery	ED rate (%)	References
Sheep	AI	D6	D11	5/6 (83)	(94)
	AI+IVC	D6 (vit)	D11	6/6 (100)	
	SCNT	D6 (vit)	D11	7/13 (54)	
	AI	D6	D13	9/9 (100)	
	AI+IVC	D6 (vit)	D13	6/6 (100)	
	SCNT	D6 (vit)	D13	9/13 (69)	
Cow	AI	D7	D16	7/19 (37)	(84)
	IVF	D7	D16	6/17 (35)	
Cow	AI	D6–D7	D14	18/20 (90)	(96)
	IVF	D6	D14	13/18 (72)	
	SCNT	D6	D14	24/33 (73)	
Cow	IVF	D7 (vit+fresh)	D14	11/20 (55)	(89)
	SCNT	D7 (vit+fresh)	D14	8/19 (42)	
Cow	IVF	D7	D12	–/227 (68)	(4)
	IVF	D7	D13	–/69 (78)	
	IVF	D7	D14	–/182 (83)	
Cow	IVF	D7	D17	5/6 (83)	(97)
	SCNT	D7	D17	12/19 (63)	
Cow	IVF	D7	D14–D15	19/20 (95)	(99)
	SCNT	D7	D14–D15	34/46 (74)	
Cow	IVF	D7	D15	6/7 (83)	(85)
Cow	AI	–	D18	10/10 (100)	(98)
	IVF	D7	D18	10/10 (100)	
	SCNT	D7	D18	24/30 (80)	
Cow	IVF	D7	D13–D14	15/20 (75)	(100)
	SCNT (transgenic cells)	D7	D13–D14	9/12 (75)	
Cow	IVF	D7	D14	20/26 (79)	(90)

AI, Artificial Insemination; IVC, In vitro culture; SCNT, Somatic Cell Nuclear Transfer; "vit", vitrified/frozen.

LINEAGES SPECIFICATION MARKERS TO ASSESS EMBRYO QUALITY IN FARM ANIMALS

In vitro embryo production enables a myriad of applications in livestock species, ranging from boosting the number of embryos obtained from females of high genetic merit to overcoming infertility problems associated to heat stress (103–105). According to the International Embryo Transfer Society

(IETS), while the number of *in vivo* derived embryos transferred seems to have stabilized in cattle, the use of *in vitro*-produced (IVP) embryos is currently increasing (742,908 embryos transferred worldwide in 2018) (106). However, despite all efforts performed to optimize assisted reproductive technologies (ARTs), embryo production systems are still not fully efficient and important differences have been reported between *in vitro* and *in vivo* embryos (107). Many studies have shown that pregnancy rates after transfer of an *in vitro* embryo are between 10 and 40% lower than with embryos generated by artificial insemination or by Multiple Ovulation Embryo Transfer (MOET) (6, 108–111). As previously mentioned, IVP embryos often show compromised development of embryonic lineages—particularly the epiblast—following embryo transfer, and it has been estimated that 80% of pregnancy failures following embryo transfer of IVP embryos occur before day 40 of pregnancy (91). Unfortunately, these rates have not improved in the last decades.

In order to improve *in vitro* embryo production techniques, it is essential to assess embryo quality, i.e., the odds of post-transfer survival, to determine which modifications of current protocols are beneficial for subsequent embryo survival. Arguably, the best embryo quality assessment would be the analysis of embryo development following embryo transfer, but this test holds two major drawbacks (1) it is expensive, time-consuming and requires the use of experimental animals and (2) it is inherently bound to intrinsic variabilities in uterine receptivity between females (112, 113). Morphological evaluation (114), widely used both in humans and farm animals to select embryos before transfer due to its non-invasive nature, is certainly useful, as pregnancy rates are higher when better-quality grade embryos are transferred (115–118). However, embryo grade is a subjective criterion; it does not always reflect competence to establish pregnancy (119), and it does not necessarily infer proper development of embryonic lineages. For instance, early mouse mutant embryos lacking a specific cell lineage cannot be visually distinguished from their wildtype counterparts, although they hardly progress beyond implantation (37, 120–123). In this perspective, the analysis of the development of specific lineages provides deeper insights of embryo quality.

Successful development of the first cell lineages is essential for implantation and further development to term (124). The most commonly used method to analyse the first lineage differentiation (i.e., ICM vs. TE) in blastocysts from livestock species has been differential cell staining, a technique based on selective permeabilization of the outer blastocyst cells which will be subsequently stained with propidium iodide (125, 126). Unfortunately, this technique only provides information on cell location, but fails to assess if those cells are properly committed to TE or ICM, as the expression of specific lineage markers is not determined. Recent studies performing single-cell transcriptomics in farms animals have enabled the identification of lineage markers. The first study using this technology in mouse pre-implantation embryos (127) was soon followed by other reports in human (24, 48), monkey (49), cow (18, 19, 128) and pig (21), which revealed relevant differences between rodents and non-rodents mammals. In bovine, two studies based on single cell qPCR analysis of IVP morulae and expanded blastocysts observed that while some classical hypoblast markers in the mouse (*GATA6*, *GSC*, and *HNF4A*) were not specific to this lineage in bovine, *SOX17*, *GATA4*, and *PDGFRA* were largely specific (18, 19). Furthermore, the core pluripotency markers *NANOG*, *SOX2*, and *OCT4* were detected in epiblast cells, although *NANOG*, *FGF4*, and *TDGF1* were deemed as the most epiblast-specific, and trophectoderm cells exclusively expressed *CDX2*, *GATA2*, *GATA3, KRT8*, *PECAM1*, or *DAB2* (18, 19). In the pig, scRNAseq of *in vivo*-derived morulae, early and late blastocysts, and spherical embryos, revealed that although *NANOG*, *SOX2*, and *OCT4* are expressed in epiblast cells, *SOX2* is the most specific epiblast marker, followed by *NANOG* (21). *GATA2* and *GATA3* were reliable trophoblast markers, while *CDX2* was barely expressed in early blastocysts, and *TEAD4* was expressed in all cell lineages. Finally, hypoblast cells were characterized by specific expression of *SOX17*, *PDGFRA*, *GATA4*, or *NID2* (21).

Expression of different lineage-specific markers can be analyzed at the protein level through embryo immunostaining (**Figure 2**). Although most commercial antibodies are designed to react with mouse and human proteins, some of them can also be used to label pig, sheep and cow embryos (**Figure 3** and **Table 3**). Antibodies against the core pluripotency markers OCT4, NANOG, and SOX2 have been regularly used to label ICM and epiblast cells. Particular caution must be paid when analyzing OCT4, as this protein is expressed in all cell lineages in bovine and porcine blastocysts (25, 26, 130, 133), being its expression restricted to the epiblast only at later stages [E11 in bovine (25)]. NANOG protein has been specifically detected in ICM cells in bovine (26, 51, 131, 134) and porcine blastocysts (21). However, SOX2 seems to be the most specific epiblast marker in pig (21, 55, 130, 135), sheep (**Figure 2**) and bovine embryos (7, 30, 31, 131, 134). Regarding TE markers, CDX2 remains the most commonly used marker, being TE-specific in pig (26, 130), sheep (**Figure 2**) and cow blastocysts (7, 25, 26). In our experience (unpublished observations, **Figure 2**) GATA3 is also a reliable TE marker in porcine, ovine and bovine embryos. Finally, regarding to hypoblast, SOX17 specifically labels hypoblast cells from the blastocyst up to the elongated conceptus in bovine (7), ovine (**Figure 2**) and porcine embryos (21, 69). Other classical hypoblast markers in mice include GATA6, ubiquitously expressed in early blastocysts and becoming restricted to hypoblast cells in late bovine (26, 51), ovine (**Figure 2**) and porcine blastocysts (130), and GATA4, ubiquitously expressed in bovine late blastocysts and becoming specifically restricted to hypoblast cells in post-hatching E10.5 embryos (51, 129), and in some cells close to the epiblast in late pig blastocysts (132).

Similarly to the conventional quality assessment in blastocysts, the developmental analysis of elongated conceptuses has been traditionally based on morphology, generally limited to conceptus length (136–139). Conceptus length constitutes a good proxy for the development of extra-embryonic membranes but such development may not be coupled to the development of the epiblast, the most sensitive lineage. In other words, the "bigger is better" concept routinely applied to assess conceptus development may be wrong, as an structure only composed by EEMs (i.e., lacking an ED) will not develop any fetus. In this

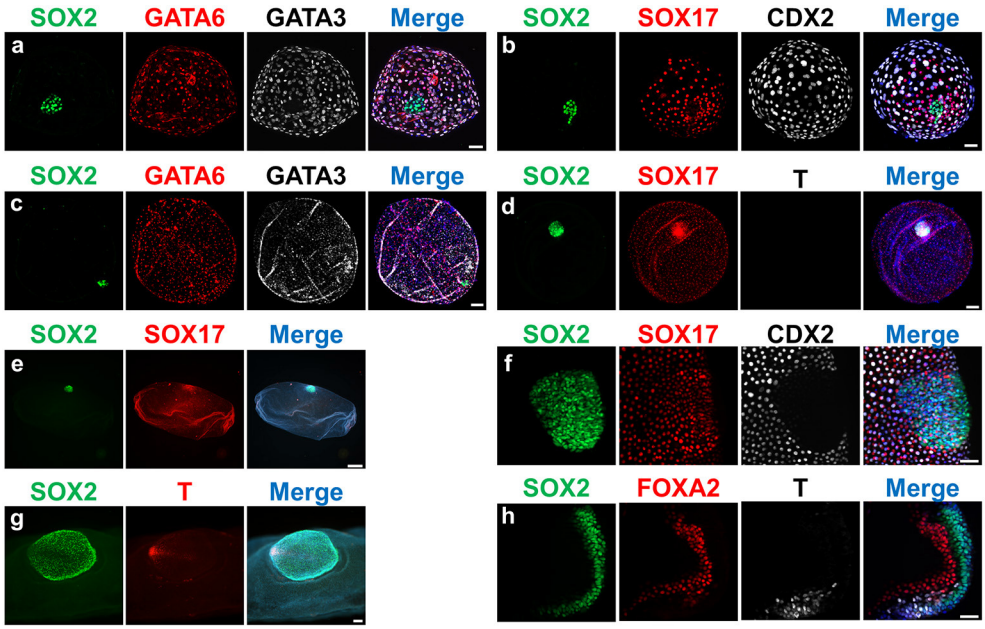

FIGURE 2 | Expression of lineage-specific markers in ovine embryos at different developmental stages. Fluorescence images of embryos stained for SOX2 (epiblast); SOX17/GATA6/FOXA2 (hypoblast/endoderm); CDX2/GATA3 (trophectoderm); T (mesoderm). Nuclei were counterstained with DAPI (merge). **(a,b)** D9 Hatched blastocysts; **(c,d)**: D11 Spherical embryos; **(e)** D13 Tubular embryo; **(f)** D13 ED without Rauber's layer; **(g)** gastrulating ED; **(h)** section of a gastrulating ED. Scale bars = 50 μm for **(a,b,f,h)**; 100 μm for **(c,d,g)**; 500 μm for panel **(e)**.

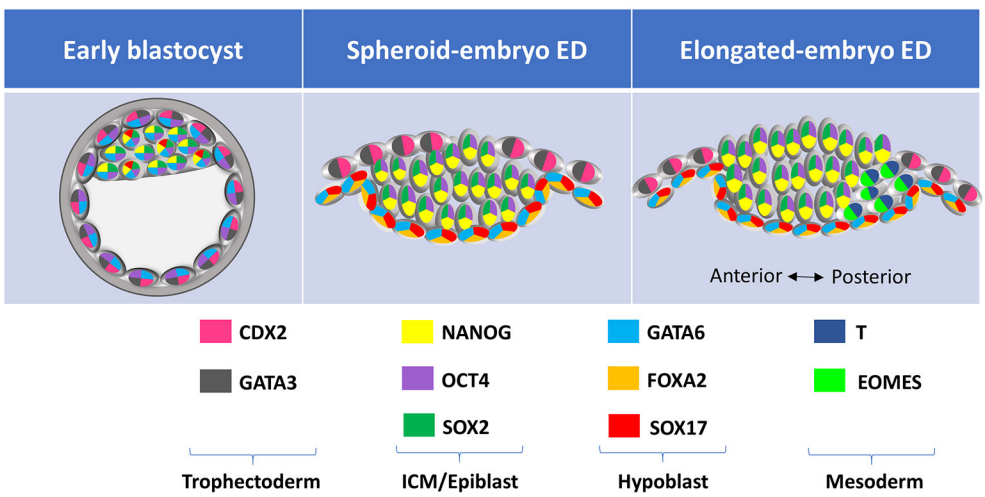

FIGURE 3 | Lineage-specific markers expressed at different developmental stages in farm ungulate embryos. ED, embryonic disc; ICM, inner cell mass; TE, trophectoderm.

regard, verifying the presence and proper development of the ED is essential to determine conceptus quality. To this aim, gastrulation markers have still not received as much attention as early lineages differentiation markers, since conceptuses at gastrulation stages are less accessible for experimental studies. However, BRACHYURY protein has been first observed in nascent mesoderm cells in the posterior epiblast of ovoid pig embryos (69, 71), and both BRACHYURY and EOMES are located in the posterior part of the ED at the same time that SOX2 expression is restricted to the anterior part in elongating sheep and cow embryos (**Figure 2**). Finally, SOX17 and FOXA2 are expressed in the migrated hypoblast and in the definitive endoderm in pig (71), sheep and cow elongating embryos (own unpublished observations, **Figure 2**).

TABLE 3 | Lineages-specific antibodies that label ungulate embryos.

Lineage	Marker	Species	Antibody	Reference
Inner cell mass/epiblast	OCT4	Bovine	Abcam, ab-19857	Own unpublished observations
			Santa Cruz, sc-8628*	(31)
			Santa Cruz, sc-9081*	(25)
		Porcine	Abcam, ab-27985	(129)
			Santa Cruz, sc-5279	(26)
			Santa Cruz, sc-8626*	(31, 55, 130)
	NANOG	Bovine	Abcam, ab-21603	(26)
			eBioscience 14-5768	(131)
		Porcine	Peprotech 500-P236	(21, 129, 132)
			Abnova, PAB6837	(130)
	SOX2	Bovine	R&D, AF2018	(131)
			Millipore, AB5603	(30)
			Biogenex, AN833-RTU	(31)
		Bovine, porcine	Santa Cruz, sc-17320*	(30, 130)
		Bovine, ovine, porcine	Invitrogen, 14-9811	(7) and own unpublished observations (**Figure 2**)
		Porcine	R&D, MAB2018	(129)
			Santa Cruz, sc-17320*	(55)
Trophectoderm	CDX2	Bovine	Abcam, ab-74339	(25)
		Bovine	Abcam, ab-7848	(31)
		Porcine, bovine	Chemicon, AB4123	(26)
		Bovine, ovine, porcine	Biogenex, MU392A-UC	(7, 130) and own unpublished observations (**Figure 2**)
	GATA3	Bovine, ovine, porcine	Abcam, ab-199428	Own unpublished observations (**Figure 2**)
Hypoblast/definitive endoderm	GATA6	Bovine	Santa Cruz, sc-9055*	(26)
		Bovine, ovine	R&D, AF1700	Own unpublished observations (**Figure 2**)
		Porcine	Abcam, Ab22600	(130)
	GATA4	Porcine	Santa Cruz, sc-25310	(129)
			Santa Cruz, sc-1237*	(132)
	SOX17	Bovine, ovine, porcine	R&D, AF1924	(7, 21, 69) and own unpublished observations (**Figure 2**)
	FOXA2	Bovine, ovine, porcine	Cell Signaling Technology, 8186S	(69) and own unpublished observations (**Figure 2**)
Mesoderm	T	Bovine, ovine, porcine	R&D, AF2085	(69) and own unpublished observations (**Figure 2**)
	EOMES	Porcine, ovine	R&D, MAB6166	(Own unpublished observations)

**These antibodies have been discontinued.*

POST-HATCHING *IN VITRO* DEVELOPMENT TO INFER EMBRYO QUALITY OF IVP EMBRYOS

Direct assessment of the developmental potential of IVP embryos beyond the blastocyst stage (i.e., during the most vulnerable period) has been traditionally hampered by the requirement of time and resource consuming *in vivo* experiments involving embryo transfer and posterior recovery (4, 89, 100, 138), as no *in vitro* system able to support embryo development beyond blastocyst hatching was available for any farm animal. In the last years, an increasing interest has been placed on developing post-blastocyst *in vitro* culture systems to better investigate embryo development and mortality during this developmental window in different mammalian species. Human embryos have been cultured in the absence of maternal tissues up to D13 (140, 141) in a system that also allows mouse post-blastocyst culture up to egg cylinders (142). This system was further improved to allow development of human embryos up to gastrulating stages, and deep embryo characterization by single-cell transcriptome and methylome mapping (143, 144).

In farm animals, hatched blastocysts attach to the bottom of the culture dish or grow in rounded form until they collapse under normal pre-hatching embryo culture conditions. Although explanted EDs were cultured *in vitro* in rabbits (145, 146), a livestock species where gastrulation also occurs in a flat embryonic disc, limited success was achieved in ungulates until recently. Pioneer studies established an *in vitro* post-hatching development (PHD) system based on agarose gel tunnels and serum- and glucose-enriched medium that achieved some expansion of the trophectoderm and certain proliferation of hypoblast cells in bovine embryos up to D15, but hypoblast migration was incomplete and epiblast cells were unable to survive (81–83). In order to promote the development of the epiblast—the most stringent cell lineage—we have developed a system based on N2B27 medium, a defined medium composed

by Neurobasal and DMEM/F12 media, and N2 and B27 supplements which was initially designed to culture neurons (147), and it was employed later for embryonic stem cells derivation and culture (148). Under this system, bovine (7) and ovine (own unpublished data) blastocysts develop beyond hatching, attaining complete hypoblast migration and epiblast survival and development into an early ED.

This pioneer system paves the way for future research focused on improving the conditions of *in vitro* embryo production or associated techniques such as embryo freezing or vitrification, as it allows direct embryo quality assessment without the need of experimental animals. The potential roles on lineages development of specific metabolites, hormones, or growth factors whose levels are altered in detrimental conditions for embryo survival, such as negative energy balance in post-partum dairy cows (90), can also be analyzed in this system.

CONCLUSIONS AND FUTURE DIRECTIONS

Being the most vulnerable period for embryo survival in ungulate species, conceptus elongation still constitutes a black box in Developmental Biology. Luckily, recent findings based on transcriptome analysis and gene ablation have started to shed light into the cell differentiation, proliferation and migration processes governing conceptus elongation, which in some cases differ greatly from those occurring in mice, the most studied mammalian model. The molecular markers of lineage differentiation in ungulates unveiled by these experiments are extremely useful to assess proper lineage development in *in vitro* produced embryos, where epiblast development has been highlighted as the major obstacle to attain a successful pregnancy. Besides, recent advances on *in vitro* culture have moved forward the limits of *in vitro* embryo development, providing a system to directly evaluate the developmental potential of IVP embryos during the most sensitive period for developmental failure. Such system provides a direct embryo quality assessment for testing diverse modifications in the IVP protocol or in associated techniques such as vitrification or freezing, aimed to improve pregnancy rates following embryo transfer.

DATA AVAILABILITY STATEMENT

The original contributions presented in the study are included in the article/supplementary material, further inquiries can be directed to the corresponding author/s.

AUTHOR CONTRIBUTIONS

All authors listed have made a substantial, direct and intellectual contribution to the work, and approved it for publication.

FUNDING

Research on conceptus elongation carried out by the authors and the publication costs of this review were funded by the projects StG-757886-ELONGAN from the European Research Council and AGL2017-58739-R from the Spanish Ministry of Economy and Competitiveness (MINECO). Images shown on **Figure 2** were taken on an equipment funded by the project ECQ2018-005184-P from MINECO. PR-I is funded by a Ramón y Cajal Contract from MINECO (RYC2018-025666-I).

ACKNOWLEDGMENTS

The authors thank the slaughterhouses Transformación Ganadera de Leganés SA, Matadero Madrid-Norte SA, and Matadero Mondejano SL (especially to Reyes Prieto Cabañas) for gently providing the ovaries required for research on ungulate lineage differentiation markers.

REFERENCES

1. Dunne LD, Diskin MG, Sreenan JM. Embryo and foetal loss in beef heifers between day 14 of gestation and full term. *Anim Reprod Sci.* (2000) 58:39–44. doi: 10.1016/S0378-4320(99)00088-3
2. Bennett GL, Leymaster KA. Integration of ovulation rate, potential embryonic viability and uterine capacity into a model of litter size in swine. *J Anim Sci.* (1989) 67:1230–41. doi: 10.2527/jas1989.6751230x
3. Maddox-Hyttel P, Alexopoulos NI, Vajta G, Lewis I, Rogers P, Cann L, et al. Immunohistochemical and ultrastructural characterization of the initial post-hatching development of bovine embryos. *Reproduction.* (2003) 125:607–23. doi: 10.1530/reprod/125.4.607
4. Berg DK, van Leeuwen J, Beaumont S, Berg M, Pfeffer PL. Embryo loss in cattle between Days 7 and 16 of pregnancy. *Theriogenology.* (2010) 73:250–60. doi: 10.1016/j.theriogenology.2009.09.005
5. Diskin MG, Morris DG. Embryonic and early foetal losses in cattle and other ruminants. *Reprod Domest Anim.* (2008) 43(Suppl 2):260–7. doi: 10.1111/j.1439-0531.2008.01171.x
6. Santos JE, Thatcher WW, Chebel RC, Cerri RL, Galvao KN. The effect of embryonic death rates in cattle on the efficacy of estrus synchronization programs. *Anim Reprod Sci.* (2004) 82–83:513–35. doi: 10.1016/j.anireprosci.2004.04.015
7. Ramos-Ibeas P, Lamas-Toranzo I, Martinez-Moro A, de Frutos C, Quiroga AC, Zurita E, et al. Embryonic disc formation following post-hatching bovine embryo development *in vitro*. *Reproduction.* (2020) 160:579–89. doi: 10.1530/REP-20-0243
8. Piliszek A, Madeja ZE. Pre-implantation development of domestic animals. *Curr Top Dev Biol.* (2018) 128:267–94. doi: 10.1016/bs.ctdb.2017.11.005
9. Korotkevich E, Niwayama R, Courtois A, Friese S, Berger N, Buchholz F, et al. The apical domain is required and sufficient for the first lineage segregation in the mouse embryo. *Dev Cell.* (2017) 40:235–47.e7. doi: 10.1016/j.devcel.2017.01.006
10. Maître JL, Turlier H, Illukkumbura R, Eismann B, Niwayama R, Nédélec F, et al. Asymmetric division of contractile domains couples cell positioning and fate specification. *Nature.* (2016) 536:344–8. doi: 10.1038/nature18958
11. Artus J, Hue I, Acloque H. Preimplantation development in ungulates: a 'menage a quatre' scenario. *Reproduction.* (2020) 159:R151–R72. doi: 10.1530/REP-19-0348
12. Wicklow E, Blij S, Frum T, Hirate Y, Lang RA, Sasaki H, et al. HIPPO pathway members restrict SOX2 to the inner cell mass where it promotes ICM fates in the mouse blastocyst. *PLoS Genet.* (2014) 10:e1004618. doi: 10.1371/journal.pgen.1004618
13. Ralston A, Cox BJ, Nishioka N, Sasaki H, Chea E, Rugg-Gunn P, et al. Gata3 regulates trophoblast development downstream of Tead4 and in

parallel to Cdx2. *Development.* (2010) 137:395–403. doi: 10.1242/dev.038828
14. Strumpf D, Mao CA, Yamanaka Y, Ralston A, Chawengsaksophak K, Beck F, et al. Cdx2 is required for correct cell fate specification and differentiation of trophectoderm in the mouse blastocyst. *Development.* (2005) 132:2093–102. doi: 10.1242/dev.01801
15. Hirate Y, Hirahara S, Inoue K, Suzuki A, Alarcon VB, Akimoto K, et al. Polarity-dependent distribution of angiomotin localizes Hippo signaling in preimplantation embryos. *Curr Biol.* (2013) 23:1181–94. doi: 10.1016/j.cub.2013.05.014
16. Niwa H, Toyooka Y, Shimosato D, Strumpf D, Takahashi K, Yagi R, et al. Interaction between Oct3/4 and Cdx2 determines trophectoderm differentiation. *Cell.* (2005) 123:917–29. doi: 10.1016/j.cell.2005.08.040
17. Ng RK, Dean W, Dawson C, Lucifero D, Madeja Z, Reik W, et al. Epigenetic restriction of embryonic cell lineage fate by methylation of Elf5. *Nat Cell Biol.* (2008) 10:1280–90. doi: 10.1038/ncb1786
18. Wei Q, Zhong L, Zhang S, Mu H, Xiang J, Yue L, et al. Bovine lineage specification revealed by single-cell gene expression analysis from zygote to blastocyst. *Biol Reprod.* (2017) 97:5–17. doi: 10.1093/biolre/iox071
19. Negron-Perez VM, Zhang Y, Hansen PJ. Single-cell gene expression of the bovine blastocyst. *Reproduction.* (2017) 154:627–44. doi: 10.1530/REP-17-0345
20. Gerri C, McCarthy A, Alanis-Lobato G, Demtschenko A, Bruneau A, Loubersac S, et al. Initiation of a conserved trophectoderm program in human, cow and mouse embryos. *Nature.* (2020) 587:443–7. doi: 10.1038/s41586-020-2759-x
21. Ramos-Ibeas P, Sang F, Zhu Q, Tang WWC, Withey S, Klisch D, et al. Pluripotency and X chromosome dynamics revealed in pig pre-gastrulating embryos by single cell analysis. *Nat Commun.* (2019) 10:500. doi: 10.1038/s41467-019-08387-8
22. Kong Q, Yang X, Zhang H, Liu S, Zhao J, Zhang J, et al. Lineage specification and pluripotency revealed by transcriptome analysis from oocyte to blastocyst in pig. *FASEB J.* (2020) 34:691–705. doi: 10.1096/fj.201901818RR
23. Niakan KK, Eggan K. Analysis of human embryos from zygote to blastocyst reveals distinct gene expression patterns relative to the mouse. *Dev Biol.* (2013) 375:54–64. doi: 10.1016/j.ydbio.2012.12.008
24. Blakeley P, Fogarty NM, del Valle I, Wamaitha SE, Hu TX, Elder K, et al. Defining the three cell lineages of the human blastocyst by single-cell RNA-seq. *Development.* (2015) 142:3151–65. doi: 10.1242/dev.123547
25. Berg DK, Smith CS, Pearton DJ, Wells DN, Broadhurst R, Donnison M, et al. Trophectoderm lineage determination in cattle. *Dev Cell.* (2011) 20:244–55. doi: 10.1016/j.devcel.2011.01.003
26. Kuijk EW, Du Puy L, Van Tol HT, Oei CH, Haagsman HP, Colenbrander B, et al. Differences in early lineage segregation between mammals. *Dev Dyn.* (2008) 237:918–27. doi: 10.1002/dvdy.21480
27. Bou G, Liu S, Sun M, Zhu J, Xue B, Guo J, et al. CDX2 is essential for cell proliferation and polarity in porcine blastocysts. *Development.* (2017) 144:1296–306. doi: 10.1242/dev.141085
28. Cauffman G, Van de Velde H, Liebaers I, Van Steirteghem A. Oct-4 mRNA and protein expression during human preimplantation development. *Mol Hum Reprod.* (2005) 11:173–81. doi: 10.1093/molehr/gah155
29. Kirchhof N, Carnwath JW, Lemme E, Anastassiadis K, Schöler H, Niemann H. Expression pattern of Oct-4 in preimplantation embryos of different species. *Biol Reprod.* (2000) 63:1698–705. doi: 10.1095/biolreprod63.6.1698
30. Goissis MD, Cibelli JB. Functional characterization of CDX2 during bovine preimplantation development *in vitro*. *Mol Reprod Dev.* (2014) 81:962–70. doi: 10.1002/mrd.22415
31. Daigneault BW, Rajput S, Smith GW, Ross PJ. Embryonic POU5F1 is required for expanded bovine blastocyst formation. *Sci Rep.* (2018) 8:7753. doi: 10.1038/s41598-018-25964-x
32. Fogarty NME, McCarthy A, Snijders KE, Powell BE, Kubikova N, Blakeley P, et al. Genome editing reveals a role for OCT4 in human embryogenesis. *Nature.* (2017) 550:67–73. doi: 10.1038/nature24033
33. Stamatiadis P, Boel A, Cosemans G, Popovic M, Bekaert B, Guggilla R, et al. Comparative analysis of mouse and human preimplantation development following POU5F1 CRISPR/Cas9 targeting reveals interspecies differences. *Hum Reprod.* (2021) 36:1242–52. doi: 10.1093/humrep/deab027
34. Sakurai N, Takahashi K, Emura N, Hashizume T, Sawai K. Effects of downregulating TEAD4 transcripts by RNA interference on early development of bovine embryos. *J Reprod Dev.* (2017) 63:135–42. doi: 10.1262/jrd.2016-130
35. Akizawa H, Kobayashi K, Bai H, Takahashi M, Kagawa S, Nagatomo H, et al. Reciprocal regulation of TEAD4 and CCN2 for the trophectoderm development of the bovine blastocyst. *Reproduction.* (2018) 155:563–71. doi: 10.1530/REP-18-0043
36. Nishioka N, Yamamoto S, Kiyonari H, Sato H, Sawada A, Ota M, et al. Tead4 is required for specification of trophectoderm in pre-implantation mouse embryos. *Mech Dev.* (2008) 125:270–83. doi: 10.1016/j.mod.2007.11.002
37. Yagi R, Kohn MJ, Karavanova I, Kaneko KJ, Vullhorst D, DePamphilis ML, et al. Transcription factor TEAD4 specifies the trophectoderm lineage at the beginning of mammalian development. *Development.* (2007) 134:3827–36. doi: 10.1242/dev.010223
38. Degrelle SA, Campion E, Cabau C, Piumi F, Reinaud P, Richard C, et al. Molecular evidence for a critical period in mural trophoblast development in bovine blastocysts. *Dev Biol.* (2005) 288:448–60. doi: 10.1016/j.ydbio.2005.09.043
39. Lamas-Toranzo I, Galiano-Cogolludo B, Cornudella-Ardiaca F, Cobos-Figueroa J, Ousinde O, Bermejo-Alvarez P. Strategies to reduce genetic mosaicism following CRISPR-mediated genome edition in bovine embryos. *Sci Rep.* (2019) 9:14900. doi: 10.1038/s41598-019-51366-8
40. Lamas-Toranzo I, Martinez-Moro A, E OC, Millan-Blanca G, Sanchez JM, Lonergan P, et al. RS-1 enhances CRISPR-mediated targeted knock-in in bovine embryos. *Mol Reprod Dev.* (2020) 87:542–9. doi: 10.1002/mrd.23341
41. Lamas-Toranzo I, Fonseca Balvis N, Querejeta-Fernandez A, Izquierdo-Rico MJ, Gonzalez-Brusi L, Lorenzo PL, et al. ZP4 confers structural properties to the zona pellucida essential for embryo development. *Elife.* (2019) 8:e48904. doi: 10.7554/eLife.48904
42. Meyer AE, Pfeiffer CA, Brooks KE, Spate LD, Benne JA, Cecil R, et al. New perspective on conceptus estrogens in maternal recognition and pregnancy establishment in the pigdagger. *Biol Reprod.* (2019) 101:148–61. doi: 10.1093/biolre/ioz058
43. Plusa B, Piliszek A, Frankenberg S, Artus J, Hadjantonakis AK. Distinct sequential cell behaviours direct primitive endoderm formation in the mouse blastocyst. *Development.* (2008) 135:3081–91. doi: 10.1242/dev.021519
44. Artus J, Piliszek A, Hadjantonakis AK. The primitive endoderm lineage of the mouse blastocyst: sequential transcription factor activation and regulation of differentiation by Sox17. *Dev Biol.* (2011) 350:393–404. doi: 10.1016/j.ydbio.2010.12.007
45. Chazaud C, Yamanaka Y. Lineage specification in the mouse preimplantation embryo. *Development.* (2016) 143:1063–74. doi: 10.1242/dev.128314
46. Frankenberg SR, de Barros FR, Rossant J, Renfree MB. The mammalian blastocyst. *Wiley Interdiscip Rev Dev Biol.* (2016) 5:210–32. doi: 10.1002/wdev.220
47. Bessonnard S, De Mot L, Gonze D, Barriol M, Dennis C, Goldbeter A, et al. Gata6, Nanog and Erk signaling control cell fate in the inner cell mass through a tristable regulatory network. *Development.* (2014) 141:3637–48. doi: 10.1242/dev.109678
48. Petropoulos S, Edsgard D, Reinius B, Deng Q, Panula SP, Codeluppi S, et al. Single-cell RNA-seq reveals lineage and X chromosome dynamics in human preimplantation embryos. *Cell.* (2016) 165:1012–26. doi: 10.1016/j.cell.2016.03.023
49. Nakamura T, Okamoto I, Sasaki K, Yabuta Y, Iwatani C, Tsuchiya H, et al. A developmental coordinate of pluripotency among mice, monkeys and humans. *Nature.* (2016) 537:57–62. doi: 10.1038/nature19096
50. Stirparo GG, Boroviak T, Guo G, Nichols J, Smith A, Bertone P. Integrated analysis of single-cell embryo data yields a unified transcriptome signature for the human pre-implantation epiblast. *Development.* (2018) 145:dev158501. doi: 10.1242/dev.158501
51. Kuijk EW, van Tol LT, Van de Velde H, Wubbolts R, Welling M, Geijsen N, et al. The roles of FGF and MAP kinase signaling in the segregation of the epiblast and hypoblast cell lineages in bovine and human embryos. *Development.* (2012) 139:871–82. doi: 10.1242/dev.071688
52. Cauffman G, De Rycke M, Sermon K, Liebaers I, Van de Velde H. Markers that define stemness in ESC are unable to identify the totipotent

cells in human preimplantation embryos. *Hum Reprod.* (2009) 24:63–70. doi: 10.1093/humrep/den351
53. Williams BS, Biggers JD. Polar trophoblast (Rauber's layer) of the rabbit blastocyst. *Anat Rec.* (1990) 227:211–22. doi: 10.1002/ar.1092270210
54. van Leeuwen J, Rawson P, Berg DK, Wells DN, Pfeffer PL. On the enigmatic disappearance of Rauber's layer. *Proc Natl Acad Sci U S A.* (2020) 117:16409–17. doi: 10.1073/pnas.2002008117
55. Sun R, Lei L, Liu S, Xue B, Wang J, Shen J, et al. Morphological changes and germ layer formation in the porcine embryos from days 7-13 of development. *Zygote.* (2015) 23:266–76. doi: 10.1017/S0967199413000531
56. Enders AC, Lantz KC, Liu IK, Schlafke S. Loss of polar trophoblast during differentiation of the blastocyst of the horse. *J Reprod Fertil.* (1988) 83:447–60. doi: 10.1530/jrf.0.0830447
57. Geisert RD, Brookbank JW, Roberts RM, Bazer FW. Establishment of pregnancy in the pig: II. Cellular remodeling of the porcine blastocyst during elongation on day 12 of pregnancy. *Biol Reprod.* (1982) 27:941–55. doi: 10.1095/biolreprod27.4.941
58. Waclawik A, Kaczmarek MM, Blitek A, Kaczynski P, Ziecik AJ. Embryo-maternal dialogue during pregnancy establishment and implantation in the pig. *Mol Reprod Dev.* (2017) 84:842–55. doi: 10.1002/mrd.22835
59. Guillomot M, Turbe A, Hue I, Renard JP. Staging of ovine embryos and expression of the T-box genes Brachyury and Eomesodermin around gastrulation. *Reproduction.* (2004) 127:491–501. doi: 10.1530/rep.1.00057
60. Bazer FW, Spencer TE, Johnson GA, Burghardt RC, Wu G. Comparative aspects of implantation. *Reproduction.* (2009) 138:195–209. doi: 10.1530/REP-09-0158
61. Johnson AD, Alberio R. Primordial germ cells: the first cell lineage or the last cells standing? *Development.* (2015) 142:2730–9. doi: 10.1242/dev.113993
62. Gao Y, Hyttel P, Hall VJ. Dynamic changes in epigenetic marks and gene expression during porcine epiblast specification. *Cell Reprogram.* (2011) 13:345–60. doi: 10.1089/cell.2010.0110
63. Oestrup O, Hall V, Petkov SG, Wolf XA, Hyldig S, Hyttel P. From zygote to implantation: morphological and molecular dynamics during embryo development in the pig. *Reprod Domest Anim.* (2009) 44(Suppl. 3):39–49. doi: 10.1111/j.1439-0531.2009.01482.x
64. Hall VJ, Jacobsen JV, Rasmussen MA, Hyttel P. Ultrastructural and molecular distinctions between the porcine inner cell mass and epiblast reveal unique pluripotent cell states. *Dev Dyn.* (2010) 239:2911–20. doi: 10.1002/dvdy.22424
65. van Leeuwen J, Berg DK, Pfeffer PL. Morphological and gene expression changes in cattle embryos from hatched blastocyst to early gastrulation stages after transfer of *in vitro* produced embryos. *PLoS One.* (2015) 10:e0129787. doi: 10.1371/journal.pone.0129787
66. Hertig AT, Rock J, Adams EC. A description of 34 human ova within the first 17 days of development. *J Anat.* (1956) 98:435–93. doi: 10.1002/aja.1000980306
67. Luckett WP. Origin and differentiation of the yolk sac and extraembryonic mesoderm in presomite human and rhesus monkey embryos. *J Anat.* (1978) 152:59–97. doi: 10.1002/aja.1001520106
68. Bedzhov I, Zernicka-Goetz M. Self-organizing properties of mouse pluripotent cells initiate morphogenesis upon implantation. *Cell.* (2014) 156:1032–44. doi: 10.1016/j.cell.2014.01.023
69. Kobayashi T, Zhang H, Tang WWC, Irie N, Withey S, Klisch D, et al. Principles of early human development and germ cell program from conserved model systems. *Nature.* (2017) 546:416–20. doi: 10.1038/nature22812
70. Gaivão MM, Rambags BP, Stout TA. Gastrulation and the establishment of the three germ layers in the early horse conceptus. *Theriogenology.* (2014) 82:354–65. doi: 10.1016/j.theriogenology.2014.04.018
71. Wolf XA, Serup P, Hyttel P. Three-dimensional immunohistochemical characterization of lineage commitment by localization of T and FOXA2 in porcine peri-implantation embryos. *Dev Dyn.* (2011) 240:890–7. doi: 10.1002/dvdy.22602
72. Idkowiak J, Weisheit G, Plitzner J, Viebahn C. Hypoblast controls mesoderm generation and axial patterning in the gastrulating rabbit embryo. *Dev Genes Evol.* (2004) 214:591–605. doi: 10.1007/s00427-004-0436-y
73. Alev C, Wu Y, Kasukawa T, Jakt LM, Ueda HR, Sheng G. Transcriptomic landscape of the primitive streak. *Development.* (2010) 137:2863–74. doi: 10.1242/dev.053462
74. Tam PP, Beddington RS. The formation of mesodermal tissues in the mouse embryo during gastrulation and early organogenesis. *Development.* (1987) 99:109–26. doi: 10.1242/dev.99.1.109
75. Eakin GS, Behringer RR. Diversity of germ layer and axis formation among mammals. *Semin Cell Dev Biol.* (2004) 15:619–29. doi: 10.1016/j.semcdb.2004.04.008
76. Hue I, Renard JP, Viebahn C. Brachyury is expressed in gastrulating bovine embryos well ahead of implantation. *Dev Genes Evol.* (2001) 211:157–9. doi: 10.1007/s004270100138
77. Blomberg Le A, Garrett WM, Guillomot M, Miles JR, Sonstegard TS, Van Tassell CP, et al. Transcriptome profiling of the tubular porcine conceptus identifies the differential regulation of growth and developmentally associated genes. *Mol Reprod Dev.* (2006) 73:1491–502. doi: 10.1002/mrd.20503
78. Talbot NC, Caperna TJ, Edwards JL, Garrett W, Wells KD, Ealy AD. Bovine blastocyst-derived trophectoderm and endoderm cell cultures: interferon tau and transferrin expression as respective *in vitro* markers. *Biol Reprod.* (2000) 62:235–47. doi: 10.1095/biolreprod62.2.235
79. Ramos-Ibeas P, Calle A, Pericuesta E, Laguna-Barraza R, Moros-Mora R, Lopera-Vasquez R, et al. An efficient system to establish biopsy-derived trophoblastic cell lines from bovine embryos. *Biol Reprod.* (2014) 91:15. doi: 10.1095/biolreprod.114.118430
80. Ramos-Ibeas P, Nichols J, Alberio R. States and origins of mammalian embryonic pluripotency *in vivo* and in a dish. *Curr Top Dev Biol.* (2018) 128:151–79. doi: 10.1016/bs.ctdb.2017.11.002
81. Brandao DO, Maddox-Hyttel P, Lovendahl P, Rumpf R, Stringfellow D, Callesen H. Post hatching development: a novel system for extended *in vitro* culture of bovine embryos. *Biol Reprod.* (2004) 71:2048–55. doi: 10.1095/biolreprod.103.025916
82. Vajta G, Alexopoulos NI, Callesen H. Rapid growth and elongation of bovine blastocysts *in vitro* in a three-dimensional gel system. *Theriogenology.* (2004) 62:1253–63. doi: 10.1016/j.theriogenology.2004.01.007
83. Machado GM, Ferreira AR, Pivato I, Fidelis A, Spricigo JF, Paulini F, et al. Post-hatching development of *in vitro* bovine embryos from day 7 to 14 *in vivo* versus *in vitro*. *Mol Reprod Dev.* (2013) 80:936–47. doi: 10.1002/mrd.22230
84. Bertolini M, Beam SW, Shim H, Bertolini LR, Moyer AL, Famula TR, et al. Growth, development, and gene expression by *in vivo*- and *in vitro*-produced day 7 and 16 bovine embryos. *Mol Reprod Dev.* (2002) 63:318–28. doi: 10.1002/mrd.90015
85. Loureiro B, Block J, Favoreto MG, Carambula S, Pennington KA, Ealy AD, et al. Consequences of conceptus exposure to colony-stimulating factor 2 on survival, elongation, interferon-τ secretion, and gene expression. *Reproduction.* (2011) 141:617–24. doi: 10.1530/REP-10-0511
86. Block J, Fischer-Brown AE, Rodina TM, Ealy AD, Hansen PJ. The effect of *in vitro* treatment of bovine embryos with IGF-1 on subsequent development in utero to Day 14 of gestation. *Theriogenology.* (2007) 68:153–61. doi: 10.1016/j.theriogenology.2007.04.045
87. Fischer-Brown AE, Lindsey BR, Ireland FA, Northey DL, Monson RL, Clark SG, et al. Embryonic disc development and subsequent viability of cattle embryos following culture in two media under two oxygen concentrations. *Reprod Fertil Dev.* (2004) 16:787–93. doi: 10.1071/RD04026
88. Bertolini M, Mason JB, Beam SW, Carneiro GF, Sween ML, Kominek DJ, et al. Morphology and morphometry of *in vivo*- and *in vitro*-produced bovine concepti from early pregnancy to term and association with high birth weights. *Theriogenology.* (2002) 58:973–94. doi: 10.1016/S0093-691X(02)00935-4
89. Alexopoulos NI, Maddox-Hyttel P, Tveden-Nyborg P, D'Cruz NT, Tecirlioglu TR, Cooney MA, et al. Developmental disparity between *in vitro*-produced and somatic cell nuclear transfer bovine days 14 and 21 embryos: implications for embryonic loss. *Reproduction.* (2008) 136:433–45. doi: 10.1530/REP-07-0392
90. Desmet KLJ, Marei WFA, Richard C, Sprangers K, Beemster GTS, Meysman P, et al. Oocyte maturation under lipotoxic conditions induces carryover transcriptomic and functional alterations during post-hatching development

of good-quality blastocysts: novel insights from a bovine embryo-transfer model. *Hum Reprod.* (2020) 35:293–307. doi: 10.1093/humrep/dez248
91. Ealy AD, Wooldridge LK, McCoski SR. BOARD INVITED REVIEW: post-transfer consequences of *in vitro*-produced embryos in cattle. *J Anim Sci.* (2019) 97:2555–68. doi: 10.1093/jas/skz116
92. Chavatte-Palmer P, Camous S, Jammes H, Le Cleac'h N, Guillomot M, Lee RS. Review: Placental perturbations induce the developmental abnormalities often observed in bovine somatic cell nuclear transfer. *Placenta.* (2012) 33(Suppl.):S99–S104. doi: 10.1016/j.placenta.2011.09.012
93. Hall V, Hinrichs K, Lazzari G, Betts DH, Hyttel P. Early embryonic development, assisted reproductive technologies, and pluripotent stem cell biology in domestic mammals. *Vet J.* (2013) 197:128–42. doi: 10.1016/j.tvjl.2013.05.026
94. Tveden-Nyborg P, Peura TT, Hartwich KM, Walker SK, Maddox-Hyttel P. Morphological characterization of pre- and peri-implantation *in vitro* cultured, somatic cell nuclear transfer and *in vivo* derived ovine embryos. *Reproduction.* (2005) 130:681–94. doi: 10.1530/rep.1.00850
95. Fabreges D, Daniel N, Duranthon V, Peyrieras N. Control of the proportion of inner cells by asymmetric divisions and the ensuing resilience of cloned rabbit embryos. *Development.* (2018) 145:dev152041. doi: 10.1242/dev.152041
96. Ideta A, Urakawa M, Aoyagi Y, Saeki K. Early development in utero of bovine nuclear transfer embryos using early G1 and G0 phase cells. *Cloning Stem Cells.* (2007) 9:571–80. doi: 10.1089/clo.2007.0017
97. Rodríguez-Alvarez L, Sharbati J, Sharbati S, Cox JF, Einspanier R, Castro FO. Differential gene expression in bovine elongated (Day 17) embryos produced by somatic cell nucleus transfer and *in vitro* fertilization. *Theriogenology.* (2010) 74:45–59. doi: 10.1016/j.theriogenology.2009.12.018
98. Degrelle SA, Jaffrezic F, Campion E, Le Cao KA, Le Bourhis D, Richard C, et al. Uncoupled embryonic and extra-embryonic tissues compromise blastocyst development after somatic cell nuclear transfer. *PLoS One.* (2012) 7:e38309. doi: 10.1371/journal.pone.0038309
99. Smith CS, Berg DK, Berg M, Pfeffer PL. Nuclear transfer-specific defects are not apparent during the second week of embryogenesis in cattle. *Cell Reprogram.* (2010) 12:699–707. doi: 10.1089/cell.2010.0040
100. van Leeuwen J, Berg DK, Smith CS, Wells DN, Pfeffer PL. Specific epiblast loss and hypoblast impairment in cattle embryos sensitized to survival signalling by ubiquitous overexpression of the proapoptotic gene BAD. *PLoS One.* (2014) 9:e96843. doi: 10.1371/journal.pone.0096843
101. Oda M, Shiota K, Tanaka S. Trophoblast cell lineage in cloned mouse embryos. *Dev Growth Differ.* (2010) 52:285–91. doi: 10.1111/j.1440-169X.2010.01173.x
102. Hirasawa R, Matoba S, Inoue K, Ogura A. Somatic donor cell type correlates with embryonic, but not extra-embryonic, gene expression in postimplantation cloned embryos. *PLoS One.* (2013) 8:e76422. doi: 10.1371/journal.pone.0076422
103. Ealy AD, Drost M, Hansen PJ. Developmental changes in embryonic resistance to adverse effects of maternal heat stress in cows. *J Dairy Sci.* (1993) 76:2899–905. doi: 10.3168/jds.S0022-0302(93)77629-8
104. Looney CR, Lindsey BR, Gonseth CL, Johnson DL. COMMERCIAL ASPECTS OF OOCYTE RETRIEVAL AND IN-*VITRO* FERTILIZATION (IVF) FOR EMBRYO PRODUCTION IN PROBLEM COWS. *Theriogenology.* (1994) 41:67–72. doi: 10.1016/S0093-691X(05)80050-0
105. Block J, Bonilla L, Hansen PJ. Efficacy of *in vitro* embryo transfer in lactating dairy cows using fresh or vitrified embryos produced in a novel embryo culture medium. *J Dairy Sci.* (2010) 93:5234–42. doi: 10.3168/jds.2010-3443
106. Viana J. *Embryo Technology Newsletter.* International Embryo Transfer Society (2019).
107. Ramos-Ibeas P, Heras S, Gómez-Redondo I, Planells B, Fernández-González R, Pericuesta E, et al. Embryo responses to stress induced by assisted reproductive technologies. *Mol Reprod Dev.* (2019) 86:1292–306. doi: 10.1002/mrd.23119
108. Lucy MC. Reproductive loss in high-producing dairy cattle: where will it end? *J Dairy Sci.* (2001) 84:1277–93. doi: 10.3168/jds.S0022-0302(01)70158-0
109. Wiltbank MC, Baez GM, Garcia-Guerra A, Toledo MZ, Monteiro PL, Melo LF, et al. Pivotal periods for pregnancy loss during the first trimester of gestation in lactating dairy cows. *Theriogenology.* (2016) 86:239–53. doi: 10.1016/j.theriogenology.2016.04.037
110. Gatea AO, Smith MF, Pohler KG, Egen T, Pereira MHC, Vasconselos JLM, et al. The ability to predict pregnancy loss in cattle with ELISAs that detect pregnancy associated glycoproteins is antibody dependent. *Theriogenology.* (2018) 108:269–76. doi: 10.1016/j.theriogenology.2017.12.021
111. Pohler KG, Green JA, Geary TW, Peres RF, Pereira MH, Vasconcelos JL, et al. Predicting embryo presence and viability. *Adv Anat Embryol Cell Biol.* (2015) 216:253–70. doi: 10.1007/978-3-319-15856-3_13
112. Estrada-Cortes E, Ortiz WG, Chebel RC, Jannaman EA, Moss JI, de Castro FC, et al. Embryo and cow factors affecting pregnancy per embryo transfer for multiple-service, lactating Holstein recipients. *Transl Anim Sci.* (2019) 3:60–5. doi: 10.1093/tas/txz009
113. Geary TW, Burns GW, Moraes JG, Moss JI, Denicol AC, Dobbs KB, et al. Identification of beef heifers with superior uterine capacity for pregnancy. *Biol Reprod.* (2016) 95:47. doi: 10.1095/biolreprod.116.141390
114. Stringfellow D, Givens M. *Manual of the International Embryo Transfer Society (IETS), 4th Edn.* Champaign: IETS (2010).
115. Farin PW, Slenning BD, Britt JH. Estimates of pregnancy outcomes based on selection of bovine embryos produced *in vivo* or *in vitro*. *Theriogenology.* (1999) 52:659–70. doi: 10.1016/S0093-691X(99)00160-0
116. Hasler JF, Henderson WB, Hurtgen PJ, Jin ZQ, McCauley AD, Mower SA, et al. PRODUCTION, FREEZING AND TRANSFER OF BOVINE IVF EMBRYOS AND SUBSEQUENT CALVING RESULTS. *Theriogenology.* (1995) 43:141–52. doi: 10.1016/0093-691X(94)00020-U
117. Hasler JF. Factors affecting frozen and fresh embryo transfer pregnancy rates in cattle. *Theriogenology.* (2001) 56:1401–15. doi: 10.1016/S0093-691X(01)00643-4
118. Chebel RC, Demétrio DG, Metzger J. Factors affecting success of embryo collection and transfer in large dairy herds. *Theriogenology.* (2008) 69:98–106. doi: 10.1016/j.theriogenology.2007.09.008
119. Hansen PJ. The incompletely fulfilled promise of embryo transfer in cattle-why aren't pregnancy rates greater and what can we do about it? *J Anim Sci.* (2020) 98:skaa288. doi: 10.1093/jas/skaa288
120. Nichols J, Zevnik B, Anastassiadis K, Niwa H, Klewe-Nebenius D, Chambers I, et al. Formation of pluripotent stem cells in the mammalian embryo depends on the POU transcription factor Oct4. *Cell.* (1998) 95:379–91. doi: 10.1016/S0092-8674(00)81769-9
121. Mitsui K, Tokuzawa Y, Itoh H, Segawa K, Murakami M, Takahashi K, et al. The homeoprotein Nanog is required for maintenance of pluripotency in mouse epiblast and ES cells. *Cell.* (2003) 113:631–42. doi: 10.1016/S0092-8674(03)00393-3
122. Chazaud C, Yamanaka Y, Pawson T, Rossant J. Early lineage segregation between epiblast and primitive endoderm in mouse blastocysts through the Grb2-MAPK pathway. *Dev Cell.* (2006) 10:615–24. doi: 10.1016/j.devcel.2006.02.020
123. Kang M, Piliszek A, Artus J, Hadjantonakis AK. FGF4 is required for lineage restriction and salt-and-pepper distribution of primitive endoderm factors but not their initial expression in the mouse. *Development.* (2013) 140:267–79. doi: 10.1242/dev.084996
124. Piliszek A, Grabarek JB, Frankenberg SR, Plusa B. Cell fate in animal and human blastocysts and the determination of viability. *Mol Hum Reprod.* (2016) 22:681–90. doi: 10.1093/molehr/gaw002
125. Fouladi-Nashta AA, Alberio R, Kafi M, Nicholas B, Campbell KH, Webb R. Differential staining combined with TUNEL labelling to detect apoptosis in preimplantation bovine embryos. *Reprod Biomed Online.* (2005) 10:497–502. doi: 10.1016/S1472-6483(10)60827-9
126. Thouas GA, Korfiatis NA, French AJ, Jones GM, Trounson AO. Simplified technique for differential staining of inner cell mass and trophectoderm cells of mouse and bovine blastocysts. *Reprod Biomed Online.* (2001) 3:25–9. doi: 10.1016/S1472-6483(10)61960-8
127. Deng Q, Ramskold D, Reinius B, Sandberg R. Single-cell RNA-seq reveals dynamic, random monoallelic gene expression in mammalian cells. *Science.* (2014) 343:193–6. doi: 10.1126/science.1245316
128. Lavagi I, Krebs S, Simmet K, Beck A, Zakhartchenko V, Wolf E, et al. Single-cell RNA sequencing reveals developmental heterogeneity of blastomeres during major genome activation in bovine embryos. *Sci Rep.* (2018) 8:4071. doi: 10.1038/s41598-018-22248-2
129. du Puy L, Lopes SM, Haagsman HP, Roelen BA. Analysis of co-expression of OCT4, NANOG and SOX2 in pluripotent cells of the

porcine embryo, *in vivo* and *in vitro*. *Theriogenology.* (2011) 75:513–26. doi: 10.1016/j.theriogenology.2010.09.019
130. Cao S, Han J, Wu J, Li Q, Liu S, Zhang W, et al. Specific gene-regulation networks during the pre-implantation development of the pig embryo as revealed by deep sequencing. *BMC Genomics.* (2014) 15:4. doi: 10.1186/1471-2164-15-4
131. Meng F, Forrester-Gauntlett B, Turner P, Henderson H, Oback B. Signal inhibition reveals JAK/STAT3 pathway as critical for bovine inner cell mass development. *Biol Reprod.* (2015) 93:132. doi: 10.1095/biolreprod.115.134254
132. Rodriguez A, Allegrucci C, Alberio R. Modulation of pluripotency in the porcine embryo and iPS cells. *PLoS One.* (2012) 7:e49079. doi: 10.1371/journal.pone.0049079
133. van Eijk MJ, van Rooijen MA, Modina S, Scesi L, Folkers G, van Tol HT, et al. Molecular cloning, genetic mapping, and developmental expression of bovine POU5F1. *Biol Reprod.* (1999) 60:1093–103. doi: 10.1095/biolreprod60.5.1093
134. Khan DR, Dube D, Gall L, Peynot N, Ruffini S, Laffont L, et al. Expression of pluripotency master regulators during two key developmental transitions: EGA and early lineage specification in the bovine embryo. *PLoS One.* (2012) 7:e34110. doi: 10.1371/journal.pone.0034110
135. Liu S, Bou G, Sun R, Guo S, Xue B, Wei R, et al. Sox2 is the faithful marker for pluripotency in pig: evidence from embryonic studies. *Dev Dyn.* (2015) 244:619–27. doi: 10.1002/dvdy.24248
136. Lonergan P, Woods A, Fair T, Carter F, Rizos D, Ward F, et al. Effect of embryo source and recipient progesterone environment on embryo development in cattle. *Reprod Fertil Dev.* (2007) 19:861–8. doi: 10.1071/RD07089
137. Barnwell CV, Farin PW, Whisnant CS, Alexander JE, Farin CE. Maternal serum progesterone concentration and early conceptus development of bovine embryos produced *in vivo* or *in vitro*. *Domest Anim Endocrinol.* (2015) 52:75–81. doi: 10.1016/j.domaniend.2015.03.004
138. Clemente M, de La Fuente J, Fair T, Al Naib A, Gutierrez-Adan A, Roche JF, et al. Progesterone and conceptus elongation in cattle: a direct effect on the embryo or an indirect effect via the endometrium? *Reproduction.* (2009) 138:507–17. doi: 10.1530/REP-09-0152
139. Barnwell CV, Farin PW, Ashwell CM, Farmer WT, Galphin SP, Jr., et al. Differences in mRNA populations of short and long bovine conceptuses on Day 15 of gestation. *Mol Reprod Dev.* (2016) 83:424–41. doi: 10.1002/mrd.22640
140. Deglincerti A, Croft GF, Pietila LN, Zernicka-Goetz M, Siggia ED, Brivanlou AH. Self-organization of the *in vitro* attached human embryo. *Nature.* (2016) 533:251–4. doi: 10.1038/nature17948
141. Shahbazi MN, Jedrusik A, Vuoristo S, Recher G, Hupalowska A, Bolton V, et al. Self-organization of the human embryo in the absence of maternal tissues. *Nat Cell Biol.* (2016) 18:700–8. doi: 10.1038/ncb3347
142. Bedzhov I, Leung CY, Bialecka M, Zernicka-Goetz M. *In vitro* culture of mouse blastocysts beyond the implantation stages. *Nat Protoc.* (2014) 9:2732–9. doi: 10.1038/nprot.2014.186
143. Xiang L, Yin Y, Zheng Y, Ma Y, Li Y, Zhao Z, et al. A developmental landscape of 3D-cultured human pre-gastrulation embryos. *Nature.* (2020) 577:537–42. doi: 10.1038/s41586-019-1875-y
144. Zhou F, Wang R, Yuan P, Ren Y, Mao Y, Li R, et al. Reconstituting the transcriptome and DNA methylome landscapes of human implantation. *Nature.* (2019) 572:660–4. doi: 10.1038/s41586-019-1500-0
145. Stankova V, Tsikolia N, Viebahn C. Rho kinase activity controls directional cell movements during primitive streak formation in the rabbit embryo. *Development.* (2015) 142:92–8. doi: 10.1242/dev.111583
146. Puschel B, Bitzer E, Viebahn C. Live rabbit embryo culture. *Cold Spring Harb Protoc.* (2010) 2010:pdb prot5352. doi: 10.1101/pdb.prot5352
147. Brewer GJ, Torricelli JR, Evege EK, Price PJ. Optimized survival of hippocampal neurons in B27-supplemented Neurobasal, a new serum-free medium combination. *J Neurosci Res.* (1993) 35:567–76. doi: 10.1002/jnr.490350513
148. Nichols J, Ying QL. Derivation and propagation of embryonic stem cells in serum- and feeder-free culture. *Methods Mol Biol.* (2006) 329:91–8. doi: 10.1385/1-59745-037-5:91

Conflict of Interest: The authors declare that the research was conducted in the absence of any commercial or financial relationships that could be construed as a potential conflict of interest.

frontiers in Veterinary Science

ORIGINAL RESEARCH
published: 14 July 2021
doi: 10.3389/fvets.2021.680182

Whole-Transcriptome Analysis of LncRNAs Mediated ceRNA Regulation in Granulosa Cells Isolated From Healthy and Atresia Follicles of Chinese Buffalo

Yu Pan†, Sufang Yang†, Juanru Cheng, Qiao Lv, Qinghua Xing, Ruimen Zhang, Jingyuan Liang, Deshun Shi and Yanfei Deng**

State Key Laboratory for Conservation and Utilization of Subtropical Agro-Bioresources, Animal Reproduction Institute, Guangxi University, Nanning, China

OPEN ACCESS

Edited by:
Jordi Roca, University of Murcia, Spain

Reviewed by:
Jitender Kumar Bhardwaj, Kurukshetra University, India
Abouzar Najafi, University of Tehran, Iran

***Correspondence:**
Deshun Shi
ardsshi@gxu.edu.cn
Yanfei Deng
yanfei-dun@163.com

†These authors have contributed equally to this work

Specialty section:
This article was submitted to Animal Reproduction - Theriogenology, a section of the journal Frontiers in Veterinary Science

Received: *13 March 2021*
Accepted: *09 June 2021*
Published: *14 July 2021*

Citation:
Pan Y, Yang S, Cheng J, Lv Q, Xing Q, Zhang R, Liang J, Shi D and Deng Y (2021) Whole-Transcriptome Analysis of LncRNAs Mediated ceRNA Regulation in Granulosa Cells Isolated From Healthy and Atresia Follicles of Chinese Buffalo. Front. Vet. Sci. 8:680182. doi: 10.3389/fvets.2021.680182

Granulosa cells (GCs) are the main supporting cells in follicles and play an important role in the regulation of oocyte maturation and follicular atresia. Accumulating evidence indicates that non-coding RNAs participate in regulation of the physiological function of GCs. However, whole-transcriptome analysis for GCs of buffalo has yet to be reported. In this study, healthy follicles (HFs) and atretic follicles (AFs) were defined according to the apoptosis rate of GCs and the hormone level in follicular fluid. GCs were collected from HFs and AFs ($n = 15$, $5 < n < 8$ mm) for whole-transcriptome analysis using second-generation high-throughput sequencing. A total of 1,861 and 1,075 mRNAs, 159 and 24 miRNAs, and 123 and 100 lncRNAs, were upregulated and downregulated between HFs and AFs, respectively. Enrichment of functions and signaling pathways of these differentially expressed (DE) genes showed that most of DEmRNAs and targets of DEmiRNAs were annotated to the categories of ECM–receptor interaction and focal adhesion, as well as PI3K-AKT, mTOR, TGF-beta, Rap1, and estrogen signaling pathways. The competing endogenous RNA (CeRNA) network was also constructed based on the ceRNA theory which further revealed regulatory roles of these DERNAs in GCs of buffalo follicles. Finally, we validated that lnc4040 regulated the expression of *Hif1a* as miR-709 sponge in a ceRNA mechanism, suggesting their critical functions in GCs of buffalo follicles. These results show that lncRNAs are dynamically expressed in GCs of HFs and AFs, and interacting with target genes in a ceRNA manner, suggesting their critical functions in buffalo follicular development and atresia.

Keywords: buffalo (*Bubalus bubalis*), follicles, granulosa cells, whole-transcriptome, ceRNA

INTRODUCTION

In the process of mammalian follicle development, more than 99% of follicles become atretic and very few of follicles develop to ovulation (1). Chinese buffalo is an important large domestic animal distributed in the tropical and subtropical regions of China. It is generally believed that the sexual maturity of buffalo is later, and its postpartum estrus period is longer than that of

cattle (2, 3). As a mono-ovulating animal, follicular atresia is also an important factor restricting its reproductive performance, and the follicular atresia rate of buffalo is higher than that of cattle (4). During each estrus period, only one follicle matures and ovulates and other follicles undergo atresia during follicular development, and this occurs repeatedly throughout the developmental stages. However, the exact mechanism of cell death during this process is not fully understood. Therefore, elucidating the molecular mechanism of follicle atresia is expected to reverse the fate of follicles in buffalo, thus effectively utilizing more follicle resources and improving the reproductive efficiency of Chinese buffalo.

Previous studies have shown that follicular atresia is closely related to the apoptosis of ovarian granulosa cells (GCs) (5–8). GCs gradually shrink in size, and apoptotic bodies are formed. The chromatin is then condensed, a large amount of which is shed into the follicular fluid of atretic follicles (AFs) and the blood supply around the follicles is greatly reduced (9–12). In addition, interferon and some growth factors can also induce apoptosis. The intrinsic factors related to apoptosis are usually those associated with stress, such as nutritional deficiency, oxidative damage, and genetic damage as well as molecular stress (13). Recent studies have shown that the autophagy of GCs partially dominates the occurrence of follicular atresia (14–16).

However, the molecular mechanism of follicular atresia needs to be further explored. The development of transcriptome techniques provides an effective route to study the mechanism of follicular development and atresia. Early transcriptomics studies of follicles focused on mRNA, and researchers conducted studies at different stages of follicular development in cattle (17–20). Subsequent research showed that miRNA expression was spatiotemporal specific during bovine follicular development. In contrast to small follicles, bta-mir-144, bta-mir-202, bta-mir-451, bta-mir-652, and bta-mir-873 were all upregulated in large healthy follicles (HFs) and they targeted the signaling pathways involved in follicular cell proliferation and steroid generation (21). Long non-coding RNAs (lncRNAs) have received considerable attention for their important roles in epigenetic regulation, chromatin modification, genomic imprinting, transcriptional control, and pre-translational as well as posttranslational mRNA processing (22, 23).

The main mechanism of competing endogenous RNAs (ceRNAs) is to competitively bind miRNAs, remove the inhibitory effect of miRNAs on target genes, and improve the expression levels of target genes (24). The development of this hypothesis has given mRNAs and non-coding RNAs new and broader biological functions (25). The research between compact cumulus cells and expanded GCs found 89 lncRNAs, of which 12 are encoded within introns of genes known to be involved in GC processes. This suggested that unique non-coding RNA transcripts may contribute to the regulation of cumulus expansion and oocyte maturation (26).

In the study of mammalian follicles, researchers have obtained a large amount of transcriptomics data, which has a crucial regulatory role at all stages of follicular development (27). Several miRNAs and lncRNAs were screened for specific signal pathway regulation analysis. However, for large domestic animals, there are few such studies. Therefore, we used high-throughput sequencing to perform a whole-transcriptome analysis of GCs isolated from AFs and HFs of the Chinese buffalo, in order to obtain various types of DE-RNA molecules, and this allowed the construction of a ceRNA network to explore the molecular regulatory pathways involved. The non-coding RNAs obtained in this study can provide a strong basis for the subsequent study of the altered physiological functions of GCs during follicular development and atresia in buffalo. The aim of the study was to provide a theoretical basis and clues for follicular atresia observed in the Chinese buffalo.

RESULTS

Appearance and Classification of HFs and AFs in Buffalo

By observing exposed follicles, the surfaces of HFs were seen to be rich in capillaries and the follicular fluid was luminous yellow, while little or no capillaries were observed on the surface of AFs, and the follicular fluid was grayish white (**Figure 1A**). Follicular fluid and GCs were isolated from both HFs and AFs. The concentrations of estradiol (E_2) and progesterone (PROG) in isolated follicular fluid were measured by ELISA, and these were 126.21 ± 9.28 and 21.88 ± 1.78 ng·ml^{-1}, respectively, and the ratio was 5.77. The concentrations of E_2 and PROG in AFs were 76.63 ± 1.09 and 53.43 ± 2.68 ng·ml^{-1}, respectively, and the ratio was 1.43 (**Table 1**). The apoptosis rate of GCs in HFs was 4.93 ± 1.59, while that in AFs was 21.31 ± 1.40 (**Figure 1B** and **Table 2**). Transmission electron microscope observations showed that the morphology and submicrostructure of each organelle in HF were more normal than those in AF, there were more mitochondria in HF compared to the AF, chromatin breaks down to form granules, and a large number of vacuoles and apoptotic bodies appear in the cytoplasm of GCs in AFs (**Figure 1C**).

Overview of mRNA-Seq Data

From mRNA-seq data, 40,990 protein-coding genes were identified in the buffalo genome. The Pearson correlation coefficient calculated according to the gene fragments per kilobase of exon model per million reads mapped (FPKM) between the HFs and AFs samples showed that the consistency among the three repeated samples in the same group was more than 0.9, indicating that the repeatability between each two samples was dependable (**Figure 2A**). Their log2FC values are presented as volcano plot diagrams in **Figure 2B**. Among all of these genes, 2,936 (1,861 upregulated and 1,075 downregulated) DEmRNAs (fold change ≥ 2 and p-value < 0.05) were identified in GCs between HFs and AFs. A heat map of DEmRNAs showed the general expression profiles of the DEmRNAs in each group (**Figure 2C**).

To explore the functions of the DEmRNAs, KEGG was the main public database used regarding the pathway. The results showed that there were 42 and 72 DEmRNAs significantly enriched to ECM–receptor interactions and focal adhesion, respectively. In addition, there were 102, 48, 29, 35, and 33 enriched to the PI3K-AKT, thyroid hormone, TGF-beta, mTOR, and estrogen signaling pathways, respectively (**Figure 2D**). GO

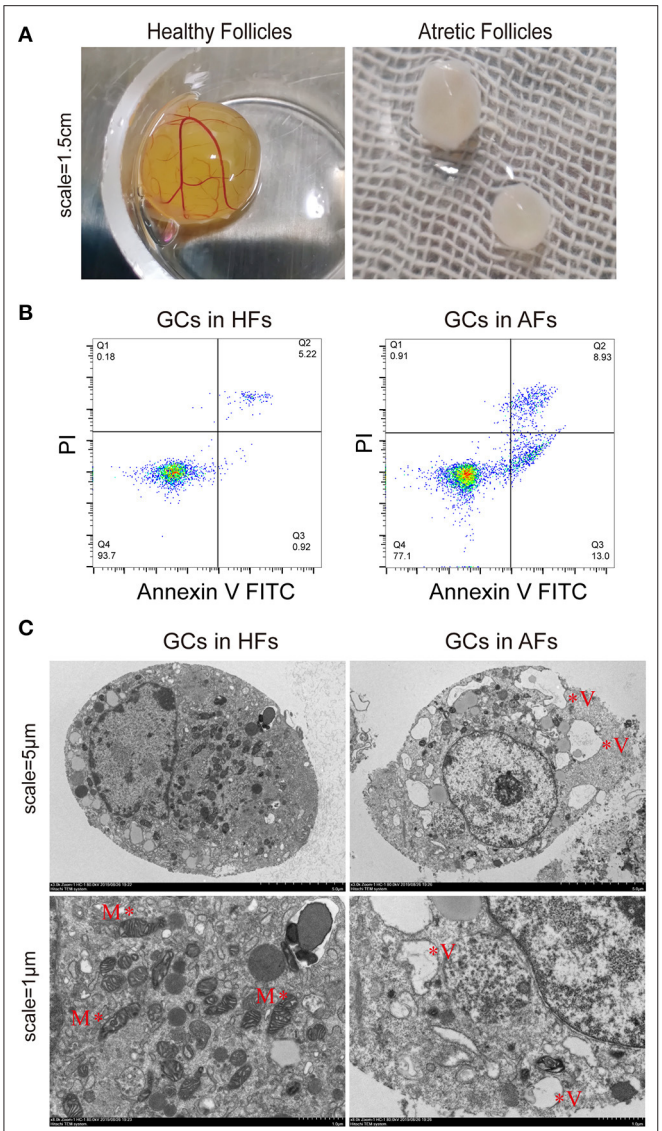

FIGURE 1 | Phenotypic detection of healthy and atretic follicles. **(A)** The appearance of follicles with scale bars = 1.5 cm: the capillaries were rich on the surface of healthy follicles, and the follicular fluid was yellow, while little or no capillaries were seen on the surface of atretic follicles, and the follicular fluid was grayish white. **(B)** The apoptosis rate of the granulosa cells ($n = 3$) of healthy and atretic follicles was assessed by flow cytometry. **(C)** Transmission electron microscope of granulosa cells in healthy and atretic follicles with scale bars = 5 and 1 μm, respectively. M indicates mitochondria, and V represents vacuoles.

TABLE 1 | Hormone levels in follicular fluid of HFs and AFs.

Follicle classification	Estrogen content ($ng \cdot ml^{-1}$)	Progesterone content ($ng \cdot ml^{-1}$)	E_2/PROG (per)	E_2/PROG
Healthy follicles ($n = 6$)	133.83	25.74	5.20	5.90 ±[a]
	124.43	23.99	5.19	
	107.76	18.29	5.89	
	167.78	27.42	6.12	
	115.70	17.55	6.59	
	125.74	19.66	6.40	
Atretic follicles ($n = 5$)	75.24	55.79	1.35	1.35 ±[b]
	72.83	48.93	1.49	
	76.59	49.07	1.56	
	79.26	62.93	1.26	
	82.20	74.36	1.11	

The data are the means ± SEM.
[a], [b]Indicate $p < 0.01$ for HFs and AFs, respectively.

annotation and GO enrichment analysis were also performed. Based on GO annotation, it was found that DEmRNAs were annotated to the cellular process, biological regulation, single-organism processes, metabolic processes, and response to stimulus under biological processes (BP), to the cells, cell parts, organelles, and organelle parts under cellular components (CC) and to the binding, catalytic activities, and molecular transducer activities under molecular functions (MF) (**Figure 2E**). In organisms, different transcripts coordinated with each other to exercise their biology and pathway-based analysis is helpful to further understand the biological functions of the transcripts.

Overview of miRNA-Seq Data

A total of 704,220 tags were generated. The results were filtered based on length (18–35 nt), and most selected tags were 22 nt in length in both the HF and AF groups (**Figure 3A**). All the clean tags were aligned with the reference genome. The tags mapped to repeat sequences were removed. Ultimately, 2,446 mature miRNAs (1,173 known and 1,273 novel) were detected, and these were drawn as a scatter plot using the expression between the different groups (**Figure 3B**). We identified miRNAs with a fold change ≥ 2 and p-values < 0.05 in a comparison of significant DEmiRNAs (159 upregulated and 24 downregulated) (**Figure 3C**). The heat maps of all DEmiRNAs were drawn to display the miRNA expression levels in different samples and to cluster miRNAs with a similar expression pattern (**Figure 3D**). Targeted mRNAs of these DEmiRNAs are listed in **Supplementary Table 1**. Pathway enrichment analysis of the targets of DEmiRNAs showed that there were 930, 884, 702, and 407 mRNAs linked to PI3K-Akt, MAPK, Ras, and mTOR signaling pathways, respectively. In addition, 799 and 400 mRNAs were linked to endocytosis and autophagy, respectively (**Figure 3E**).

Overview of lncRNA-Seq Data

The expressions of 3,488 known and 1,338 novel transcripts were identified. Two different softwares, namely, CNCI (version 2) (28) and CPC (29) (http://cpc.cbi.pku.edu.cn/), were used to assess the protein-coding potential of novel transcripts by default parameters. Novel transcripts were mapped with the SwissProt database to assess protein annotation. The intersection results of both non-protein-coding potential and non-protein annotation were chosen as the new lncRNAs (1,344) (**Figure 4A**). The lncRNAs obtained were classified into five classes according to their location relative to protein-coding genes, and these were named intergenic, bidirectional, intronic, antisense, and sense

TABLE 2 | Apoptotic rate of GCs in HFs and AFs.

	GCs of HFs			GCs of AFs		
Q1 (%)	0.18	0.07	0.13	0.91	3.60	2.30
Q2 (%)	5.22	5.77	0.63	8.93	5.84	21.50
Q3 (%)	0.92	1.11	1.14	13.00	12.80	1.86
Q4 (%)	93.70	93.00	98.10	77.10	77.70	74.30
Q2+Q3	6.14	6.88	1.77	21.93	18.64	23.36
Apoptosis rate (%)		4.93 ± 1.59^a			21.31 ± 1.40^b	

The data are the means ± SEM, n = 3.
[a],[b]Indicate $p < 0.01$ for HFs and AFs, respectively.

overlapping lncRNAs. The different types of lncRNAs probably have different biological functions (**Figure 4B**). A comparison of the genomic characterizations of the lncRNAs with mRNAs showed that their transcripts were similar in length distribution, except that lncRNA had relatively higher numbers of long transcripts (>4,500 bp) than mRNAs. For the number of exons, a higher percentage of lncRNAs had two to four exons. In addition, lncRNAs tended to have a shorter ORF length and a lower FPKM value (**Figures 4C–E**). Transcripts with a fold change ≥ 2 and a *p*-value < 0.05 were identified in a comparison as significant DElncRNAs (209 in final, 122 upregulated, and 87 downregulated) (**Supplementary Table 4**) were seen when a volcano plot was drawn (**Figure 4F**). Based on the expression of the DElncRNAs, the relationship between the sample and the DElncRNAs was clustered hierarchically, and a heat map is used to represent the clustering results (**Figure 4G**).

CeRNA Regulatory Network in GCS Between HFs vs. AFs

To reveal the global regulatory network of protein-coding RNAs and ncRNAs in GCs between HFs vs. AFs, a ceRNA network was constructed using DEmiRNAs, DEmRNAs, and DElncRNAs based on the ceRNA theory. In total, 1,458 DEmRNAs and 134 DElncRNAs were predicted as targets for 135 miRNAs. The lncRNA–miRNA–mRNA network was constructed by assembling all the co-expression competing triplets, which has been identified above. The connectivity of RNA in the ceRNA network was defined as the number of co-expressed targeted miRNAs. So ceRNAs with the highest connectivity were regarded as hub genes, which are more essential in biological networks.

In this ceRNA network, miR-424-3p, miR-542-5p, miR-735-5p, mi-503-3p, miR-212-3p, miR-216-3p, and miR-2440-5p are involved in more than 100 nodes, suggesting that they may act as core regulators. In addition, lncRNAs including XR_003111160.1, XR_003106664.1, XR_003103086.1, XR_327 919.2, XR_003111331.1, XR_003103012.1, XR_003111622.1, and TCONS_00165726 participated in the network.

Because of the large number of node genes and the tedious gene interaction network, the top 30 DEmiRNAs were selected as the source genes to simplify visualization using Cytoscape software (v3.6.0) (http://www.cytoscape.org/) (**Figure 5A**) with their target mRNAs. These 30 miRNAs included miR-146-3p, miR-450-3p, miR-424-3p, miR-212-3p, and miR-29-3p. GO enrichment analysis of all target mRNAs showed that most mRNAs were enriched in cell parts, binding, cellular processes, and organelles. KEGG pathways were enriched in ECM–receptor interactions, PI3K-AKT signaling pathway, protein digestion and absorption, focal adhesion, Hippo signaling pathway, mTOR signaling pathway, and various other metabolic pathways (**Figures 5B,C**).

Verification of the Regulation of *Hif1a* by ceRNA Circuitry in GCs

To further support the ceRNA hypothesis, a regulatory circuitry containing TCONS_00104040 (lnc4040), miR-709-5p (miR-709), and TCONS_00111150 (*Hif1a*) was selected for further verification. *Hif1a* can regulate the proliferation, autophagy, and cell cycle of GCs, and it also plays an important role in ovulation selection (31–33). Our initial experiments confirmed that the expression of lnc4040 was positively correlated with *Hif1a* and negatively correlated with miR-709; Western blot analysis revealed that the protein expression of *Hif1a* was significantly higher in the HF group than in the AF group (**Figures 6A,B**). We hypothesized that lnc4040 function as miRNA (miR-709) sponges to regulate the expression of *Hif1a* indirectly. To further confirm the binding events among miR-709, lnc4040, and *Hif1a*, we predicted the potential miR-709-binding site within lnc4040 and *Hif1a* by RNA22 version 2.0 (http://cm.jefferson.edu/rna22/Interactive/) (**Figure 6C**). Subsequent experiments validated the direct regulatory effect of miR-709 on *Hif1a* in 293T cells. Dual luciferase expression vectors carrying the wild-type (WT) miR-709-binding sites or one of the mutated versions of the miR-709-binding sites were constructed. MiR-709 mimics by co-transfection inhibited luciferase activity by the luciferase vectors carrying the mutations in site 1 (mut-1) or both sites 1 and 2 (mut-3), but not by the luciferase vectors carrying the WT *Hif1a*-binding sites or the mutation in binding site 2 (mut-2) (**Figure 6D**). This suggests that the binding site 1 of *Hif1a* might play the major role in miR-709 regulation of *Hif1a*. We also found that miR-709 can significantly inhibit the luciferase activity (**Figure 6E**). The HIF1A protein expression level in cultured GCs was decreased after miR-709-mimic transfection and conversely was increased after miR-709-inhibitor transfection (**Figure 6F**). Moreover, after overexpression of lnc4040, the downregulation of HIF1A protein expression induced by miR-709-mimic was alleviated (**Figure 6G**). These results evidenced that lnc4040 may

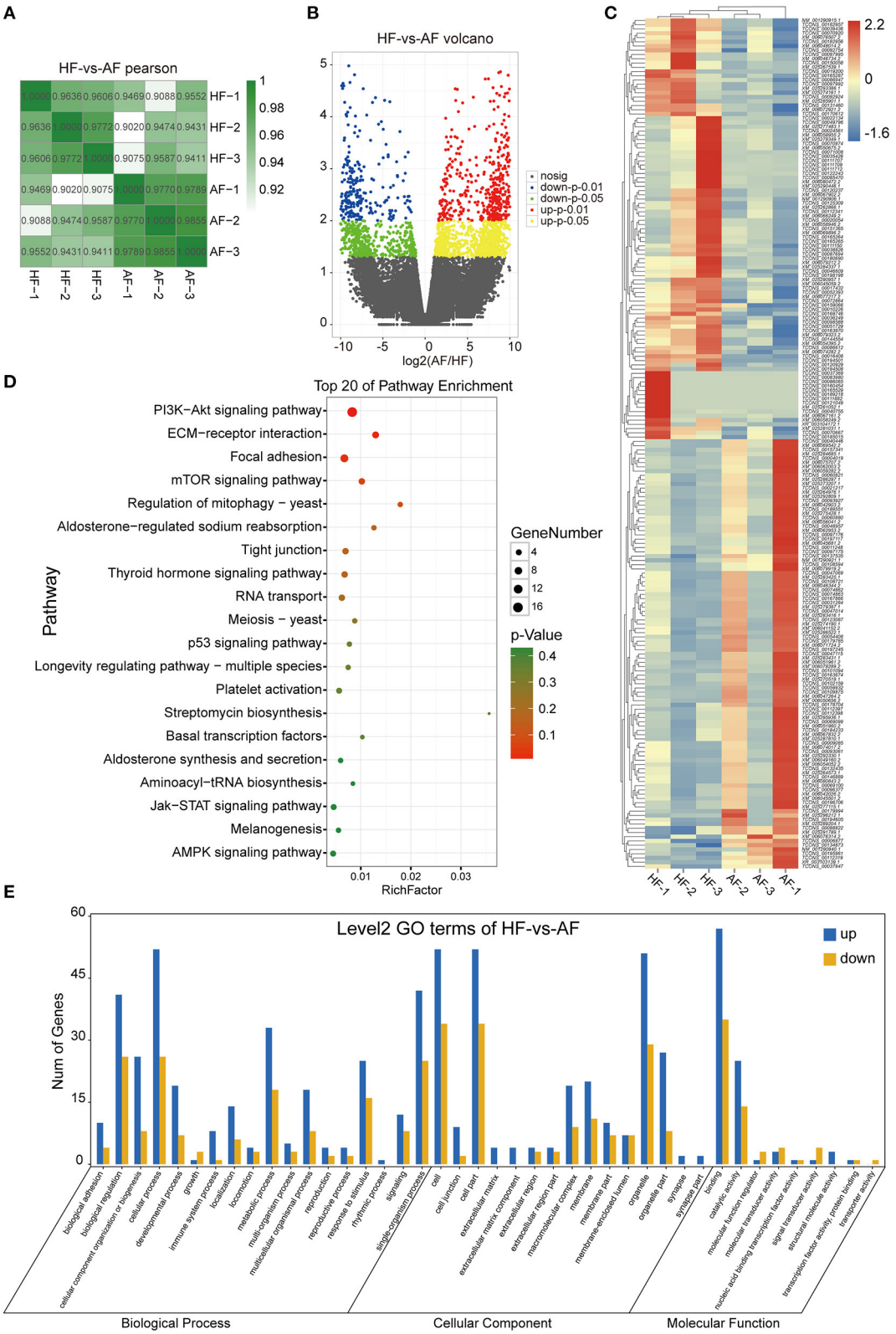

FIGURE 2 | Identification and analysis of DEmRNAs in granulosa cells between healthy and atretic follicles. **(A)** The Pearson correlation heat map between each sample. **(B)** Volcano plot diagrams showing log2FC and p-values of DEmRNAs. **(C)** Clustering heat map for DEmRNAs in each sample between the two groups. The

(Continued)

FIGURE 2 | expression of DEmRNAs was calculated with 2 as the base logarithm, and different samples and transcripts were analyzed by hierarchical cluster analysis; red and blue represent upregulation and downregulation, respectively. **(D)** Top 20 of the KEGG pathway bubble chart of DEmRNAs. The bubble size represents the number of mRNAs enriched in the pathway, and the bubble color represents the *p*-value. **(E)** GO enrichment histogram of DEmRNAs; blue and yellow represent upregulation and downregulation, respectively.

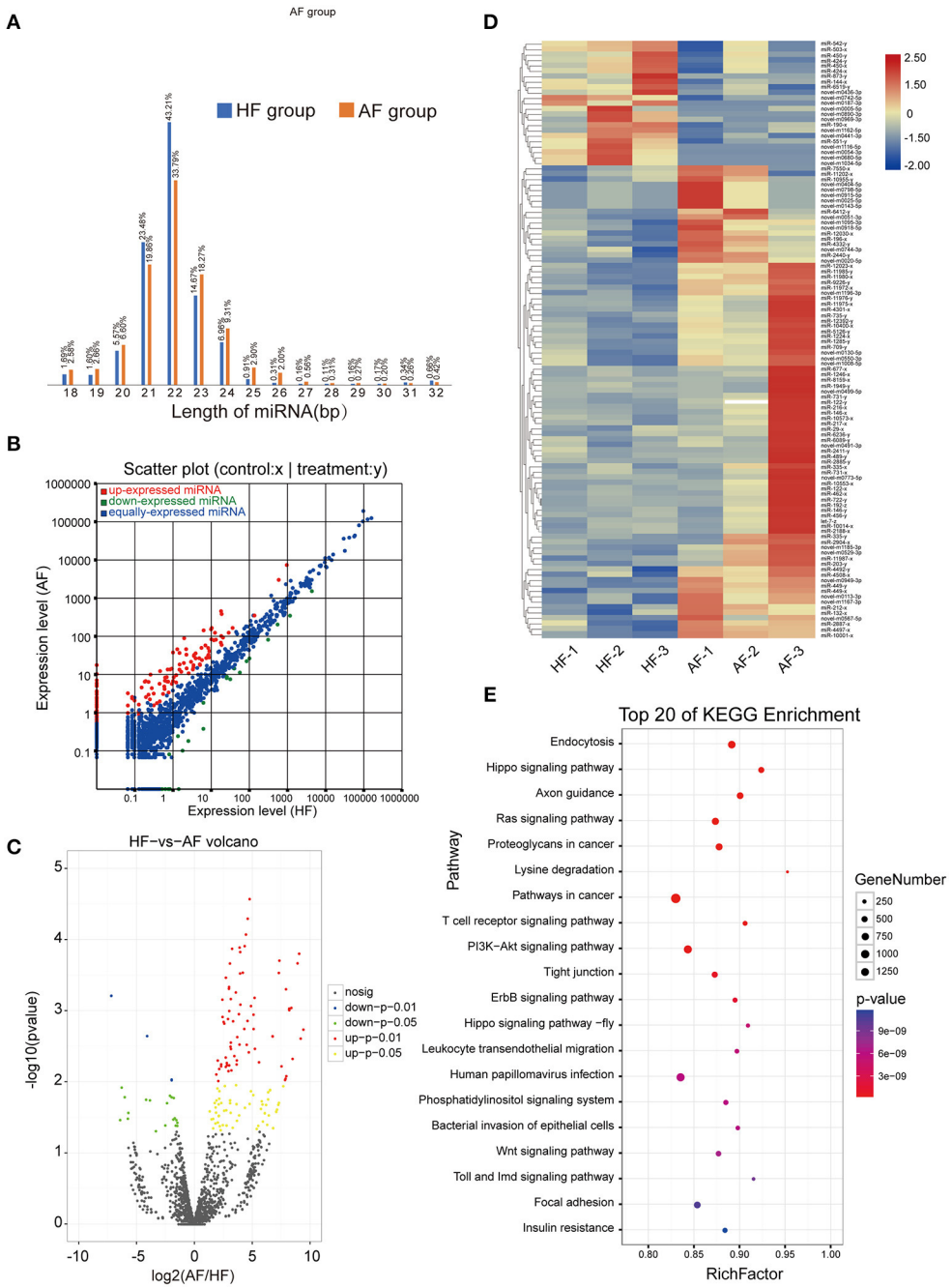

FIGURE 3 | Identification and analysis of DEmiRNAs in granulosa cells between healthy and atretic follicles. **(A)** Length statistic histogram of tags between the two groups. **(B)** The expression of identified miRNAs between the two groups was upregulated (30) and downregulated (blue). **(C)** Volcanic diagram of the expression of DEmiRNAs in different groups. **(D)** Clustering heat map for DEmiRNAs in each sample between the two groups with red for upregulation and blue for downregulation. **(E)** Top 20 of the KEGG pathway bubble chart of target mRNAs; the bubble size represents the number of mRNAs enriched in the pathway, and the bubble color represents the *p*-value.

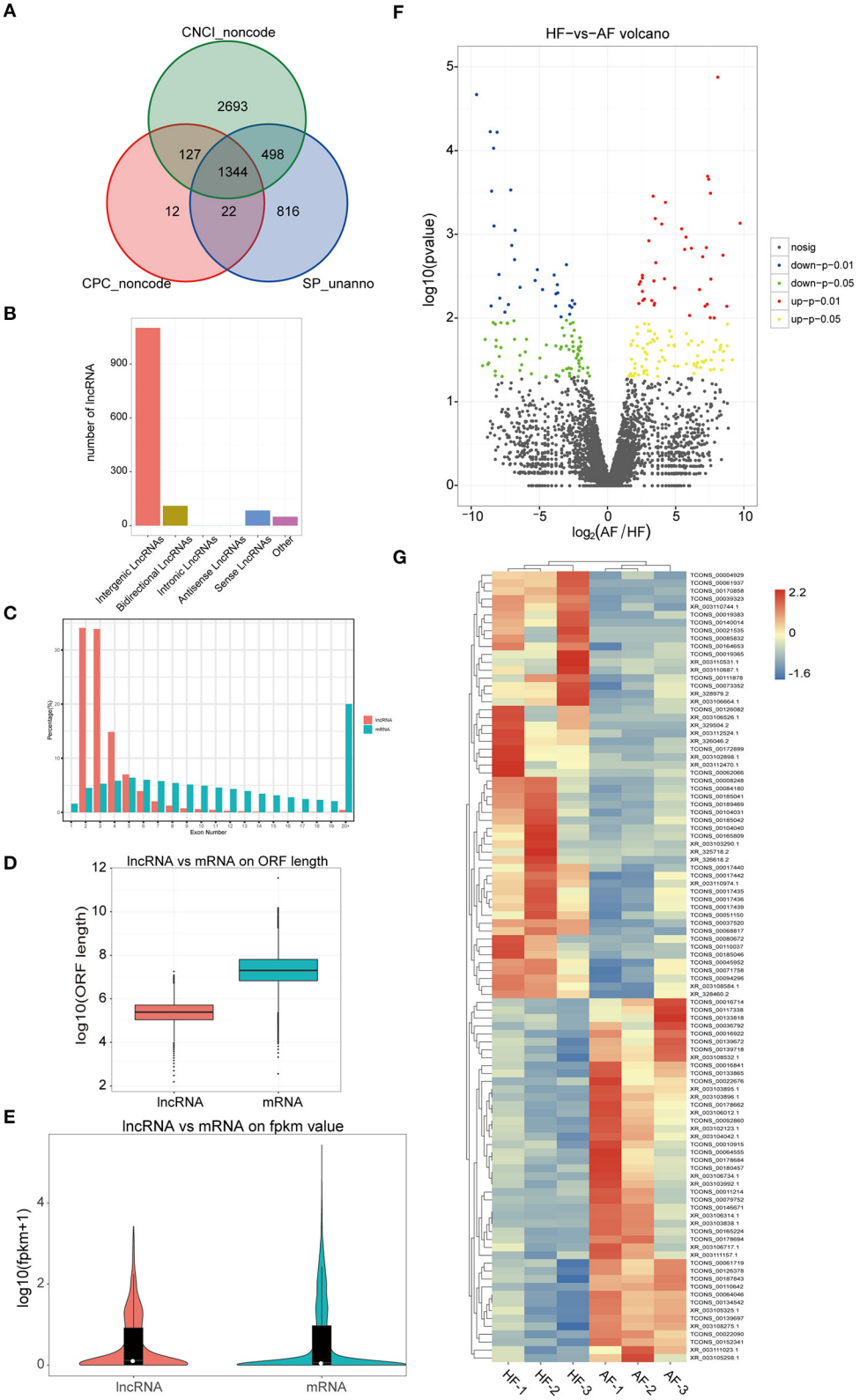

FIGURE 4 | Identification and analysis of DElncRNAs in granulosa cells between healthy and atretic follicles. **(A)** Venn diagram of the lncRNA annotation results of CPC, CNCI, and SwissProt. **(B)** LncRNA classification histogram. **(C–E)** Comparison of lncRNA with mRNA with respect to the transcript length, exon number, ORF length, and FPKM values. **(F)** Volcano plot of the expression of DElncRNAs in different groups. **(G)** Heat map of all DElncRNAs.

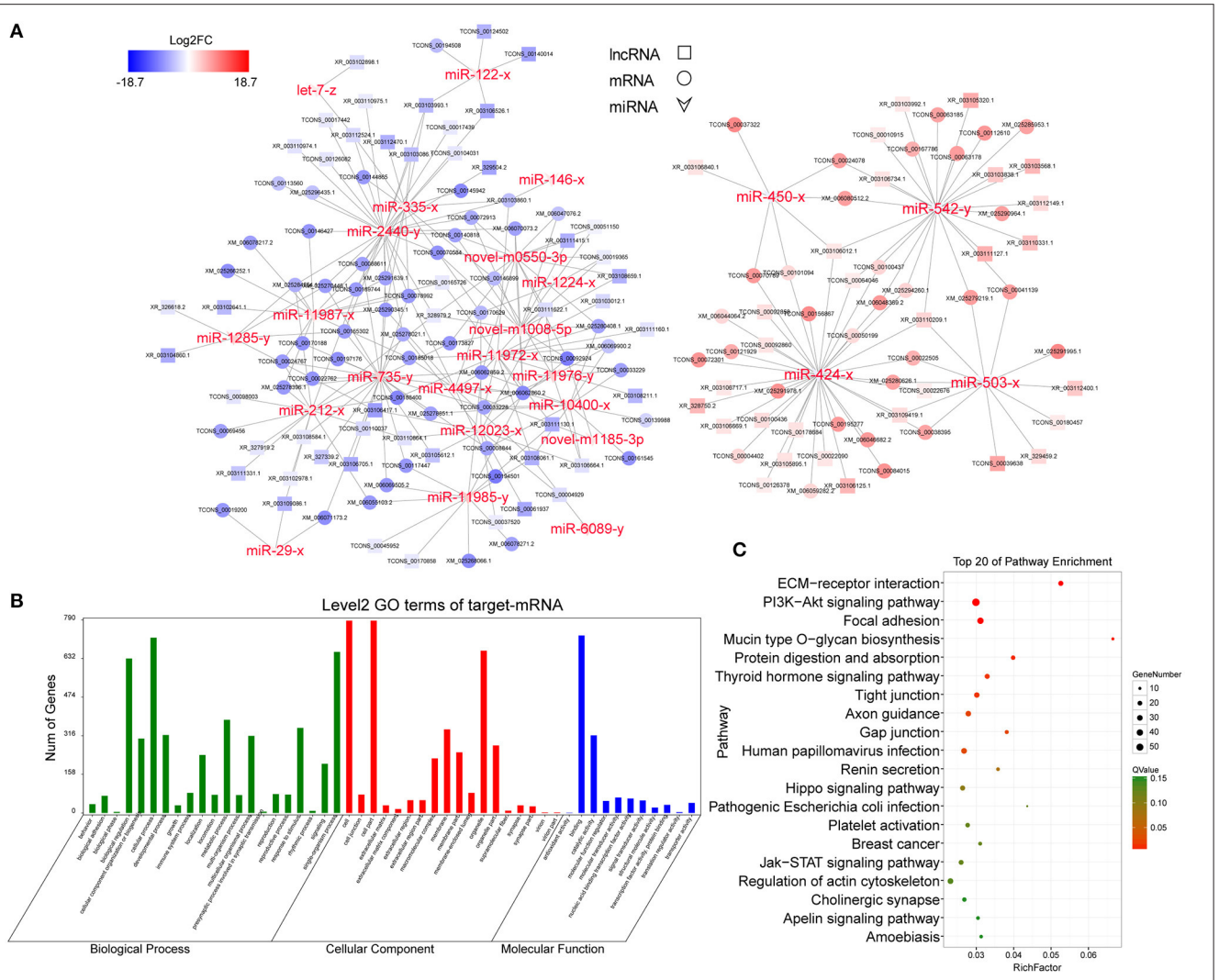

FIGURE 5 | CeRNA regulatory network and functional analysis. **(A)** CeRNA network built with the top 30 DEmiRNAs. Red and blue represent the upregulated and downregulated levels, respectively. **(B)** Level 2 GO enrichment of target mRNAs. **(C)** Top 20 KEGG pathways of target mRNAs.

function as a sponge of miR-709 to regulate the expression of *Hif1a*. In summary, our results showed that three-node lncRNA-mediated regulatory circuitry might play an essential role in GCs during follicle development.

MATERIALS AND METHODS

Tissues

All experiments regarding animals were performed in the State Key Laboratory for Conservation and Utilization of Subtropical Agro-bio-resources and were conducted in accordance with its guidelines for the care and use of laboratory animals. Ovaries were collected from a local abattoir in Nanning (from non-pregnant female buffaloes) and transported to the laboratory in sterile saline maintained at 38°C. After rinsing with 75% ethanol, the ovaries were placed on a gauze after high-pressure treatment, then sliced open, and single follicles ($5 < n < 8$ mm, $n = 20$) were separated from the ovarian tissue with ophthalmic scissors and repeatedly rinsed with 0.1 M phosphate buffer (pH 7.25).

In this experiment, a total of 15 follicles were successfully collected, and eight HFs and seven AFs were identified. Because a certain amount of follicular fluid is needed to detect hormone levels, we selected six HFs and five AFs for testing. Since the GCs collected need to be detected for apoptosis rate, electron microscopy, and subsequent RNA sequencing, we only collected enough GCs from three HFs and three AFs for experiments.

Classification of HFs and AFs

We judged the status of a follicle by the appearance of the follicle. We classified the follicles with yellowish surfaces, rich capillaries and they bright red color, uniform distribution, meanwhile clear follicular fluid as HFs. When the surfaces appeared gray to white, with fewer capillaries and turbidity in the follicular fluid in conjunction with dark masses inside the follicles or the follicles

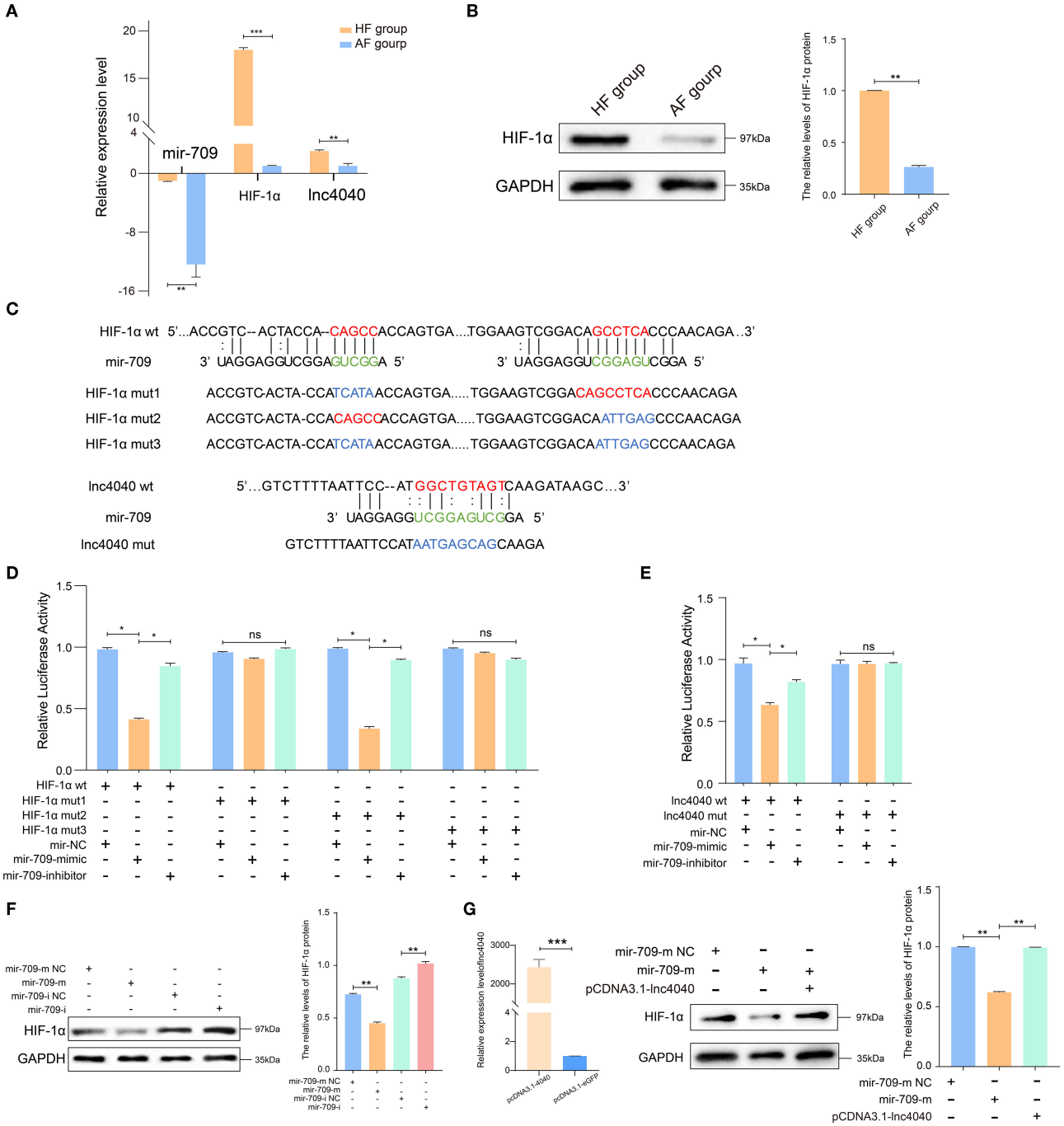

FIGURE 6 | Experimental validated of ceRNAs regulation with miR-709. **(A)** Relative expression levels of miR-709, *Hif1a*, and lnc4040 in GCs between HFs and AFs. **(B)** Expression of HIF1A protein in GCs between HFs vs. AFs and quantified by ImageJ (v1.45), error bars represent SEM ($n = 3$) $^{**}p < 0.01$. **(C)** Predicted miR-709-binding site on *Hif1a* and lnc4040, and design of luciferase reporter. **(D)** 293T cells were co-transfected with wild-type (WT) or mutant (MUT) luciferase reporters of *Hif1a* with miR-709 mimics, mimics NC, or miRNA inhibitors. The relative levels of firefly luminescence normalized to Renilla luminescence are plotted. Error bars represent SEM ($n = 3$) $^{*}p < 0.05$. **(E)** 293T cells were co-transfected with wild-type (WT) or mutant (MUT) luciferase reporters of lnc4040 with miR-709 mimics, mimics NC, or miRNA inhibitors. The relative levels of firefly luminescence normalized to Renilla luminescence are plotted. Error bars represent SEM ($n = 3$) $^{*}p < 0.05$. **(F)** Expression of HIF1A protein in GCs infected with miR-709 mimics, mimics NC, miR-709 inhibitor, and inhibitor NC and quantified by ImageJ (v1.45); error bars represent SEM ($n = 3$) $^{**}p < 0.01$. **(G)** Expression of HIF1A protein in GCs infected with miRNA mimics, mimics NC, and lnc4040 overexpression vector and quantified by ImageJ (v1.45); error bars represent SEM ($n = 3$) $^{**}p < 0.01$.

having severe internal flocculation, these were classified as AFs (34). Then, we detected the hormone content of follicular fluid (estrogen and PROG) by ELISA, the apoptosis of GCs by flow cytometric analysis, and the microstructure of GCs by TEM between HFs and AFs.

Detection of E_2 and PROG in Follicular Fluid

The follicular fluid was collected from HFs ($n = 6$) and AFs ($n = 5$), centrifuged for 2,000 ***g*** for 10 min, and E_2 and PROG were measured in the supernatants using ELISA kits (Cusabio, CSB-E08893b, Wuhan, China), and an enzyme-labeled instrument (Tecan Trading AG, Mannedorf, Switzerland) was used for measurements. All assays were validated in our laboratory by showing parallelism between serial sample dilutions and the provided assay standard curves (ranges, 40–1,000 pg/ml for E_2 and 0.5–30 ng/ml for PROG). Sensitivities of the assays were 40 pg/ml and 0.2 ng/ml, and the intra-assay coefficients of variations were 15% for each.

Detection of Apoptosis of GCs

The FITC Annexin V Apoptosis Detection Kit I (BD Pharmingen, 556547, Franklin Lakes, NJ, USA) was used to measure apoptosis. GCs were collected and washed twice with cold PBS and then resuspended in 1× binding buffer at a concentration of 1×10^6 cells/ml. Five microliters of FITC Annexin V and 5 μl PI were added, and the cells were gently vortexed and then incubated for 15 min at room temperature (25°C) in the dark. Four hundred microliters of 1× binding buffer was then added to each tube per test, and the samples were analyzed by flow cytometry (ACCURI C6, BD, Franklin Lakes, NJ, USA) within 1 h.

TEM Staining of GCs

GCs were collected and washed twice with cold PBS, and the cell suspension was fixed at 4°C by mixing with an equal volume of fixing solution: 2.5% glutaraldehyde and 0.1 M phosphate buffer as solvent (Servicebio, G1102, Wuhan, China) for 2–4 h. The cells were transferred to centrifuge tubes and spun to get the cell pellets, and then washed three times with 0.1 M PBS. Dehydration was performed by placing the samples in the following solvents for 15 min each: 50% ethanol, 70% ethanol, 80% ethanol, 90% ethanol, 95% ethanol, two changes of 100% ethanol, and two changes of acetone. The samples were then infiltrated with 1:1 acetone: EMbed 812 (SPI, West Chester, PA 90529-77-4, USA) for 2–4 h followed by 2:1 acetone: EMbed 812 overnight in a desiccator without covering and then pure EMbed 812 for 5–8 h in a 37°C oven. Then, the samples were embedded by baking in a 60°C oven for 48 h. Ultrathin sections (60–80 nm) were cut with an ultramicrotome (Leica UC7, Leica, Wetzlar, Germany). Sections were stained with uranyl acetate in pure ethanol for 15 min and then rinsed with distilled water. Then, they were stained with lead citrate for 15 min and again rinsed with distilled water. The sections were air-dried overnight and observed on a TEM (HT7700, Hitachi, Tokyo, Japan).

RNA Preparation and Sequencing Analysis

Total RNA was extracted from the GCs of HFs and AFs by using the TRIzol™ Reagent (Life Technologies, Mt Waverley, VIC, Australia) according to the manufacturer's protocol. The protocol was as follows: drastic mechanic vibration after add 1 mL of TRIzol® reagent (50–100 mg tissue or 5–10 × 10^6 cells), add 0.2 ml of chloroform and leave for 2–3 min (room temperature), centrifuge (12,000×***g***, 4°C for 15 min), add 0.5 ml of isopropanol and leave for 5–10 min (room temperature), centrifuge (12,000×***g***, 4°C for 10 min) for RNA deposition, and then add 1 ml 75% ethanol for RNA washing. RNA quality and integrity were estimated with an Agilent 2100 Bioanalyzer and RNA 6000 Nano Kit Reagents (Agilent Technologies, Santa Clara, CA, USA). Only high-quality RNA samples (concentration ≥ 250 ng/μl, RIN ≥ 7.0, total content ≥ 20 ng) were used to construct the sequencing libraries.

RNA-Seq

Details of the mRNA-seq, miRNA-seq, and lncRNA-seq methods are described in detail in **Supplementary Material**.

CeRNA Regulatory Network

Correlations of expression between mRNAs, miRNAs, and lncRNAs were evaluated using the Spearman rank correlation coefficient (SCC). Pairs with SCC < −0.7 were selected such as those with negatively co-expressed lncRNA–miRNA pairs or mRNA–miRNA pairs, or those where both mRNA and lncRNA were miRNA target genes and also where all the RNAs were differentially expressed. Pairs with Pearson correlation coefficients (PCC) > 0.9 were selected as co-expressed lncRNA–mRNA pairs, where both the mRNAs and lncRNAs in the pair were targeted and co-expressed negatively with a common miRNA. As a result, only the gene pairs with a p-value < 0.05 were selected. Pathway significant enrichment analysis used the KEGG pathway as a unit, and the hypergeometric test was used to determine whether the pathway was significantly enriched in differentially expressed transcripts when compared with the background of the whole transcripts.

Quantitative Real-Time PCR (qRT-PCR) Experimental Validation

qRT-PCR was performed to validate the expression levels of DEmRNAs, DElncRNAs, and DEmiRNAs. Total RNA was extracted by using the TRIzol™ Reagent (Life Technologies, Mt Waverley, VIC, Australia) according to the manufacturer's protocol. First-strand cDNA was synthesized from 1 μg of total RNA with the HiScript® II QRT SuperMix (Vazyme, Cat#R223, Nanjing, China) for qPCR. In addition, 1 μg of small RNA was used for cDNA synthesis using a miRNA 1st-Strand cDNA Synthesis Kit (reaction contains 10 μl of 2× RT Mix, 2 μl of random hexamers, 2 μl of HiScript II Enzyme Mix, and 1 pg−1 μg total RNA from the samples, added with ddH_2O to a final volume of 20 μl) (Vazyme, Cat#MR101, China) with the stem-loop primers designed using the stem-loop sequence (GTCGTATCCAGGGTCCGAGGTATT CGCACTGGATACGAC) except for the internal reference, U6.

qPCR was performed on the Applied Biosystems™ 7500 Real-Time PCR Systems using 10 μl of ChamQ™ Universal SYBR® qPCR Master Mix (Vazyme, Cat#Q711), lnRcute lncRNA qPCR Detection Kit (Cat#FP402, Tiangen, Beijing, China), and miRNA Universal SYBR® qPCR Master Mix (Vazyme, Cat#MQ101) in each 20-μl reaction volume per well by following the manufacturer's instructions. The $2^{-\Delta\Delta CT}$ method was used to normalize and determine the RNA level relative to an internal reference gene, beta-actin (Cs1g05000.1) or U6 (35). All primers used are listed in **Supplementary Table 3**.

Dual-Luciferase Reporter Assay

PsiCHECK 2.0-*Hif1a* WT and psiCHECK 2.0-*Hif1a* mut 1, 2, and 3 and psiCHECK 2.0-lnc4040 WT and psiCHECK 2.0-lnc4040 mut were constructed and validated by DNA sequencing. 293T cells (5×10^4 per well) were seeded in 24-well plates and grown to a density of 70–80%. Cotransfection of cells was performed using 50 nM miR-709 mimic, NC, and 25 nM miR-709-inhibitor, NC (RiboBio, Guangzhou, China), or a 0.5 μg reporter vector by X-tremeGENE™ HP DNA Transfection Reagent (6366244001, Roche, Basel, Switzerland). Twenty-four hours after transfection, culture medium was removed, cells were gently washed with PBS once, and 100 μl of passive lysis buffer was added and incubated at 37°C for 10–12 min. Cells were lysed by pipetting up and down several times and centrifuged at 5,000 rpm for 4 min to remove debris, and 10–20 μl was used to assay for luciferase activity using dual luciferase reporter assay (GeneCopoeia, LF004, Rockville, MD USA) in a single injector luminometer. The method refers to the previous study (36).

Vector Construction and Transfection

The lncRNA overexpression vector was constructed using the linear sequence of lnc4040 amplified from GCs by PCR. They were then cloned into the pcDNA3.1-EGFP vector in accordance with the manufacturer's protocol using the NheI and KpnI restriction sites. GCs were collected from follicular fluid and cultured to P2 with 10% FBS (Gibco-BRL, Grand Island, NE, USA) added to normal DMEM (Gibco-BRL, Grand Island, USA). miRNA mimics, mimics NC, and lncRNA overexpression vector were transiently transfected into GCs using Lipofectamine 3000 reagent (Invitrogen, Carlsbad, CA, USA). GCs were collected 48 h after transfection, and proteins were extracted for further experiments.

Western Blot Analysis

Total proteins from GCs were homogenized using RIPA buffer (Servicebio, G2002, Wuhan, China). Protein concentrations were determined using the BCA Protein Assay Kit (Solarbio, PC0020, Wuhan, China). Proteins were separated by 10% sodium dodecyl sulfate polyacrylamide gel electrophoresis, transferred to a polyvinylidene fluoride membrane (Millipore, IEVH00005, Burlington, MA, USA), and then incubated with antibodies (HIF1A, Novus, NB100, Littleton, CO, USA; GAPDH, Proteintech, 60004-1-Ig, Wuhan, China) overnight at 4°C and then with HRP-conjugated secondary antibody for 1 h at room temperature. Pictures were captured by an imaging system (UVP).

Statistical Analysis

The quantitative results are presented as means ± SEM based on at least three independent experiments. Significant variance in multiple comparisons was performed using multiple *t*-tests and one-way ANOVA with GraphPad Prism version 8.0 (GraphPad Software, La Jolla, CA, USA). Differences were considered significant when p-values ≤ 0.05.

DISCUSSION

At present, there is no exact method to judge the difference between healthy and atresia-associated buffalo follicles. Previous judgment on the appearance of sheep follicles was reported (37), and this was applied to naked follicles collected and observed in these studies. The hormone levels in follicular fluid were also used as an important basis for judging whether the follicle was in the process of atresia. The ratio of E_2 to PROG in follicular fluid has been discussed differently in different species. The PROG/E_2 ratio of ≥10 usually indicated follicle atresia in bovine (38), and the E_2/PROG ratio of healthy camel follicles was 22.8 while that of AFs was 0.08 (39), and in swine, follicles with a PROG/E_2 ratio of <5 were always classified as HF (40). Through a comprehensive comparison of the hormone ratios and appearance, it was found that the ratio of E_2 to PROG in follicular fluid for HFs was 5.77 and that for AFs was 1.43 in our study. Follicular atresia is mainly attributed to GC apoptosis (1, 41–43), and the apoptosis rate of GCs in HFs is basically <10%, while that in AFs can be as high as 30% (44–46). In bovine, the apoptosis rate of follicular GCs with <10% apoptotic cells was designated as HFs (44). In this study, the apoptosis rate of GCs in HFs was 4.93 ± 1.59; that is, the proportion of healthy cells was about 95%, which was consistent with previous studies. The accuracy of sequencing and grouping was guaranteed by the comprehensive determination of three indicators.

In this study, whole-transcriptome RNA sequencing was performed for the first time on buffalo ovarian GCs, and the differences between HFs and AFs at the RNA level were analyzed systematically. Our study found 2,936 DEmRNAs (**Supplementary Table 2** for details), among which *Serpine2*, *Inha*, *Hif1a*, *Fst*, *Jak3*, *Cyp19a1*, and *Vegfa* were the top ones with the highest expression levels, and these were highly expressed in HF. *Serpine2* was at the highest level in GCs of growing dominant bovine follicles (47). This is in accordance with the report that the expression of *Serpine2* was regulated by follicle-stimulating hormone (FSH) and growth factors in non-luteinizing bovine GCs, and the authors proposed that it could regulate atresia in bovine follicles (48). This is consistent with the high expression of *Serpine2* in AFs, which further indicates that *Serpine2* is needed in GCs of AFs. *In vitro* studies on follicle wall explants confirmed the significant differential expression of *Inha* and *Fst* during follicle development in the laying hen (49). Moreover, several specific mRNAs expressed in GCs during follicular development detected in previous studies were confirmed in this experiment (50–52).

There were also many reports on the regulation of follicular development by miRNA in GCs. A previous study confirmed

that miR-21-3p inhibits bovine GC autophagy by targeting VEGFA so as to regulate follicular atresia (53). In addition, miRNA-10001-3p and miRNA-12030-3p were shown to regulate VEGFA and FST, which suggests that both these factors probably act synergistically during buffalo follicular atresia. *Hif1a*, as a regulator of VEGF, has been shown to induce autophagy of follicular GCs *via* FSH (31). In our study, it was found that *Hif1a* expressed highly in HFs, suggesting that it might promote autophagy of GCs in order to maintain the dynamic balance of follicular development and protect the follicles from entering atresia.

One of the uppermost markers of ovarian differentiation, FOXL2, is necessary for the normal development of GCs (30, 54), and its expression was the highest in these cells, followed by stromal cells, and it was not expressed in oocytes (54, 55). It was predicted that miR-212-3p may target FOXL2 in buffalo GCs, and the results of sequencing and quantitative analysis confirmed the high expression of FOXL2 and the low expression of miR-212-3p in HFs. The results seen for SOX9, which has the opposite effect to FOXL2, showed that its expression in AFs was higher than that in HFs and it is a target by miR-424-3p. This finding is important within the context of the regulation of follicular atresia.

By visualizing the network diagram, several pairs of important ceRNA relationships are seen. These include a key miRNA, miR-424-3p, which is predicted to target four DEmRNAs in GCs between HFs and AFs, including FGFR1 (TCONS_00004077), SGK1 (XM_006059282.2), SOX9 (XM_025279387.1), and THBS (XM_025294260.1). In addition, miR-212-3p is predicted to target FOXL2 (XM_025290957.1), JAK3 (TCONS_00098588), and LDHA (XM_006056061.2). Also, miR-709-5p is seen to target *Hif1a* (TCONS_00111150) and INHBB (XM_025277483.1). All these target mRNAs regulate cell proliferation, apoptosis, and response to hormones and play regulatory roles at different stages of follicular development.

The ceRNA hypothesis was first proposed by Pandolf in 2011. He presented a unifying hypothesis regarding how mRNAs, transcribed pseudogenes, and lncRNAs "communicate" to each other using microRNA response elements (MREs) (56). MiRNAs can bind to the target mRNAs, inhibiting their translation or leading to their degradation, thus achieving the function of posttranscriptional regulation of gene expression. In addition to pseudogenes, mRNAs and lncRNAs can function as ceRNAs.

In this study, 49.6% of DEmRNAs were predicted as the targets of 135 DEmiRNAs, which constituted 4,309 DEmiRNA–DEmRNA interactions. Half of the DEmRNAs were not used during construction of the ceRNA network because the SCCs of expression between mRNA and miRNA were $<$-0.7. Also, the PCC of the targeting relationship with miRNA was $>$0.9 and the p-values were $<$ 0.05. These DEmRNAs competitively bound 134 DElncRNAs as ceRNAs. Because miRNAs play a critical role in the connection and regulation of different ceRNAs, particular attention was paid to the following miRNAs: miR-212-3p, miR-424-3p, and miR-709-5p. MiR-212 had been shown to be highly induced by LH in GCs, thus reducing the expression of CTBP1 protein (57). An increase in follicular levels of miR-212 was also observed following administration of an ovulatory dose of hCG (58). Studies on miR-424 showed that it is associated with therapeutic targets for a variety of diseases, such as muscular dystrophy, liver cancer, HPV, and vascular remodeling as well as regulating the STAT, NOTCH, and HIF1A signaling pathways (59–62).

In our study, XR_003106012.1 and XR_003106717.1 were found to competitively bind to miR-424-3p and TCONS_00104040 was competitively bound to miR-709-5p. It suggests that lncRNA may function as miRNA sponges to participate the regulation of follicular development. However, it should be pointed out that most of DElncRNAs were not included in the ceRNA network. Therefore, it is assumed that these lncRNAs are involved in the regulation of follicular development *via* other mechanisms. These may include a requirement for transcription or splicing of an RNA, due to DNA elements within the lncRNA promoter or gene body that function independently of the transcription, induction of DNA methylation, and modification of chromatin or serve as transcription enhancers (63).

During follicular development, miRNAs act as key regulators to modulate the upregulation or downregulation of important GC processes such as proliferation, apoptosis, differentiation, transcriptional regulation, and modification. As a consequence, through the regulation of GCs, it may be possible to control the development of dominant follicles to mature follicles and ovulate, while the non-dominant or unselected follicles gradually proceed to atresia, so as to regulate the dynamic development of follicles and maintain the balance of ovarian development. In this process, some lncRNAs can act as ceRNAs to competitively bind the MRE of miRNAs, which may indirectly affect the expression of particular mRNAs. Our experimental validation demonstrated that lnc4040 function as miRNA (miR-709) sponges to regulate the abundance of HIF1α. Thus, we proposed that lncRNA can regulate the abundance of key transcription factors in a ceRNA manner, then fine-tune the expression of cell-related genes in GCs during follicle development. However, further work is needed to elucidate their functions in buffalo follicular atresia.

In general, we have carried out an in-depth molecular analysis of GCs in HFs and AFs. Taking the buffalo as an entry point, we can temporarily fill in the gaps in the non-coding RNA data of this species in the field of reproduction. The buffalo could also serve as a model for mono-ovulating mammals, which could be useful for other mono-ovulating livestock. Next studies will investigate the role of non-coding RNAs in regulating the physiological state and function of GCs, thus affecting follicle development and atresia in Chinese buffalo.

DATA AVAILABILITY STATEMENT

The datasets presented in this study can be found in online repositories. The names of the repository/repositories and accession number(s) can be found in the article/**Supplementary Material**.

ETHICS STATEMENT

The animal study was reviewed and approved by Animal Care & Welfare Committee of Guangxi University.

AUTHOR CONTRIBUTIONS

YP, SY, DS, and YD designed the research. YP, JC, QL, and QX performed the research. YP, RZ, and JL analyzed the data. SY provided the experimental material. YP, DS, and YD wrote the paper. DS and YD provided the supervision and funding. All authors contributed to the article and approved the submitted version.

FUNDING

The research was funded by the National Natural Science Foundation of China (grant nos. 31860644 and 31760334), Natural Science Foundation of Guangxi Province (grant nos. 2019GXNSFDA185002, AA17204051, and 2018GXNSFAA281007), and Nanning Scientific Research Technological Development Foundation (grant nos. 20192087 and 20194147).

ACKNOWLEDGMENTS

We are also grateful to Dr. Dev Sooranna, Imperial College London, for the English language edits of the manuscript.

SUPPLEMENTARY MATERIAL

The Supplementary Material for this article can be found online at: https://www.frontiersin.org/articles/10.3389/fvets.2021.680182/full#supplementary-material

REFERENCES

1. Tilly JL, Kowalski KI, Johnson AL, Hsueh AJ. Involvement of apoptosis in ovarian follicular atresia and postovulatory regression. *Endocrinology*. (1991) 129:2799–801. doi: 10.1210/endo-129-5-2799
2. Warriach HM, McGill DM, Bush RD, Wynn PC, Chohan KR. A review of recent developments in buffalo reproduction - a review. *Asian Austral J Anim*. (2015) 28:451–5. doi: 10.5713/ajas.14.0259
3. Barile VL. Improving reproductive efficiency in female buffaloes. *Livest Prod Sci*. (2005) 92:183–94. doi: 10.1016/j.livprodsci.2004.06.014
4. Perera B. Reproductive cycles of buffalo. *Anim Reprod Sci*. (2011) 124:194–9. doi: 10.1016/j.anireprosci.2010.08.022
5. Manabe N, Goto Y, Matsuda-Minehata F, Inoue N, Maeda A, Sakamaki K, et al. Regulation mechanism of selective atresia in porcine follicles: regulation of granulosa cell apoptosis during atresia. *J Reprod Dev*. (2004) 50:493–514. doi: 10.1262/jrd.50.493
6. Bhardwaj JK, Sharma RK. Scanning electron microscopic changes in granulosa cells during follicular atresia in Caprine ovary. *Scanning*. (2011) 33:21–4. doi: 10.1002/sca.20217
7. Sharma R, Bhardwaj J. Granulosa cell apoptosis *in situ* in caprine ovary. *Biology*. (2007) 7:1111–4.
8. Sharma R, Bhardwaj J. *In situ* evaluation of granulosa cells during apoptosis in caprine ovary. *Int J Integr Biol*. (2009) 5.
9. Takagi K, Yamada T, Miki Y, Umegaki T, Nishimura M, Sasaki J. Histological observation of the development of follicles and follicular atresia in immature rat ovaries. *Acta Med Okayama*. (2007) 61:283–98. doi: 10.18926/AMO/32892
10. Rodgers RJ, Irving-Rodgers HF. Morphological classification of bovine ovarian follicles. *Reproduction*. (2010) 139:309–18. doi: 10.1530/REP-09-0177
11. Maeda A, Goto Y, Matsuda-Minehata F, Cheng Y, Inoue N, Manabe N. Changes in expression of interleukin-6 receptors in granulosa cells during follicular atresia in pig ovaries. *J Reprod Develop*. (2007) 53:727–36. doi: 10.1262/jrd.19011
12. Eppig JJ, Schroeder AC. Capacity of mouse oocytes from preantral follicles to undergo embryogenesis and development to live young after growth, maturation, and fertilization *in vitro*. *Biol Reprod*. (1989) 41:268–76. doi: 10.1095/biolreprod41.2.268
13. Quirk SM, Harman RM, Cowan RG. Regulation of Fas antigen (Fas, CD95)-mediated apoptosis of bovine granulosa cells by serum and growth factors. *Biol Reprod*. (2000) 63:1278–84. doi: 10.1095/biolreprod63.5.1278
14. Choi J, Jo M, Lee E, Choi D. Induction of apoptotic cell death *via* accumulation of autophagosomes in rat granulosa cells. *Fertil Steril*. (2011) 95:1482–6. doi: 10.1016/j.fertnstert.2010.06.006
15. Choi JY, Jo MW, Lee EY, Yoon BK, Choi DS. The role of autophagy in follicular development and atresia in rat granulosa cells. *Fertil Steril*. (2010) 93:2532–7. doi: 10.1016/j.fertnstert.2009.11.021
16. Choi J, Jo M, Lee E, Choi D. AKT is involved in granulosa cell autophagy regulation *via* mTOR signaling during rat follicular development and atresia. *Reproduction*. (2014) 147:73–80. doi: 10.1530/REP-13-0386
17. Evans AC, Ireland JL, Winn ME, Lonergan P, Smith GW, Coussens PM, et al. Identification of genes involved in apoptosis and dominant follicle development during follicular waves in cattle. *Biol Reprod*. (2004) 70:1475–84. doi: 10.1095/biolreprod.103.025114
18. Girard A, Dufort I, Douville G, Sirard M-A. Global gene expression in granulosa cells of growing, plateau and atretic dominant follicles in cattle. *Reprod Biol Endocrinol*. (2015) 13:17. doi: 10.1186/s12958-015-0010-7
19. Sisco B, Hagemann LJ, Shelling AN, Pfeffer PL. Isolation of genes differentially expressed in dominant and subordinate bovine follicles. *Endocrinology*. (2003) 144:3904–13. doi: 10.1210/en.2003-0485
20. Zielak AE, Forde N, Park SD, Doohan F, Coussens PM, Smith GW, et al. Identification of novel genes associated with dominant follicle development in cattle. *Reprod Fertil Dev*. (2007) 19:967–75. doi: 10.1071/RD07102
21. Sontakke SD, Mohammed BT, McNeilly AS, Donadeu FX. Characterization of microRNAs differentially expressed during bovine follicle development. *Reproduction*. (2014) 148:271–83. doi: 10.1530/REP-14-0140
22. Lee JT. Epigenetic regulation by long non-coding RNAs. *Science*. (2012) 338:1435–9. doi: 10.1126/science.1231776
23. Zhang F-L, Li N, Wang H, Ma J-M, Shen W, Li L. Zearalenone exposure induces the apoptosis of porcine granulosa cells and changes long noncoding RNA expression to promote antiapoptosis by activating the JAK2-STAT3 pathway. *J Agric Food Chem*. (2019) 67:12117–28. doi: 10.1021/acs.jafc.9b05189
24. Thomson DW, Dinger ME. Endogenous microRNA sponges: evidence and controversy. *Nat Rev Genet*. (2016) 17:272–83. doi: 10.1038/nrg.2016.20
25. Feng X, Li F, Wang F, Zhang G, Pang J, Ren C, et al. Genome-wide differential expression profiling of mRNAs and lncRNAs associated with prolificacy in Hu sheep. *Biosci Rep*. (2018) 38:BSR20171350. doi: 10.1042/BSR20171350
26. Yerushalmi GM, Salmon-Divon M, Yung Y, Maman E, Kedem A, Ophir L, et al. Characterization of the human cumulus cell transcriptome during final follicular maturation and ovulation. *Mol Hum Reprod*. (2014) 20:719–35. doi: 10.1093/molehr/gau031
27. Zhang Y, Yan Z, Qin Q, Nisenblat V, Chang HM, Yu Y, et al. Transcriptome landscape of human folliculogenesis reveals oocyte and granulosa cell interactions. *Mol Cell*. (2018) 72:1021–34 e4. doi: 10.1016/j.molcel.2018.10.029
28. Sun L, Luo H, Bu D, Zhao G, Yu K, Zhang C, et al. Utilizing sequence intrinsic composition to classify protein-coding and long non-coding transcripts. *Nucleic Acids Res*. (2013) 41:e166. doi: 10.1093/nar/gkt646
29. Kong L, Zhang Y, Ye Z-Q, Liu X-Q, Zhao S-Q, Wei L, et al. CPC: assess the protein-coding potential of transcripts using sequence features and support vector machine. *Nucleic Acids Res*. (2007) 35:W345–9. doi: 10.1093/nar/gkm391

30. Schmidt D, Ovitt CE, Anlag K, Fehsenfeld S, Gredsted L, Treier AC, et al. The murine winged-helix transcription factor Foxl2 is required for granulosa cell differentiation and ovary maintenance. *Development*. (2004) 131:933–942. doi: 10.1242/dev.00969
31. Zhou J, Yao W, Li C, Wu W, Li Q, Liu H. Administration of follicle-stimulating hormone induces autophagy *via* upregulation of HIF-1alpha in mouse granulosa cells. *Cell Death Dis*. (2017) 8:e3001. doi: 10.1038/cddis.2017.371
32. Szymanska M, Manthe S, Shrestha K, Girsh E, Harlev A, Kisliouk T, et al. Sirtuin-1 inhibits endothelin-2 expression in human granulosa-lutein cells *via* HIF1A and epigenetic modifications. *Biol Reprod*. (2020) 2020:ioaa199. doi: 10.1093/biolre/ioaa199
33. Yalu R, Oyesiji AE, Eisenberg I, Imbar T, Meidan R. HIF1A-dependent increase in endothelin 2 levels in granulosa cells: role of hypoxia, LH/cAMP, and reactive oxygen species. *Reproduction*. (2015) 149:11–20. doi: 10.1530/REP-14-0409
34. Sharma RK, Singh R, Bhardwaj JK, Saini S. Topographic and ultrastructural variations in isthmus segment of oviduct during oestrous cycle in Caprines. *Scanning*. (2013) 35:344–8. doi: 10.1002/sca.21073
35. Livak KJ, Schmittgen TD. Analysis of relative gene expression data using real-time quantitative PCR and the 2[-Delta Delta C(T)] method. *Methods*. (2001) 25:402–8. doi: 10.1006/meth.2001.1262
36. Hong LJ, Gu T, He YJ, Zhou C, Hu Q, Wang XW, et al. Genome-wide analysis of circular RNAs mediated ceRNA regulation in porcine embryonic muscle development. *Front Cell Dev Biol.* (2019) 7:289. doi: 10.3389/fcell.2019.00289
37. Moor RM, Hay MF, Dott HM, Cran DG. Macroscopic identification and steroidogenic function of atretic follicles in sheep. *J Endocrinol*. (1978) 77:309–18. doi: 10.1677/joe.0.0770309
38. Grimes RW, Matton P, Ireland JJ. A comparison of histological and non-histological indices of atresia and follicular function. *Biol Reprod*. (1987) 37:82–8. doi: 10.1095/biolreprod37.1.82
39. Kafi M, Maleki M, Davoodian N. Functional histology of the ovarian follicles as determined by follicular fluid concentrations of steroids and IGF-1 in *Camelus dromedarius*. *Res Vet Sci*. (2015) 99:37–40. doi: 10.1016/j.rvsc.2015.01.001
40. Zhang J, Liu Y, Yao W, Li Q, Liu H, Pan Z. Initiation of follicular atresia: gene networks during early atresia in pig ovaries. *Reproduction*. (2018) 156:23–33. doi: 10.1530/REP-18-0058
41. Palumbo A, Yeh J. *In situ* localization of apoptosis in the rat ovary during follicular atresia. *Biol Reprod*. (1994) 51:888–95. doi: 10.1095/biolreprod51.5.888
42. McRae RS, Johnston HM, Mihm M, O'Shaughnessy PJ. Changes in mouse granulosa cell gene expression during early luteinization. *Endocrinology*. (2005) 146:309–17. doi: 10.1210/en.2004-0999
43. Irving-Rodgers HF, van Wezel IL, Mussard ML, Kinder JE, Rodgers RJ. Atresia revisited: two basic patterns of atresia of bovine antral follicles. *Reproduction*. (2001) 122:761–75. doi: 10.1530/reprod/122.5.761
44. Feng WG, Sui HS, Han ZB, Chang ZL, Zhou P, Liu DJ, Tan JH, et al. Effects of follicular atresia and size on the developmental competence of bovine oocytes: a study using the well-in-drop culture system. *Theriogenology*. (2007) 67:1339–50. doi: 10.1016/j.theriogenology.2007.01.017
45. Yu YS, Sui HS, Han ZB, Li W, Luo MJ, Tan JH. Apoptosis in granulosa cells during follicular atresia: relationship with steroids and insulin-like growth factors. *Cell Res*. (2004) 14:341–6. doi: 10.1038/sj.cr.7290234
46. Blondin P, Dufour M, Sirard MA. Analysis of atresia in bovine follicles using different methods: flow cytometry, enzyme-linked immunosorbent assay, and classic histology. *Biol Reprod*. (1996) 54:631–7. doi: 10.1095/biolreprod54.3.631
47. Bédard J, Brûlé S, Price CA, Silversides DW, Lussier JG. Serine protease inhibitor-E2 (SERPINE2) is differentially expressed in granulosa cells of dominant follicle in cattle. *Mol Reprod Dev*. (2003) 64:152–65. doi: 10.1002/mrd.10239
48. Cao M, Nicola E, Portela VM, Price CA. Regulation of serine protease inhibitor-E2 and plasminogen activator expression and secretion by follicle stimulating hormone and growth factors in non-luteinizing bovine granulosa cells *in vitro*. *Matrix Biol*. (2006) 25:342–54. doi: 10.1016/j.matbio.2006.05.005
49. Lovell TM, Gladwell RT, Groome NP, Knight PG. Ovarian follicle development in the laying hen is accompanied by divergent changes in inhibin A, inhibin B, activin A and follistatin production in granulosa and theca layers. *J Endocrinol*. (2003) 177:45–55. doi: 10.1677/joe.0.1770045
50. Richani D, Constance K, Lien S, Agapiou D, Stocker WA, Hedger MP, et al. Cumulin and FSH cooperate to regulate inhibin B and activin B production by human granulosa-lutein cells *in vitro*. *Endocrinology*. (2019) 160:853–62. doi: 10.1210/en.2018-01026
51. Ndiaye K, Castonguay A, Benoit G, Silversides DW, Lussier JG. Differential regulation of Janus kinase 3 (JAK3) in bovine preovulatory follicles and identification of JAK3 interacting proteins in granulosa cells. *J Ovarian Res*. (2016) 9:71. doi: 10.1186/s13048-016-0280-5
52. McFee RM, Rozell TG, Cupp AS. The balance of proangiogenic and antiangiogenic VEGFA isoforms regulate follicle development. *Cell Tissue Res*. (2012) 349:635–47. doi: 10.1007/s00441-012-1330-y
53. Ma L, Zheng Y, Tang X, Gao H, Liu N, Gao Y, et al. miR-21-3p inhibits autophagy of bovine granulosa cells by targeting VEGFA *via* PI3K/AKT signaling. *Reproduction*. (2019) 158:441–52. doi: 10.1530/REP-19-0285
54. Cocquet J, Pailhoux E, Jaubert F, Servel N, Xia X, Pannetier M, et al. Evolution and expression of FOXL2. *J Med Genet*. (2002) 39:916–21. doi: 10.1136/jmg.39.12.916
55. Pannetier M, Fabre S, Batista F, Kocer A, Renault L, Jolivet G, et al. FOXL2 activates P450 aromatase gene transcription: towards a better characterization of the early steps of mammalian ovarian development. *J Mol Endocrinol*. (2006) 36:399–413. doi: 10.1677/jme.1.01947
56. Salmena L, Poliseno L, Tay Y, Kats L, Pandolfi PP. A ceRNA hypothesis: the Rosetta Stone of a hidden RNA language? *Cell*. (2011) 146:353–8. doi: 10.1016/j.cell.2011.07.014
57. Fiedler SD, Carletti MZ, Hong X, Christenson LK. Hormonal regulation of MicroRNA expression in periovulatory mouse mural granulosa cells. *Biol Reprod*. (2008) 79:1030–7. doi: 10.1095/biolreprod.108.069690
58. Schauer SN, Sontakke SD, Watson ED, Esteves CL, Donadeu FX. Involvement of miRNAs in equine follicle development. *Reproduction*. (2013) 146:273–82. doi: 10.1530/REP-13-0107
59. Tian Q, Li Y, Wang F, Li Y, Xu J, Shen Y, et al. MicroRNA detection in cervical exfoliated cells as a triage for human papillomavirus-positive women. *J Natl Cancer Inst*. (2014) 106:dju241. doi: 10.1093/jnci/dju241
60. Han H, Du Y, Zhao W, Li S, Chen D, Zhang J, et al. PBX3 is targeted by multiple miRNAs and is essential for liver tumour-initiating cells. *Nat Commun*. (2015) 6:8271. doi: 10.1038/ncomms9271
61. Ghosh G, Subramanian IV, Adhikari N, Zhang X, Joshi HP, Basi D, et al. Hypoxia-induced microRNA-424 expression in human endothelial cells regulates HIF-α isoforms and promotes angiogenesis. *J Clin Invest*. (2010) 120:4141–54. doi: 10.1172/jci42980
62. Connolly M, Paul R, Farre-Garros R, Natanek SA, Bloch S, Lee J, et al. miR-424-5p reduces ribosomal RNA and protein synthesis in muscle wasting. *J Cachexia Sarcopenia Muscle*. (2018) 9:400–16. doi: 10.1002/jcsm.12266
63. Kopp F, Mendell JT. Functional classification and experimental dissection of long noncoding RNAs. *Cell*. (2018) 172:393–407. doi: 10.1016/j.cell.2018.01.011

Conflict of Interest: The authors declare that the research was conducted in the absence of any commercial or financial relationships that could be construed as a potential conflict of interest.

frontiers in Veterinary Science

ORIGINAL RESEARCH
published: 19 July 2021
doi: 10.3389/fvets.2021.668158

Characterization of the Impact of Density Gradient Centrifugation on the Profile of the Pig Sperm Transcriptome by RNA-Seq

Yu Lian[1†], *Marta Gòdia*[1†‡], *Anna Castello*[1,2], *Joan Enric Rodriguez-Gil*[3], *Sam Balasch*[4], *Armand Sanchez*[1,2] *and Alex Clop*[1,5*]

[1] Centre for Research in Agricultural Genomics (CRAG), CSIC-IRTA-UAB-UB, Campus UAB, Barcelona, Spain, [2] Unit of Animal Science, Department of Animal and Food Science, Autonomous University of Barcelona, Barcelona, Spain, [3] Unit of Animal Reproduction, Department of Animal Medicine and Surgery, Autonomous University of Barcelona, Barcelona, Spain, [4] Grup Gepork S.A., Barcelona, Spain, [5] Consejo Superior de Investigaciones Científicas, Barcelona, Spain

OPEN ACCESS

Edited by:
Isabel Barranco,
University of Bologna, Italy

Reviewed by:
Jean Feugang,
Mississippi State University, United States
Margarida Fardilha,
University of Aveiro, Portugal

***Correspondence:**
Alex Clop
alex.clop@cragenomica.es

[†]These authors have contributed equally to this work and share first authorship

[‡]**Present address:**
Marta Gòdia,
Animal Breeding and Genomics, Wageningen University and Research, Wageningen, Netherlands

Specialty section:
This article was submitted to Animal Reproduction–Theriogenology, a section of the journal Frontiers in Veterinary Science

Received: 15 February 2021
Accepted: 22 June 2021
Published: 19 July 2021

Citation:
Lian Y, Gòdia M, Castello A, Rodriguez-Gil JE, Balasch S, Sanchez A and Clop A (2021) Characterization of the Impact of Density Gradient Centrifugation on the Profile of the Pig Sperm Transcriptome by RNA-Seq. Front. Vet. Sci. 8:668158. doi: 10.3389/fvets.2021.668158

RNA-Seq data from human semen suggests that the study of the sperm transcriptome requires the previous elimination from the ejaculates of somatic cells carrying a larger load of RNA. Semen purification is also carried to study the sperm transcriptome in other species including swine and it is often done by density gradient centrifugation to obtain viable spermatozoa from fresh ejaculates or artificial insemination doses, thereby limiting the throughput and remoteness of the samples that can be processed in one study. The aim of this work was to evaluate the impact of purification with density gradient centrifugation by BoviPure™ on porcine sperm. Four boar ejaculates were purified with BoviPure™ and their transcriptome sequenced by RNA-Seq was compared with the RNA-Seq profiles of their paired non-purified sample. Seven thousand five hundred and nineteen protein coding genes were identified. Correlation, cluster, and principal component analysis indicated high—although not complete—similarity between the purified and the paired non-purified ejaculates. 372 genes displayed differentially abundant RNA levels between treatments. Most of these genes had lower abundances after purification and were mostly related to translation, transcription and metabolic processes. We detected a significant change in the proportion of genes of epididymal origin within the differentially abundant genes (1.3%) when compared with the catalog of unaltered genes (0.2%). In contrast, the proportion of testis-specific genes was higher in the group of unaltered genes (4%) when compared to the list of differentially abundant genes (0%). No proportion differences were identified for prostate, white blood, lymph node, tonsil, duodenum, skeletal muscle, liver, and mammary gland. Altogether, these results suggest that the purification impacts on the RNA levels of a small number of genes which are most likely caused by the removal of epididymal epithelial cells but also premature germinal cells, immature or abnormal spermatozoa or seminal exosomes with a distinct load of RNAs.

Keywords: sperm RNA, RNA-Seq, sperm purification, differentially abundant gene, somatic cell, germline cell, exosome

INTRODUCTION

Despite being a matter of debate for many years, the presence and role of sperm RNA is beginning to be elucidated. The analysis of the spermatozoon transcriptome can shed light on the previous, present or future roles of the genes involved in spermatogenesis, early embryo development, and transgenerational inheritance (1). The sperm's transcriptomic landscape has been profiled in a large number of animal species including human, mice, cattle, pig, and horse (1), and several research groups focus their efforts to identify molecular markers associated to semen quality and fertility in human (2), cattle (3), horse (4) and swine (5–10). Transcriptomic evaluations of the ejaculated spermatozoa are often preceded by a purification step to remove somatic and prokaryotic cells often by using a commercial colloidal silica suspension (e.g., PureSperm®, BoviPure™, Nidacon, Sweden) in order to prepare density gradients and purify the sperm cells (11–14). This step is considered to be necessary since spermatozoa carry small amounts of RNA that are also highly fragmented when compared with the somatic cells that could be present in the ejaculate. The sperm transcriptome profile could be thus overshadowed by the profiles from these somatic cells. However, the purification step with gradient cell centrifugation requires viable spermatozoa only available in fresh ejaculates or in frozen straws prepared for artificial insemination. The use of fresh ejaculates limits the number of samples that can be simultaneously processed in an experiment and the remoteness of their geographical location. In terms of logistics, studies requiring large number of samples would benefit if they could extract RNA from frozen material. In pigs, ejaculates from artificial insemination studs often contain small amounts of epithelial cells but the presence of somatic and non-spermatozoa germline cells is rare and associated to inflammatory processes of the reproductive tract (Michael Kleve-Feld, Personal Communication). Our group has always purified the porcine ejaculates with BoviPure™ when characterizing the boar sperm transcriptome (5, 6, 8, 15) to be on the safe side since the potential impact of an even tiny presence of somatic cells on the semen transcriptome profile is unknown. The objective of this pilot study was to assess the changes on the porcine ejaculate's transcriptome after BoviPure™ purification and discuss the potential underlying causes. To achieve this goal, we compared the transcriptomes of purified vs. paired non-purified ejaculates from four male pigs.

MATERIALS AND METHODS

Sample Collection

Four fresh ejaculates showing good semen quality parameters (**Supplementary Table 1**) were obtained each from a different Pietrain boar from a commercial farm using the gloved hand method (16), diluted (1:2) immediately into the prepared fresh commercial extender and stored at 16°C. The ejaculates were privately owned for non-research purposes and the owners provided consent for their use for research. Specialized professionals at the farm collected the ejaculates following standard routine procedures and guidelines.

Sample Processing and RNA Extraction

For each ejaculate, we collected two aliquots. One aliquot was purified (P) with the BoviPure™ (Nidacon; Mölndal, Sweden) colloid centrifugation method. The other aliquot was not purified (NP). For the P samples, a maximum of 11 mL of ejaculate and 1 billion cells were placed over 3 mL of BoviPure™ in 15 mL RNase-free tubes. The tubes were then centrifuged at 300 × g for 20 min at 20°C. After centrifugation, all the upper phases were removed. The cell pellet were transferred to a new 15 mL RNase-free tube with 10 mL RNase-free PBS and centrifuged at 1,500 × g for 10 min at 20°C. The supernatant was removed and the pellets were stored at −80°C in 1 mL Trizol® for further use for RNA extraction. A detailed description of the purification protocol with BoviPure™ is provided by Gòdia et al. (5). For the NP aliquots, 1.5 mL of ejaculate was centrifuged at 14,000 g for 4 min at 20°C and the supernatant was removed. The pellet was then eluted in 1 mL of Trizol® and stored at −80°C until RNA extraction.

Total RNA was extracted from the eight samples as described in Gòdia et al. (5). Briefly, between 47 and 300 million cells were pre-lysed using a 5 mL sterile syringe with a 25 G needle for 5 and 2 min of vigorous vortex. After adding 200 μL of chloroform, the samples were incubated for 3 min at room temperature. Then, the samples were centrifuged at 12,000 × g for 15 min and the supernatants were transferred to new RNase-free tubes, in which 500 μL of isopropanol was added. These samples were then centrifuged at 12,000 × g for 10 min. The supernatants were removed carefully and the pellets were washed with 500 μL of 75% (v/v) ethanol solution. The samples were centrifuged at 13,000 × g for 5 min and dried out at room temperature for 10 min. The dried samples were resuspended in 30 μL of ultrapure water. All the centrifugations were performed at 4°C. All the RNA samples were subjected to DNase treatment with the Turbo DNA-free™ kit (Thermo Fisher Scientific; CA, USA) following the manufacturer's instructions. The RNAs were quantified with Qubit™ RNA HS Assay kit (Invitrogen; CA, USA).

In order to have an initial evaluation of the purity of the extracted RNA defined as RNA originating exclusively from sperm cells and devoid of DNA, for each sample, we used three qPCR assays that assess the abundance of the sperm specific *PRM1* RNA, the somatic-cell specific *PTPRC* RNA and the absence of genomic DNA (gDNA) using SYBR® Select Master Mix (Thermo Fisher Scientific; CA, USA) and done in triplicate as previously described (5). Total RNA abundance was quantified with Qubit RNA HS Assay kit (Invitrogen; CA, USA).

RNA-Seq Library Preparation

Sequencing libraries were prepared with the SMARTer Stranded Total RNA-Seq Kit v2—Pico Input Mammalian (Takara Bio)

Abbreviations: Cq, quantification cycle; DAG, differentially abundant gene; FPKM, fragments per kilobase of transcript per million mapped reads; GO, Gene Ontology; NP, non-purified sample; P, purified sample; PCA, Principal component analysis; TIN, transcript integrity number; tRNA, transfer RNA.

using Dual Indexing strategy, starting with 10 ng of RNA quantified with the Qubit NRA HS Assay Kit (Thermo Fisher Scientific) and following the manufacturer's instructions. The final libraries were quality controlled on a Bioanalyzer (Agilent) using a High Sensitivity DNA Kit. The libraries were sequenced in an Illumina's HiSeq4000 system to generate 76 bp long paired-end reads following the manufacturer's protocol for dual indexing. Image analysis, base calling and quality scoring of the run were processed using the manufacturer's software Real Time Analysis (v 2.7.7) and followed by generation of FASTQ sequence files.

RNA-Seq Mapping and Analysis

Total RNA-Seq reads were evaluated for quality control by FastQC software (v, 0.11.5) (https://www.bioinformatics.babraham.ac.uk). Low-quality reads (Phred –Q $<$ 20 and read length $<$ 25 bp) and sequencing adaptors were trimmed with Trimmomatic v.0.33 (17). Trimmed reads were aligned to the pig reference genome (Sscrofa 11.1) using HISAT2 v.2.1.0 (18) with the default parameters. Duplicate reads were removed with PicardTools v11.0.5 MarkDuplicates (http://picard.sourceforge.net). RNA levels of the genes annotated in the porcine genome (Ensembl v.101) were quantified as Fragments Per Kilobase of transcript per Million mapped reads (FPKM), with StringTie v.1.3.4 (19). The genes with FPKM $\leq$ 1 were excluded from further analysis. Differential gene abundance between P and NP was carried out by DESeq2 (20) and only these genes showing absolute $\log_2$ fold-change $\geq$ 1.5 and False Discovery Rate (FDR) $\leq$ 0.05 between P and NP were considered to be differentially abundant.

To determine whether the RNA-Seq quality metrics of the P and NP samples were significantly different, we used R to carry the Wilcoxon signed-rank test. The pairwise relationships between NP and the paired P transcriptomes were assessed by linear regression and with the Pearson correlation coefficient considering the purification treatment and the sample identifier. The hierarchical cluster dendrogram and the corresponding Selective Inference *p*-values were carried with the R package "pvclust" (21), and the Principal Component Analysis (PCA) and the correlation plot with the R package "ggplot2" (22). RNA transcript integrity (TIN) was calculated with RseQC v.2.6.4 (23) using the Ensembl v.101 pig annotation. TIN indicates the proportion of a gene that is covered by reads ranging from 0 (no coverage) to 100 (fully covered transcript). The TINs across paired samples was compared with the Wilcoxon signed-rank test.

To assess whether the differences in gene abundance identified between P and NP were really caused by the purification step and were not stochastic, we randomly shuffled the 8 samples into two groups of four samples each, 10 times and compared each time, the transcriptome profiles of the two groups with DESeq2 (20).

Gene Ontology (GO) enrichment analysis was performed with Cytoscape v.3.8.2 (24) plugin BiNGO v.3.0.4 using EBI porcine Gene Ontology Annotation Database (release: 2021-02-01) with default settings. Only the significant corrected *p*-values with FDR correction were considered.

Evaluation of the Potential Tissue of Origin of the Differentially Abundant Genes Between Purified and Non-purified Samples

We carried an analysis to determine the potential tissue or cell type of origin of differentially abundant genes (DAG) between NP and P. We used a two-tailed Fisher's Exact Test to compare the proportion of genes with tissue-specific expression between the DAG and the non-DAG groups. We used an RNA-Seq dataset from an experiment carried by the Roslin Institute on 27 porcine tissues as part of the FAANG project (https://www.faang.org) with the NCBI's BioProject Accession Number PRJEB19386. The gene expression values (FPKM) of this dataset are available at the European Bioinformatics Institute ArrayExpress expression atlas (https://www.ebi.ac.uk/gxa/home) archive under file E-MTAB-5895. The catalog included two male and two female Duroc juveniles. All pigs were between four and six months old. The file provided tissue expression results from males and females separately. This dataset includes epididymis, penis, tonsil, amygdala, mesenteric lymph node, lung alveolus, liver, heart, adipose tissue, omentum, several central nervous system areas, skeletal muscle, spleen, several sections of the digestive tract, cortex of kidney, pituitary gland, and uterus. Tonsil was only analyzed in males. Obviously, the reproductive tissues were only represented by the one corresponding sex. We averaged the FPKM expression of the tissues analyzed in both males and females. We interrogated the genes with specific expression in epididymis as a male reproductive tissue and tonsil and lymph node as a tissue representing leukocytes which can be also be present in sperm. We also queried duodenum and skeletal muscle as two control tissues that are not expected to contribute cells to sperm.

We considered that a gene has a tissue-specific expression when its RNA FPKM in the target tissue was $>$20 and the FPKM in all the other tissues in the dataset was $<$5. Duodenum, tonsils and skeletal muscle did not show any tissue-specific gene. Thus, for these tissues we allowed up to three additional tissues with FPKM $>$ 5. The genes identified following these conditions were considered as nearly tissue-specific. Then, we compared the abundance of these tissue-specific genes in the list of DAGs and the list of non-DAGs from our study.

We repeated this analysis using the GTEx Portal (dbGaP accession number phs000424.v8.ps), which contains RNA-Seq data from 54 human tissues including the prostate and testis male reproductive tissues as well as several representative of adipose tissue, artery, central nervous system, digestive tract, female reproductive organs, whole blood, EBV transformed lymphocytes, heart, kidney, skeletal muscle, skin, salivary gland, spleen, and thyroid. We used Ensembl BioMart (version 104) to identify the human orthologs of all the genes identified in our sperm (DAG and non-DAG) experiment. We queried the GTEx dataset using these human orthologous genes. We targeted prostate and testis as male reproductive tissues, EBV-transformed lymphocytes, and whole blood representing lymphocytes, which can be also found in sperm and liver, nerve tibial and mammary

gland as control tissues which should not contain cell types that could be also found in sperm.

RESULTS AND DISCUSSION

RNA Extraction and qPCR Results

RNA extractions showed very similar yields between the P and NP groups (**Supplementary Table 2**). Moreover, all the minus reverse transcription of the control samples showed no amplification of *PRM1* and *PTPRC* and the qPCR on the intergenic region was undetectable in all P and NP samples, thereby indicating no DNA contamination (**Supplementary Table 2**). The eight samples presented quantification cycles (Cq) ranging between 15.7 and 17.6 for the *PRM1* sperm-specific gene (**Supplementary Table 2**). In contrast, the Cq for *PTPRC* blood-specific gene for the P samples ranged between 35.6 and 37.2, and between 32.6 and 37.6 in NP (**Supplementary Table 2**). The $\Delta Cq_{PTPRC-PRM1}$, calculated as the Cq for *PTPRC* minus the Cq for *PRM1* ranged between 18.1 and 21.0 in P, and 17 to 20.4 in NP, which means that, in average and as expected, the *PTPRC* assay had lower signal when compared to the *PRM1* assay in P than in NP (**Supplementary Table 2**). The NP aliquot of sample B2 showed more *PTPRC* signal ($\Delta Cq_{PTPRC-PRM1}$) than any other of the eight samples thereby suggesting a degree of somatic cell presence in this sample.

Sequencing Metrics

We sequenced an average of 67.6 million reads per sample. Of these, an average of 7.6 million reads were uniquely mapped to the porcine genome and used for downstream analysis (**Supplementary Table 3**). There were no significant differences between the sequencing metrics of P vs. NP samples (**Supplementary Table 3**).

Description and General Comparison of the P and NP Transcriptomes

Using HISAT2, we identified an average of 7,519 protein coding genes with FPKM $\geq$ 1 and 1,870 genes with FPKM $\geq$ 10 (**Supplementary Table 4**). The genes displaying most abundant RNA levels included *PRM1*, *HSPB9*, *OAZ3*, *TSSK6*, and *TPPP2*, among others and were mostly related to sperm biology (**Supplementary Table 4**).

Linear regression and correlation analysis based on the RNA levels of the 7,519 protein coding genes showed high correlations (between 0.93 in B4 and 0.99 in B3) between P and NP (**Figure 1**). Hierarchical clustering analysis of the 8 samples showed that the samples do not tend to group by the purification treatment but by their sample of origin (**Figure 2A**). Nevertheless, PCA seemed to separate NP and P into two different groups based on their principal component 1 (**Figure 2B**). Principal component 1 biggest contributors were *TTC38* followed by *PPARA*, *TRMU*, and *FAM118A*, which together explained 57.2% of this component (**Supplementary Table 5**). We searched the GTEx portal (dbGaP accession number phs000424.v8.ps) to determine the expression of these genes in human tissues. *TTC38* is mostly expressed in liver, small intestine, colon and whole blood and *PPARA* and *TRMU* have ubiquitous expression. On the contrary, *FAM118A* displays highest expression in testis, where spermatogenesis takes part, and prostate, which, at least in humans (25) and horse (26), contributes exosomes and can also provide epithelial cells to the human ejaculates (27). *TTC38*'s and *FAM118A*'s functions are not well known. *PPARA* is a transcription factor involved in energy metabolism and mitochondrial and peroxisomal function (28). *TRMU* is a mitochondrial tRNA modifying gene (29) thus related to protein synthesis. Sample B4 showed the largest disparity between NP and P of all the samples in all these analyses.

Contrarily to what happens in somatic cells, most sperm RNAs are fragmented. Thus, we also evaluated RNA fragmentation by measuring TIN, which ranges between 0 and 100 indicating from full fragmentation to full integrity of the transcript, and found similar ($p = 0.37$) TIN in the NP [mean $\pm$ standard deviation (SD) $= 19.44 \pm 16.04$] and the P (mean $\pm$ SD $= 17.89 \pm 15.45$) samples thereby indicating no major differences between both groups (**Supplementary Table 6**). This is probably due to the fact that the DAGs total RNAs represent a small proportion of the whole sperm transcriptome abundance (**Supplementary Table 4**).

Differential RNA Abundance Analysis Between P and NP

We also carried differential abundance analysis to identify these genes with different RNA levels in P when compared to NP, a scenario that could be potentially caused by the removal of somatic cells, premature germline cells, immature, and morphologically abnormal spermatozoa or seminal plasma exosomes from the ejaculates. We used the 7,519 genes with FPKM $\geq$ 1 for the differential analysis using a paired sample design. Three hundred and seventy-two of the genes with FPKM $\geq$ 1 and 81 of the genes with FPKM $\geq$ 10 showed significant differential RNA abundance between P and NP (**Supplementary Table 4**) and were thus considered DAGs. To check whether the list of DAGs was stochastic or really owed to technical differences produced by the purification step, we randomly shuffled 10 times the eight samples into two four-sample groups and carried differential gene abundance analysis between both groups. These analyses showed between none and five DAGs in each comparison (**Supplementary Table 7**), thereby suggesting that the purification step has an impact on the RNA abundance of some genes. Most of the 372 DAGs showed a decreased RNA abundance in the P samples (**Supplementary Table 4**) which indicates that some cell types, organelles or vesicles were removed during the purification step. Only *TNNI3*, *CTXN1*, *SLC27A5*, *HSPA12B*, and ENSSSCG00000032730 presented increased RNA levels in P in at least three of the four samples (**Supplementary Table 4**). According to the GTEx portal (dbGaP accession number phs000424.v8.ps), *TNNI3*, a component of the striated muscle filaments, is exclusively expressed in the heart although one study linked it to prostate cancer (30). *CTXN1* is most highly expressed in the brain but it is also present at lower levels in several other tissues including testis, and its function is

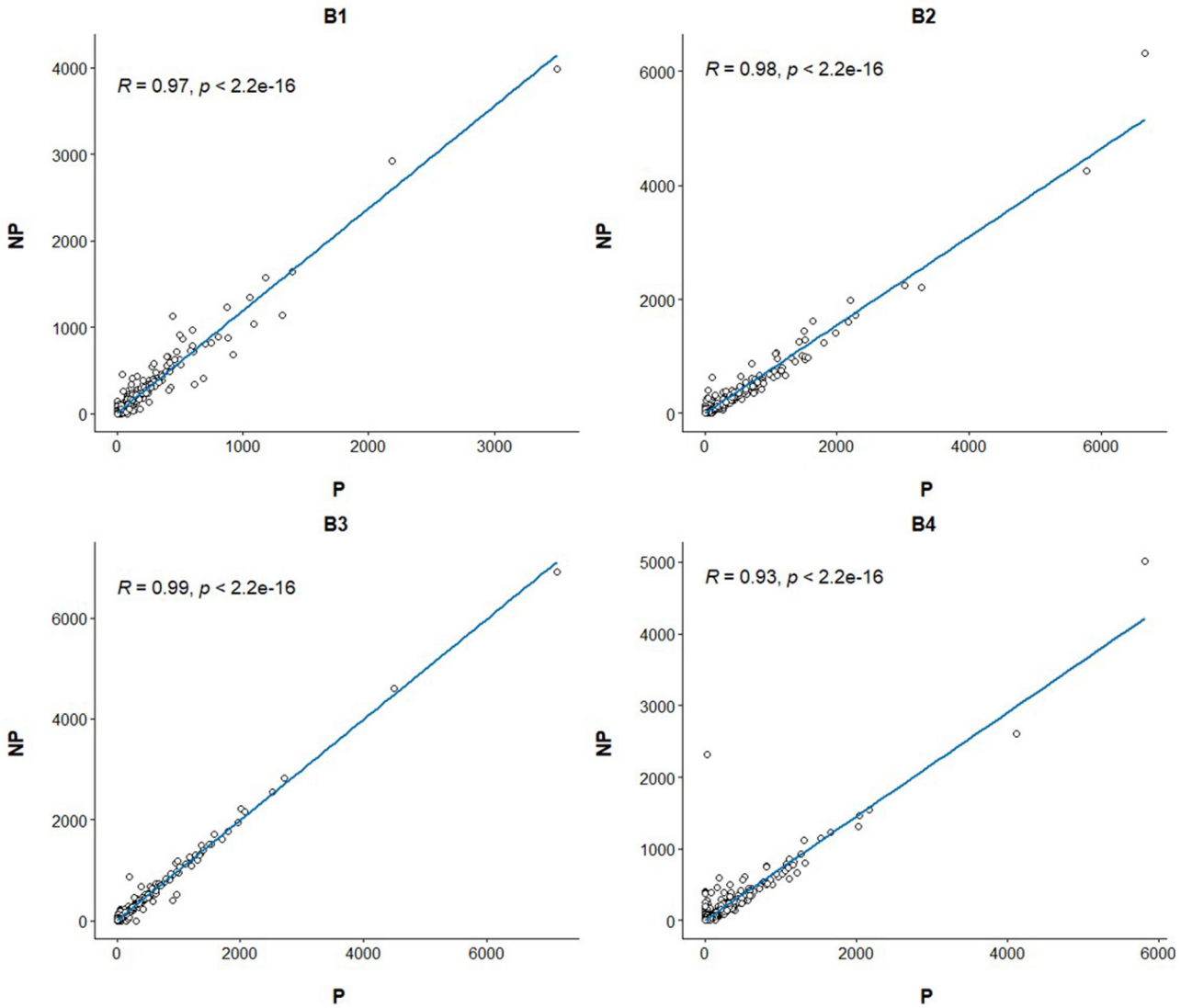

FIGURE 1 | Linear regression and Pearson correlation of the transcriptome profiles between the purified and non-purified aliquots for the four ejaculates. The Pearson correlation and its *p*-value are annotated at the top left of each plot.

related to brain biology (31). *SLC27A5* is exclusively expressed in liver and is associated to lipid metabolism and bile synthesis (32). *HSPA12B* is highly abundant in spleen, lung, breast, and adipose tissues and has been related to heart injury (33) and lung cancer (34). Thus, no particular link with the cells expected to be found in the ejaculates could be drew for these genes. *TNNI3*, *SLC27A5*, *HSPA12B*, and ENSSSCG00000032730 presented low average abundance across the eight samples (FPKM < 5) and even if significant, this data, should be considered with caution as it could be spurious. *CTXN1* displayed a much larger average abundance (FPKM = 85) and it is more likely to be real. Its increased levels in P indicate that a particular entity in the ejaculate—perhaps a particular sub-population of sperm cells—carrying this gene are more likely to be present after purification. However, as this is the only gene showing clear presence in the sperm and an increase in P, we cannot exclude the possibility that this was a spurious result. The 372 DAGs were enriched for GO terms related to translation and transcription and metabolic processes (**Supplementary Table 8**) and in fact, the list contained a large number of ribosomal proteins (e.g., *RPS3A*, *RPS27A*, and *RPL7*). The DAG group was clearly enriched over the non-DAG list for RPL and RPS ribosomal protein genes (Two-Tailed Fisher's Exact Test $p <$ 1.9E-53), which showed decreased levels in P when compared to NP. The majority of the DAGs showed an average abundance below 10 FPKM (**Supplementary Table 4**). Among the list of DAGs with average abundance above 10 FPKM, the top 10 that showed most significant differences included four ribosomal proteins and six genes with distinct functions (**Table 1**). These 10 genes are expressed in a wide catalog of tissues (GTEx portal;

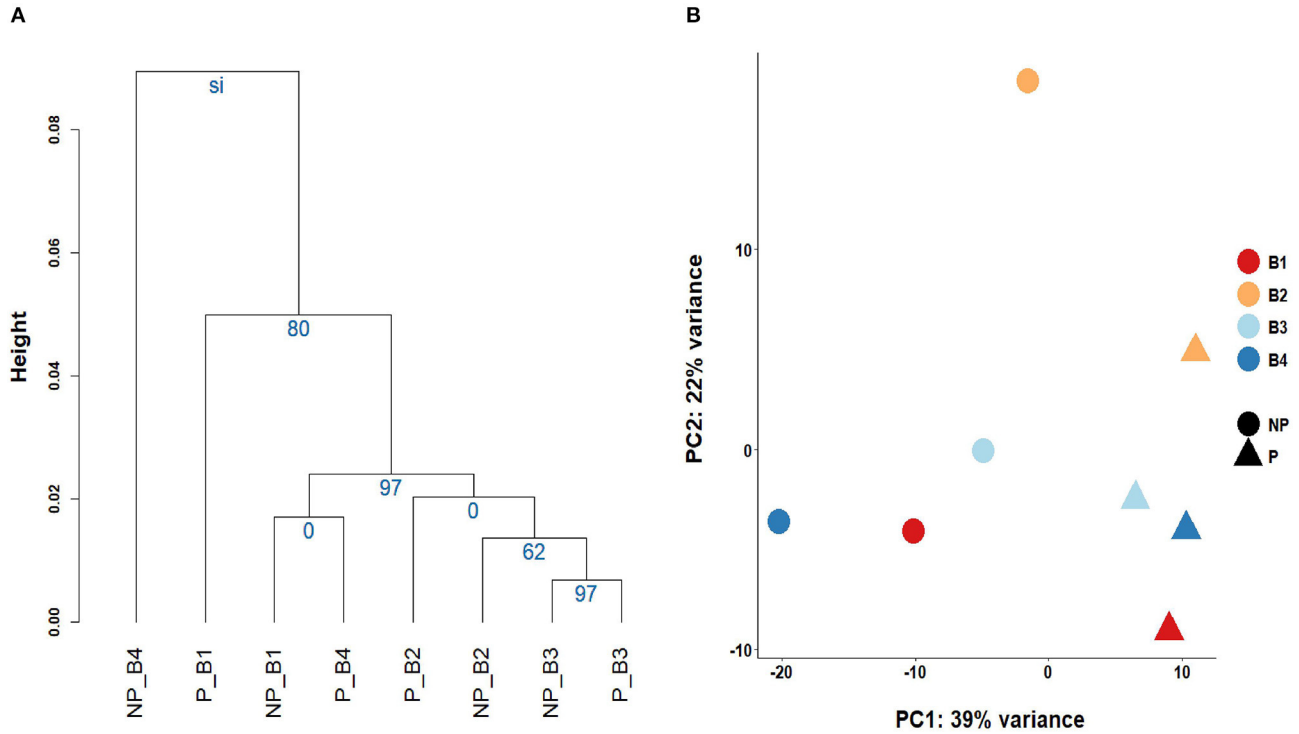

FIGURE 2 | Grouping of the sperm transcriptomes of the eight samples. **(A)** Cluster analysis and the Selective Inference *p*-values. **(B)** Principal Component Analysis biplot.

dbGaP accession number phs000424.v8.ps), but preferentially in EBV-transformed lymphocytes and most of them also in the female reproductive organs (**Table 1**). *PTMA* is related to cell proliferation (35), immunity (36), and chromatin remodeling (37) and it is also expressed in rat spermatocytes and spermatids but its functions in these cells are unknown (38). *NANS* is involved in the synthesis of sialic acid in multiple cell types and cellular processes (39) and within the catalog of human tissues, it is most highly expressed in the prostate but it is also present in other tissues including sperm. Sialic acid is a key component of the sperm glycocalyx assembled during sperm development, maturation and upon contact with the seminal fluid and is related to sperm. *TMSB4X* is linked to actin polymerization and cytoskeleton organization (40) and is most highly expressed in EBV transformed lymphocytes. *EEF1A1* delivers tRNA to the ribosome for translation elongation (41). One study carried RNA-Seq on chromatoid bodies isolated from testicles from GRTH knock-in mice with a sterile phenotype lacking elongated spermatids and spermatozoa (42). Chromatoid bodies are typically present in the cytoplasm of spermatocytes and round spermatids but are absent in elongating spermatids and spermatozoa and seem to be crucial for spermatogenesis. In this study, the authors identified an increased presence of genes related to transcript regulation, including *EEF1A1* in the mutant when compared to the wild type mice. *RACK1* acts as a scaffold assisting and modulating protein-protein interactions to recruit, assemble or regulate signaling molecules (43) and is a component of the 40S ribosomal subunit (44). The interaction between RACK1 and the AChE-R acetylcholinesterase splice variant in the spermatocytes of transgenic mice overexpressing *AChE-R* and displaying reduced sperm differentiation and sperm count showed that the interactions between AChE-R with RACK1 and enolase-α may be related to these sperm related phenotypes (45).

To get a glimpse of the tissue or cell type of origin of the DAGs group, we compared the proportion of the 372 DAGs with preferential expression in the porcine epididymis, a male reproductive organ known to contribute RNAs to the ejaculate (46), the tonsils and lymph node, that contain leukocytes, which could be also present in sperm. We also queried duodenum and skeletal muscle as control tissues that should not contain cell types also present in sperm. Three hundred and sixty-six DAG and 6,992 non-DAG genes were also present in the E-MTAB-5895 porcine gene expression catalog. Fifty-seven genes displayed specific expression in the epididymis, 5 and 13 of which were DAG and non-DAG, respectively (**Table 2**). Thus, 1.3% of the DAGs and 0.2% of the non-DAGs showed epididymis-specific expression. The two-tailed Fisher's Exact Test showed a clear difference ($p = 0.001$) between the abundance of epididymis specific genes in the DAG list when compared to the non-DAG group. Skeletal muscle and duodenum showed 48 and 5 tissue-specific genes, respectively. Five and one genes showed tissue-specific expression in the tonsils and lymph node, respectively, but none of these was present in our porcine sperm samples.

TABLE 1 | Ten most differentially abundant genes with FPKM ≥ 10 between the purified and paired non-purified samples.

Ensembl identifier	Gene name	FDR	Average FPKM	B1 P/NP	B2 P/NP	B3 P/NP	B4 P/NP	Average P/NP	Human tissues with highest expression according to the GTEx Portal
ENSSSCG00000041806	–	5.74E-14	40	0.06	0.11	0.29	0.17	0.16	
ENSSSCG00000037274	Prothymosin Alpha (*PTMA*)	2.31E-12	32	0.08	0.31	0.14	0.07	0.15	Quite ubiquotous but mostly expressed in EBV-transformed lymphocytes. Low expression in testis.
ENSSSCG00000005373	N-Acetylneuraminate Synthase (*NANS*)	2.31E-12	16	0.03	0.23	0.30	0.10	0.16	Highest expression in the prostate and colon.
ENSSSCG00000009019	Ribosomal Protein S3A (*RPS3A*)	2.92E-12	13	0.10	0.26	0.17	0.06	0.15	Mostly expressed in the female reproductive organs and EBV-transformed lymphocytes.
ENSSSCG00000032111	Ribosomal Protein L7 *(RPL7*)	1.86E-11	15	0.09	0.47	0.14	0.14	0.21	Mostly expressed in the female reproductive organs and EBV-transformed lymphocytes.
ENSSSCG00000012119	Thymosin Beta 4 X-Linked (*TMSB4X*)	3.66E-11	16	0.09	0.16	0.12	0.20	0.14	Mostly expressed in EBV-transformed lymphocytes, spleen, lung, and whole blood.
ENSSSCG00000004489	Eukaryotic Translation Elongation Factor 1 Alpha 1 (*EEF1A1*)	4.45E-11	93	0.07	0.48	0.29	0.10	0.24	Mostly expressed in cultured fibroblasts, EBV-transformed lymphocytes, ovary, and uterus.
ENSSSCG00000033019	Ribosomal Protein L12 (*RPL12*)	5.8E-11	16	0.05	0.20	0.17	0.10	0.13	Most highly expressed in EBV-transformed lymphocytes, ovary, cultured fibroblasts, and cervix.
ENSSSCG00000029724	Receptor For Activated C Kinase 1 (*RACK1*)	6.6E-11	19	0.09	0.26	0.28	0.17	0.20	Most highly expressed in ovary, EBV-transformed lymphocytes, cultured fibroblasts, and cervix.
ENSSSCG00000031088	Ribosomal Protein S7 (*RPS7*)	7.0E-11	81	0.10	0.58	0.33	0.28	0.32	Most highly expressed in ovary, EBV-transformed lymphocytes and cultured fibroblasts.

B1 P/NP, Ratio of the FPKM in the purified and the FPKM in the non-purified in B1; B2 P/NP, Ratio of the FPKM in purified and the FPKM in non-purified in B2; B3 P/NP, Ratio of the FPKM in purified and the FPKM in non-purified in B3; B4 P/NP, Ratio of the FPKM in purified and the FPKM in non-purified in B4; Average P/NP, Average of the ratio of the FPKM in purified and the FPKM in non-purified in the four samples.

For these three tissues we allowed up to three additional tissues with FPKM > 5. None of these four tissues showed a statistical difference between DAGs and non-DAGs (**Table 2**).

We carried the same analysis on the dataset of gene expression in 54 human tissues from the GTEx Portal (dbGaP accession number phs000424.v8.ps) querying testis and prostate as male reproductive organs, EBV transformed lymphocytes and whole blood as representatives of leukocytes and liver, nerve tibial and mammary gland as negative controls. Three hundred and twenty-seven and 6,304 DAGs and non-DAGs had a human ortholog present in the GTEx catalog (**Table 2**). Only testis, liver, and nerve tibial showed tissue-specific genes (**Table 2**). For prostate, EBV transformed lymphocytes, whole blood and mammary gland, we selected those genes which showed FPKM > 20 in the target tissue and FPKM > 5 in not more than three additional tissues. The list of testis-specific genes were the only ones that showed a statistically significant difference between DAGs and non-DAGs ($p = 5.4E-07$) but these genes were enriched in the non-DAG group (**Table 2**).

The genes *HBB*, *CDH1*, *PTPRC*, *KRT1*, *KRT10*, *CXCL8*, and *KLK3* previously used to determine the presence of leukocytes, epithelial cells, and prostate in human (47) and pig (5) showed no detectable levels of RNA in P and NP. Only *HBB* presented moderate abundance (FPKM = 36) in the NP sample from B4 (**Supplementary Table 4**). This data indicates that most NP samples are free of detectable levels of RNAs from somatic cell origin but that B4 may have contained a sufficient proportion of leukocytes to provide detectable levels of *HBB*. This is in line with the results on the cluster and PCA analyses which showed that the NP sample of B4 clustered and mapped apart from all the other samples and the fact that this sample showed the highest abundance for 266 of the 372 DAGs.

In light of these results, we wanted to explore whether the contribution of each sample to the list of DAGs was homogeneous or on the contrary, there was high variability between samples. We carried four differential abundance analyses between P and the paired NP samples but this

TABLE 2 | Number of tissue-specific or nearly tissue-specific genes in the DAG and non-DAG groups and *p*-value of the comparison of the proportion of these genes in both groups.

Tissue	Number of tissue-specific genes	Number of tissue-specific genes present in pig sperm	Number of nearly tissue-specific genes	Number of nearly tissue-specific genes present in pig sperm	Number in DAG	Number in non-DAG	*P*-value
Epididymis	57	18	N/A	N/A	5	13	0.001
Skeletal muscle	48	6	N/A	N/A	0	6	1
Duodenum	5	2	N/A	N/A	0	2	1
Lymph node	1	0	14	1	0	1	1
Tonsils	5	0	50	10	2	8	0.08
Testis	908	295	N/A	N/A	0	295	5.40E-07
Prostate	5	0	16	3	1	2	0.14
EBV transformed lymphocytes	13	0	149	40	0	40	0.26
Whole blood	7	0	105	6	0	6	1
Mammary	0	0	7	0	0	0	1
Liver	85	3	N/A	N/A	0	3	1
Nerve tibial	2	1	N/A	N/A	0	1	1

Number in DAG, number of tissue-specific or nearly tissue-specific genes in the DAG group. Number in non-DAG, number of tissue-specific or nearly tissue-specific genes in the non-DAG group. P-value, P-value of the two-tailed Fisher's Exact Test comparing the proportion of tissue specific or nearly tissue-specific genes in the DAG vs. the non-DAG groups. N/A, non applicable.

time, removing each time, a different sample and thus carrying the comparison on only three ejaculates. The results demonstrated that the removal of sample B4 caused the most dramatic reduction of the number of DAGs when compared to the original differential abundance analysis carried on the four samples (**Supplementary Table 9**). Despite this outcome, the correlation between the NP and P transcriptomes of B4 was still high ($R^2 = 0.93$) which shows that even in this sample, the BoviPure^{TM} purification did not have a dramatic impact of the overall transcriptome profile of this sample. Remarkably, the removal of B2 did not show any relevant change in the number of DAGs which, contrarily to what was indicated by the $\Delta Cq_{PTPRC-PRM1}$, suggests no particular contamination of somatic cell RNAs. The semen quality phenotypes of the fresh ejaculate of B4 before purification showed lower ejaculate volume but all the other parameters (sperm cell concentration, sperm cell viability, percentage of spermatozoa with head, tail, or neck abnormalities, percentage of sperm cells with proximal or distal droplets and percentage of motile spermatozoa), did not deviate from the values observed in the other three samples (**Supplementary Table 1**). Therefore, we could not link the difference on the transcriptome of this sample to the semen quality phenotypes.

A somehow surprising finding was the clear enrichment of RPL and RPS ribosomal protein genes in the DAG group over the non-DAG list (Two-Tailed Fisher's Exact Test $p < 1.9E-53$), which showed decreased abundance in P when compared to NP. As intact ribosomal RNAs (rRNAs) are depleted in sperm to warrant translational silencing (48), we hypothesize that spermatozoa may also have reduced RNA levels of proteins forming the ribosomal sub-units. If true, this would indicate that the DAGs are contributed mostly by non-sperm entities.

This is also supported by the enriched abundance of human testis specific genes in the non-DAG list. We hypothesize that these non-DAG genes are specific to the later stages of spermatogenesis and they are present in the mature spermatozoa, which are not removed by the BoviPure^{TM} treatment. As a matter of fact, the list of 295 sperm-specific genes present in the non-DAG include important genes related to sperm biology and function such as *PRM1*, *PRM2*, *CATSPER1*, *CATSPERD*, *DAZL*, and several members of the *SPATA* and *SPACA* families among others (**Supplementary Table 10**).

As reviewed by Fedder in 1996, research in human semen has identified the presence of leukocytes, squamous epithelial cells, Sertoli cells, spermatogonia, spermatocytes, and spermatids (49). In addition, the presence of epithelial cells from the epididymis (50) and the prostate (27) have been also confirmed. In swine, sperm from artificial insemination studs rarely contain leukocytes but low levels of epithelial cells are frequently found (Michael Kleve-Feld, Personal Communication). We detected 57 pig epididymis-specific genes, 18 of which were present in our boar sperm samples. The DAG group was enriched for such genes, which indicates the removal of epididysomal cells or exosomes after the purification. On the other side, we did not find statistically significant differences in the proportion of human prostate-specific genes between the DAG and the non-DAG groups. This could be indicating that the prostate did not contribute a detectable level of epithelial cells or exosomes to the pig sperm but it could also be caused by the small number of human prostate's nearly specific genes, only 16, that we identified in the study, with

resulted in only one and two genes present in the DAG and the non-DAG lists, respectively. Notwithstanding, the absence of detectable levels of prostate cells in sperm is also supported by the null presence of *KLK3* in all the NP and P samples.

The presence of epididymal material in sperm could be due to either epithelial cells or exosomes or a combination of both. Seminal exosomes have been found in the boar sperm (51). RNA-Seq data from human (52) and porcine (46) seminal exosomes showed that the RNA cargo of these vesicles is mostly made up of short RNAs but also include protein-coding RNAs. In pigs, RNA-Seq of the small RNA fraction of seminal exosomes from ejaculates displaying normal semen quality parameters showed that 25.3% of the sequencing reads corresponded to messenger RNAs (mRNAs). As the objective of this study was on microRNAs, the authors did not provide additional detail on the messenger RNAs present in the boar exosomes (46). Whether the BoviPure^{TM} purification removes the seminal vesicles is unknown. From the one side, BoviPure^{TM} separates the seminal fluid from the mature spermatozoa which should eliminate the exosomes present in the fluid. But on the other side, seminal exosomes also bind to the sperm's cell membrane and their removal after gradient-based protocols is uncertain. We don't know whether these exosomes unbind from the sperm during the purification or whether the sperm cells bound to exosomes have a distinct density that could remove them after purification. This also happens for the NP samples as they were subjected to a 14,000 g centrifugation for 4 minutes. Exosomes sedimentation often uses ultra-centrifugations of at least 120,000 g for 70 min. However, whether the sperm bound exosomes will sediment alongside with the sperm is unsure. In consequence, we hypothesize that the most likely largest contributor to the DAG list are epididysomal epithelial cells. A somatic cell has been estimated to contain in average between 10 and 30 picograms of RNA, in contrast with an average of 15 femtograms for a human spermatozoon. In addition, our own estimation suggests that the porcine sperm contains in average 1.6 femtograms per cell (5). Hence, the presence of an even tiny proportion of these epithelial cells in the sperm might be able to contribute detectable levels of RNA in the sample.

In order to further identify the origin of the RNAs impacted by BoviPure^{TM}, future studies should be carried. To determine the contribution of abnormal or immature spermatozoa, the comparison should include an additional control consisting of an aliquot treated with somatic cell lysis buffer or sonication. The comparison between the three conditions should be still taken with caution as the SDS present in the lysis buffer could solubilise the sperm's membrane and remove its midpiece, which contains a large number of mitochondria thereby altering the resulting transcriptome (13). The contribution of the seminal exosomes could be further elucidated by purifying these vesicles by either ultra-centrifugation, or filtration by gradient based protocols and comparing the resulting transcriptome with that of the NP and P samples. This experiment should be accompanied by the exploration under the electron microscope of extracellular vesicles in the purified and non-purified samples. In any case, the results identified in swine cannot be translated to humans because the pig semen contains a much lower proportion of somatic cells than the men's ejaculate.

CONCLUSION

Three of the four ejaculates had undetectable levels of somatic cell RNA markers before purification, thereby showing an agreement with the low levels of non-sperm cells typically found in samples from boar artificial insemination studs. We found strong indications that the purification with BoviPure^{TM} has a mild but noticeable impact on the RNA abundance of some genes and that this was originated by the removal of non-sperm cell entities with the most likely contribution of epididymal epithelial cells. The evaluation of the 10 most differentially abundant genes also indicated the removal of premature germline cells—even immature or morphologically abnormal spermatozoa—as well as leukocytes with a distinct RNA cargo. In light of these results, our group feels comfortable with the use of non-purified samples for the interrogation of the relationship between spermatozoon RNAs and semen quality traits. However, this should be decided by each research group in accordance to the experimental design and objective of their study.

DATA AVAILABILITY STATEMENT

The data presented in the study are deposited in the NCBI's short read archive repository, accession numbers SRR14117413, SRR14117412, SRR14117411, SRR14117410, SRR14117409, SRR14117408, SRR14117407, and SRR14117406.

ETHICS STATEMENT

Ethical review and approval was not required for the animal study because this study was done on ejaculates that were privately owned by a commercial farm for non-research purposes. The owners provided consent for their use for research. Specialized professionals at the farm collected the ejaculates following standard routine procedures and guidelines.

AUTHOR CONTRIBUTIONS

AS and ACl conceived and designed the experiments. SB collected the samples. JR-G carried the phenotypic analysis. ACa carried the qPCR analyses. MG performed sperm purifications and RNA extractions. YL and MG made the bioinformatics and statistics analysis. YL, MG, and ACl analyzed the data. ACl, YL, JR-G, and MG wrote the manuscript. All authors discussed the data and read and approved the contents of the manuscript.

FUNDING

This work was supported by the Spanish Ministry of Economy and Competitiveness (MINECO) under grant AGL2013-44978-R and grant AGL2017-86946-R and by the CERCA Programme/Generalitat de Catalunya. AGL2017-86946-R was also funded by the Spanish State Research Agency (AEI) and the European Regional Development Fund (ERDF). We thank the Agency for Management of University and Research Grants (AGAUR) of the Generalitat de Catalunya (Grant Numbers 2014 SGR 1528 and 2017 SGR 1060). We also acknowledge financial support from the Spanish Ministry of Science and Innovation, through the Severo Ochoa Programme for Centers of Excellence in R&D SEV-2015-0533 and CEX2019-000902-S. YL thanks the China Scholarship Council for her PhD scholarship. We acknowledge support of the publication fee by the CSIC Open Access Publication Support Initiative through its Unit of Information Resources for Research (URICI).

SUPPLEMENTARY MATERIAL

The Supplementary Material for this article can be found online at: https://www.frontiersin.org/articles/10.3389/fvets.2021.668158/full#supplementary-material

Supplementary Table 1 | Phenotypic values for several semen quality parameters of the four ejaculates used in this study.

Supplementary Table 2 | RNA extraction and qPCR data. P_B1, Purified sample of B1; NP_B1, Non-purified sample of B1; P_B2, Purified sample of B2; NP_B2, Non-purified sample of B2; P_B3, Purified sample of B3; NP_B3, Non-purified sample of B3; P_B4, Purified sample of B4; NP_B4, Non-purified sample of B4; P_average, Average value of the purified samples; NP_average, Average value of the non-purified samples.

Supplementary Table 3 | Sequencing metrics. P_B1: Purified sample of B1; NP_B1: Non-purified sample of B1; P_B2: Purified sample of B2; NP_B2: Non-purified sample of B2; P_B3: Purified sample of B3; NP_B3: Non-purified sample of B3; P_B4: Purified sample of B4; NP_B4: Non-purified sample of B4.

Supplementary Table 4 | Gene abundance across the eight samples for the 7,519 protein coding genes with average FPKM $\geq$ 1. DAG, Differentially abundant gene; FDR, False Discovery Rate; P_B1, Purified sample of B1; NP_B1, Non-purified sample of B1; P_B2, Purified sample of B2; NP_B2, Non-purified sample of B2; P_B3, Purified sample of B3; NP_B3, Non-purified sample of B3; P_B4, Purified sample of B4; NP_B4, Non-purified sample of B4.

Supplementary Table 5 | Major gene contributors to principal component 1 of the Principal Component Analysis.

Supplementary Table 6 | Transcript Integrity Number values across the eight samples. P_B1, Purified sample of B1; NP_B1, Non-purified sample of B1; P_B2, Purified sample of B2; NP_B2, Non-purified sample of B2; P_B3, Purified sample of B3; NP_B3, Non-purified sample of B3; P_B4, Purified sample of B4; NP_B4, Non-purified sample of B4.

Supplementary Table 7 | Results of the 10 shuffles to organize the eight samples into 2 four-sample random groups. P_B1, Purified sample of B1; NP_B1, Non-purified sample of B1; P_B2, Purified sample of B2; NP_B2, Non-purified sample of B2; P_B3, Purified sample of B3; NP_B3, Non-purified sample of B3; P_B4, Purified sample of B4; NP_B4, Non-purified sample of B4. Random shuffles are identified as Random1, Random2, Random3, Random4, Random5, Random6, Random7, Random8, Random9, Random10. A and B denote the randomly generated groups in each shuffle.

Supplementary Table 8 | Results of the Gene Ontology analysis of the 372 differentially abundant genes between the purified and the non-purified samples.

Supplementary Table 9 | List of differentially abundant genes when including the four ejaculates and when removing the ejaculates B1, B2, B3, or B4. The second row shows the number of DAGs identified in that analyses. Down, gene showing significantly decreased RNAs levels in P when compared to NP. Up, gene showing significantly increased RNAs levels in P when compared to NP.

Supplementary Table 10 | List of tissue-specific or nearly tissue-specific genes for pig epididymis, lymph node, tonsil, duodenum and skeletal muscle and for human prostate, testis, EBV transformed lymphocytes, whole blood, liver, and nerve tibial that are also present in the pig sperm. The last column shows whether that particular gene belonged to the DAG or the non-DAG group.

REFERENCES

1. Gòdia M, Swanson G, Krawetz SA. A history of why fathers' RNA matters. *Biol Reprod.* (2018) 99:147–59. doi: 10.1093/biolre/ioy007
2. Jodar M, Sendler E, Moskovtsev SI, Librach CL, Goodrich R, Swanson S, et al. Absence of sperm RNA elements correlates with idiopathic male infertility. *Sci Transl Med.* (2015) 7:295re6. doi: 10.1126/scitranslmed.aab1287
3. Keles E, Malama E, Bozukova S, Siuda M, Wyck S, Witschi U, et al. The micro-RNA content of unsorted cryopreserved bovine sperm and its relation to the fertility of sperm after sex-sorting. *BMC Genomics.* (2021) 22:30. doi: 10.1186/s12864-020-07280-9
4. Suliman Y, Becker F, Wimmers K. Implication of transcriptome profiling of spermatozoa for stallion fertility. *Reprod Fertil Dev.* (2018) 30:1087–98. doi: 10.1071/RD17188
5. Gòdia M, Mayer FQ, Nafissi J, Castelló A, Rodríguez-Gil JE, Sánchez A, et al. A technical assessment of the porcine ejaculated spermatozoa for a sperm-specific RNA-seq analysis. *Syst Biol Reprod Med.* (2018) 64:291–303. doi: 10.1080/19396368.2018.1464610
6. Gòdia M, Estill M, Castelló A, Balasch S, Rodríguez-Gil JE, Krawetz SA, et al. A RNA-seq analysis to describe the boar sperm transcriptome and its seasonal changes. *Front Genet.* (2019) 10:299. doi: 10.3389/fgene.2019.00299
7. Gòdia M, Castelló A, Rocco M, Cabrera B, Rodríguez-Gil JE, Balasch S, et al. Identification of circular RNAs in porcine sperm and evaluation of their relation to sperm motility. Sci Rep. (2020) 10:7985. doi: 10.1038/s41598-020-64711-z
8. Ablondi M, Gòdia M, Rodriguez-Gil JE, Sánchez A, Clop A. Characterisation of sperm piRNAs and their correlation with semen quality traits in swine. *Anim Genet.* (2021) 52:114–20. doi: 10.1111/age.13022
9. Fraser L, Brym P, Pareek CS, Mogielnicka-Brzozowska M, Paukszto, Jastrzebski JP, et al. Transcriptome analysis of boar spermatozoa with different freezability using RNA-Seq. *Theriogenology.* (2020) 142:400–13. doi: 10.1016/j.theriogenology.2019.11.001
10. Alvarez-rodriguez M, Martinez C, Wright D, Barranco I, Roca J, Rodriguez-martinez H. The transcriptome of pig spermatozoa, and its role in fertility. *Int J Mol Sci.* (2020) 21:1572. doi: 10.3390/ijms21051572
11. Das PJ, McCarthy F, Vishnoi M, Paria N, Gresham C, Li G, et al. Stallion sperm transcriptome comprises functionally coherent coding and regulatory RNAs as revealed by microarray analysis and RNA-seq. *PLoS One.* (2013) 8:e56535. doi: 10.1371/journal.pone.0056535
12. Gòdia M, Reverter A, González-Prendes R, Ramayo-Caldas Y, Castelló A, Rodríguez-Gil JE, et al. A systems biology framework integrating GWAS and RNA-seq to shed light on the molecular basis of sperm quality in swine. *Genet Sel Evol.* (2020) 52:1–21. doi: 10.1186/s12711-020-00592-0
13. Mao S, Goodrich RJ, Hauser R, Schrader SM, Chen Z, Krawetz SA. Evaluation of the effectiveness of semen storage and sperm purification methods for spermatozoa transcript profiling. *Syst Biol Reprod Med.* (2013) 59:287–95. doi: 10.3109/19396368.2013.817626
14. Nätt D, Kugelberg U, Casas E, Nedstrand E, Zalavary S, Henriksson P, et al. Human sperm displays rapid responses to diet. *PLoS Biol.* (2019) 17:e3000559. doi: 10.1371/journal.pbio.3000559

15. Godia M, Castello A, Rocco M, Cabrera B, Rodriguez-Gil J, Sanchez A, et al. Identification of circular RNAs in porcine sperm and their relation to sperm motility. *Sci. Rep*. (2019). doi: 10.1101/608026
16. King GJ, W MJ. A comparison of two methods for boar semen collection. *J Anim Sci.* (1973) 36:563–5. doi: 10.2527/jas1973.363563x
17. Bolger AM, Lohse M, Usadel B. Trimmomatic: a flexible trimmer for Illumina sequence data. *Bioinformatics.* (2014) 30:2114–20. doi: 10.1093/bioinformatics/btu170
18. Kim D, Langmead B, Salzberg SL. HISAT: a fast spliced aligner with low memory requirements. *Nat Methods.* (2015) 12:357–60. doi: 10.1038/nmeth.3317
19. Pertea M, Pertea GM, Antonescu CM, Chang T, Mendell JT, Salzberg SL. StringTie enables improved reconstruction of a transcriptome from RNA-seq reads. *Nat Biotechnol.* (2015) 33:290–5. doi: 10.1038/nbt.3122
20. Love MI, Huber W, Anders S. Moderated estimation of fold change and dispersion for RNA-seq data with DESeq2. *Genome Biol.* (2014) 15:550. doi: 10.1186/s13059-014-0550-8
21. Suzuki R, Shimodaira H. Pvclust: An R package for assessing the uncertainty in hierarchical clustering. *Bioinformatics.* (2006) 22:1540–2. doi: 10.1093/bioinformatics/btl117
22. Wickham H. *ggplot2: Elegant Graphics for Data Analysis.* (2016) Available online at: https://ggplot2.tidyverse.org (accessed April 23, 2021).
23. Wang L, Nie J, Sicotte H, Li Y, Eckel-Passow JE, Dasari S, et al. Measure transcript integrity using RNA-seq data. *BMC Bioinformatics.* (2016) 17:58. doi: 10.1186/s12859-016-0922-z
24. Shannon P, Markiel A, Ozier O, Baliga NS, Wang JT, Ramage D, et al. Cytoscape: a software environment for integrated models. *Genome Res.* (1971) 13:426.
25. Aalberts M, van Dissel-Emiliani FMF, van Adrichem NPH, van Wijnen M, Wauben MHM, Stout TAE, et al. Identification of distinct populations of prostasomes that differentially express prostate stem cell antigen, annexin A1, and GLIPR2 in humans. *Biol Reprod.* (2012) 86:1–8. doi: 10.1095/biolreprod.111.095760
26. Aalberts M, Sostaric E, Wubbolts R, Wauben MWM, Nolte-'T Hoen ENM, Gadella BM, et al. Spermatozoa recruit prostasomes in response to capacitation induction. *Biochim Biophys Acta Proteins Proteomics.* (2013) 1834:2326–35. doi: 10.1016/j.bbapap.2012.08.008
27. Andrade-Rocha FT. Assessment of exfoliated prostate cells in semen: Relationship with the secretory function of the prostate. *Am J Clin Pathol.* (2007) 128:788–93. doi: 10.1309/9ELYPH61DBD8AXYC
28. Vamecq J, Latruffe N. Medical significance of peroxisome proliferator-activated receptors. *Lancet.* (1999) 354:141–8. doi: 10.1016/S0140-6736(98)10364-1
29. Sasarman F, Antonicka H, Horvath R, Shoubridge EA. The 2-thiouridylase function of the human MTU1 (TRMU) enzyme is dispensable for mitochondrial translation. *Hum Mol Genet.* (2011) 20:4634–43. doi: 10.1093/hmg/ddr397
30. Gupta A, Shukla N, Nehra M, Gupta S, Malik B, Mishra AK, et al. A pilot study on the whole exome sequencing of prostate cancer in the indian phenotype reveals distinct polymorphisms. *Front Genet.* (2020) 11:874. doi: 10.3389/fgene.2020.00874
31. Levchuk LA, Ivanova SA, Semke VY. Effects of neuroprotector cortexin on the dynamics of neuroendocrine system parameters in patients with organic emotionally labile (asthenic) disorders. *Bull Exp Biol Med.* (2013) 155:75–7. doi: 10.1007/s10517-013-2083-7
32. Sharma V, Hiller M. Loss of enzymes in the bile acid synthesis pathway explains differences in bile composition among mammals. *Genome Biol Evol.* (2018) 10:3211–7. doi: 10.1093/gbe/evy243
33. Zhao Y, Liu C, Liu J, Kong Q, Mao Y, Cheng H, et al. HSPA12B promotes functional recovery after ischaemic stroke through an eNOS-dependent mechanism. *J Cell Mol Med.* (2018) 22:2252–62. doi: 10.1111/jcmm.13507
34. Ma H, Lu T, Zhang X, Li C, Xiong J, Huang L, et al. HSPA12B: a novel facilitator of lung tumor growth. *Oncotarget.* (2015) 6:9924–36. doi: 10.18632/oncotarget.3533
35. Letsas KP, Frangou-Lazaridis M. Surfing on prothymosin alpha proliferation and anti-apoptotic properties. *Neoplasma.* (2006) 53:92–6.
36. Ioannou K, Derhovanessian E, Tsakiri E, Samara P, Kalbacher H, Voelter W, et al. Prothymosin α and a prothymosin α-derived peptide enhance TH1-type immune responses against defined HER-2/neu epitopes. *BMC Immunol.* (2013) 14:43. doi: 10.1186/1471-2172-14-43
37. Gómez-Márquez J. Function of prothymosin α in chromatin decondensation and expression of thymosin β-4 linked to angiogenesis and synaptic plasticity. *Ann N Y Acad Sci.* (2007) 1112:201–9. doi: 10.1196/annals.1415.020
38. Ferrara D, Izzo G, Pariante P, Donizetti A, D'Istria M, Aniello F, et al. Expression of prothymosin alpha in meiotic and post-meiotic germ cells during the first wave of rat spermatogenesis. *J Cell Physiol.* (2010) 224:362–8. doi: 10.1002/jcp.22131
39. Schnaar RL, Gerardy-Schahn R, Hildebrandt H. Sialic acids in the brain: gangliosides and polysialic acid in nervous system development, stability, disease, and regeneration. *Physiol Rev.* (2014) 94:461–518. doi: 10.1152/physrev.00033.2013
40. Cassimeris L, Safer D, Nachmias VT, Zigmond SH. Thymosin beta 4 sequesters the majority of G-actin in resting human polymorphonuclear leukocytes. *J Cell Biol.* (1992) 119:1261–70. doi: 10.1083/jcb.119.5.1261
41. Knight JRP, Gavin Garland G, Pöyry T, Mead E, Vlahov N, Sfakianos A, et al. Control of translation elongation in health and disease. *Dis Model Mech.* (2020) 13:dmm043208. doi: 10.1242/dmm.043208
42. Anbazhagan R, Kavarthapu R, Coon SL, Dufau ML. Role of phosphorylated gonadotropin-regulated testicular RNA helicase (GRTH/DDX25) in the regulation of germ cell specific mRNAs in chromatoid bodies during spermatogenesis. *Front Cell Dev Biol.* (2020) 8:580019. doi: 10.3389/fcell.2020.580019
43. Schechtman D, Mochly-Rosen D. Adaptor proteins in protein kinase C-mediated signal transduction. *Oncogene.* (2001) 20:6339–47. doi: 10.1038/sj.onc.1204778
44. Rabl J, Leibundgut M, Aitade SF, Haag A, Ban N. Crystal structure of the eukaryotic 60S ribosomal subunit in complex with initiation factor 1. *Science.* (2011) 331:730–6. doi: 10.1126/science.1198308
45. Mor I, Sklan EH, Podoly E, Pick M, Kirschner M, Yogev L, et al. Acetylcholinesterase-R increases germ cell apoptosis but enhances sperm motility. *J Cell Mol Med.* (2008) 12:479–95. doi: 10.1111/j.1582-4934.2008.00231.x
46. Xu Z, Xie Y, Zhou C, Hu Q, Gu T, Yang J, et al. Expression pattern of seminal plasma extracellular vesicle small RNAs in boar semen. *Front Vet Sci.* (2020) 7:585276. doi: 10.3389/fvets.2020.585276
47. Jodar M, Sendler E, Moskovtsev SI, Librach CL, Goodrich R, Swanson S, et al. Response to Comment on "Absence of sperm RNA elements correlates with idiopathic male infertility." *Sci Transl Med*. (2016) 8:353tr1. doi: 10.1126/scitranslmed.aaf4550
48. Kierszenbaum AL, Tres LL, Hill C, Carolina N. Structural and transcriptional features of the mouse spermatid genome. *J Cell Biol.* (1975) 65:258–70. doi: 10.1083/jcb.65.2.258
49. Fedder J. Nonsperm cells in human semen: with special reference to seminal leukocytes and their possible influence on fertility. *Arch Androl.* (1996) 36:41–65. doi: 10.3109/01485019608987883
50. Weiser D, Mietens A, Stadler B, Ježek D, Schuler G, Middendorff R. Contractions transport exfoliated epithelial cells through the neonatal epididymis. *Reproduction.* (2020) 160:109–16. doi: 10.1530/REP-19-0617
51. Du J, Shen J, Wang Y, Pan C, Pang W, Diao H, et al. Boar seminal plasma exosomes maintain sperm function by infiltrating into the sperm membrane. *Oncotarget.* (2016) 7:58832–47. doi: 10.18632/oncotarget.11315

52. Vojtech L, Woo S, Hughes S, Levy C, Ballweber L, Sauteraud RP, et al. Exosomes in human semen carry a distinctive repertoire of small non-coding RNAs with potential regulatory functions. *Nucleic Acids Res.* (2014) 42:7290–304. doi: 10.1093/nar/gku347

Conflict of Interest: SB was employed by the company Group Gepork S.A. The authors declare that this study received funding from MINECO, AGAUR, Generalitat de Catalunya and MICINN. The funder was not involved in the study design, collection, analysis, interpretation of data, the writing of this article or the decision to submit it for publication.

The remaining authors declare that the research was conducted in the absence of any commercial or financial relationships that could be construed as a potential conflict of interest.

frontiers in Veterinary Science

ORIGINAL RESEARCH
published: 19 July 2021
doi: 10.3389/fvets.2021.703101

A Combined Flow Cytometric Semen Analysis and miRNA Profiling as a Tool to Discriminate Between High- and Low-Fertility Bulls

Federica Turri†, Emanuele Capra*†, Barbara Lazzari, Paola Cremonesi, Alessandra Stella and Flavia Pizzi*

Institute of Agricultural Biology and Biotechnology, National Research Council (IBBA-CNR), Lodi, Italy

OPEN ACCESS

Edited by:
Isabel Barranco, University of Bologna, Italy

Reviewed by:
Arumugam Kumaresan, National Dairy Research Institute (ICAR), India
Albert Salas-Huetos, Harvard University, United States
Arlindo A. Moura, Federal University of Ceara, Brazil

***Correspondence:**
Federica Turri
federica.turri@ibba.cnr.it

†*These authors have contributed equally to this work and share first authorship*

Specialty section:
This article was submitted to Animal Reproduction - Theriogenology, a section of the journal Frontiers in Veterinary Science

Received: *30 April 2021*
Accepted: *15 June 2021*
Published: *19 July 2021*

Citation:
Turri F, Capra E, Lazzari B, Cremonesi P, Stella A and Pizzi F (2021) A Combined Flow Cytometric Semen Analysis and miRNA Profiling as a Tool to Discriminate Between High- and Low-Fertility Bulls. Front. Vet. Sci. 8:703101. doi: 10.3389/fvets.2021.703101

Predicting bull fertility is one of the main challenges for the dairy breeding industry and artificial insemination (AI) centers. Semen evaluation performed in the AI center is not fully reliable to determine the level of bull fertility. Spermatozoa are rich in active miRNA. Specific sperm-borne miRNAs can be linked to fertility. The aim of our study is to propose a combined flow cytometric analysis and miRNA profiling of semen bulls with different fertility to identify markers that can be potentially used for the prediction of field fertility. Sperm functions were analyzed in frozen-thawed semen doses (CG: control group) and high-quality sperm (HQS) fraction collected from bulls with different field fertility levels (estimated relative conception rate or ERCR) by using advanced techniques, such as the computer-assisted semen analysis system, flow cytometry, and small RNA-sequencing. Fertility groups differ for total and progressive motility and in the abnormality degree of the chromatin structure ($P < 0.05$). A backward, stepwise, multiple regression analysis was applied to define a model with high relation between *in vivo* (e.g., ERCR) and *in vitro* (i.e., semen quality and DE-miRNA) fertility data. The analysis produced two models that accounted for more than 78% of the variation of ERCR (CG: $R^2 = 0.88$; HQS: $R^2 = 0.78$), identifying a suitable combination of parameters useful to predict bull fertility. The predictive equation on CG samples included eight variables: four kinetic parameters and four DNA integrity indicators. For the HQS fraction, the predictive equation included five variables: three kinetic parameters and two DNA integrity indicators. A significant relationship was observed between real and predicted fertility in CG ($R^2 = 0.88$) and HQS fraction ($R^2 = 0.82$). We identified 15 differentially expressed miRNAs between high- and low-fertility bulls, nine of which are known (miR-2285n, miR-378, miR-423-3p, miR-191, miR-2904, miR-378c, miR-431, miR-486, miR-2478) while the remaining are novel. The multidimensional preference analysis model partially separates bulls according to their fertility, clustering three semen quality variable groups relative to motility, DNA integrity, and viability. A positive association between field fertility, semen quality parameters, and specific miRNAs was revealed. The integrated approach could provide a model for bull selection in AI centers, increasing the reproductive efficiency of livestock.

Keywords: bull, sperm, semen quality, sequencing, miRNA, fertility

INTRODUCTION

Prediction of bull fertility is one of the crucial factors dictating optimum efficiency in the livestock production system. Considering that, in dairy cattle, the selection and reproductive management are based on the use of artificial insemination (AI), the assessment of the level of bull fertility nowadays is one of the main challenges for AI centers and cattle breeders.

At present, quality parameters routinely applied in semen evaluation tests performed in AI centers are not fully reliable to determine a bull's fertility level. Field fertility, in terms of the ability of bulls to make cows pregnant through AI, is affected by a wide range of factors, such as health status, genetic traits, full functionality of reproductive organs, herd management, semen quality, and cryopreservation protocols. Reproductive efficiency of AI bulls is predicted by direct measure of fertility. The most utilized method of measuring male fertility is related to the non-return rate (NRR) although low-to-moderate correlation has been observed between the semen quality criteria currently used and the NRR (1). The estimated relative conception rate (ERCR) is a measure of the fertility of an individual sire and is predictable and repeatable over the whole productive life of an AI sire if data relative to the semen quality have been collected (2).

Studies on male fertility focus also on the assessment of several semen quality parameters after freezing and thawing, on the evaluation of the relationship of *in vitro* semen quality with field data, with the aim to exclude low-potential-fertility bulls from breeding programs, thus saving considerable time and economic resources. As genomic selection for male fertility is not widely implemented, semen evaluation for the prediction of male fertility has a greater impact on breeding outcomes (3). Thus, an urgent need to improve semen evaluation techniques and fertility prediction models is evident.

Several advanced technologies can be used to examine the quality of spermatozoa—such as computer-assisted semen analysis (CASA) and flow cytometry (FCM)—which can provide accurate and objective evaluation of sperm function. With the existing methods, it is easier to identify low-fertility (LF) bulls, but ranking those with moderate-to-high fertility is more complicated (1). Some researchers, such as Sellem et al. (4), Gliozzi et al. (5), and Kumaresan et al. (6), aimed to identify the most suitable spermatic parameters for semen fertility prediction, combining several *in vitro* assessments and obtaining an accuracy of the developed model for male fertility prediction in cattle species of $R^2 = 0.39$, $R^2 = 0.84$, and $R^2 = 0.83$, respectively. These studies demonstrate that the combination of kinetic semen parameters and DNA analysis based on FCM, such as DNA sperm integrity, seems to be able to distinguish among fertility levels in bulls even in the high-fertility (HF) range.

Moreover, the integration of several tests, from the evaluation of semen quality with advanced technologies to sperm molecular investigation, such as small RNA profiling, is a promising approach to achieve a better understanding of sperm functions as well as to evaluate semen quality and predict bull fertility (7).

Mature spermatozoa contain coding and non-coding RNAs, some of which are involved in the regulation of many physiological pathways related to spermatogenesis, sperm maturation, and early embryonic development with the potential to modulate sperm morpho-functional features as well as male reproductive ability (8). Among small RNA species, miRNAs are associated with sperm cell fertility status and embryo development (9). In bulls, different profiles of sperm miRNA were investigated and associated with different sperm quality and fertility levels (1, 4, 7, 8, 10).

In our study, we hypothesize that bulls with moderate-to-high fertility can be identified by a difference in semen quality and by the analysis of miRNA expression.

An integrated approach between advanced semen quality analysis and miRNA profiling of cryopreserved semen in HF and LF bulls is proposed to identify markers and build a model that can be potentially used for the prediction of male field fertility.

MATERIALS AND METHODS

Semen Source and Field Fertility Evaluation

Frozen semen samples from 10 mature progeny-tested Italian Holstein–Friesian bulls of known reproductive ability were purchased from INSEME S.p.A bull AI center (Modena, Italy). The bulls were classified according to field fertility data expressed as the ERCR, provided by the Italian Holstein Breeders Association (ANAFI). To calculate the ERCR, the 56-day NRR to service was adjusted for several factors, including farm, year and month of insemination, parity, days open of the cow at first insemination, bull, bull progeny, and cow. The ERCR represents the effect of the bull on the NRR (expressed as a percentage) of cows inseminated in the herd and is determined by the difference between that NRR value for a particular bull and the average NRR values obtained with the semen of other bulls. As its calculation is based on a large number of services from many different herds, the ERCR is considered a highly accurate measurement to identify HF and LF bulls (11). On average, 1,541 inseminations per bull (with a range of 106–11,036 inseminations) were used to estimate ERCR. Bulls with a reliability of ERCR > 80 were considered (Reliability = 100 × [1 – (1 – (number of inseminations / (number of inseminations + 200))½) × 2.3]). According to the distribution of bulls based on the ERCR, five HF and five LF bulls were identified in the distribution tails. The bulls included in the present study, routinely used in AI, displayed a narrow fertility range, as ERCR values ranged from −2.09 to 4.09 (**Table 1**). For each bull, two different batches were collected in two seasons, summer (August–September) and winter (February–March) and analyzed. The semen was packaged in 0.5-ml straws (each containing 20×10^6 spermatozoa), frozen with a commercial egg yolk–based extender, and stored in liquid nitrogen. For each bull, the frozen-thawed semen doses were evaluated before (control group: CG) and immediately after Percoll density gradient centrifugation (high-quality sperm, HQS, fraction).

Isolation of Spermatozoa Through Percoll Gradient

HQS fractions were isolated as described by Capra et al. (7). For each bull, 10 frozen semen doses (20×10^6 cells per dose)

TABLE 1 | Field fertility details of the bulls involved in the study.

Bulls	ERCR	Fertility	N. of insemination	Reliability (%)
1	2.38	High	4,202	99
2	1.97	High	3,209	98
3	4.09	High	2,371	98
4	1.99	High	4,074	99
5	2.84	High	16,767	99
6	−2.41	Low	346	85
7	−1.73	Low	1,892	97
8	−2.90	Low	1,427	96
9	−1.82	Low	2,929	98
10	−1.83	Low	360	86

were simultaneously thawed in a water bath at 37°C for 20 s and pooled. The pool (5 mL) of each bull was split into two aliquots of 2.5 mL that were overlaid on a dual-layer (90–45%) discontinuous Percoll gradient (Sigma-Aldrich, St. Louis, USA) in two 15-ml conical tubes and centrifuged at 700 × *g* for 30 min at 20°C. The Percoll layers were prepared by diluting Percoll solution in as indicated by Parrish et al. (12). The Percoll gradient is a colloidal suspension of silica particles coated with polyvinylpyrrolidone. By using two discontinuous layers (45 and 90%) by centrifugation it is possible to obtain a different sedimentation according to sperm motion. The HQS fraction obtained from each of the two tubes (replicates) was washed in Tyrode's albumin lactate pyruvate (TALP) sperm medium (12) at 700 × *g* for 10 min at 20°C; the obtained pellets were resuspended in 150 μl of TALP. Aliquots from each replicate were kept at −80°C until RNA extraction.

Evaluation of Sperm Characteristics

Two technical replicates for each bull, for the two seasons, were evaluated for total motility and sperm kinetic parameters by CASA and sperm viability, acrosomal status, and DNA integrity by FCM immediately after thawing (CG) and after Percoll separation in the HQS fraction obtained.

CASA

Total motility and sperm kinetics parameters were assessed by the CASA system (ISAS® v1, Proiser, R + D S.L., Paterna, Spain) combined with a phase contrast microscope (Nikon Optiphot) equipped with a negative phase contrast 10× objective and integrated warmer stage and connected to a video camera (Proiser 782M, Proiser R+D).

Semen from CG was evaluated as raw without dilution, and 5 μl of semen pellet obtained after Percoll density gradient centrifugation (HQS fraction) were diluted in 5 μl TALP sperm medium (13) prewarmed at 37°C. Next, 10 μl of diluted semen were placed on a prewarmed (37°C) Makler® chamber. During the analysis, the microscope heating stage was maintained at 37°C. Images were relayed, digitized, and analyzed by the ISAS® v1 software with user-defined settings as follows: frames acquired, 25; frame rate, 20 Hz; minimum particle area 20 microns^2; maximum particle areas 70 microns^2; progressivity of the straightness 70%. CASA kinetics parameters were total motility (MOT TOT, %), progressive motility (PRG, %), curvilinear velocity (VCL, μm/s), straight-line velocity (VSL, μm/s), average path velocity (VAP, μm/s), linearity coefficient (LIN, % = VSL/VCL × 100), amplitude of lateral head displacement (ALH, μm), straightness coefficient (STR, % = VSL/VAP × 100), wobble coefficient (WOB, % = VAP/VCL × 100), and beat cross frequency (BCF, Hz).

FCM Analysis

Measurements were recorded using a Guava® EasyCyte™ 5HT microcapillary flow cytometer (Merck KGaA, Darmstadt, Germany; distributed by IMV Technologies) equipped with fluorescent probes excited by a 20-mW argon ion laser (488 nm). Forward-scatter (FSC) vs. side-scatter (SSC) plots were used to separate sperm cells from debris. Non-sperm events were excluded from further analysis. Fluorescence detection was set with three photomultiplier tubes: detector FL-1 (green: 525/30 nm), detector FL-2 (yellow/orange: 586/26 nm), and detector FL-3 (red: 690/50 nm). Calibration was carried out using standard beads (Guava® Easy Check Kit, Merck Millipore). A total of 5,000 sperm events per sample for each bull were analyzed at a flow rate of 200 cells/s. Compensation for spectra overlap between fluorochromes was set according to the procedures outlined by Roederer (14).

Data were acquired and analyzed using CytoSoft and EasyCompDNA software (Merck KGaA, Darmstadt, Germany; distributed by IMV Technologies), respectively.

Sperm Viability

The LIVE-DEAD® Sperm Viability Kit (Life Technologies Italia, Italy) was used for the analysis of plasma membrane integrity as described by Gliozzi et al. (5). The kit contained the membrane-permeant nucleic acid stain SYBR®14 and the conventional dead cell stain propidium iodide (PI). Both dyes can be used to label DNA. After staining, live sperm cells with intact cell membranes fluoresced bright green, whereas cells with damaged cell membranes fluoresced red. Aliquots of semen extended with Easy Buffer (2.0×10^5 spermatozoa/ml) were supplemented with SYBR®14 0.1 μM and PI 12 μM (final dilutions) according to manufacturer instructions. After gentle mixing and 10 min incubation at 37°C in the dark, three replicates per sample were performed. Debris particles were gated out according to the intensity of green and red fluorescence. Three sperm populations were detected on the FL-1/FL-3 dot plot: viable (green), dead (red), and moribund (double-stained) spermatozoa.

Acrosomal Membrane Integrity

Acrosomal membrane integrity was assessed using Easykit 5 (ref. 025293; IMV Technologies). This kit is used to measure the level of disrupted acrosome within viable or dead sperm populations. The ready-to-use 96-well plate was filled with 200 mL of embryonic holding solution (ref. 019449; IMV Technologies), and 40,000 sperm were added during 45 min at 37°C protected from light in basal condition. The signal was read with the

Guava® EasyCyte™ 5HT microcapillary flow cytometer, and a total of 5,000 events were acquired. Percentages of sperm with either intact or damaged plasma membrane as well as intact or damaged acrosome were computed. Spermatozoa with disrupted acrosomes were labeled with a green probe. Dead spermatozoa with damaged plasma membrane were labeled with a red fluorochrome.

Sperm Chromatin Structure Assay

The Sperm Chromatin Structure Assay was assessed as previously described in other studies of ours (5, 15) by using acridine orange, a planar molecule that intercalates into double-stranded DNA but stacks on single-stranded DNA causing a metachromatic shift from green (double-stranded DNA) to red fluorescence (single-stranded DNA), when exposed to the 488 nm laser light of the flow cytometer. The technique is based on the susceptibility of sperm DNA to acid-induced denaturation as low pH treatment causes partial DNA denaturation in sperm with altered chromatin structure. The assessments were performed using the sperm chromatin structure assay (16): 3.0×10^5 cells were diluted in 200 μl of TNE buffer (0.01 M Tris-HCl, 0.15 M NaCl, 1 mM EDTA, pH 7.4) and added to 400 μl of an acidic solution (Triton X-100 0.1%, 0.15 M NaCl, 0.08 N HCl; pH 1.2). After 30 s, cells were stained with 1.2 ml of acridine orange solution (6 μg/ml in 0.1 M citric acid, 0.2 M Na_2HPO_4, 1 mM EDTA, 0.15 M NaCl; pH 6). Samples were protected from light and incubated at room temperature for 2.5 min; after that, two replicates per sample were acquired and analyzed using, respectively, CytoSoft and EasyCompDNA software (Merck KGaA, Darmstadt, Germany; distributed by IMV Technologies) and expressed as Alpha-T, which is indicative of the shift from green to red fluorescence, is expressed as the ratio of red to total fluorescence intensity [red/(red + green)], and quantifies the degree of abnormal chromatin structure with an increased susceptibility to acid-induced denaturation; standard deviation of Alpha-T (ATSD), which shows the extent of abnormality in the chromatin structure within a population; DNA fragmentation index (%DFI), which indicates the percentage of sperm with fragmented DNA; and percentage of sperm with high green fluorescence (%HG), which is representative of the percentage of immature cells with reduced nuclear condensation (incomplete histone-protamine exchange). The FCM instrument was AO-saturated prior to analysis by running the AO equilibration solution.

RNA Extraction

Two technical replicates of the HQS Percoll fraction (obtained from 10 frozen semen doses each) from each bull sperm ($n = 10$) collected in two seasons (summer and winter) were used for RNA isolation. RNA was extracted as previously described (7). Briefly, the sperm cell pellet was initially homogenized and solubilized in 800 μl of TRIzol with incubation at 65°C for 15 min. RNA was then purified using the NucleoSpin®miRNA kit (Macherey-Nagel, Germany). RNA concentration and quality were determined by the Agilent 2100 Bioanalyzer (Santa Clara, CA) (**Supplementary File 1**). The isolated RNAs were stored at −80°C until use.

Library Preparation and Sequencing

Libraries were generated using the Illumina Truseq Small RNA Preparation kit according to the manufacturer's instructions and the protocol described by Capra et al. (7). Libraries from the 10 bulls (five HF, five LF) in the two seasons (winter and summer) were pooled together for each technical replicate and concentrated (15× libraries pool) with Agencourt®AMPure® XP (Beckman, Coulter, Brea, CA) (1 Vol. sample: 1.8 Vol. beads), thus obtaining two pools of libraries representing the two technical replicates. The two pools were purified on a Pippin Prep system (Sage Science, MA, USA) to recover the 125–167 nt fraction containing mature miRNAs. The quality and yield after sample preparation were measured with an Agilent 2200 Tape Station, High Sensitivity D1000. Libraries were sequenced on two lanes of Illumina Hiseq 2000 (San Diego, CA).

miRNA Detection and Bioinformatics Analysis

miRNA detection and discovery were carried out with Mirdeep2 on Illumina high-quality trimmed sequences. *Bos taurus* miRNAs available at miRBase (http://www.mirbase.org/) were used to accomplish known miRNA detection on the trimmed sequences. Known miRNAs from related species (sheep, goat, and horse) available at miRBase were also input into Mirdeep2 to support the individuation of novel miRNAs. The Mirdeep2 quantifier module was used to quantify expression and retrieve counts for the detected known and novel miRNAs. Differential expression analyses between the HF and LF bulls and in different seasons were run with the Bioconductor edgeR package (17). Principal component analysis (PCA) was performed with Genesis (18).

Statistical Analysis

Data obtained from *in vitro* semen evaluation (CASA and FCM measurements) were analyzed using the SAS™ package v 9.4 (SAS Institute Inc., Cary, NC, USA) with different statistical models to evaluate the following:

1) Isolation of sperm fractions and evaluation of sperm separation.

   The general linear model procedure (PROC GLM) was used to (i) evaluate the effect of technical replicates on semen quality parameters in the HQS fraction—the model included as fixed effects the bull and the replicate nested in the sperm fraction—and (ii) verify the efficiency of the sperm separation from the CG to HQS fractions. The model included the fixed effect of the sperm fraction and of the bull.

2) Relations between *in vitro* semen quality and *in vivo* fertility.

   PROC GLM was used to assess *in vitro* sperm quality in function of the ERCR (HF and LF bulls). The model included the fixed effects of fertility rank, categorized as LF (ERCR $\leq$ 1.0) and HF (ERCR $\geq$ 1) and season of semen collection (two levels as follows: winter, February to March, and summer, August to September).

A backward stepwise multiple regression analysis (PROC REG) was used to obtain a model with high relation between sperm quality parameters and ERCR. The redundant parameters were excluded from analysis. The procedure started with a model

that contained all *in vitro* sperm parameters and repeatedly eliminated non-significant variables, using a significance level of $P < 0.05$ to retain variables. The real values of the significant variables obtained from each bull as determined by backward elimination were included in an equation (real values were multiplied for the estimated parameters, calculated by backward elimination) to calculate the predicted fertility values. Correlation between real and predicted fertility values was then assessed.

A multidimensional preference analysis (MDPREF) was then conducted to explore the *in vitro* semen quality traits and miRNA expression that correlated with the level of bull fertility. MDPREF is a PCA of data performed using the PROC PRINQUAL procedure of SAS (19). This procedure finds linear and non-linear transformations of variables, using the method of alternating least squares, which optimizes properties of the transformed variables' correlation or covariance matrix. In the current case, a MDPREF biplot with bull fertility level (HF and LF) in rows and *in vitro* semen quality traits and miRNA expression in columns best represents the relationships among the fertility scores. MDPREF identifies the variability that is most salient to the preference patterns of the fertility levels toward the *in vitro* semen quality and miRNAs expression and extracts this as the first principal component.

Results are given as adjusted least squares means ± standard error means (LSM ± SEM).

TABLE 2 | Sperm quality variables assessed after thawing (Control Group = CG) and after Percoll separation in High and Low Quality Sperm Fraction (HQS, LQS).

Sperm parameters	CG	HQS Fraction	LQS Fraction
MOT TOT	73.14 ± 2.51[a]	81.02 ± 2.51[b]	11.15 ± 2.51[c]
PROG	49.15 ± 2.03[a]	52.49 ± 2.03[a]	7.84 ± 2.03[b]
VSL	53.29 ± 2.39[a]	62.80 ± 2.39[b]	42.24 ± 2.39[c]
VCL	86.26 ± 3.59[a]	112.27 ± 3.59[b]	66.78 ± 3.59[c]
VAP	61.94 ± 2.65[a]	75.98 ± 2.65[b]	47.02 ± 2.65[c]
LIN	62.06 ± 1.77[a]	55.25 ± 1.77[b]	63.05 ± 1.77[c]
STR	85.91 ± 0.98[a]	81.81 ± 0.98[b]	88.69 ± 0.98[c]
WOB	72.01 ± 1.48[a]	67.00 ± 1.48[b]	70.33 ± 1.48[b]
ALH	2.85 ± 0.11[a]	3.67 ± 0.11[b]	2.30 ± 0.11[c]
BCF	10.05 ± 0.34[a]	9.03 ± 0.34b	8.33 ± 0.34[b]
VIAB	44.40 ± 2.14[a]	64.31 ± 2.22[b]	24.23 ± 2.22[c]
VIA	25.10 ± 1.62[a]	39.16 ± 1.68[b]	8.56 ± 1.68[c]
VDA	1.96 ± 0.14[a]	1.60 ± 0.15[a]	1.00 ± 0.15[b]
ALPHAT	0.4123 ± 0.001147[a]	0.4072 ± 0.001147[b]	0.4060 ± 0.001183[b]
ATSD	0.0102 ± 0.000597[ab]	0.0118 ± 0.000597[b]	0.0132 ± 0.000616[c]
%DFI	1.60 ± 0.22[a]	0.92 ± 0.22[b]	1.82 ± 0.23[a]
%HG	1.84 ± 0.20[a]	2.05 ± 0.20[a]	3.18 ± 0.21[b]

MOT TOT, total motility; PROG, cells progressive motility; VSL, straight-line velocity; VCL, curvilinear velocity; VAP, average path velocity; LIN, linear coefficient; STR, straightness coefficient; WOB, wobble coefficient; ALH, amplitude of lateral head displacement; BCF, beat cross-frequency; VIAB, viable sperm; VIA, viable with intact acrosome; VDA, viable with disrupted acrosome; ALPHA-T, red/(red+ green) fluorescence intensity; ATSD, Alpha-T standard deviation; %DFI, fragmented DNA sperm; %HG, high green fluorescence sperm.

[a,b,c]values within a row with different superscripts differ significantly at $P < 0.05$.

RESULTS

Isolation of Sperm Fractions and Evaluation of Sperm Separation

No significant differences were observed among technical replicates concerning semen quality parameters in HQS fractions (**Supplementary Table 1**). Sperm cells were successfully enriched in HQS fractions (**Table 2**) after Percoll centrifugation considering MOT TOT, PROG, VSL, VCL, VAP, ALH, VIAB, VIA, VDA, Alpha-T, and %DFI variables, and a significant ($P < 0.05$) improvement of the sperm quality occurred in the HQS fraction with respect to the CG.

Existing Relations Between *in vitro* Semen Quality and *in vivo* Fertility

No significant effects on *in vitro* semen quality were observed according to the semen collection season. *In vitro* sperm quality parameters according to the fertility level, assessed on both the CG and HQS fraction, are presented in **Table 3**. A significant ($P < 0.05$) improvement of MOT TOT and PROG was found in CG/HF bulls with respect to the CG/LF group. Significant differences were also observed for Alpha-T, showing a major abnormality in the degree of chromatin structure in LF bulls. In the CG/HF bulls, higher values were found with respect to LF bulls for VIAB and VIA variables as well as a lower percentage of sperm with fragmented DNA (%DFI) and percentage of sperm with immature cells with reduced nuclear condensation (%HG) although not with significant values. In the HQS fraction, an increase ($P < 0.05$) of the abnormality degree of chromatin structure (Alpha-T) was also noticed in LF bulls with respect to the HF bulls.

A backward elimination analysis was performed to obtain a fertility prediction model between *in vitro* (sperm quality parameters) and *in vivo* (ERCR) fertility on both CG and HQS fraction. The initial model applied on both CG and HQS fraction was ERCR= MOT TOT + PROG + VSL + VCL + VAP + LIN + STR + WOB + ALH + BCF + VIAB + VIA + VDA + ALPHAT + ATSD + %DFI + %HG.

The analysis produced two final models that accounted for more than 78% of the variation of ERCR (CG: $R^2 = 0.88$; HQS fraction: $R^2 = 0.78$). The predictive equation of the final model on CG included eight variables (ERCR = ALPHAT + %DFI + ATSD + %HG + STR + VAP + VCL + WOB): four DNA integrity indicators (ALPHA-T: F-value 7.31, $P = 0.0205$, %DFI: F-value 31.65, $P = 0.0002$; ATSD: F-value 20.85, $P = 0.0008$; %HG: F-value 20.31, $P = 0.0009$), and four kinetic parameters (STR: F-value 15.27, $P = 0.0024$; VAP: F-value 12.54, $P = 0.0046$; VCL: F-value 12.09, $P = 0.0052$; WOB: F-value 10.01, $P = 0.0090$).

On HQS fraction, the predictive equation of the final included five variables (ERCR= ALPHAT + %DFI + MOT TOT + PROG + VSL): two DNA integrity indicators (ALPHA-T: F-value 43.07, $P < 0.0001$; %DFI: F-value 19.07, $P = 0.0008$), and three kinetic parameters (MOT: F-value 6.19, $P = 0.0272$, PROG: F-value 6.23, $P = 0.0268$; VSL: F-value 6.76, $P = 0.0220$).

TABLE 3 | *In vitro* sperm quality parameters assessed on frozen-thawed semen doses by CASA and FCM of 10 Holstein bulls based on fertility ranking in the CG and HQS fraction (LSM ± SEM).

Fraction	CG				HQS Fraction			
	HF		LF		HF		LF	
Parameters	LSM	SEM	LSM	SEM	LSM	SEM	LSM	SEM
MOT TOT	83.27[a]	4.00	63.02[b]	4.00	83.96	4.66	78.04	4.66
PROG	54.49[a]	3.07	43.80[b]	3.07	52.35	4.12	52.64	4.12
VSL	54.01	3.31	52.57	3.31	60.77	6.29	64.83	6.29
VCL	90.19	4.49	82.33	4.49	111.95	6.49	112.60	6.49
VAP	64.34	3.45	59.53	3.45	75.18	6.46	76.78	6.46
LIN	59.76	2.58	64.36	2.58	53.28	3.74	57.23	3.74
STR	83.73[a]	1.38	88.09[b]	1.30	79.51	1.97	84.11	1.97
WOB	71.16	2.13	72.85	2.13	66.27	3.13	67.73	3.13
ALH	2.96	0.14	2.73	0.14	3.69	0.18	3.65	0.18
BCF	9.85	0.38	10.25	0.38	8.48[a]	0.34	9.58[b]	0.34
VIAB	48.73	4.26	40.07	4.26	66.89	2.97	62.42	3.14
VIA	28.12	2.66	22.08	2.66	36.82	4.04	42.11	4.27
VDA	1.88	0.25	2.04	0.25	1.54	0.17	1.70	0.18
ALPHA-T	0.4097[a]	0.0016	0.4150[b]	0.0016	0.4025[a]	0.0020	0.4119[b]	0.0020
ATSD	0.0093	0.0009	0.0112	0.0009	0.0113	0.0006	0.0124	0.0006
%DFI	1.3337	0.3215	1.8830	0.3215	0.7327	0.2314	1.1106	0.2314
%HG	1.5775	0.2210	2.1160	0.2210	2.0627	0.1672	2.0502	0.1672

MOT TOT, total motility; PROG, cells progressive motility; VSL, straight-line velocity; VCL, curvilinear velocity; VAP, average path velocity; LIN, linear coefficient; STR, straightness coefficient; WOB, wobble coefficient; ALH, amplitude of lateral head displacement, BCF, beat cross-frequency; VIAB, viable sperm; VIA, viable with intact acrosome; VDA, viable with disrupted acrosome; ALPHA-T, red/(red + green) fluorescence intensity; ATSD, Alpha-T standard deviation; %DFI, fragmented DNA sperm; %HG, high green fluorescence sperm.
[a,b]values within a row with different superscripts differ significantly at $P < 0.05$.

Figure 1 highlights the high correlation ($R^2 = 0.88$, Adjusted $R^2 = 0.8091$; $P < 0.05$. $R^2 = 0.82$, Adjusted $R^2 = 0.7062$; $P < 0.05$) between real and predicted fertility found in CG and HQS fraction, respectively.

Small RNA Sequencing, miRNA Identification and Profile Across HF and LF Bulls

Small RNA sequencing resulted in 145,180,999 reads after trimming and quality filtering with an average production of about 3.62 million reads per sample. An average of 632,000 miRNAs was detected by Mirdeep2 for each sample with the identifications of 923 unique miRNAs in total. Among these, 579 were known *Bos taurus* miRNAs, 98 were homologous of known miRNAs from other species, and 246 were new candidate miRNAs (**Supplementary File 2**). PCA performed on the 200 most abundant miRNAs grouped same animal closed together independently the season of semen collection and only partially separated HF (right lower corner) and LF (left upper corner) bulls (**Figure 2**). In fact, no significant variation was observed in miRNA expression from sperm collected in the two different seasons. On the contrary, comparison of HF and LF bulls results in 15 differentially expressed miRNAs (DE-miRNAs), nine of which were known, and the remaining were novel (**Supplementary File 3**). DE-miRNAs were prevalently highly expressed in the LF bulls (bta-miR-2285n, Novel:19_18865, Novel:4_36841, Novel:22_25699, Novel:21_25145, bta-miR-2478, bta-miR-2904, bta-miR-486, bta-miR-378c, bta-miR-378, bta-miR-423-3p) except for bta-miR-191, bta-miR-431, Novel:1_635 and Novel:6_40383, which show higher expression levels in the HF group (**Figure 3**).

Possible Existing Association Between *in vitro* Semen Quality, Observed Fertility, and Differentially Expressed miRNAs

MDPREF was used to study the relationship between *in vitro* semen quality parameters and miRNA expression in relation to the observed field fertility (**Figure 4**). In the model, most of the variability is reached with the first two components (∼76%). On the biplot, the trait scores are joined to the origin by the trait vector. The analysis produced two dimensions that seem to separate bulls according to their level of fertility (LF, HF), with the HF group more precisely clustered. Considering both *in vitro* sperm quality and miRNA expression, the first two components separated the vectors in three specific clusters, one relative to sperm motility and kinetics parameters (MOT TOT, MOT PROG, VCL, VAP, VSL, LIN, WOB, BCF, STR), the second one relative to DNA integrity indicators (Alpha-T, ATSD, %DFI, %HG), and the last one relative to sperm viability indicators (VIAB, VIA). The DNA integrity indicators (considered as damage) showed a positive relation with the group of bulls with LF, indicating also a positive relation with bta-miR-378c, bta-miR-423-3p, and bta-miR-486. Sperm viability indicators showed a positive relation with the group of HF bulls and

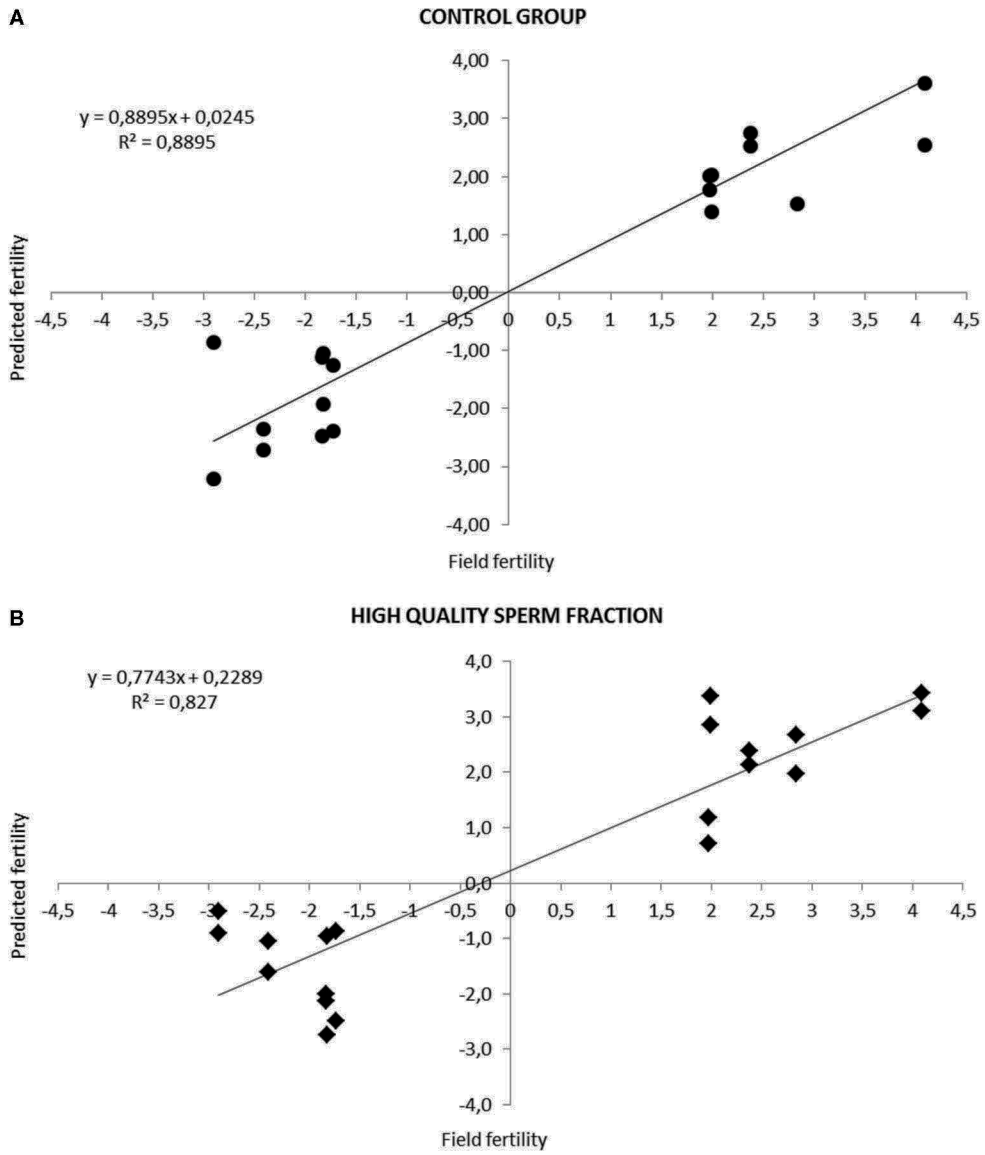

FIGURE 1 | Relationship between fertility rates predicted by the equation based on the combination of different sperm quality parameters and the observed field fertility in CG **(A)** and HQS fraction **(B)**. The line shows the trend in the data.

miR-191. In **Supplementary File 4** the correlation matrix of the Multi-Dimensional Preference analysis, showing the correlation between sperm quality and miRNAs, and the equation with select sperm quality parameters and miRNAs.

DISCUSSION

The current study was conducted with the aim to identify semen quality and miRNA biomarkers with the final goal to predict the fertility status in bulls. To categorize the most suitable parameters and provide a reliable prediction of bull fertility (among HF and LF bulls), we combined several *in vitro* sperm characteristics, assessed with advanced techniques such as CASA and FCM as well as miRNA expression by small RNA-sequencing with field fertility (ERCR).

In our study, the HQS fraction was successfully fractioned after Percoll gradient, showing good reproducibility between technical replicates and attenuating sample variabilities (20, 21). The improved HQS fraction was characterized by sperm with significant faster motion characteristics, more vital, with a better condition of the membrane integrity with respect to the CG. Similar results were observed for motility and membrane integrity in our previous study (7) and by Arias et al. (22). Although the average low levels of DNA damage shown were below the threshold for subfertility, in the HQS fraction, we observed a significant reduction of three variables out of four descriptive of DNA damage in contrast with Arias et al. (22) and

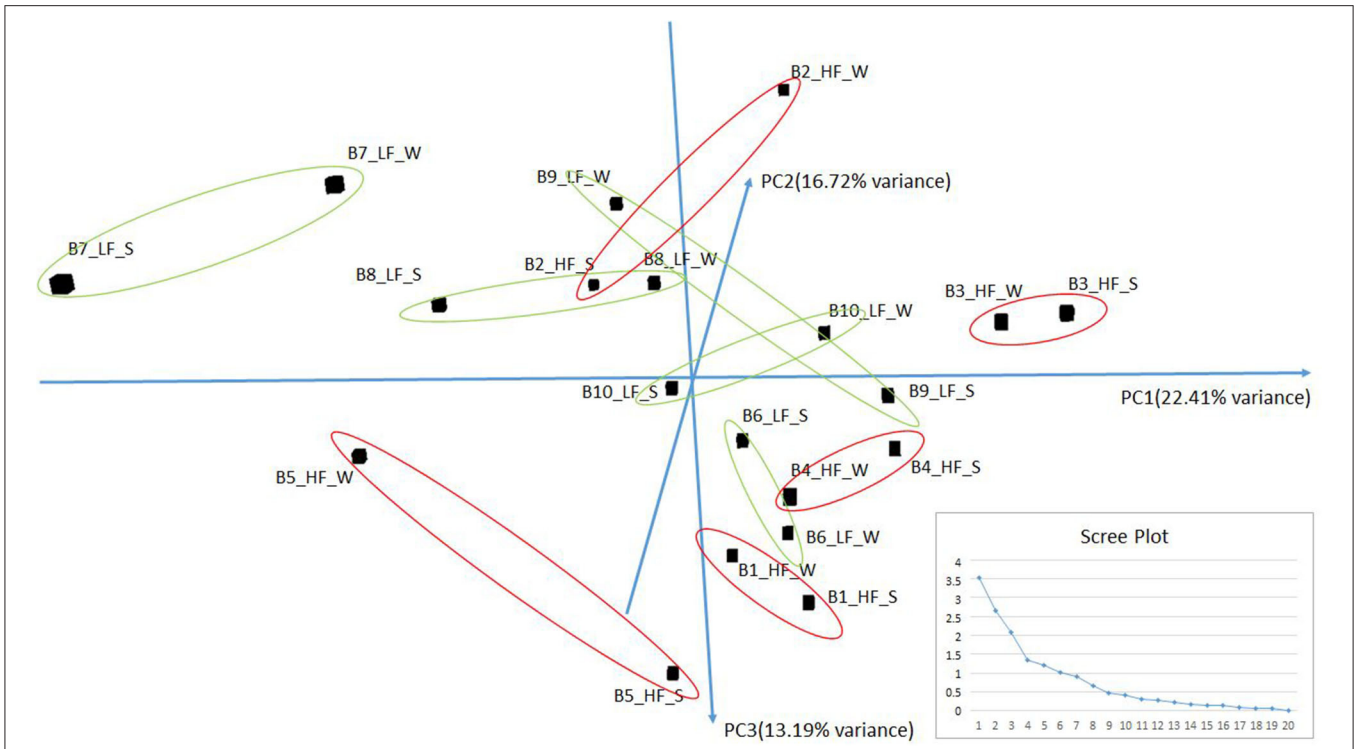

FIGURE 2 | PCA of the more abundant miRNAs ($n = 200$) found in HF and LF bulls in the two seasons: Summer (S) and Winter (W). The scree plot, in the lower right corner of the figure, was reported to explore the optimal groups of the PCA (*x*-axis: principal component, *y*-axis: eigenvalues).

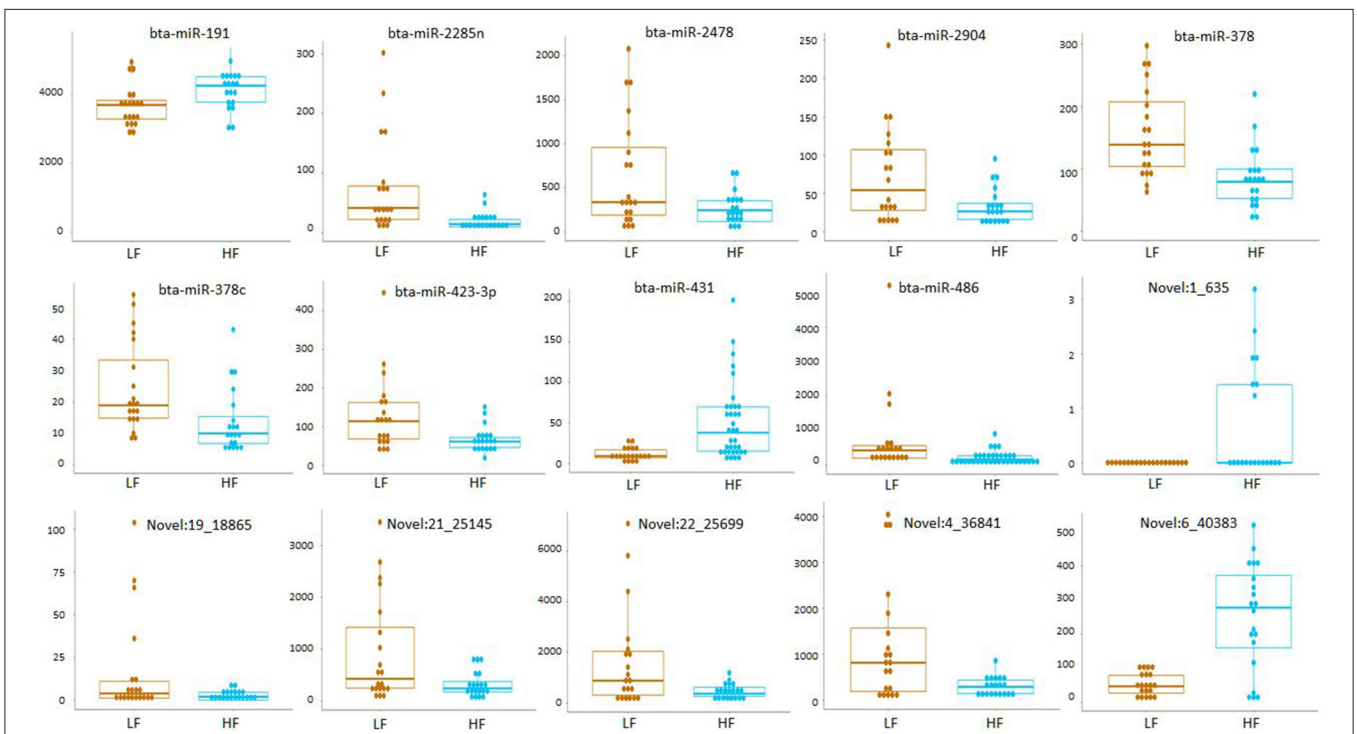

FIGURE 3 | Read count of DE-miRNAs between HF and LF bulls.

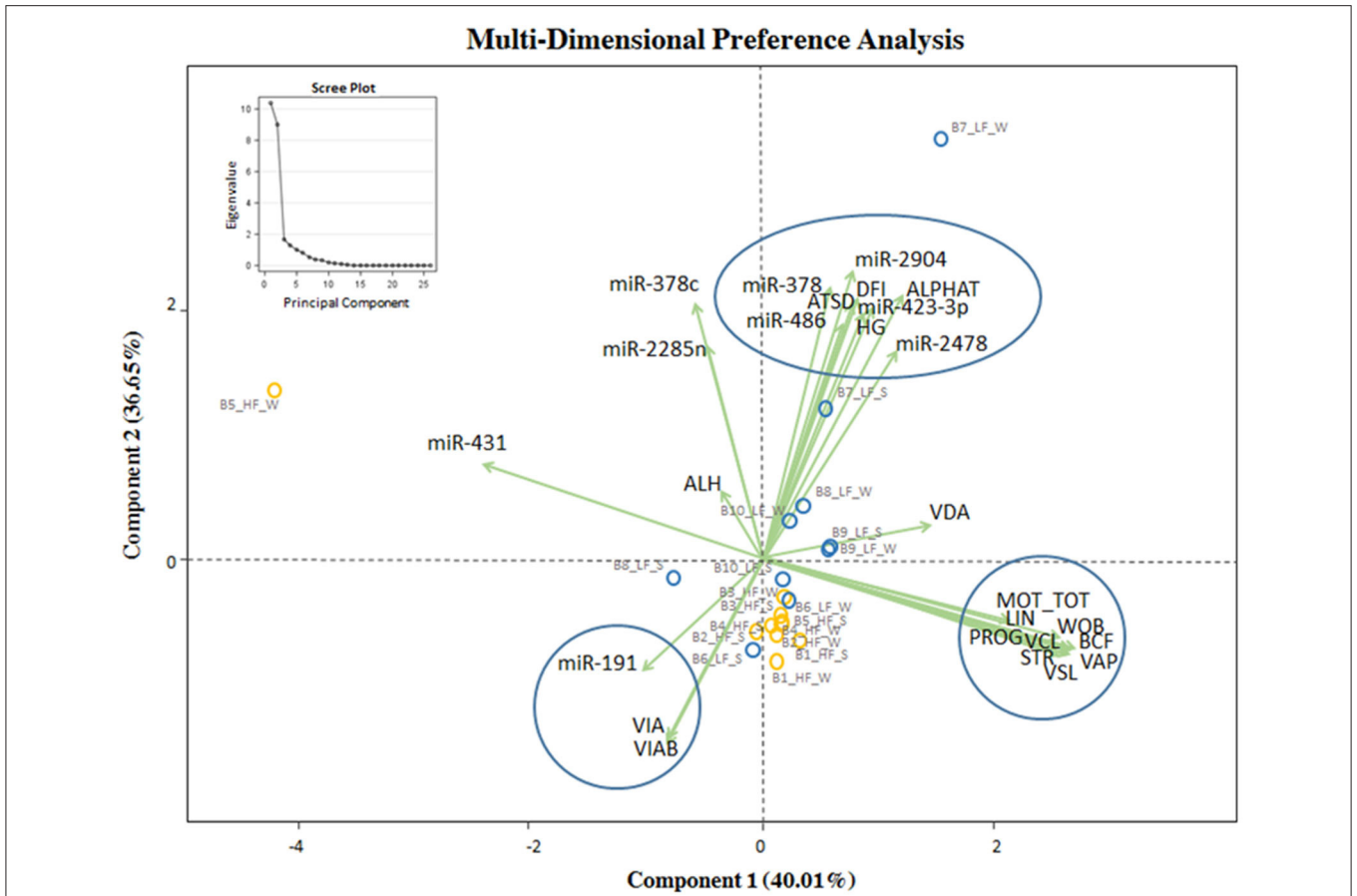

FIGURE 4 | MDPREF analysis biplot based on the combination of *in vitro* sperm quality parameters, miRNA, and observed field fertility. The dots indicate the exact position of HF and LF bulls (yellow and blue, respectively) between the two components. The ellipse and circles represent the clustering relative to *in vitro* sperm quality parameters and miRNA: sperm motility and kinetics parameters (MOT TOT, MOT PROG, VCL, VAP, VSL, LIN, WOB, BCF, STR, on the right); DNA integrity and miRNA indicators (Alpha-T, ATSD, %DFI, %HG in the upper part); viability and acrosomal status and miRNA indicators (VIA, VIAB, in the lower part). The scree plot, in the upper left corner of the figure, was reported to explore the optimal groups of the PCA.

Castro et al. (23), who did not find any significant difference for chromatin deficiency after Percoll gradient selection.

As reproductive success depends on the ability of the sperm cell to transfer information to the developing embryo, we analyzed many variables strictly related to sperm functions. According to our results, in the CG group, descriptors such as total and progressive motility were significantly higher in bulls with superior fertility. These results are in agreement with Gliozzi et al. (5) and in contrast to Kumaresan et al. (6) and García-Macías et al. (24) who did not observed any significant differences in bulls' kinetic parameters between fertility groups. Motility is the most commonly used parameter in routine assessments performed in AI centers, but its correlation with fertility is not universally accepted (5), partially due to differences in estimation methods, CASA settings, thawing temperature, and media used for dilution (25). To overcome this problem and to be sure to evaluate the potential real fraction involved in sperm fertilization (in terms of semen quality and miRNA expression), we isolated the HQS fraction of cryopreserved semen. In the CG, other variables discriminated bulls according to their fertility level, such as the abnormality degree of chromatin structure (Alpha-T), in a significant way, and viable sperm (VIAB) and intact acrosome (VIA) as demonstrated by other studies for viability (5, 6, 26), acrosome integrity (4), and DNA (5, 6, 27), confirming the importance of these evaluations strictly correlated with sperm capacitation, *in vivo* fertilization, and early embryo development. Considering the HQS fraction, we observed that the Alpha-T variable can significantly discriminate among bull fertility levels, showing a lower DNA damage in bulls with superior fertility. In this group also total motility, viability, and %DFI have shown better values although not with statistically significant values.

In literature, high accuracy levels of the models for bull fertility prediction were achieved, such as reported in our previous study (5) and by Kumaresan et al. (6), both around an efficiency of R^2 = 0.83–0.84. Our model developed in an earlier study (5), which provided the stepwise backward selection procedure application, has allowed us to reach, in this study, a major accuracy level equal to R^2 = 0.88 in the CG and R^2 = 0.82 in the HQS fraction. In both cases, the models include variables relative to kinetic parameters and DNA integrity indicators, accounting for most

of the differences observed in bull fertility. Sperm motility traits and parameters related to chromatin structure were previously recognized as variables highly related with fertility and useful in the development of fertility predictive models (5, 28, 29). To our knowledge only Waterhouse et al. (30) and Gliozzi et al. (5) apply the stepwise backward selection procedures with the aim to develop models that associate *in vitro* semen quality with fertility prediction. Among the numerous variables evaluated, they found that only sperm motility traits and parameters related to chromatin structure are associated with field fertility, in agreement with our results, confirming that this model could be easily implemented in bull AI centers, which routinely evaluate sperm motility and may instruct external laboratories to assess DNA integrity. Recently, Alves et al. (31) reviewed the important role of miRNAs in physiological processes related to spermatozoa biogenesis, maturation, oocyte fecundation, and embryo development.

In cattle, different studies reported miRNA profile alteration associated with different sperm quality levels and fertility phenotypes. A previous study by qPCR miRNA profiling with a customized panel of bovine-specific miRNAs reported several miRNAs altered in HF and LF bulls isolated directly from cryopreserved semen (1, 10) or after purification with Percoll separation (8). Small-RNA sequencing of high and low motile fractions isolated from cryopreserved sperm using Percoll gradient, together showed variation of quality parameters and significant changes in miRNA expression (7). In this work, we characterized the miRNA content in the HQS fraction of HF and LF bulls collected in two different seasons. The relative expression of the most expressed miRNAs clearly shows that miRNA expression is strictly related to the animal and is not influenced by the season of collection. Although this is the first study reporting an individual-specific bull miRNA expression, the small non-coding RNA repertoire was recently reported to be different across cattle breeds and probably associated to animal genotypes (4).

HF and LF bulls present a subset of DE-miRNAs. Among 9 *Bos taurus* DE-miRNAs (miR-2285n, miR-378, miR-423-3p, miR-19, miR-2904, miR-378c, miR-431, miR-486, miR-2478), miR-2285n, miR-378 and miR-486 have already been proven to change their expression levels between low and high motile sperm populations in our previous study (7). The highest expression of miR-2285n and miR-486 in the semen of LF bulls was in agreement with the highest level of those miRNAs in the low motile fraction. MiR-486 expression in sperm was observed to change during sperm maturation in semen isolated from caput/caudal regions in mouse (32). MiR-486 function in controlling spermatogonial stem cell stemness gene expression and growth properties with a potential role in spermatogenesis and male fertility was recently described in mice (33). On the contrary, miR-378 observed to be overexpressed in the high motile fraction was upregulated in the LF bulls. In cattle, mir-378 was previously reported to be indirectly associated with semen quality (34). Single nucleotide polymorphisms in the inner centromere protein potentially affecting spermatogenesis and normal morphological characteristics of Holstein bull sperm was reported to influence the binding capacity to bta-miR-378 (34). Within other DE-miRNAs found in our study, miR-423-3p, highly expressed in the LF group, was previously detected to be positively correlated with the severity of asthenozoospermia in human sperm (35). Interestingly, within the only two miRNA positively associated with HF bulls, miR-191 showed a strong positive correlation with the fertilization rate of blastocysts (FR), in human *in vitro* fertilization experiments (36).

The MDPREF model, applied in this study to evaluate the relationship between *in vitro* semen quality parameters, miRNA expression on frozen-thawed motile sperm fraction, and observed bull fertility, seems to be able to discriminate bulls according to their level of fertility with more precision for the HF bulls. Semen quality variables are clustered in three specific groups, relative to sperm motility and kinetics parameters, to DNA integrity indicators, and to sperm viability indicators.

In our model, variables relative to sperm motility and kinematics have not shown any association between miRNAs and observed bull fertility, and a positive relation was revealed among sperm viability and DNA integrity indicators, miRNA expression, and bull fertility.

The DNA integrity indicators, which are descriptive of damage, positively correlate with LF bulls as well as with some miRNAs (miR-378, miR-486, miR-2285) previously reported to be differentially expressed between the low and high motile sperm fractions (7). However, no data concerning parameters related to DNA integrity was previously reported (7). Bulls of superior fertility correlate also with superior sperm viability indicators, in terms of viable sperm and viable sperm with intact acrosome and with miR-191 levels. Previous investigations on mir-191-5p expression related to sperm quality parameters show a significant correlation with sperm morphology but not with sperm density and viability in humans (36).

CONCLUSION

In this study, we provide a reliable model to predict bull fertility, easily implementable in bull AI centers, which routinely evaluate sperm motility and may instruct external laboratories to assess DNA integrity, confirming the relationship between bull *in vitro* semen quality and *in vivo* fertility. Through an advanced semen quality assessment, which combines kinetic semen parameters originating from the CASA system and DNA analysis based on FCM, supported by statistical models, it was possible to establish that semen from LF bulls differs from that of HF individuals mainly in terms of sperm DNA integrity. Also viability and acrosome integrity concur to discriminate bulls according their fertility level.

We investigated differentially expressed miRNAs in the high-quality sperm fraction of bulls as candidate markers for evaluating fertility status. Fifteen miRNAs were differentially expressed in bulls with contrasting fertility. With our study, we applied a first statistical model integrating the relative expression of known DE-miRNAs and semen *in vitro* quality parameters to propose a solution to predict fertility that potentially could be used for further studies in the field in a wider population. As a

novelty, the application of the MDPREF analysis demonstrated that a positive correlation was present among specific *in vitro* quality parameters (as motility viability and DNA integrity indicators), specific miRNAs, and bull fertility status.

Further studies are needed to evaluate these specific miRNAs as qualitative biomarkers for the prediction of assessment of sperm quality and the prediction of bull fertility. The integrated approach between advanced semen quality analysis and miRNA profiling could provide a model for prediction of fertility that might be beneficial to AI centers in the selection of bulls and facilitate the elimination of subfertile subjects or ejaculates with low fertilizing capacity.

DATA AVAILABILITY STATEMENT

The datasets presented in this study can be found in online repositories. The names of the repository/repositories and accession number(s) can be found below: the Sequence Read Archive (SRA) database, on NCBI server, and accession number: PRJNA727990.

ETHICS STATEMENT

Ethical review and approval was not required for the animal study because the commercial frozen semen doses used in this study were acquired from an approved commercial artificial insemination bull centers.

AUTHOR CONTRIBUTIONS

EC, FP, FT, and AS conceived the study. FT isolated the spermatozoa fractions through Percoll gradient and evaluated sperm characteristics and carried out the statistical analysis. EC and PC performed the RNA extraction, libraries preparation and sequencing. BL carried out the bioinformatic analysis. EC carried out pathway analysis. FP acquired the funding and supervised the project. EC and FT wrote the manuscript and generated the figures. All authors read and approved the final manuscript.

FUNDING

This work was supported by the project CNR-DISBA Cambiamenti Climatici (7009 - FOE 2019).

SUPPLEMENTARY MATERIAL

The Supplementary Material for this article can be found online at: https://www.frontiersin.org/articles/10.3389/fvets.2021.703101/full#supplementary-material

Supplementary Table 1 | Effect of technical replicate on sperm quality variables assessed after Percoll separation in the High Quality Sperm Fraction (HQS). (LSM ± SEM).

Supplementary File 1 | Example of Eukaryote Total RNA Pico profile obtained with Agilent Bionalizer for the sample B9_LF_S.

Supplementary File 2 | Total raw and normalized counts for miRNAs expressed in sperm in HF and LF bulls and different seasons, including technical replicates.

Supplementary File 3 | edgeR output for differential expression analysis between HF and LF bulls and different seasons.

Supplementary File 4 | Correlation matrix of the Multi-Dimensional Preference analysis.

Supplementary File 5 | Novel miRNA precursors sequences identified in High Fertility (HF) and Low Fertility (LF) bulls.

Supplementary File 6 | Novel miRNA mature sequences identified in High Fertility (HF) and Low Fertility (LF) bulls.

REFERENCES

1. Fagerlind M, Stålhammar H, Olsson B, Klinga-Levan K. Expression of miRNAs in bull spermatozoa correlates with fertility rates. *Repr Dom Anim.* (2015) 50:587–94. doi: 10.1111/rda.12531
2. Clay JS, McDaniel BT. Computing mating bull fertility from DHI Nonreturn data. *J Dairy Sci.* (2001) 84:1238–45. doi: 10.3168/jds.S0022-0302(01)74585-7
3. Gross N, Peñagaricano F, Khatib H. Integration of whole-genome DNA methylation data with RNA sequencing data to identify markers for bull fertility. *Anim Genet.* (2020) 51:502–10. doi: 10.1111/age.12941
4. Sellem E, Broekhuijse MLWJ, Chevrier L, Camugli S, Schmitt E, Schibler L, et al. Use of combinations of *in vitro* quality assessments to predict fertility of bovine semen. *Theriogenology.* (2015) 84:1447–54. doi: 10.1016/j.theriogenology.2015.07.035
5. Gliozzi TM, Turri F, Manes S, Cassinelli C, Pizzi F. The combination of kinetic and flow cytometric semen parameters as a tool to predict fertility in cryopreserved bull semen. *Animal.* (2017) 11:1975–82. doi: 10.1017/S1751731117000684
6. Kumaresan A, Johannisson A, Al-Essawe EM, Morrell JM. Sperm viability, reactive oxygen species, and DNA fragmentation index combined can discriminate between above- and below-average fertility bulls. *J Dairy Sci.* (2017) 100:5824–36. doi: 10.3168/jds.2016-12484
7. Capra E, Turri F, Lazzari B, Cremonesi P, Gliozzi TM, Fojadelli I, et al. Small RNA sequencing of cryopreserved semen from single bull revealed altered miRNAs and piRNAs expression between high- and low-motile sperm populations. *BMC Genomics.* (2017) 18:14. doi: 10.1186/s12864-016-3394-7
8. Alves MBR, De Arruda RP, De Bem THC, Florez-Rodriguez SA, de Sá Filho MF, Belleannée C, et al. Sperm-borne miR-216b modulates cell proliferation during early embryo development via K-RAS. *Sci Rep.* (2019) 9:10358. doi: 10.1038/s41598-019-46775-8
9. Liu WM, Pang RTK, Chiu PCN, Wong BPC, Lao K, Lee KF, et al. Sperm-borne microRNA-34c is required for the first cleavage division in mouse. *Proc Natl Acad Sci USA.* (2012) 109:490–4. doi: 10.1073/pnas.1110368109
10. Menezes ESB, Badial PR, El Debaky H, Husna AU, Ugur MR, Kaya A, et al. Sperm miR-15a and miR-29b are associated with bull fertility. *Andrologia.* (2020) 52:e13412. doi: 10.1111/and.13412
11. Ibrahim NM, Gilbert GR, Loseth KJ, Crabo BG. Correlation between clusterin-positive spermatozoa determined by flow cytometry in bull semen and fertility. *J Androl.* (2000) 21:887–94.
12. Parrish JJ, Krogenaes A, Susko-Parrish JL. Effect of bovine sperm separation by either swim-up or Percoll method on success of in vitro fertilization and early embryonic development. *Theriogenology.* (1995) 44:859–69. doi: 10.1016/0093-691X(95)00271-9
13. Bavister BD, Leibfried ML, Lieberman. Development of preimplantation embryos of the golden hamster in a defined culture medium. *Biol Reprod.* (1983) 28:235–47. doi: 10.1095/biolreprod28.1.235
14. Roederer M. *Compensation (An Informal Perspective).* (2000). Available online at: http://www.drmr.com/compensation (accessed April 28, 2021).
15. Toschi P, Capra E, Anzalone DA, Lazzari B, Turri F, Pizzi F, et al. Maternal peri-conceptional undernourishment perturbs offspring sperm methylome. *Reproduction.* (2020) 159:513–23. doi: 10.1530/REP-19-0549

16. Evenson DP, Jost L. Sperm chromatin structure assay is useful for fertility assessment. *Methods Cell Sci.* (2000) 22:169–89. doi: 10.1023/A:1009844109023
17. Robinson MD, McCarthy DJ, Smyth GK. edgeR: a Bioconductor package for differential expression analysis of digital gene expression data. *Bioinformatics.* (2010) 26:139–40. doi: 10.1093/bioinformatics/btp616
18. Sturn A, Quackenbush J, Trajanoski Z. Genesis: cluster analysis of microarray data. *Bioinformatics.* (2002) 18:207–8. doi: 10.1093/bioinformatics/18.1.207
19. Linting M, Meulman JJ, Groenen PJ, van der Kooij AJ. Nonlinear principal components analysis, introduction and application. *Psychol Methods.* (2007) 12:336–58. doi: 10.1037/1082-989X.12.3.336
20. Mengual L, Ballesca JL, Ascaso C, Oliva R. Marked differences in protamine content and P1/P2 ratios in sperm cells from percoll fractions between patients and controls. *J Androl.* (2003) 24:438–47. doi: 10.1002/j.1939-4640.2003.tb02692.x
21. Morrell JM, Johannisson A, Dalin AM, Rodriguez-Martinez H. Morphology and chromatin integrity of stallion spermatozoa prepared by density gradient and single layer centrifugation through silica colloids. *Reprod Domest Anim.* (2008) 44:512–7. doi: 10.1111/j.1439-0531.2008.01265.x
22. Arias ME, Andara K, Briones E, Felmer R. Bovine sperm separation by Swim-up and density gradients (Percoll and BoviPure): effect on sperm quality, function and gene expression. *Reprod Biol.* (2017) 17:126–32. doi: 10.1016/j.repbio.2017.03.002
23. Castro LS, Siqueira AFP, Hamilton TRS, Mendes CM, Visintin JA, Assumpção MEOA. Effect of bovine sperm chromatin integrity evaluated using three different methods on in vitro fertility. *Theriogenology.* (2018) 107:142–8. doi: 10.1016/j.theriogenology.2017.11.006
24. García-Macías V, de Paz P, Martínez-Pastor F, Álvarez M, Gomes-Alves S, Bernardo J, et al. DNA fragmentation assessment by flow cytometry and Sperm-Bos-Halomax (bright-field microscopy and fluorescence microscopy) in bull sperm. *Int J Androl.* (2007) 30:88–98. doi: 10.1111/j.1365-2605.2006.00723.x
25. Contri A, Valorz C, Faustini M, Wegher L, Carluccio A. Effect of semen preparation on casa motility results in cryopreserved bull spermatozoa. *Theriogenology.* (2010) 74:424–35. doi: 10.1016/j.theriogenology.2010.02.025
26. Christensen P, Labouriau R, Birck A, Boe-Hansen GB, Pedersen J, Borchersen S. Relationship among seminal quality measures and field fertility of young dairy bulls using low-dose inseminations. *J Dairy Sci.* (2011) 94:1744e54. doi: 10.3168/jds.2010-3087
27. Birgitte Narud B, Klinkenberg G, Khezri A, Zeremichael TT, Stenseth EB, Nordborg A. Differences in sperm functionality and intracellular metabolites in Norwegian Red bulls of contrasting fertility. *Theriogenology.* (2020) 157:24–32. doi: 10.1016/j.theriogenology.2020.07.005
28. Gillan L, Kroetsch T, Maxwell WMC, Evans G. Assessment of *in vitro* sperm characteristics in relation to fertility in dairy bulls. *Anim Reprod Sci.* (2008) 103:201–14. doi: 10.1016/j.anireprosci.2006.12.010
29. Oliveira LZ, de Arruda RP, de Andrade AFC, Celeghini ECC, Reeb PD, Martins JPN, et al. Assessment of in vitro sperm characteristics and their importance in the prediction of conception rate in a bovine timed-AI program. *Anim Reprod Sci.* (2013) 137:145–55. doi: 10.1016/j.anireprosci.2013.01.010
30. Waterhouse KE, Haugan T, Kommisrud E, Tverdal A, Flatberg G, Farstad W, et al. Sperm DNA damage is related to field fertility of semen from young Norwegian Red bulls. *Reprod Fertil Dev.* (2006) 18:781–8. doi: 10.1071/RD06029
31. Alves MBR, Celeghini ECC, Belleannée C. From sperm motility to sperm-borne microRNA signatures: new approaches to predict male fertility potential. *Front Cell Dev Biol.* (2020) 8:791. doi: 10.3389/fcell.2020.00791
32. Nixon B, Stanger SJ, Mihalas BP, Reilly JN, Anderson AL, Dun MD, et al. Next generation sequencing analysis reveals segmental patterns of microRNA expression in mouse epididymal epithelial cells. *PLoS ONE.* (2015) 10:e0135605. doi: 10.1371/journal.pone.0135605
33. Liu SS, Maguire EM, Bai YS, Huang L, Liu Y, Xu L. A novel regulatory axis, CHD1L-MicroRNA 486-matrix metalloproteinase 2, controls spermatogonial stem cell properties. *Mol Cell Biol.* (2019) 39:e00357–18. doi: 10.1128/MCB.00357-18
34. Liu J, Sun Y, Yang C, Zhang Y, Jiang Q, Huang J, et al. Functional SNPs of INCENP affect semen quality by alternative splicing mode and binding affinity with the target Bta-miR-378 in Chinese Holstein Bulls. *PLoS ONE.* (2016) 11:e0162730. doi: 10.1371/journal.pone.0162730
35. Zhang R, Zuo Y, Cao S. Upregulated microRNA-423-5p promotes oxidative stress through targeting glutathione S-transferase mu 1 in asthenozoospermia. *Mol Reprod Dev.* (2021) 8:158–66. doi: 10.1002/mrd.23454
36. Xu H, Wang X, Wang Z, Li J, Xu Z, Miao M, et al. MicroRNA expression profile analysis in sperm reveals hsa-mir-191 as an auspicious omen of in vitro fertilization. *BMC Genomics.* (2020) 21:165. doi: 10.1186/s12864-020-6570-8

Conflict of Interest: The authors declare that the research was conducted in the absence of any commercial or financial relationships that could be construed as a potential conflict of interest.

frontiers in Veterinary Science

ORIGINAL RESEARCH
published: 26 July 2021
doi: 10.3389/fvets.2021.679947

Non-targeted Metabolomics Reveals Metabolic Characteristics of Porcine Atretic Follicles

Jiayuan Mo[1†], Le Sun[1†], Juanru Cheng[2†], Yujie Lu[1], Yaochang Wei[1], Guangsheng Qin[2], Jing Liang[1] and Ganqiu Lan[1*]*

[1] College of Animal Science and Technology, Guangxi University, Nanning, China, [2] Key Laboratory of Buffalo Genetics, Guangxi Buffalo Research Institute, Chinese Academy of Agricultural Science, Nanning, China

Follicular atresia is one of the main factors limiting the reproductive power of domestic animals. At present, the molecular mechanisms involved in porcine follicular atresia at the metabolic level remain unclear. In this study, we divided the follicles of Bama Xiang pigs into healthy follicles (HFs) and atretic follicles (AFs) based on the follicle morphology. The expression of genes related to atresia in granulosa cells (GCs) and the concentration of hormones in the follicular fluid (FF) from HFs and AFs were detected. We then used liquid chromatography–mass spectrometry-based non-targeted metabolomic approach to analyze the metabolites in the FF from HFs and AFs. The results showed that the content of estradiol was significantly lower in AFs than in HFs, whereas that of progesterone was significantly higher in AFs than that in HFs. The expression of *BCL2*, *VEGFA*, and *CYP19A1* was significantly higher in HFs than in AFs. In contrast, the expression of *BAX* and *CASPASE3* was significantly lower in HFs. A total of 18 differential metabolites (DMs) were identified, including phospholipids, bioactive substances, and amino acids. The DMs were involved in 12 metabolic pathways, including arginine biosynthesis and primary bile acid biosynthesis. The levels of eight DMs were higher in the HF group than those in the AF group ($p < 0.01$), and those of 10 DMs were higher in the AF group than those in the HF group ($p < 0.01$). These findings indicate that the metabolic characteristics of porcine AFs are lower levels of lipids such as phospholipids and higher levels of amino acids and bile acids than those in HFs. Disorders of amino acid metabolism and cholic acid metabolism may contribute to porcine follicular atresia.

Keywords: Bama Xiang pig, follicular atresia, non-targeted metabolomics, LC-MS, follicular fluid

OPEN ACCESS

Edited by:
Jordi Roca,
University of Murcia, Spain

Reviewed by:
Mallikarjun Bidarimath,
Cornell University, United States
Abouzar Najafi,
University of Tehran, Iran

***Correspondence:**
Ganqiu Lan
gqlan@gxu.edu.cn
Jing Liang
liangjing@gxu.edu.cn

[†]These authors have contributed equally to this work and share first authorship

Specialty section:
This article was submitted to Animal Reproduction - Theriogenology, a section of the journal Frontiers in Veterinary Science

Received: *12 March 2021*
Accepted: *25 June 2021*
Published: *26 July 2021*

Citation:
Mo J, Sun L, Cheng J, Lu Y, Wei Y, Qin G, Liang J and Lan G (2021) Non-targeted Metabolomics Reveals Metabolic Characteristics of Porcine Atretic Follicles. Front. Vet. Sci. 8:679947. doi: 10.3389/fvets.2021.679947

INTRODUCTION

Reproductive ability, which is a base index, typically refers to productivity in the porcine industry. In mammals, the ovary produces generative cells. The number of follicles is an index that determines the reproductive ability of female animals, especially polyembryonic animals. However, when more than 90% of the follicles degenerate before ovulation, the condition is termed follicular atresia (1). It is well-known that follicular cells include not only oocytes but also follicular fluid (FF) and granulosa cells (GCs). Many factors affect follicular atresia; however, GC apoptosis is the

main molecular mechanism (2, 3). Additionally, the physiological activities of the hypothalamus–pituitary–gonadal axis occupy an influential position in follicular atresia (4). The molecules in FF, such as hormones [including melatonin (5) and growth hormone (6)] and cytokines [transforming growth factor beta (TGF-β) superfamily (7), insulin-like growth factor (IGF) (8), interleukin-6 (IL6) (9), and epidermal growth factor (EGF) (10)], also affect follicular atresia. Because of the transfer of plasma and the secretion of follicle cells, the FF component is highly complex. The concentration of FF components may be inconsistent in diverse follicular cell types, especially between atretic follicles (AFs) and healthy follicles (HFs). Nishimoto et al. (11) studied the difference between HFs and AFs in cattle and proposed that glucose and lactic acid may be markers of follicular atresia in FF. However, the consistency of these indices in Bama Xiang pigs is unknown.

Fortunately, sequencing technology has quickly developed with the development of biotechnology and computer technology. After RNA sequencing (RNA-seq) explained the difference at the transcription level, proteomics explained the difference at the translation level. Metabolomics is an emerging omics technology that explains differences at the metabolic level. We can perform qualitative and quantitative analyses of all small molecule metabolites (<1 kDa) in specific biological samples (such as blood, urine, and FF) by metabolomics. This technology is suitable for the study of physiological mechanisms and the discovery of biomarkers (12). At present, metabolomics based on FF samples have shown great potential in reproductive medicine. It is used to identify biomarkers that assess oocyte quality to predict the outcome of assisted reproduction (13). Additionally, metabolomic analysis of FF screened out biomarkers of multiple reproductive diseases such as polycystic ovary syndrome (14), endometriosis (10), and infertility (15) and characterized their global metabolic profile to provide a reference for the clinical diagnosis of these diseases and an in-depth study of their pathogenesis. This study indicated that this method can be used to identify biomarkers in animal husbandry and veterinary medicine.

Bama Xiang pigs are a Chinese indigenous pig and are famous for their small size, excellent meat quality, and early maturation (16). Bama Xiang boars produce sperm in the seminiferous tubules at the age of 29 days, and the sex maturation time is 76 days. For Bama Xiang sows, the sex maturation time is 110 days (17). However, the litter size of Bama Xiang pigs is lower than that of many Chinese indigenous breeds, such as Meishan pigs, Bamei pigs, and Erhualian pigs. Therefore, using metabolomics to identify biomarkers between HFs and AFs will be of great benefit in improving the understanding of Bama Xiang pig reproduction traits. Meanwhile, because of the parallels with humans in anatomy and physiology, Bama Xiang pigs could be used in human medical research (18–21). Our study used a liquid chromatography–mass spectrometry (LC–MS)-based non-targeted metabolomic approach for the first time to analyze the FF of HFs and AFs in Bama Xiang pigs. The results will further increase the understanding of the mechanism of follicular atresia in Bama Xiang pigs and provide a reference for experimental animals to benefit human reproduction studies.

MATERIALS AND METHODS

Follicle Classification

A total of 10 ovaries were collected from the right side of 6-month-old Bama Xiang pigs from the Bama Xiang Pig Agriculture and Animal Husbandry Co., Ltd. (Guangxi, China). After collection, the ovaries were rinsed with physiological saline, placed in a heat preservation pot containing physiological saline at 37°C with high-pressure processing, and transported to the laboratory within 2 h. After rinsing with 75% ethanol, the ovaries were washed with physiological saline at 37°C. Ophthalmic scissors were used to cut open and separate a single follicle (3 mm $< n <$ 5 mm) from the ovarian tissue. The single follicle was repeatedly rinsed with 0.1 M phosphate buffer (pH 7.25). As previously mentioned (22), we divided the follicles into HF and AF groups based on follicle morphology. The morphology of the follicle mainly included the following two aspects: the appearance of the follicle (such as color, capillary, and transparency) (23) and state of cumulus–oocyte complex (COC) and GCs.

Collection of Granulosa Cells and Follicular Fluid

After morphological classification, we removed the oocytes, and the remaining liquids (including FF and GCs) were mixed. The FF and GCs were separated by centrifugation (4°C, 1,200 rpm, 5 min). After washing 2–3 times with precooled phosphate buffered saline, the collected GCs were mixed with 1 ml TRIzol and stored at −80°C. The FF was centrifuged again (4°C, 8,000 rpm, 5 min) to collect the supernatant. Then, 30 μl of the supernatant was used to detect the concentration of estradiol (E2) and progesterone (PROG), and the rest was stored at −80°C for LC–MS analysis. In the same individual, we collected only one HF and one AF sample. A total of 10 samples each were collected from the HF group and AF group.

Measurements of Estradiol and Progesterone

The hormone levels related to follicular atresia, such as E2 (24) and PROG (25) in FF, were measured using ELISA kits (Shanghai Enzyme Biotechnology Co., Ltd., China, ml002366, ml002422) to confirm the follicle classification. A total of 20 FF samples were analyzed using a microplate reader (Infinite M200 PRO, TECAN) according to the manufacturer's instructions. All assays were validated in our laboratory by showing parallels between serial sample dilutions and the provided assay standard curve (range: E2, 2.5–80 pg/ml; PROG, 0.625–20 ng/ml). Sensitivity of the E2 and PROG assays was 0.1 pg/ml and 0.1 ng/ml, respectively. The intra-assay coefficient of variation was <15% for each.

cDNA Synthesis and Quantitative RT-PCR for Related Genes

The TRIzol Reagent (Ambion, Life Technologies, New York, USA), chloroform, isopropanol, and ethanol were used to extract the total RNA. RNase-free water was used to dissolve total RNA from GCs. Oligo $(dT)_{23}VN$ (10 μM), 4× gDNA wiper Mix, and RNase-free ddH_2O at 42°C were used for 2 min to remove the DNA from the GCs. We used the 5× HiScript II

TABLE 1 | Quantitative real-time PCR primers of genes.

Name	Primer sequence (5′-3′)	Length (bp)	Reference/ accession numbers
BAX-F	GCCGAAATGTTTGCTGAC	154	AJ606301
BAX-R	GCCGATCTCGAAGGAAGT		
BCL2-F	GATGCCTTTGTGGAGCTGTATG	145	AB271960
BCL2-R	CCCGTGGACTTCACTTATGG		
CASPASE3-F	TGGATGCTGCAAATCTCA	327	NM_214131
CASPASE3-R	TCCCACTGTCCGTCTCAA		
CYP19A1-F	GCTGCTCATTGGCTTAC	187	NM_214431
CYP19A1-R	TCCACCTATCCAGACCC		
VEGFA-F	CCTTGCTGCTCTACCTCC	239	NM_214084
VEGFA-R	CTCCAGACCTTCGTCGTT		
GAPDH-F	GGACTCATGACCACGGTCCAT	220	AF017079
GAPDH-R	TCAGATCCACAACCGACACGT		

Select qRT SuperMix II at 50°C for 15 min to convert the RNA into cDNA (Vazyme, R223-01, China) (26). Prior to quantitative RT-PCR (qRT-PCR) amplification, the sequences of primers for *BAX*, *BCL2*, *CASPASE3*, *CYP19A1*, *VEGFA*, and *GAPDH* (**Table 1**) were designed using the Oligo 7.0 software. qRT-PCR was performed on an Applied Biosystems 7500 Real-Time PCR System (ABI7500; Applied Biosystems, Carlsbad, CA, USA) using ChamQ Universal SYBR qPCR Master Mix (Vazyme, Q711-02/03, China) following the manufacturer's instructions. The relative expression of each gene was calculated using the $2^{-\Delta\Delta Ct}$ method with *GAPDH* as the reference gene.

Follicular Fluid Sample Preparation

Prior to FF metabolite analysis, a 50-μl FF sample with 125 μl of methanol and 125 μl of acetonitrile was added to 1.5-ml Eppendorf (EP) tubes, vortexed for 30 s to precipitate protein, underwent a low-temperature ultrasound for 15 min, and then was centrifuged (13,000 rpm, 20 min, 4°C). The supernatant fractions were collected and evaporated using a vacuum concentrator. The resulting dry residues were redissolved in 50 μl of acetonitrile:water (1:1) and centrifuged again (13,000 rpm, 20 min, 4°C). Finally, the liquid supernatant was transferred to sampler vials for analysis using a ultraperformance LC–MS (UPLC-MS) system (27).

Ultraperformance Liquid Chromatography–Mass Spectrometry Instrument and Parameters

A Dionex liquid chromatograph instrument (UltiMate3000, Thermo Fisher Scientific, USA) was utilized. It contained a liquid phase pump (HPG-3400 SD, Thermo Fisher Scientific, USA), column temperature box (TCC-3000 SD, Thermo Fisher Scientific, USA), and an autosampler (WPS-3000SL, Thermo Fisher Scientific, USA). An ACQUITY UPLCBEHC18 column (50 × 2.1 mm, 1.7 μm) was also used. The ion source was a quadrupole electrostatic field orbit trap high-resolution mass spectrometer Q-Exactive (Thermo Fisher Scientific, USA) heated electrospray (Thermo Fisher Scientific, USA). The scanning mode was full MS and full MS/dd-MS2 (**Table 2**) (27).

TABLE 2 | Instrument operation program of UPLC-MS/MS analysis.

Item	Parameter	Item	Parameter
Column temperature	30°C	Mass range	80–1,200 m/z
Autosampler temperature	4°C	Sheath gas flow rate	30 psi
Sample injection volume	2 μl	Auxiliary gas flow rate	10 psi
Mobile phase A	Water plus 0.1% formic acid	Transmission Capillary temperature	320°C
Mobile phase B	Methanol	Primary scan resolutions	70,000
Spray voltage	3.0 kV	Secondary scan resolutions	17,500

Data Analysis

The original data were processed using the Compound Discover 3.1 software for peak alignment of metabolites, to correct the retention time of metabolites, and to extract the peak area of metabolites. To identify the metabolite structures, accurate mass matching (<25 ppm) and matching with secondary spectra were used in the experiment. The peak areas of all metabolites were imported into the SIMCA-P program (version 14.1, Umetrics) for multivariate analysis, consisting of unsupervised principal component analysis (PCA) and supervised orthogonal partial least squares discriminant analysis (OPLS-DA). PCA was used to determine intragroup aggregation and inter-group separation tendencies, whereas OPLS-DA was performed to further determine inter-group differences. The OPLS-DA models were validated based on the interpretation of variation in Y (R2Y) and forecast ability based on the model (Q2) in cross-validation and permutation tests by applying 200 iterations. Univariate analyses were performed, including independent-samples *t*-test and fold change analysis. Significant differential metabolites (DMs) were screened using variable importance in projection (VIP) scores (VIP > 1) obtained from the OPLS-DA model and *p*-values ($p < 0.05$) using the *t*-test. In addition, the metabolic pathway analysis network tools MetPA (http://metpa.metabolomics.ca), MetaboAnalyst (https://www.metaboanalyst.ca/MetaboAnalyst/home.xhtml), and the Encyclopedia of Genes and Genomes in the Kyoto Protocol (KEGG, http://www.genome.jp/kegg/) were used to identify potentially disordered metabolic pathways. The differences between groups for hormone concentration and the qRT-PCR results were analyzed using independent-samples *t*-test analysis in SAS 9.2, and the results are expressed as the mean ± standard error of the mean. Unless otherwise stated, differences were considered statistically significant at $p < 0.05$.

RESULTS

Appearance of Follicles

We identified one HF and one AF from the same ovary. The COCs, GCs, and FF were noticeably different between HFs and AFs. The cumulus, ooplasm, zona pellucida, GCs, and FF were

damaged or deteriorated in AFs (**Table 3**). In follicles of the same size, more blood vessels were observed in the HFs than in the AFs (**Figure 1**).

Determination of Estradiol and Progesterone in Follicular Fluid

Each sample in the HF and AF groups was analyzed three times. A total of 60 records of E2 and PROG were used to carry out the independent-samples *t*-test analysis in SAS 9.2. The concentrations of E2 in the HF and AF were 35.20 ± 8.30 and 16.43 ± 3.06 pg/ml, respectively. The concentrations of PROG in the HF and AF were 6.41 ± 2.45 and 11.89 ± 2.14 ng/ml, respectively. Compared with the HF, in the AF, the content of E2 in the FF was significantly reduced ($p < 0.01$) and that of PROG was significantly increased ($p < 0.01$) (**Figure 2A**).

TABLE 3 | Classification of follicles based on the state of COCs and granulosa cells.

Classification	COCs	GCs	FF
HF	Compact cumulus and translucent ooplasm	Large quantity and compact	Clear
AF	Strongly extended or absent cumulus and dark ooplasm, and damaged zona pellucida	Few quantity and Quicksand shaped	Turbid

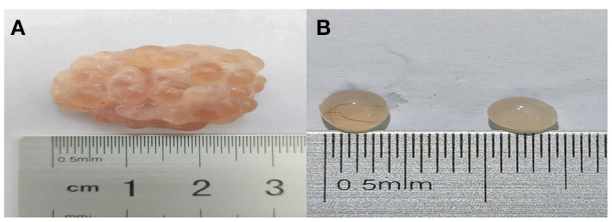

FIGURE 1 | The morphologies of the ovary and follicles of Bama Xiang pig. **(A)** The right ovary of the Bama Xiang pig. **(B)** The healthy follicle (left side) and atretic follicle (right side) in the same ovary of Bama Xiang pig.

Expressions of Genes Related to Atresia in Granulosa Cells

Similar to the content of E2 and PROG, the expression of genes related to atresia in GCs from the HF and AF was assessed three times in each sample. A total of 60 records of each gene from the 20 samples, including *BCL2*, *VEGFA*, *CYP19A1*, *BAX*, and *CASPASE3*, were used to carry out the independent-samples *t*-test analysis using SAS 9.2 software. While we used the gene expression of HF as 1, the expression levels of *BCL2*, *VEGFA*, *CYP19A1*, *BAX*, and *CASPASE3* in AF were 0.22 ± 0.14, 0.53 ± 0.19, 0.53 ± 0.20, 2.26 ± 0.59, and 3.05 ± 1.76, respectively. The expression of *BCL2*, *VEGFA*, and *CYP19A1* in HF was significantly higher than that in AF ($p < 0.01$). The expression of *BAX* and *CASPASE3* in HF was significantly lower than that in AF ($p < 0.01$) (**Figure 2B**).

Metabolite Profiles of Follicular Fluid

To obtain an overview of the FF metabolic characteristics of Bama Xiang pig follicular atresia, non-targeted metabolic profiling was conducted using the UPLC–MS/MS method. In this experiment, 3,044 peaks in the positive and negative ion modes were obtained. After filtering using the mzCloud database, HMDB database, total ion chromatograms, molecular weight, retention time, peak area, and peak intensity, a total of 994 metabolites were matched. The PCA showed that the R2X model interpretation rates for the two groups under the positive and negative ion mode conditions were 0.62 and 0.679, respectively. Four quality control (QC) samples gathered together not only in the positive PCA score plot but also in the negative PCA score plot (**Figure 3**). The OPLS-DA showed that samples from the two groups were well-separated, and each tended to cluster in the same group (**Figures 4A,B**). In the positive ion mode of OPLS-DA, R2Y and Q2 were 0.986 and 0.517, respectively, whereas in the negative ion mode, R2Y and Q2 were 0.979 and 0.38, respectively. The intercepts of permutation tests in the positive ion mode and negative ion mode were −0.257 and −0.353,

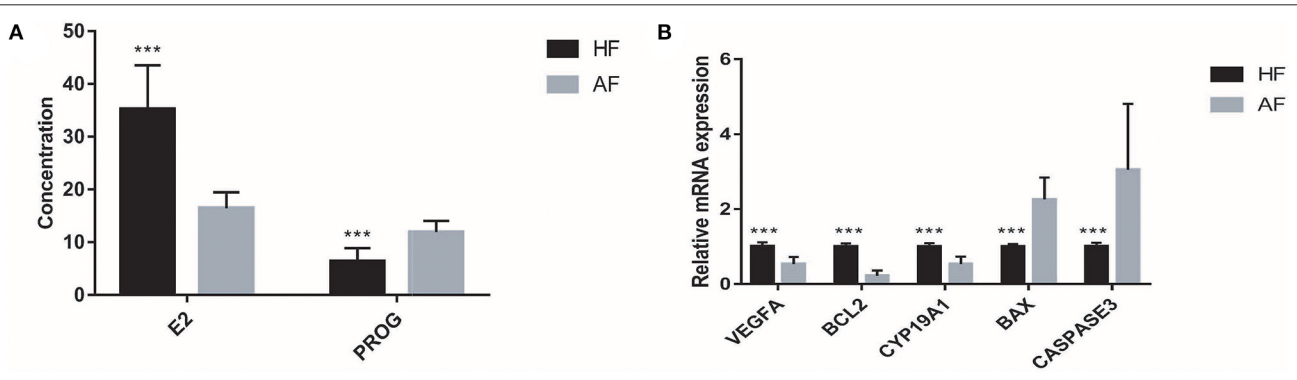

FIGURE 2 | The hormone contents and gene expressions in the healthy follicle (HF) and atretic follicle (AF) samples. **(A)** The contents of estradiol (E2) and progesterone (PROG) in the follicular fluid (FF) from HF and AF, respectively. **(B)** The relative mRNA expressions of *VEGFA*, *BCL2*, *CYP19A1*, *BAX*, and *CASPASE3* genes in the HF and AF samples, respectively. *** highly significant difference between the two groups ($p < 0.01$).

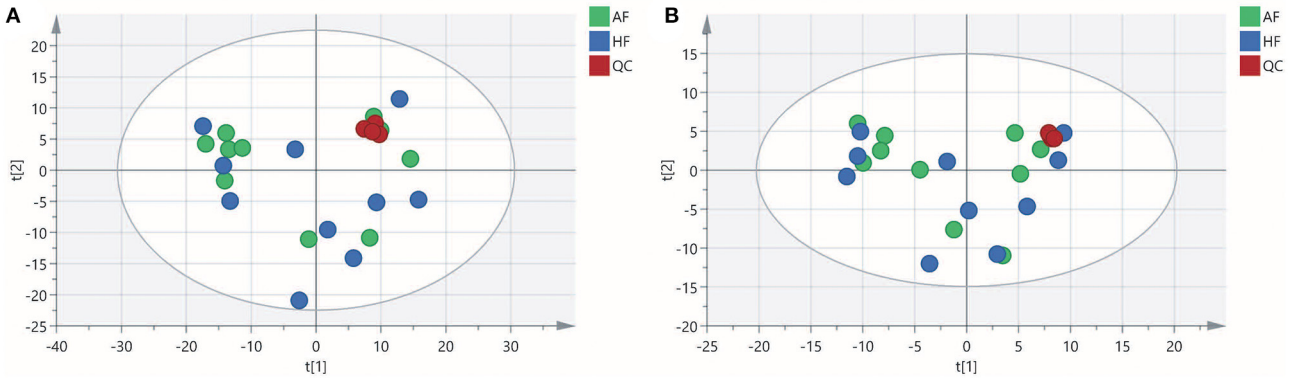

FIGURE 3 | Principal component analysis (PCA) score plot of the healthy follicle (HF) and atretic follicle (AF) groups. **(A)** PCA score plot for the two groups analyzed in the positive ion mode. **(B)** PCA score plot for the two groups analyzed in the negative ion mode. t[1] was the first principal component; t[2] was the second principal component.

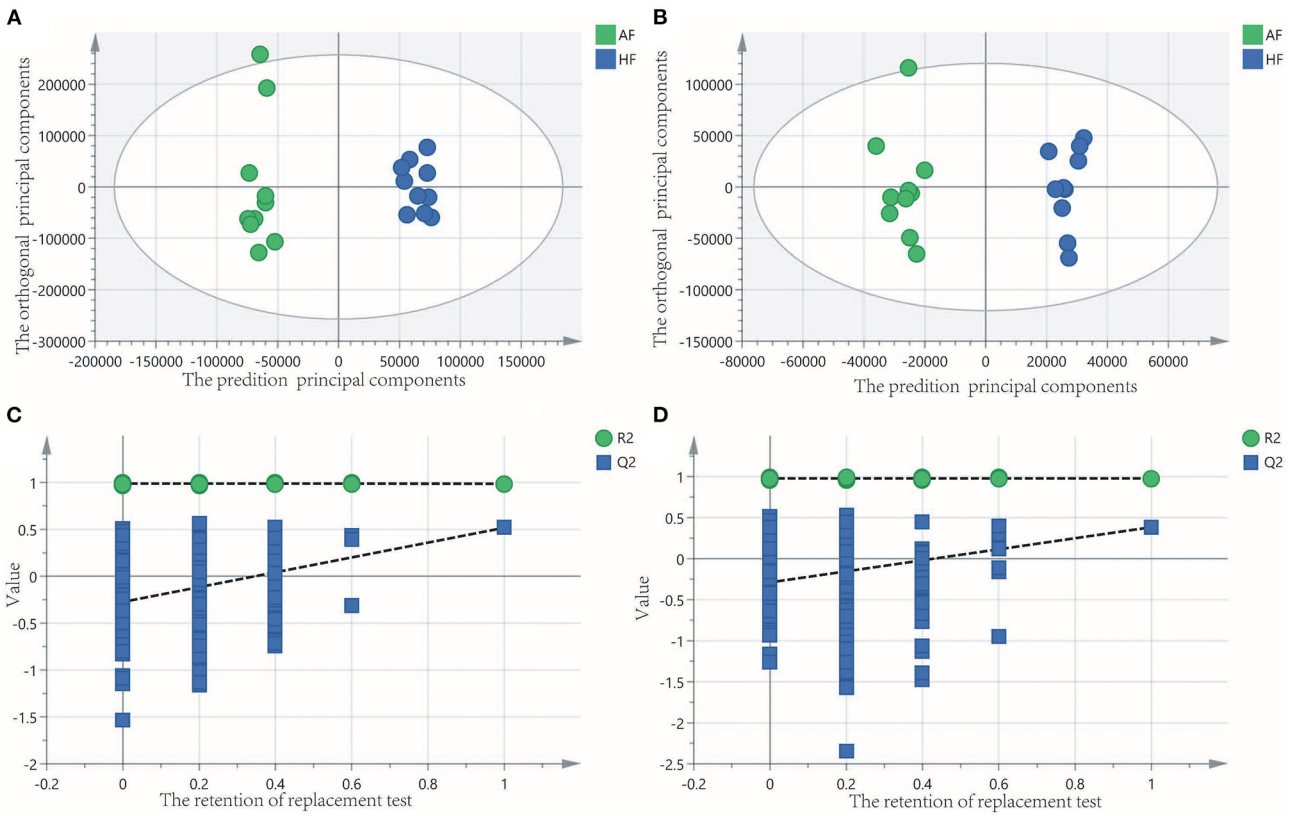

FIGURE 4 | Orthogonal partial least squares discriminant analysis (OPLS-DA) of score and permutation test plot for the healthy follicle (HF) and atretic follicle (AF) groups. **(A,C)** were in the positive ion mode; **(B,D)** were in the negative ion mode. The intercept limit of Q2 was calculated by the regression line, which was the plot of Q2 from the permutation test in the OPLS-DA model.

respectively (**Figures 4C,D**). A total of 18 metabolites, including L-glutamine, beta-lysine, testosterone cypionate, and L-arginine, were identified as DMs between the HF and AF groups (**Table 4**, **Figure 5**). The levels of eight DMs, including palmitamide, octadecanamide, and tetradecanamide, were higher in the HF than in the AF ($p < 0.01$), and those of 10 DMs, including L-glutamine, L-arginine, and guanine, were higher in the AF than in the HF ($p < 0.01$) (**Figure 6**). Using MetaboAnalyst 4.0 to analyze the 18 DMs showed that they were completely enriched in 12 metabolic pathways, such as arginine biosynthesis, alanine,

TABLE 4 | Information of 18 differential metabolites.

Name	MW (Da)	RT (min)	FC	VIP	Ion mode
15-Methylpalmitate	287.28188	14.06	0.21	14.7694	P
LysoPC (0:0/16:0)	495.33163	17.93	1.59	7.09451	P
Platelet-activating factor (PAF)	523.36237	18.781	2.22	5.17624	P
Palmitamide	255.25574	18.496	4.69	1.68894	P
Octadecanamide	283.28693	19.172	9.71	1.56161	P
L-Glutamine	146.06888	0.744	0.67	1.4515	P
7alpha-Hydroxy-3-oxo-4-cholestenoic acid	430.30736	16.088	0.67	1.40831	P
L-Pyroglutamic acid	129.04248	0.58	0.78	1.25267	P
Beta-lysine	146.10531	0.538	0.72	1.21497	P
Testosterone cypionate	412.2969	17.669	0.65	1.20554	P
Guanine	151.04914	1.451	0.77	1.16932	P
Lyso-PAF	481.35226	18.524	1.53	1.14234	P
Tetradecanamide	227.22444	17.649	6.99	1.05941	P
L-Arginine	174.11136	1.288	0.70	1.04384	P
Metenolone enanthate	414.31281	17.8	0.47	1.00324	N
LysoPE(18:0/0:0)	481.31663	17.914	1.72	5.40505	N
LysoPE(20:0/0:0)	509.34799	18.872	2.18	3.83837	N
Myristyl sulfate	294.18663	17.563	0.65	2.37024	N

Fold changes (FC) were calculated as the peak area average levels in the HF group relative to those in the AF group. A fold changes > 1 indicates relatively higher concentration in the HF group, whereas a fold change of < 1 indicates a concentration lower than that in the AF group. MW, molecular weight; RT, retention time; VIP, variable importance in projection; P, positive ion mode; N, negative ion mode.

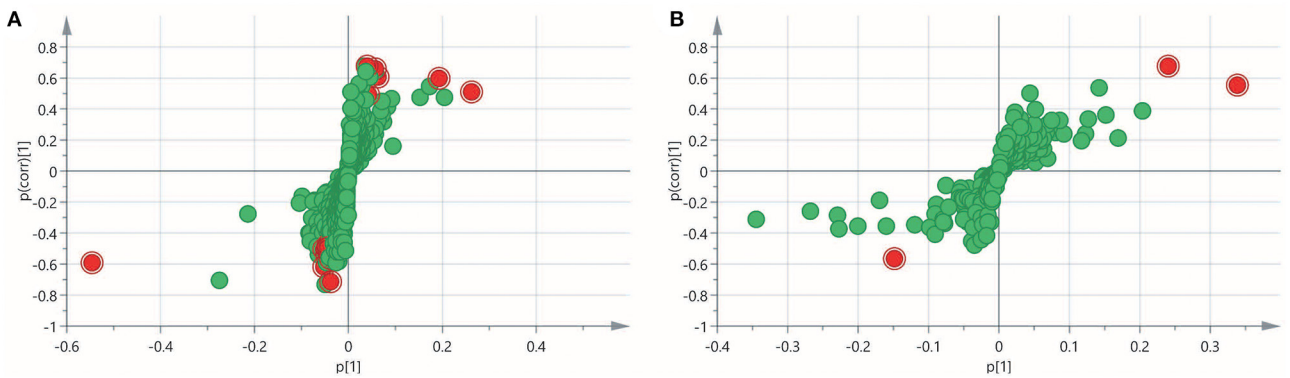

FIGURE 5 | Variable importance in projection (VIP) score plot for the healthy follicle (HF) and atretic follicle (AF) groups. **(A)** The VIP score plot for the two groups analyzed in the positive ion mode. **(B)** The VIP score plot for the two groups analyzed in the negative ion mode. p[1] was the load of each substance under the first principal component; p(corr)[1] was the correlation between each substance and the first principal component. The red plots were the differential metabolites.

aspartate, and glutamate metabolism, and primary bile acid (BA) biosynthesis (**Table 5**).

DISCUSSION

First, we identified HFs and AFs based on the appearance of the follicles. We then measured the concentration of hormones in FF and gene expression in GCs to prove the identification accuracy of HFs and AFs. Similar to the research on *VEGFA* (28) in follicular atresia, the expression of *VEGFA* was approximately two times higher in the HF than in the AF in our study. Furthermore, HFs appeared to have more blood vessels than AFs. This result indicated that the expression of *VEGFA* gene in HF plays a key role in blood vessel generation to maintain the health of the follicles. Meanwhile, the expression of *BAX* (29), *BCL2* (29, 30), *CASPASE3* (30), and *CYP19A1* (31) and the concentration of E2 (24) and PROG (25) were significantly different, which is consistent with the results of prior research. All these studies illustrated that the grouping of our study was reasonable.

The results of this study suggest that the concentrations of bioactive phospholipid substances, including lysophosphatidylcholine [LysoPC (0-0/16:0)], lysophosphatidylethanolamine [LysoPE (18:0/0-0 and 20:0/0-0)], platelet-activating factor (PAF), and

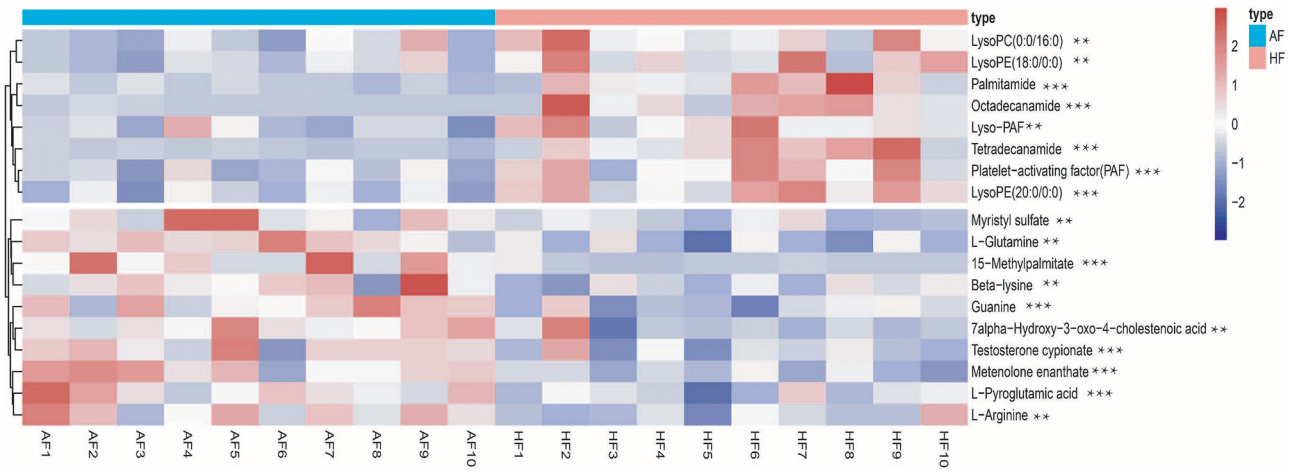

FIGURE 6 | Heatmap of the different metabolites in the follicular fluid of the healthy follicle (HF) and atretic follicle (AF) groups. ** significant difference ($p < 0.05$); *** highly significant difference ($p < 0.01$).

TABLE 5 | Results of metabolic pathway enrichment analysis.

Pathway name	Match status	*P*	Impact	Details
Arginine biosynthesis	2/14	0.0032727	0.07614	KEGG
Aminoacyl-tRNA biosynthesis	2/48	0.036071	0.0	KEGG
D-Glutamine and D-glutamate metabolism	1/6	0.038151	0.0	KEGG
Nitrogen metabolism	1/6	0.038151	0.0	KEGG
Purine metabolism	2/65	0.062718	0.01281	KEGG
Ether lipid metabolism	1/20	0.12213	0.08434	KEGG
Glutathione metabolism	1/28	0.16709	0.00709	KEGG
Alanine, aspartate and glutamate metabolism	1/28	0.16709	0.11378	KEGG
Glyoxylate and dicarboxylate metabolism	1/32	0.18879	0.0	KEGG
Arginine and proline metabolism	1/38	0.22038	0.05786	KEGG
Pyrimidine metabolism	1/39	0.22554	0.0	KEGG
Primary bile acid biosynthesis	1/46	0.26078	0.0	KEGG

Metabolic pathway analysis of differential metabolites.

1-*O*-hexadecyl-lyso-sn-glycero-3-phosphocholine (Lyso-PAF), are lower in the AF than in the HF. *In vivo*, LPC and LPE can be converted into PC and PE by acylation, which is mediated by lysophospholipid acyltransferases (LPLATs). PC and PE are the most abundant phospholipids and important structural and functional components of the biological membrane in all mammals (32, 33). The physiological significance of LPE remains unknown, but LPC has been shown to participate in several physiological activities as an effective lipid mediator. LPC is beneficial for GC growth and oocyte maturation by activating the extracellular signal-regulated kinases and nitric oxide (NO) (34). The exogenous addition of LPC could reduce the inhibitory effect of zearalenone on the oocyte maturation process (35). Similar to our study, some recent studies based on FF metabolomics have found more evidence that LPC and LPE are involved in the regulation of follicle development (36, 37). PAF is considered to be the most potent lipid mediator known to date, and the remodeling pathway mediated by LysoPAF is one of the important pathways of PAF biosynthesis (38). PAF has been reported to promote ovulation, facilitate oocyte maturation *in vitro*, enhance extracellular matrix formation around luteal cells, and promote the growth of vascular networks (39). This result is consistent with our findings, as the expression of *VEGFA* was higher in the HF than in the AF, and more blood vessels were observed in HFs. In contrast, estrogen has been proven to cause accumulation of PAF in the ovary by inhibiting the activity of PAF-acetylhydrolase, and the level of PAF is positively correlated with estrogen (40). More importantly, testosterone cypionate as a testosterone can transform to E2 by aromatase reaction (41), and testosterone cypionate level in the AF was significantly higher than that in the HF. Therefore, we hypothesized that testosterone cypionate in the HF was transformed into E2 to promote the accumulation of PAF, which benefited oocyte maturation and maintenance of HFs. However, further research is required to determine the relationship between these factors and follicular atresia. In our results, phospholipid levels were higher in the HF than in the AF. The level of phospholipids that promote follicle development may be achieved by the activation of extracellular signal-regulated kinases and production of NO; the lack of phospholipids may lead to damage of the zona pellucida and GCs, which further results in the deterioration of FF.

An interesting finding of our study was that the levels of amino acids such as L-glutamine, L-pyroglutamic acid, and L-arginine in FF samples were increased by atresia. However, studies have shown that L-pyroglutamic acid can be converted into glutamate to synthesize glutathione (GSH). Reduced GSH is a powerful antioxidant that protects GCs against oxidative stress caused by reactive oxygen species, maintaining normal mitochondrial function and inhibiting cell apoptosis (42). L-arginine improves

oocyte maturation and embryo development by increasing NO production (43). These amino acids appear to have a positive effect on follicle development; however, they are upregulated in the FF of AFs, which seems contradictory. However, the concentration of amino acids was not higher. A higher concentration of amino acids means that the balance of osmotic pressure is affected, and the disruption of normal amino acid metabolism may damage the balance of intracellular osmotic pressure and ammonia level in FF, which may injure the oocyte and GCs (44). Therefore, disorders of amino acid metabolism may be one of the factors contributing to follicular atresia in pigs.

Additionally, this study revealed differences in BA metabolism. We compared the FF from HFs and AFs and found that in the FF from AFs, cholic acid (primary BA, $p < 0.1$) and its synthetic precursor 7-hydroxy-3-oxy-4-cholesteric acid were significantly upregulated, while secondary BAs, including glycoursodeoxycholic acid ($p < 0.1$) and glycodeoxycholic acid ($p < 0.1$), were downregulated. BAs are cytotoxic molecules, and excessive BAs have been proven to disrupt the mitochondrial function of cells, induce oxidative stress, and ultimately damage the ovary (45). The aliphatic side chain of primary BAs is conjugated to an amide linkage (N-acyl amidation) with glycine or taurine to form secondary BAs and reduce BA toxicity (46). Our results indicated that cholic acid synthesis was increased and the degradation was decreased, which led to the accumulation of cholic acid in AFs. Finally, the disruption of cholic acid metabolism may damage the follicles by inducing oxidative stress.

CONCLUSION

In summary, this study analyzed the different metabolic profiles of FF between HFs and AFs in Bama Xiang pigs. Our results revealed that the metabolic characteristics of porcine AFs are lower levels of lipids (such as phospholipids) and higher levels of amino acids and BAs than those in HFs. Disorders of amino acid metabolism and cholic acid metabolism may contribute to follicular atresia in pigs.

DATA AVAILABILITY STATEMENT

The raw data supporting the conclusions of this article will be made available by the authors, without undue reservation.

ETHICS STATEMENT

The animal study was reviewed and approved by the College of Animal Science & Technology, Guangxi University (Ethics approval reference number: GXU-2021-055).

AUTHOR CONTRIBUTIONS

JM, LS, and JC designed the study, conducted the experiments, and drafted the paper. YL, YW, and GQ conducted parts of the experiments. JL and GL revised the paper. All authors have read and agreed to the published version of the manuscript.

FUNDING

This study was supported by the National Modern Agricultural Industrial Technology System (nycytxgxcxtd-15-01) and the Science and Technology Major Project of Guangxi (Guike-AA17292002).

ACKNOWLEDGMENTS

We thank the National Natural Science Foundation of China for funding this research. We would like to thank the State Key Laboratory for Conservation and Utilization of Subtropical Agro-bioresources for the instrument support.

REFERENCES

1. Meng L, Teerds K, Tao J, Wei H, Jaklofsky M, Zhao Z, et al. Characteristics of circular RNA expression profiles of porcine granulosa cells in healthy and atretic antral follicles. *Int J Mol Sci.* (2020) 21:5217. doi: 10.3390/ijms 21155217
2. Shan X, Yu T, Yan X, Wu J, Fan Y, Guan X, et al. Proteomic analysis of healthy and atretic porcine follicular granulosa cells. *J Proteomics.* (2021) 232:104027. doi: 10.1016/j.jprot.2020.104027
3. Racine C, Genêt C, Bourgneuf C, Dupont C, Plisson-Petit F, Sarry J, et al. New anti-müllerian hormone target genes involved in granulosa cell survival in women with polycystic ovary syndrome. *J Clin Endocrinol Metab.* (2021) 106:e1271–89. doi: 10.1210/clinem/dgaa879
4. Muthulakshmi S, Hamideh PF, Habibi HR, Maharajan K, Kadirvelu K, Mudili V. Mycotoxin zearalenone induced gonadal impairment and altered gene expression in the hypothalamic-pituitary-gonadal axis of adult female zebrafish (Danio rerio). *J Appl Toxicol.* (2018) 38:1388–97. doi: 10.1002/jat.3652
5. He Y, Deng H, Jiang Z, Li Q, Shi M, Chen H, et al. Effects of melatonin on follicular atresia and granulosa cell apoptosis in the porcine. *Mol Reprod Dev.* (2016) 83:692–700. doi: 10.1002/mrd.22676
6. Socha JK, Hrabia A. Response of the chicken ovary to GH treatment during a pause in laying induced by fasting. *Domest Anim Endocrinol.* (2019) 69:84–95. doi: 10.1016/j.domaniend.2019.05.001
7. Chu YL, Xu YR, Yang WX, Sun Y. The role of FSH and TGF-beta superfamily in follicle atresia. *Aging.* (2018) 10:305–21. doi: 10.18632/aging.101391
8. Mazerbourg S, Monget P. Insulin-like growth factor binding proteins and igfbp proteases: a dynamic system regulating the ovarian folliculogenesis. *Front Endocrinol.* (2018) 9:134. doi: 10.3389/fendo.2018.00134
9. Bromfield JJ, Sheldon IM. Lipopolysaccharide reduces the primordial follicle pool in the bovine ovarian cortex ex vivo and in the murine ovary in vivo. *Biol Reprod.* (2013) 88:98. doi: 10.1095/biolreprod.112.106914
10. Max MC, Bizarro-Silva C, Bufalo I, Gonzalez SM, Lindquist AG, Gomes RG, et al. *In vitro* culture supplementation of EGF for improving the survival of equine preantral follicles. *In Vitro Cell Dev Biol Anim.* (2018) 54:687–91. doi: 10.1007/s11626-018-0296-9
11. Nishimoto H, Hamano S, Hill GA, Miyamoto A, Tetsuka M. Classification of bovine follicles based on the concentrations of steroids, glucose and lactate in follicular fluid and the status of accompanying follicles. *J Reprod Dev.* (2009) 55:219–24. doi: 10.1262/jrd.20114
12. Patti GJ, Yanes O, Siuzdak G. Metabolomics: the apogee of the omic triology. *Nat rev Mol Cell Bio.* (2013) 13:263. doi: 10.1038/nrm3314

13. Bracewell-Milnes T, Saso S, Abdalla H, Nikolau D, Norman-Taylor J, Johnson M, et al. Metabolomics as a tool to identify biomarkers to predict and improve outcomes in reproductive medicine: a systematic review. *Hum Reprod Update.* (2017) 23:723–36. doi: 10.1093/humupd/dmx023
14. Sun Z, Chang HM, Wang A, Song J, Zhang X, Guo J, et al. Identification of potential metabolic biomarkers of polycystic ovary syndrome in follicular fluid by SWATH mass spectrometry. *Reprod Biol Endocrinol.* (2019) 17:45. doi: 10.1186/s12958-019-0490-y
15. Castiglione MM, Iuliano A, Schettini S, Petruzzi D, Ferri A, Colucci P, et al. NMR metabolic profiling of follicular fluid for investigating the different causes of female infertility: a pilot study. *Metabolomics.* (2019) 15:19. doi: 10.1007/s11306-019-1481-x
16. Yang Y, Adeola AC, Xie HB, Zhang YP. Genomic and transcriptomic analyses reveal selection of genes for puberty in Bama Xiang pigs. *Zool Res.* (2018) 39:424–30. doi: 10.24272/j.issn.2095-8137.2018.068
17. Wang LY, Lin AG, Wang LX, Li K, Yang GS, He RG, et al. *Animal Genetic Resources in China Pigs*. Beijing: China Agriculture Press (2011). p. 237.
18. Zhai X, Han W, Wang M, Guan S, Qu X. Exogenous supplemental NAD+ protect myocardium against myocardial ischemic/reperfusion injury in swine model. *Am J Transl Res.* (2019) 11:6066–74.
19. Ning X, Yang K, Shi W, Xu C. Comparison of hypertrophic scarring on a red Duroc pig and a Guangxi Mini Bama pig. *Scars Burns Healing.* (2020) 6:2059513120930903. doi: 10.1177/2059513120930903
20. Guo M, Liu J, Guo F, Shi J, Wang C, Bible PW, et al. Panax quinquefolium saponins attenuate myocardial dysfunction induced by chronic ischemia. *Cell Physiol Biochem.* (2018) 49:1277–88. doi: 10.1159/000493407
21. Zhu TY, Ai J, Nie CH, Zhou GH, Chen XH, Zhang YL, et al. Feasibility of computed tomography-guided irreversible electroporation for porcine kidney ablation. *J Cancer Res Ther.* (2020) 16:1125–8. doi: 10.4103/jcrt.JCRT_594_19
22. Zhang J, Liu Y, Yao W, Li Q, Liu H, Pan Z. Initiation of follicular atresia: gene networks during early atresia in pig ovaries. *Reproduction.* (2018) 156:23–33. doi: 10.1530/REP-18-0058
23. Kita Y, Shindou H, Shimizu T. Cytosolic phospholipase A2 and lysophospholipid acyltransferases. *Biochim Biophys Acta Mol Cell Biol Lipids.* (2019) 1864:838–45. doi: 10.1016/j.bbalip.2018.08.006
24. Li M, Zhou S, Wu Y, Li Y, Yan W, Guo Q, et al. Prenatal exposure to propylparaben at human-relevant doses accelerates ovarian aging in adult mice. *Environ Pollut.* (2021) 285:117254. doi: 10.1016/j.envpol.2021.117254
25. Pargianas M, Kosmas I, Papageorgiou K, Kitsou C, Papoudou-Bai A, Batistatou A, et al. Follicle inhibition at the primordial stage without increasing apoptosis, with a combination of everolimus, verapamil. *Mol Biol Rep.* (2020) 47:8711–26. doi: 10.1007/s11033-020-05917-2
26. Wang M, Bhullar NK. Selection of suitable reference genes for QRT-PCR gene expression studies in rice. *Methods Mol Biol.* (2021) 2238:293–312. doi: 10.1007/978-1-0716-1068-8_20
27. Luo ZZ, Shen LH, Jiang J, Huang YX, Bai LP, Yu SM, et al. Plasma metabolite changes in dairy cows during parturition identified using untargeted metabolomics. *J Dairy Sci.* (2019) 102:4639–50. doi: 10.3168/jds.2018-15601
28. Gao X, Zhang J, Pan Z, Li Q, Liu H. The distribution and expression of vascular endothelial growth factor A (VEGFA) during follicular development and atresia in the pig. *Reprod Fertil Dev.* (2020) 32:259–66. doi: 10.1071/RD8508
29. Zhang T, BaSang WD, Chang W, Huo S, Ma X, Ju X, et al. Dynamics of apoptosis-related gene expression during follicular development in yak. *J Anim Physiol Anim Nutr.* (2021). doi: 10.1111/jpn.13527. [Epub ahead of print].
30. Liu H, Tian Z, Guo Y, Liu X, Ma Y, Du X, et al. Microcystin-leucine arginine exposure contributes to apoptosis and follicular atresia in mice ovaries by endoplasmic reticulum stress-upregulated Ddit3. *Sci Total Environ.* (2021) 756:144070. doi: 10.1016/j.scitotenv.2020.144070
31. Li Q, Du X, Liu L, Liu H, Pan Z, Li Q. Upregulation of miR-146b promotes porcine ovarian granulosa cell apoptosis by attenuating CYP19A1. *Domest Anim Endocrinol.* (2021) 74:106509. doi: 10.1016/j.domaniend.2020.106509
32. Van der Veen JN, Kennelly JP, Wan S, Vance JE, Vance DE, Jacobs RL. The critical role of phosphatidylcholine and phosphatidylethanolamine metabolism in health and disease. *Biochim Biophys Acta Biomembr.* (2017) 1859:1558–72. doi: 10.1016/j.bbamem.2017.04.006
33. Kim EA, Kim JA, Park MH, Jung SC, Suh SH, Pang MG, et al. Lysophosphatidylcholine induces endothelial cell injury by nitric oxide production through oxidative stress. *J Matern Fetal Neonatal Med.* (2009) 22:325–31. doi: 10.1080/14767050802556075
34. Sriraman V, Modi SR, Bodenburg Y, Denner LA, Urban RJ. Identification of ERK and JNK as signaling mediators on protein kinase C activation in cultured granulosa cells. *Mol Cell Endocrinol.* (2008) 294:52–60. doi: 10.1016/j.mce.2008.07.011
35. Lai FN, Liu XL, Li N, Zhang RQ, Zhao Y, Feng YZ, et al. Phosphatidylcholine could protect the defect of zearalenone exposure on follicular development and oocyte maturation. *Aging.* (2018) 10:3486–506. doi: 10.18632/aging.101660
36. Wen X, Kuang Y, Zhou L, Yu B, Chen Q, Fu Y, et al. Lipidomic components alterations of human follicular fluid reveal the relevance of improving clinical outcomes in women using progestin-primed ovarian stimulation compared to short-term protocol. *Med Sci Monit.* (2018) 24:3357–65. doi: 10.12659/MSM.906602
37. Song J, Wang X, Guo Y, Yang Y, Xu K, Wang T, et al. Novel high-coverage targeted metabolomics method (SWATHtoMRM) for exploring follicular fluid metabolome alterations in women with recurrent spontaneous abortion undergoing in vitro fertilization. *Sci Rep.* (2019) 9:10873. doi: 10.1038/s41598-019-47370-7
38. Lordan R, Tsoupras A, Zabetakis I, Demopoulos CA. Forty years since the structural elucidation of platelet-activating factor (PAF): historical, current, and future research perspectives. *Molecules.* (2019) 24:4414. doi: 10.3390/molecules24234414
39. Vandenberghe L, Heindryckx B, Smits K, Szymanska K, Ortiz-Escribano N, Ferrer-Buitrago M, et al. Platelet-activating factor acetylhydrolase 1B3 (PAFAH1B3) is required for the formation of the meiotic spindle during in vitro oocyte maturation. *Reprod Fertil Dev.* (2018) 30:1739–50. doi: 10.1071/RD18019
40. Pritchard PH. The degradation of platelet-activating factor by high-density lipoprotein in rat plasma. Effect of ethynyloestradiol administration. *Biochem J.* (1987) 246:791–4. doi: 10.1042/bj2460791
41. Colleluori G, Aguirre L, Napoli N, Qualls C, Villareal DT, Armamento-Villareal R. Testosterone therapy effects on bone mass and turnover in hypogonadal men with type 2 diabetes. *J Clin Endocrinol Metab.* (2021). doi: 10.1210/clinem/dgab181. [Epub ahead of print].
42. Circu ML, Aw TY. Glutathione and apoptosis. *Free Radic Res.* (2008) 42:689–706. doi: 10.1080/10715760802317663
43. Zeng X, Mao X, Huang Z, Wang F, Wu G, Qiao S. Arginine enhances embryo implantation in rats through PI3K/PKB/mTOR/NO signaling pathway during early pregnancy. *Reproduction.* (2013) 145:1–7. doi: 10.1530/REP-12-0254
44. Wang W, Zhang W, Liu J, Sun Y, Li Y, Li H, et al. Metabolomic changes in follicular fluid induced by soy isoflavones administered to rats from weaning until sexual maturity. *Toxicol Appl Pharmacol.* (2013) 269:280–9. doi: 10.1016/j.taap.2013.02.005
45. Ommati MM, Farshad O, Niknahad H, Arabnezhad MR, Azarpira N, Mohammadi HR, et al. Cholestasis-associated reproductive toxicity in male and female rats: the fundamental role of mitochondrial impairment and oxidative stress. *Toxicol Lett.* (2019) 316:60–72. doi: 10.1016/j.toxlet.2019.09.009
46. Di Ciaula A, Garruti G, Lunardi BR, Molina-Molina E, Bonfrate L, Wang DQ, et al. Bile acid physiology. *Ann Hepatol.* (2017) 16:s4–14. doi: 10.5604/01.3001.0010.5493

Conflict of Interest: The authors declare that the research was conducted in the absence of any commercial or financial relationships that could be construed as a potential conflict of interest.

Publisher's Note: All claims expressed in this article are solely those of the authors and do not necessarily represent those of their affiliated organizations, or those of the publisher, the editors and the reviewers. Any product that may be evaluated in this article, or claim that may be made by its manufacturer, is not guaranteed or endorsed by the publisher.

frontiers in Veterinary Science

ORIGINAL RESEARCH
published: 05 August 2021
doi: 10.3389/fvets.2021.694247

The Proteome of Equine Oviductal Fluid Varies Before and After Ovulation: A Comparative Study

Pablo Fernández-Hernández[1,2†], Federica Marinaro[3†], María Jesús Sánchez-Calabuig[4], Luis Jesús García-Marín[1,5], María Julia Bragado[1,6], Lauro González-Fernández[1,6‡] and Beatriz Macías-García[1,2*‡]*

[1] Research Group of Intracellular Signaling and Technology of Reproduction (Research Institute INBIO G+C), University of Extremadura, Cáceres, Spain, [2] Department of Animal Medicine, Faculty of Veterinary Sciences, University of Extremadura, Cáceres, Spain, [3] Stem Cell Therapy Unit, Jesús Usón Minimally Invasive Surgery Centre, Cáceres, Spain, [4] Department of Animal Medicine and Surgery, Faculty of Veterinary Sciences, University Complutense of Madrid, Madrid, Spain, [5] Department of Physiology, Faculty of Veterinary Sciences, University of Extremadura, Cáceres, Spain, [6] Department of Biochemistry and Molecular Biology and Genetics, Faculty of Veterinary Sciences, University of Extremadura, Cáceres, Spain

OPEN ACCESS

Edited by:
Jordi Roca, University of Murcia, Spain

Reviewed by:
Ivan Cunha Bustamante-Filho, Universidade do Vale do Taquari - Univates, Brazil
Arumugam Kumaresan, National Dairy Research Institute (ICAR), India

***Correspondence:**
Lauro González-Fernández
lgonfer@unex.es
Beatriz Macías-García
bemaciasg@unex.es

[†] These authors have contributed equally to this work and share first authorship

[‡] These authors share senior authorship

Specialty section:
This article was submitted to Animal Reproduction - Theriogenology, a section of the journal Frontiers in Veterinary Science

Received: *12 April 2021*
Accepted: *25 June 2021*
Published: *05 August 2021*

Citation:
Fernández-Hernández P, Marinaro F, Sánchez-Calabuig MJ, García-Marín LJ, Bragado MJ, González-Fernández L and Macías-García B (2021) The Proteome of Equine Oviductal Fluid Varies Before and After Ovulation: A Comparative Study. Front. Vet. Sci. 8:694247. doi: 10.3389/fvets.2021.694247

Equine fertilization cannot be performed in the laboratory as equine spermatozoa do not cross the oocyte's zona pellucida *in vitro*. Hence, a more profound study of equine oviductal fluid (OF) composition at the pre-ovulatory and post-ovulatory stages could help in understanding what components are required to achieve fertilization in horses. Our work aimed to elucidate the proteomic composition of equine OF at both stages. To do this, OF was obtained postmortem from oviducts of slaughtered mares ipsilateral to a pre-ovulatory follicle ($n = 4$) or a recent ovulation ($n = 4$); the samples were kept at −80°C until analysis. After protein extraction and isobaric tags for relative and absolute quantification (iTRAQ) labeling, the samples were analyzed by nano-liquid chromatography coupled to tandem mass spectrometry (LC-MS/MS). The analysis of the spectra resulted in the identification of a total of 1,173 proteins present in pre-ovulatory and post-ovulatory samples; among these, 691 were unique for *Equus caballus*. Proteins from post-ovulatory oviductal fluid were compared with the proteins from pre-ovulatory oviductal fluid and were categorized as upregulated (positive log fold change) or downregulated (negative log fold change). Fifteen proteins were found to be downregulated in the post-ovulatory fluid and 156 were upregulated in the post-ovulatory OF compared to the pre-ovulatory fluid; among the upregulated proteins, 87 were included in the *metabolism of proteins* pathway. The identified proteins were related to *sperm–oviduct interaction, fertilization*, and *metabolism*, among others. Our data reveal consistent differences in the proteome of equine OF prior to and after ovulation, helping to increase our understanding in the factors that promote fertilization and early embryo development in horses.

Keywords: horse, oviductal fluid, ovulation, mass spectrometry, proteome, domestic animal reproduction

INTRODUCTION

Assisted reproductive technologies (ARTs) are commonly used in the field of reproduction to obtain embryos in domestic species (1). Currently, *in vitro* fertilization (IVF) is the technique of choice to produce embryos *in vitro* in domestic species such as bovine (2). The first report of unequivocal successful IVF in domestic species was published in rabbits in 1954 (3, 4). In this report, the authors

used spermatozoa recovered from the female's reproductive tract after artificial insemination to perform IVF (3). Until that moment, IVF failure was associated with the lack of adequate induction of sperm capacitation, a maturational process in which the spermatozoon needs to fully acquire its fertilizing capacity (4, 5). Since then, fertilization media were designed for each species based on the composition of the reproductive fluids, which consistently vary among species (bovine, human, mice, and porcine) (6, 7). Unfortunately, despite the efforts of different research groups around the world, the *in vitro* production of equine embryos is still very inefficient, in part due to the low success rate of *in vitro* fertilization that varies from 0 to 33% (8, 9).

Recent research demonstrates that the failure of equine IVF is most likely attributable to the inability of the spermatozoa to penetrate the oocyte's zona pellucida (10) and, hence, to a suboptimal composition of the fertilization media that results in ineffective sperm capacitation (9, 11). This theory is supported by the fact that oviductal transfer of *in vitro* matured equine oocytes in an inseminated mare results in embryonic development at similar rates to those obtained from spontaneous ovulations (12). Interestingly, it has been described that equine IVF conditions support the binding of stallion spermatozoa to the zona pellucida, but they fail to induce the acrosome reaction and other capacitation-related events (8). Therefore, mimicking the conditions of the oviductal environment could be the key for successful equine IVF as it provides the ideal microenvironment for fertilization, promoting adequate sperm capacitation (8). A deeper understanding of the composition of oviductal secretions is required to better mimic the oviductal milieu and to ensure sperm capacitation *in vitro* in the horse.

Oviductal fluid (OF) is composed of ions, hormones, growth factors, metabolites, and proteins, among other compounds (6). The oviduct is lined with an epithelium coated by OF, which is composed of secretions of these cells and of blood plasma filtrate (11). Hence, the oviduct provides a dynamic microenvironment that changes according to the stage of the estrus cycle (13), ovulation site (14), oviductal region (15), and the presence of gametes or embryos (16). At present, the addition of natural reproductive fluids to commercial IVF media has been shown to improve embryo quality and yield in cows (2), highlighting the importance of studying the composition of oviductal secretions to improve current ARTs in domestic species (17).

The composition of the OF greatly varies depending on the species in study; hence, the results obtained from a single species cannot be extrapolated to others (18). In the particular case of horses, the difficult anatomical approach of the oviduct, the limited number of equine slaughterhouses, and the low amount of OF produced (11) render the addition of native oviductal fluid to the IVF media unfeasible in horses.

For these reasons, to fully develop an equine IVF protocol and to increase the embryo yield and the quality of the embryos produced *in vitro*, a more profound study of the physiology of the oviduct and the composition of its secretions is of outmost importance (8). Previous studies have reported the metabolome of equine OF (11) or the proteome of OF in mares during early embryo development (19), but more research is required to fully unravel the key factors leading to successful fertilization *in vitro* in horses.

One of the main components of the OF are proteins, but their functions are still under study (6, 18). In horses, consistent differences in the proteomic composition of the oviductal secretions in pregnant mares compared to non-pregnant counterparts, and also in the ipsilateral and contralateral oviduct where the embryo is allocated, have been described (19). In this regard, some authors claim that unsuccessful *in vitro* fertilization is related to the lack of specific proteins in the fertilization medium that may be impeding complete sperm capacitation (6).

Thus, in the present work, we aimed to elucidate the proteomic composition of equine OF at the pre-ovulatory and post-ovulatory stages. Besides, the different protein compositions between both stages were also contrasted. Our results show that the proteome of equine OF varies prior to and post-ovulation. Interestingly, enrichment analysis of the upregulated proteins revealed that 15 proteins were found to be downregulated and 156 were upregulated in post-ovulatory OF compared to pre-ovulatory OF. Using the enrichment analysis approach, the main categories identified were directly related with metabolism. The Reactome pathway analysis showed that, in the proteins identified as upregulated in the post-ovulatory OF, 87 of them were included in the *metabolism of proteins* pathway and 56 were enclosed in the *developmental biology* pathway, revealing an intense protein turnover during early embryo development in horses.

MATERIALS AND METHODS

Collection of Oviductal Fluid

Oviducts were obtained immediately postmortem at a commercial slaughterhouse, on three separate days. At evisceration, the entire reproductive tract was extracted and carefully inspected. The ovaries were examined and those tracts with a pre-ovulatory follicle $\geq$35 mm in diameter (as confirmed after opening the follicle using a scalpel blade), associated with uterine edema on examination of the opened endometrial surface (vivid endometrial folds with a gelatinous appearance), were sampled as pre-ovulatory (pre-OV). When the ovaries had evidence of a recent ovulation, as confirmed after sectioning the ovary to examine the presence of a corpus hemorrhagicum or juvenile corpus luteum (CL) identified as a luteal structure with a large, red central clot and a luteinized wall that was still visibly crenulated, the reproductive tracts were classified as post-ovulatory (post-OV) and also harvested. The oviduct and the attached ovary containing the pre-ovulatory follicle or the CL were separated from the uterus distally to the uterotubal junction, the ovary was dissected, and the oviduct was carefully dried with a tissue and placed into a Petri dish within ~30 min of slaughter. A non-heparinized hematocrit capillary tube (Merck, Madrid, Spain) attached to a 5-ml syringe by a silicone tube was inserted into the ampulla of the oviduct through the infundibular opening. Gentle aspiration was performed to recover fluid, and the fluid retrieved was expressed into 500-µl tubes. Aspiration was repeated for a total of at least three times per oviduct. The retrieved fluid was centrifuged for 2 min in

a microcentrifuge at room temperature (RT) to remove large cellular masses. The supernatant was retrieved, transferred to a clean tube, and placed in dry ice until its arrival at the laboratory (4–5 h). Once at the laboratory, the OF was centrifuged at 16,000 × *g* at 4°C for 20 min and the supernatant transferred to a clean tube. The volume obtained was measured using a micropipette, and the samples were then kept at −80°C until analysis. A total of four pre-ovulatory OF samples and four post-ovulatory OF samples were submitted for proteomic analysis. Each sample was extracted from an individual female ($n = 8$ samples in total). Between 8 and 10 μl per sample was used for proteomic analysis.

Protein Digestion and Tagging With the iTRAQ® 8-Plex Reagent

After sample thawing, the total protein concentration of each sample was determined using the Pierce 660-nm protein assay kit (Pierce, Rockford, IL, USA). For digestion, 40 μg of protein from each replicate and condition (pre-ovulatory OF, $n = 4$; post-ovulatory OF, $n = 4$) was precipitated by the methanol/chloroform method. Protein pellets were resuspended and denatured in 20 μl of triethylammonium bicarbonate (TEAB; 7 M urea/2 M thiourea, 0.1 M, pH 7.5; SERVA Electrophoresis GmbH, Heidelberg, Germany), reduced with 1 μl of 50 mM Tris (2-carboxyethyl)phosphine (TCEP; AB SCIEX, Foster City, CA, USA), pH 8.0, at 37°C for 60 min, and followed by 2 μl of 200 mM cysteine-blocking reagent (methyl methanethiosulfonate, MMTS; Pierce) for 10 min at RT. The samples were diluted up to 120 μl to reduce the urea/thiourea concentration with 50 mM TEAB. Digestions were initiated by adding 2 μg of sequencing grade modified trypsin (Sigma-Aldrich, St. Louis, MO, USA) to each sample in a ratio of 1:20 (*w*/*w*), which were then incubated at 37°C overnight on a shaker. Sample digestions were evaporated to dryness.

Each trypsin-digested sample, previously reconstituted with 80 μl of 70% ethanol/50 mM TEAB, was labeled at RT for 2 h with a half unit of iTRAQ Reagent 8-plex kit (AB SCIEX, Foster City, CA, USA). Isobaric tags for relative and absolute quantification (iTRAQ) labeling was performed according to the following schema: iTRAQ 113 reagent: pre-ovulatory OF R1; iTRAQ 114 reagent: pre-ovulatory OF R2; iTRAQ 115 reagent: pre-ovulatory OF R3; iTRAQ 116 reagent: pre-ovulatory OF R4; iTRAQ 117: post-ovulatory OF R1; iTRAQ 118 reagent: post-ovulatory OF R2; iTRAQ 119 reagent: post-ovulatory OF R3; and iTRAQ 121 reagent: post-ovulatory OF R4. After labeling, the samples were combined and the reaction stopped by evaporation in a SpeedVac. Salts were washed using a Sep-Pak C18 cartridge (Waters, Milford, MA, USA).

Liquid Chromatography and Mass Spectrometry Analysis

A 2-μg aliquot of each sample was subjected to 2D nano-liquid chromatography electrospray ionization tandem mass spectrometry (LC-ESI-MS/MS) analysis using a nano-liquid chromatography system (Eksigent Technologies NanoLC Ultra-1D Plus, AB SCIEX, Foster City, CA, USA) coupled to a high-speed TripleTOF 5600 mass spectrometer (SCIEX, Foster City, CA, USA) with a Nanospray III source. The injection volume was 5 μl. The analytical column used was a silica-based reversed-phase nanoACQUITY UPLC 75-μm × 15-cm column (Waters), with 1.7 μm particle size. The trap column was an Acclaim PepMap 100 column (ThermoFisher Scientific, Waltham, MA, USA), with 5 μm particle diameter and 100 Å pore size, switched on-line with the analytical column. The loading pump delivered a solution of 0.1% formic acid in water at 2 μl/min. The nano-pump provided a flow rate of 250 nl/min and was operated under gradient elution conditions using 0.1% formic acid in water as mobile phase A and 0.1% formic acid in acetonitrile as mobile phase B. Gradient elution was performed according to the following scheme: isocratic conditions of 96% A/4% B for 5 min, a linear increase to 40% B in 205 min, then a linear increase to 90% B for an additional 15 min, isocratic conditions of 90% B for 10 min, and a return to the initial conditions in 2 min. The total gradient length was 250 min.

Data acquisition was performed with the TripleTOF 5600 system. Ionization occurred under the following conditions: ion spray voltage floating (ISVF), 2,800 V; curtain gas (CUR), 20; interface heater temperature (IHT), 150; ion source gas 1 (GS1), 20; and declustering potential (DP), 85 V. All data were acquired using the information-dependent acquisition (IDA) mode with Analyst TF 1.7 software (AB SCIEX, Foster City, CA, USA). For the IDA parameters, a 0.25-s MS survey scan in the mass range of 350–1,250 Da was followed by 30 MS/MS scans of 150 ms in the mass range of 100–1,500 Da (total cycle time, 4.5 s). Switching criteria were set to ions greater than the mass-to-charge ratio (*m*/*z*) 350 and smaller than *m*/*z* 1,250, with a charge state of 2–5 and an abundance threshold of more than 90 counts per second. Former target ions were excluded for 20 s. The IDA rolling collision energy (CE) parameters script was used for automatically controlling the CE.

Data Analysis and Statistics

The MS/MS spectra were exported to mgf format using Peak View v1.2.0.3 and searched using Mascot Server 2.5.1, OMSSA 2.1.9, X!TANDEM 2013.02.01.1, and Myrimatch 2.2.140 against a composite target/decoy database built from the *Equus caballus* reference proteome sequences at UniProt Knowledgebase (January 2020), together with commonly occurring contaminants. After recalibration of patent ion mass measurements using high-scoring X!TANDEM hits, the search engines were configured to match potential peptide candidates with mass error tolerance of 10 ppm and fragment ion tolerance of 0.02 Da, allowing for up to two missed tryptic cleavage sites and isotope error (^{13}C) of 1, considering a fixed MMTS modification of cysteine and variable oxidation of methionine, pyroglutamic acid from glutamine or glutamic acid at the peptide N-terminus, acetylation of the protein N-terminus, and modifications of lysine, tyrosine, and peptide N-terminus with iTRAQ 8-plex reagents. Score distribution models were used to compute the peptide-spectrum match *p*-values (20), and spectra recovered by a false discovery rate (FDR) ≤ 0.01 (peptide-level) filter were selected for quantitative analysis. Approximately 5% of the signals with the lowest quality were removed prior to further analysis. Differential regulation was

measured using linear models (21), and statistical significance was measured using *q*-values (FDR). All analyses were conducted using software from Proteobotics (Madrid, Spain).

RESULTS

Proteomic analysis resulted in the identification of a total of 1,173 proteins that were present in pre-ovulatory and post-ovulatory OF. Only the characterized proteins with at least one peptide and FDR < 0.01 have been presented (**Supplementary Table 1**).

For enrichment analyses, the UniProt[1] accession numbers were associated with the gene names and Ensembl[2] IDs by using the databases for *E. caballus* proteins, genes, and transcripts from DAVID Bioinformatics[3] (22, 23) and g:Profiler[4] (24). Enrichment analysis of the proteins identified in the OF was performed using the Functional Annotation Tool provided by DAVID Bioinformatics. Gene Ontology (GO) (molecular function, cellular component, and biological process), Kyoto Encyclopedia of Genes and Genomes (KEGG), and UniProt keywords were used as the annotation databases. Among the initial 1,173 proteins, the DAVID software recognized 691 unique proteins from the *E. caballus* species (**Supplementary Table 2A**). Enrichment analysis of these 691 proteins revealed that 54.3% (375 among the initial 691) were associated with the *extracellular exosome* category (GO:0070062) and 111 with the *cytoplasm* category (GO:0005737). Reactome[5] pathway analysis of the identified proteins belonging to these two GO categories was performed by exploring the corresponding gene names in the *Homo sapiens* database (**Supplementary Tables 2B,C**). Additionally, Voronoi pathway visualizations (Reacfoam) (**Figure 1**) showed that proteins belonging to the categories *extracellular exosome* (GO:0070062) and *cytoplasm* (GO:0005737) were almost equally involved to pathways related to metabolism, immune system, cell cycle, and developmental biology, among others. On the other hand, proteins from the category *extracellular exosome* showed a unique involvement in the processes of hemostasis and organelle biogenesis and maintenance, while proteins from the category cytoplasm were involved in signal transduction processes. Moreover, proteins from *extracellular exosome* were associated with disease-related pathways. To represent protein changes in pre- and post-ovulatory equine OF, the iTRAQ results (1,173 characterized proteins) were analyzed to obtain log2 fold changes. Proteins from post-ovulatory OF were compared with the proteins from pre-ovulatory OF and were categorized as upregulated (positive log fold change) or downregulated (negative log fold change) (**Figure 2**). Only differentially expressed upregulated or downregulated proteins categorized as "likely" or "confident" (FDR < 0.05 and FDR < 0.01, respectively) and with $p < 0.05$ were taken into consideration and are listed in **Figure 1**, **Supplementary Table 3**. Among the identified proteins, 15 were found to be downregulated in post-ovulatory OF compared to the pre-ovulatory counterpart and 156 were upregulated in post-ovulatory OF compared to pre-ovulatory OF.

Enrichment analysis of the upregulated and downregulated proteins was performed on the corresponding Ensembl IDs using the g:GOSt Functional profiling tool[6] of g:Profiler. Ensembl IDs were examined as ordered query in the *E. caballus* database, taking into consideration only annotated genes. GO molecular function, cellular component, and biological process and KEGG were used as the annotation databases (**Supplementary Tables 4A, 5A**). Furthermore, pathway analyses of the downregulated and upregulated proteins in equine post-ovulatory vs. pre-ovulatory OFs were performed exploring the corresponding gene names in the *H. sapiens* database (**Supplementary Tables 4B, 5B**). Representative pictures of the enriched GO and KEGG categories in downregulated and upregulated proteins were obtained uploading gene symbols in the *E. caballus* database of the bioinformatics tool Omicsbean[7] (**Figure 3**).

Interestingly, when the enrichment analysis was performed for the 15 downregulated proteins (**Supplementary Table 4A**), seven of them (47% of the proteins) were included in the category *metabolic pathways* (KEGG:01100). The downregulated proteins under this category were aminoacylase 1 (ACY1), glutathione S-transferase Mu 1 and 3 (GSTM1 and GSTM3, respectively), glutamine–fructose-6-phosphate aminotransferase 1 (GFPT1), NME/NM23 nucleoside diphosphate kinase 1 (NME2), lactate dehydrogenase B (LDHB), and phosphoglycerate dehydrogenase (PHGDH).

On the other hand, when the 154 upregulated proteins were investigated using an enrichment analysis approach, the main categories identified were directly related to metabolism (**Supplementary Table 5A**). In the *metabolic process* category (GO:0008152), 116 proteins (75% of the initial 167 upregulated transcripts) were enclosed, *organic substance metabolic process* (GO:0071704) involved 110 proteins (71%), and *cellular metabolic process* (GO:0071704) included 109 proteins (71%), while in *nitrogen compound metabolic process* (GO:0006807) and *primary metabolic process* (GO:0044238), 107, and 105 proteins were included, respectively. Of note is that 35% of the proteins were involved in *peptide metabolic process* (GO:0006518), suggesting an active protein synthesis and remodeling in the post-ovulatory phase. Moreover, 124 (81%) post-ovulatory upregulated proteins were localized in the *cytoplasm* (GO:0005737), in particular in the *cytosolic ribosome* (GO:0005840; 31%). Interestingly, eight upregulated proteins in post-ovulatory OF were grouped into the categories *single fertilization* (GO:0007338), *sperm–egg recognition* (GO:0035036), and *binding of sperm to zona pellucida* (GO:0007339). The proteins involved in these categories were the T-complex 1 (TCP1) and its chaperonin-containing TCP1 subunits 2, 3, 5, 7, and 8 (CCT2, CCT3, CCT5, CCT7, and CCT8, respectively), together with sperm autoantigenic protein 17 (SPA17). Moreover,

[1]https://www.uniprot.org/
[2]https://www.ensembl.org/index.html
[3]https://david.ncifcrf.gov/
[4]https://biit.cs.ut.ee/gprofiler/convert
[5]https://reactome.org/
[6]https://biit.cs.ut.ee/gprofiler/gost
[7]http://www.omicsbean.cn/

A

Results summary	
postOV / preOV	
70,10%	truly null fraction (π0, proportion of contrasts under the null hypothesis)
97	confident.up (q-value < 0.01, positive log fold change)
83	likely.up (q-value < 0.05, positive log fold change)
418	putative.up (q-value > 0.05 but p-value < 1-π0, positive log fold change)
663	no differentially regulated
24	putative.down (q-value > 0.05 but p-value < 1-π0, negative log fold change)
8	likely.down (q-value < 0.05, negative log fold change)
9	confident.down (q-value < 0.01, negative log fold change)
1302	# hypotheses tested
197	# hypotheses significant with q < 0.05

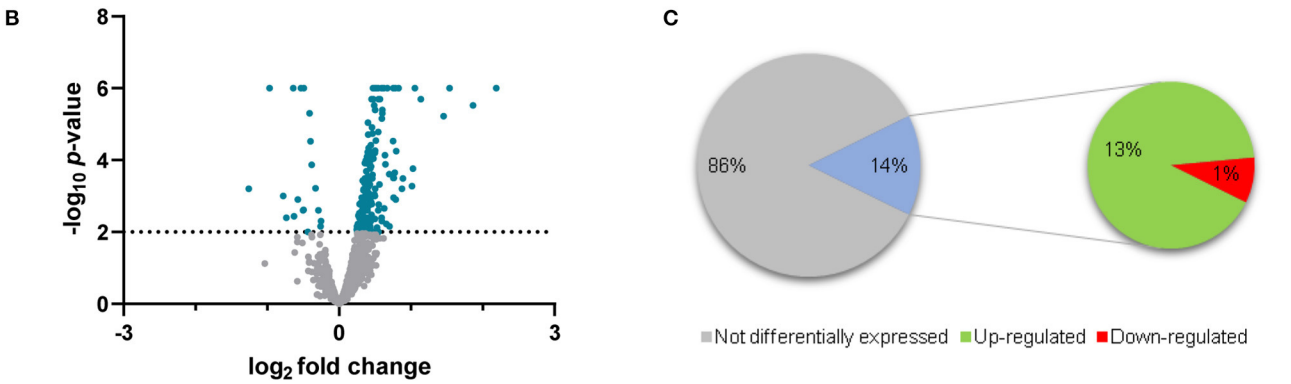

FIGURE 1 | Summary of data analysis for the comparison of post-ovulatory oviductal fluid (post-OF) vs. pre-ovulatory oviductal fluid (pre-OF). **(A)** The number of expressed proteins (upregulated, downregulated, or non-differentially regulated—*left column*) and their degrees of confidence (*right column*) are represented. A total of 1,302 hypotheses were tested. Log2 fold changes and *q*-values (false discovery rate, FDR) were considered to identify the differentially expressed (upregulated and downregulated) proteins in the post-OF vs. the pre-OF group. **(B)** Volcano plot representing the differentially and non-differentially expressed proteins. Only proteins with $q < 0.05$ and $-\log_{10} p > 2$ were considered differentially expressed (*blue*). Positive log2 fold changes represent upregulated proteins and negative log2 fold changes represent downregulated proteins. **(C)** For ease of analysis in *Equus caballus* databases, repeated, unresolved, and uncharacterized proteins were removed. A total of 1,173 unique, inferred, and characterized proteins (listed in **Supplementary Table 1**) were finally analyzed according to their log2 fold changes and *q*-values (FDR). Proteins with *q*-values (FDR) > 0.05 were considered not differentially expressed (1,002 proteins, 86%). Proteins with $q < 0.05$ were considered differentially expressed (171 proteins, 14%). Positive fold changes represent upregulated proteins (156 proteins, 13%), whereas negative fold changes represent downregulated proteins (15 proteins, 1%). The figures were created with Microsoft Excel and GraphPad Prism.

five out of these eight proteins were under the *category zona pellucida receptor complex* (GO:0002199). STRING[8] was used to investigate the protein–protein interaction networks. Protein names were searched in the *H. sapiens* database as multiple protein query. STRING revealed that all these proteins, except SPA17, were also specifically associated with the highest edge confidence (**Figure 4**), so it may be assumed that they contribute to a shared function. In addition, the Reactome pathway analysis of the upregulated proteins showed their involvement in the categories *metabolism of proteins* (R-HSA-392499), *cellular responses to stress* (R-HSA-2262752), and *developmental biology* (R-HSA-1266738), among others (**Supplementary Table 5B**). An enrichment analysis of the upregulated proteins belonging to these categories was performed with GO, confirming their involvement not only as *structural constituent of ribosome* (GO:0003735) and in *peptide metabolic process* (GO:0006518) (**Supplementary Table 5C**) but also in *reactive oxygen species metabolic process* (GO:0072593) (**Supplementary Table 5D**).

It is worth mentioning that among the upregulated proteins, there were albumin (ALB), the secretoglobin SCGB1A1, versican (VCAN), myosin heavy chain 9 (MYH9), and gelsolin (GSN).

DISCUSSION

The present work explores the proteome of equine OF in the peri-ovulatory period. Our data reveal that consistent differences exist in the composition of equine OF obtained from oviducts ipsilateral to a pre-ovulatory follicle and the one obtained after ovulation, coinciding with previous results in bovine (25). Interestingly, the enrichment analysis revealed that,

[8]https://string-db.org/

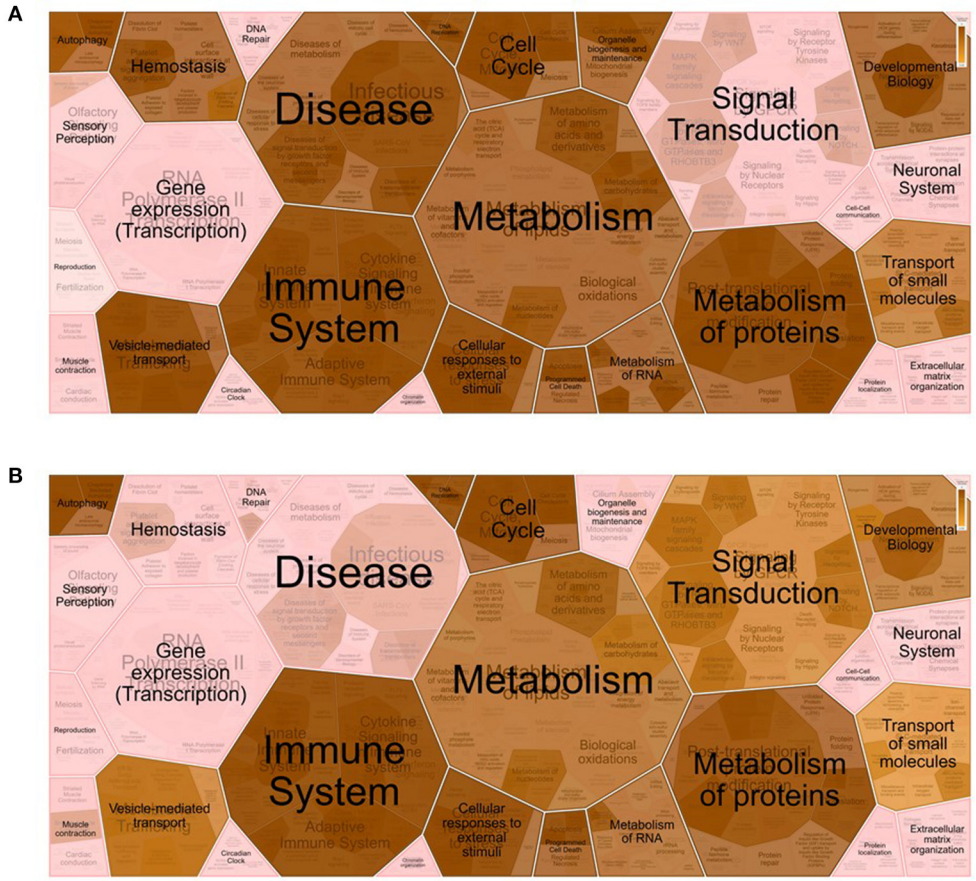

FIGURE 2 | Voronoi pathway visualization (Reacfoam) for the identified proteins from equine oviductal fluid belonging to the Gene Ontology (GO) categories *extracellular exosome* (GO:0070062) **(A)** and *cytoplasm* (GO:0005737) **(B)**. A Reactome overrepresentation pathway analysis of the identified proteins listed in the above-mentioned GO categories (see **Supplementary Table 2**) was performed with the analysis tool of Reactome (https://reactome.org/) by exploring the corresponding gene names in the *Homo sapiens* database. The *p*-values are shown with the gradient from *pink* ($p > 0.05$) through *light brown* ($0.05 < p < 0$) to *dark brown* ($p \approx 0$).

among the 691 unique proteins recognized for *E. caballus*, 375 (54.3%) were associated with the *extracellular exosome* category (GO:0070062). Hence, the majority of the identified proteins in equine OF may be involved in cell-to-cell communication as the identified protein cargo may be delivered from the oviductal milieu to the gametes/embryos in membrane-enclosed microparticles, as also demonstrated in other species (18, 26). The second category obtained in the enrichment analysis was *cytoplasm* (GO:0005737; 200 identified proteins), which corresponds with 28.9% of all the identified proteins, as also described in other species in which 13–27% of all the identified proteins were shown to have a cytoplasmic origin (18). The cytoplasmic origin of the proteins could be related to epithelial cell breakdown during OF extraction, or, most likely, they could be derived from apocrine or non-canonical secretory pathways (27, 28). Interestingly, these cytoplasmic proteins have also been described to have an exosomal origin (28). In our samples, the enrichment analysis revealed that 111 proteins identified as having a cytoplasmic origin (55.5%) were also enclosed in the *extracellular exosome* category (data not shown). Hence, it is likely that this cytoplasmic protein cargo is delivered by extracellular vesicles to the gametes and embryos.

The Reactome pathway analysis showed that, in the proteins identified as upregulated in post-ovulatory OF, 87 of them were included in the *metabolism of proteins* pathway and 56 were enclosed in the *developmental biology* pathway, revealing an intense protein turnover during early embryo development in horses, as demonstrated in other species (29). Interestingly, regarding the 15 downregulated proteins found in post-ovulatory OF, eight of them exhibited an FDR < 0.01 and were classified as confident downregulated, namely, FABP3, CLU, ACY1, GFPT1, LDHB, GSTM3, NME2, and TAGLN2 (**Supplementary Table 3**).

The fatty acid-binding protein 3 FABP is part of a protein family known as fatty acid-binding proteins, in which nine isoforms are enclosed. These proteins bind to long-chain fatty acids (C16–C20) and transport them to intracellular compartments (into the peroxisome, mitochondria, or the

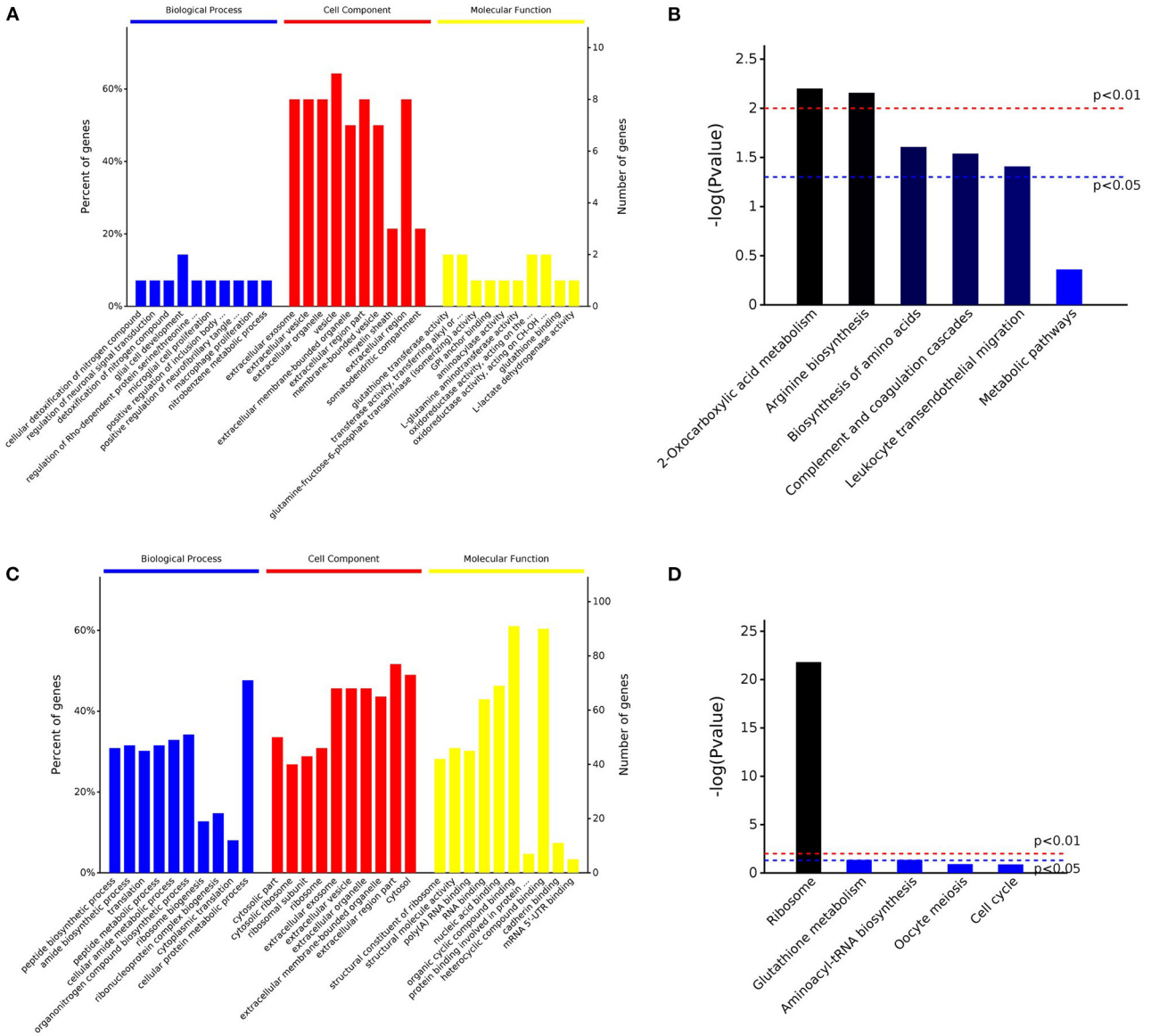

FIGURE 3 | Overview of the enrichment analysis of the downregulated and upregulated proteins in post-ovulatory oviductal fluid (OF) vs. pre-ovulatory OF. Up to 10 significantly enriched terms in the biological process (BP), cellular component (CC), and molecular function (MF) categories of the Gene Ontology (GO) analysis for downregulated **(A)** and upregulated **(C)** proteins are shown. Terms of the same category are ordered by *p*-values (cutoff $p = 0.05$), the terms on the *left* being more significant. The *left* and *right y*-axes show the percentage and number, respectively, of the involved proteins in a term **(A,C)**. Five out of the top 10 enriched KEGG pathways for the downregulated **(B)** and upregulated **(D)** proteins are shown. The significance of the results, based on genome background enrichment, is shown by *broken red* ($p = 0.01$) and *blue* ($p = 0.05$) *lines* **(B,D)**.

endoplasmic reticulum) or to the extracellular milieu, free, or enclosed in extracellular vesicles (30).

Isoform 3 of FABP is called FABP3 or heart FABP and has been demonstrated to be involved in aberrant lipid accumulation in bovine oocytes subjected to *in vitro* maturation (31). Interestingly, Smits et al. (32) showed that equine embryos produced *in vitro* showed lower messenger RNA (mRNA) expression of *FABP3* compared to *in vivo*-derived embryos, indicating that lipids could be a potential energy source for the embryo during the pre-implantation window. The lower expression of FABP3 in post-ovulatory OF compared to pre-ovulatory OF may also be linked to the fact that FABP3 overexpression induces apoptosis, as demonstrated in heart and embryonic cancer cells, and thus, its expression needs to be finely regulated when the embryo enters the oviduct (33). In porcine oviductal cells cultured *in vitro*, the changing mRNA expression of *FABP3* over the culture time has also been described, highlighting that the oviduct has the

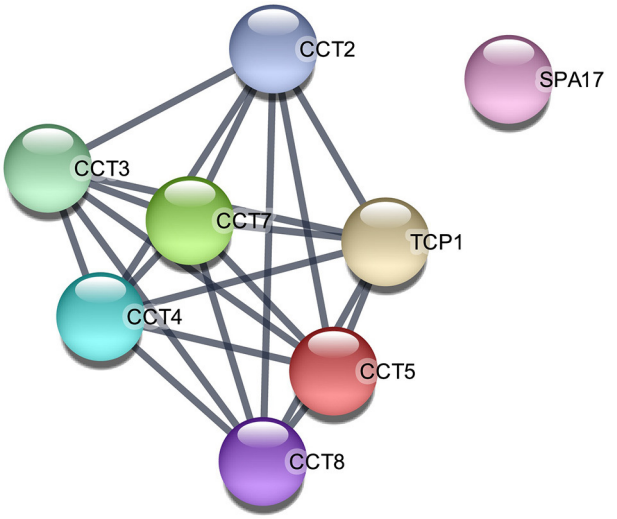

FIGURE 4 | Protein–protein interaction network among the upregulated proteins in post-ovulatory oviductal fluid belonging to the category single fertilization (GO:0007338). *Lines between nodes* indicate edges (representing protein–protein associations) with the highest confidence (0.900). The image was created with the STRING app for Cytoscape. *CCT2/CCT3/CCT5/CCT7/CCT8*, chaperonin-containing TCP1 subunits 2, 3, 5, 7, and 8, respectively; *SPA17*, sperm autoantigenic protein 17; *TCP1*, T-complex 1.

ability to modulate fatty acid metabolism. This modulation by oviductal cells could avoid possible lipotoxic effects favoring early embryo quality and survival (34), which can also explain our findings.

Regarding GFPT1, this enzyme controls the flux of glucose into the hexosamine pathway, being determinant for the production of hyaluronic acid. GFPT1 is significantly overexpressed in *in vivo* matured equine cumulus cells compared to the *in vitro* matured counterparts, explaining in part the vivid cumulus expansion observed in equine oocytes produced *in vivo* (35). In the porcine oviduct, it has been demonstrated that hyaluronic acid modulates sperm capacitation and enhances sperm survival, delaying the capacitation process (36). Hence, the lower expression of GFPT1 in equine post-ovulatory OF could be related to a physiological change in the oviductal milieu in which capacitation needs to be induced to achieve oocyte fertilization. In this sense, lactate dehydrogenase B (LADHB) is involved in lactate synthesis from pyruvate, and it is known that lactate is a core metabolite found in equine OF (11). Lactate is required to maximize mitochondrial activity and motility in equine spermatozoa incubated under capacitating conditions (37) and is also required during *in vitro* oocyte maturation (38, 39). Hence, the downregulation of LADHB in post-ovulatory OF compared to pre-ovulatory OF could also be related to the specific lactate needs of equine gametes during capacitation and fertilization. Similarly, clusterin (CLU) may also be playing a role modulating sperm capacitation in the oviduct. CLU is a chaperone found in the extracellular space and in various body fluids secretions, including equine OF (19, 40). In rabbits, CLU expression increases in the mixture of spermatozoa and OF retrieved from the oviduct 4 h post-insemination during the pre-ovulatory period (41). CLU has also been demonstrated to undergo re-localization in mice during capacitation (42) and could be supporting the final maturation process of spermatozoa in the equine oviduct, as previously demonstrated in rabbits (40).

Another protein present in the OF is GSTM3, an antioxidant enzyme involved in cell protection against oxidative stress that has been found in the uterine fluid of pregnant and non-pregnant mares (43). This protein has been detected in goat sperm surface and plays a crucial role as a zona pellucida-binding protein (44); hence, as our data and previous reports in sheep (45) show a GSTM3 downregulation in post-ovulatory OF compared to pre-ovulatory OF, this protein could be playing a crucial role in gamete interaction promoting fertilization.

The protein TAGLN2 belongs to the transgelin (TAGLN) family, which comprised three isoforms and have been identified as actin-binding proteins, which are known to stabilize the actin cytoskeleton (46). TAGLN2 is known to affect actin cross-linking blocking F-actin depolymerization and has been described to play a core role in embryo implantation in mice (46). However, equine embryos undergo fixation around day 21 post-ovulation, so the downregulation of TAGLN2 expression in post-ovulatory OF could be instead modulating actin depolymerization during sperm capacitation, promoting acrosome reaction, as previously reported in other species (47), or may be playing another role that needs to be further explored.

Nucleoside diphosphate kinase B (NME2) plays a major role in the synthesis of nucleoside triphosphates other than adenosine triphosphate. It has also been identified as a potential canonical transcription factor that regulates gene transcription through its DNA-binding activity (48) and has been described to be overexpressed in bovine OF ipsilateral to the pre-ovulatory follicle (25) in the form of extracellular vesicle cargo (49). However, the role that nucleoside diphosphate kinase B may play in equine fertilization remains to be studied. This is the same scenario for ACY1, a soluble homodimeric zinc-binding enzyme that is involved in the hydrolysis of *N*-acetylated proteins. The *N*-acylation of a protein usually leads to the extension of its half-life, and interestingly, 50–80% of all cellular proteins show formylated or acetylated N-termini. After the degradation of proteins, free amino acids can be recycled by the enzymatic hydrolysis of *N*-acylated amino acids catalyzed by aminoacylases, such as ACY1 that has a wide substrate specificity (50). Amino acid metabolism is crucial for embryo development, and a different amino acid turnover has been demonstrated to happen in the culture medium of human embryos resulting in clinical pregnancy and those that underwent reabsorption (51). Once more, the exact role that this protein may play in equine OF remains to be further studied.

In our setting, the most significantly upregulated protein was secretoglobin (SCGB1A1), coinciding with previous studies in horses in which this uteroglobin was significantly upregulated in the ipsilateral oviduct of pregnant mares (19). A similar secretoglobin (SCGB1D2) was already found to be upregulated in the human oviduct in the early luteal phase, and both secretoglobins have been associated with anti-inflammatory/immunomodulatory, anti-chemotactic, and

embryonic growth-stimulatory activities, as also proposed in horses (19, 52). The upregulated VCAN was demonstrated to promote cell motility and migration (53, 54), suggesting that the post-ovulatory oviductal microenvironment is involved in the migration process of the zygote toward the uterus. ALB upregulation in post-ovulatory OF has already been described in equine (19), while GSN was found in bovine oviductal exosomes playing a core role in sperm–oviduct interaction and early embryo development (49). Moreover, the upregulation of MYH9 in post-ovulatory OF is in agreement with a previous study on bovine post-ovulatory OF in which this protein was demonstrated to be a specific sperm-interacting protein (55). Regarding the upregulated proteins in the category *single fertilization* (GO:0007338), it has already been reported that the molecules involved in the process of sperm–egg recognition and binding are not only expressed in the spermatozoa or oocytes but can also be dispersed in OF (56). According to the STRING analysis, TCP1 and its subunits CCT2, CCT3, CCT5, CCT7, and CCT8 interact in common pathways (**Figure 4**). This result is in accordance with previous studies that hypothesized that chaperone proteins are necessary to deliver and assemble multiprotein complexes on the surface of gametes before sperm–egg interaction (57).

Our data reveal interesting differences in the proteome of equine OF prior to and post-ovulation. These findings may help to continue unraveling which factors promote fertilization and early embryo development, aiming to improve *in vitro* fertilization outcome in horses. More studies are required to achieve the proposed goal, and further studies will be carried out to keep improving our understanding regarding the physiology of oocyte fertilization in horses.

DATA AVAILABILITY STATEMENT

The datasets presented in this study can be found in online repositories. The names of the repository/repositories and accession number(s) can be found at: http://www.proteomexchange.org/, PXD025320.

ETHICS STATEMENT

Ethical review and approval was not required for the animal study because samples were retrieved from a slaughterhouse.

AUTHOR CONTRIBUTIONS

PF-H contributed to the investigation, methodology, writing the original draft, manuscript review, and editing. FM helped with the data curation, formal analysis, methodology, writing the original draft, and in manuscript review and editing. MS-C contributed to the investigation and in manuscript review and editing. LJG-M and MJB helped with manuscript review and editing and in funding acquisition. LG-F did the formal analysis, investigation, methodology, writing the original draft, and in manuscript review and editing. BM-G contributed to the conceptualization, data curation, formal analysis, funding acquisition, investigation, methodology, project administration, supervision, writing the original draft, and in manuscript review and editing. All authors contributed to the article and approved the submitted version.

FUNDING

This study was supported by the Spanish Ministry of Economy, Industry and Competitiveness and Fondo Europeo de Desarrollo Regional (FEDER) (AEI/FEDER/UE), references: AGL2017-84681-R and RYC-2017-21545 (the last awarded to BM-G). LG-F was supported by a grant Atracción y retorno de talento investigador a "Centros de I+D+i pertenecientes al Sistema Extremeño de Ciencia, Tecnología e Innovación from Junta de Extremadura" (Spain; reference: TA18008). PF-H was supported by a grant Acción II, Plan propio "Plan de Iniciación a la Investigación, Desarrollo Tecnológico e Innovación" from the University of Extremadura (reference: Beca RC4).

ACKNOWLEDGMENTS

The help of the veterinary team at the slaughterhouse (Carmen, Gerardo, and Jesús) is warmly appreciated (Incarsa, Burgos). Proteomic analysis was performed by Dr. Alberto Paradela Elizade and his research group at the CNB-CSIC (Madrid, Spain), and the proteome statistical analysis was performed by Antonio Ramos Fernández (Proteobotics, Madrid, Spain). The help of both researchers is kindly acknowledged. Analysis of the proteomics data was possible thanks to the kind suggestions of María de los Ángeles de Pedro Muñoz. The authors wish to acknowledge the suggestions provided by Dr. Shavahn Loux. This work is dedicated to Martín González Macías and to the memory of Juan Antonio García Iglesias.

SUPPLEMENTARY MATERIAL

The Supplementary Material for this article can be found online at: https://www.frontiersin.org/articles/10.3389/fvets.2021.694247/full#supplementary-material

REFERENCES

1. Galli C, Lazzari G. The manipulation of gametes and embryos in farm animals. *Reprod Domest Anim Zuchthyg.* (2008) 43(Suppl. 2):1–7. doi: 10.1111/j.1439-0531.2008.01136.x
2. Lopera-Vasquez R, Hamdi M, Maillo V, Lloreda V, Coy P, Gutierrez-Adan A, et al. Effect of bovine oviductal fluid on development and quality of bovine embryos produced *in vitro*. *Reprod Fertil Dev.* (2017) 29:621–9. doi: 10.1071/RD15238
3. Thibault C, Dauzier L, Wintenberger S. Cytological study of fecundation *in vitro* of rabbit ovum. *C R Seances Soc Biol Fil.* (1954) 148:789–90.
4. Chang MC. Fertilizing capacity of spermatozoa deposited into the fallopian tubes. *Nature.* (1951) 168:697–8. doi: 10.1038/168697b0
5. Austin C. Observations on the penetration of the sperm into the mammalian egg. *Aust J Biol Sci.* (1951) 4:581. doi: 10.1071/BI9510581
6. Coy P, Yanagimachi R. The common and species-specific roles of oviductal proteins in mammalian fertilization and embryo development. *BioScience.* (2015) 65:973–84. doi: 10.1093/biosci/biv119

7. Gardner DK, Leese HJ. Concentrations of nutrients in mouse oviduct fluid and their effects on embryo development and metabolism *in vitro*. *Reproduction.* (1990) 88:361–8. doi: 10.1530/jrf.0.0880361
8. Leemans B, Gadella BM, Stout TAE, De Schauwer C, Nelis H, Hoogewijs M, et al. Why doesn't conventional IVF work in the horse? The equine oviduct as a microenvironment for capacitation/fertilization. *Reproduction.* (2016) 152:R233–45. doi: 10.1530/REP-16-0420
9. Leemans B, Stout TAE, De Schauwer C, Heras S, Nelis H, Hoogewijs M, et al. Update on mammalian sperm capacitation: how much does the horse differ from other species? *Reproduction.* (2019) 157:R181–97. doi: 10.1530/REP-18-0541
10. Choi YH, Okada Y, Hochi S, Braun J, Sato K, Oguri N. In vitro fertilization rate of horse oocytes with partially removed zonae. *Theriogenology.* (1994) 42:795–802. doi: 10.1016/0093-691X(94)90448-R
11. González-Fernández L, Sánchez-Calabuig MJ, Calle-Guisado V, García-Marín LJ, Bragado MJ, Fernández-Hernández P, et al. Stage-specific metabolomic changes in equine oviductal fluid: new insights into the equine fertilization environment. *Theriogenology.* (2020) 143:35–43. doi: 10.1016/j.theriogenology.2019.11.035
12. Hinrichs K, Love CC, Brinsko SP, Choi YH, Varner DD. In vitro fertilization of *in vitro*-matured equine oocytes: effect of maturation medium, duration of maturation, and sperm calcium ionophore treatment, and comparison with rates of fertilization *in vivo* after oviductal Transfer1. *Biol Reprod.* (2002) 67:256–62. doi: 10.1095/biolreprod67.1.256
13. Lamy J, Gatien J, Dubuisson F, Nadal-Desbarats L, Salvetti P, Mermillod P, et al. Metabolomic profiling of bovine oviductal fluid across the oestrous cycle using proton nuclear magnetic resonance spectroscopy. *Reprod Fertil Dev.* (2018) 30:1021. doi: 10.1071/RD17389
14. Bauersachs S, Blum H, Mallok S, Wenigerkind H, Rief S, Prelle K, et al. Regulation of ipsilateral and contralateral bovine oviduct epithelial cell function in the postovulation period: a transcriptomics approach1. *Biol Reprod.* (2003) 68:1170–7. doi: 10.1095/biolreprod.102.010660
15. Maillo V, de Frutos C, O'Gaora P, Forde N, Burns GW, Spencer TE, et al. Spatial differences in gene expression in the bovine oviduct. *Reproduction.* (2016) 152:37–46. doi: 10.1530/REP-16-0074
16. Hunter RHF. Components of oviduct physiology in eutherian mammals. *Biol Rev Camb Philos Soc.* (2012) 87:244–55. doi: 10.1111/j.1469-185X.2011.00196.x
17. Avilés M, Gutiérrez-Adán A, Coy P. Oviductal secretions: will they be key factors for the future ARTs? *MHR Basic Sci Reprod Med.* (2010) 16:896–906. doi: 10.1093/molehr/gaq056
18. Saint-Dizier M, Schoen J, Chen S, Banliat C, Mermillod P. Composing the early embryonic microenvironment: physiology and regulation of oviductal secretions. *Int J Mol Sci.* (2019) 21:223. doi: 10.3390/ijms21010223
19. Smits K, Nelis H, Van Steendam K, Govaere J, Roels K, Ververs C, et al. Proteome of equine oviducal fluid: effects of ovulation and pregnancy. *Reprod Fertil Dev.* (2017) 29:1085. doi: 10.1071/RD15481
20. Ramos-Fernández A, Paradela A, Navajas R, Albar JP. Generalized method for probability-based peptide and protein identification from tandem mass spectrometry data and sequence database searching. *Mol Cell Proteomics.* (2008) 7:1748–54. doi: 10.1074/mcp.M800122-MCP200
21. Lopez-Serra P, Marcilla M, Villanueva A, Ramos-Fernandez A, Palau A, Leal L, et al. A DERL3-associated defect in the degradation of SLC2A1 mediates the Warburg effect. *Nat Commun.* (2014) 5:3608. doi: 10.1038/ncomms4608
22. Huang DW, Sherman BT, Lempicki RA. Systematic and integrative analysis of large gene lists using DAVID bioinformatics resources. *Nat Protoc.* (2009) 4:44–57. doi: 10.1038/nprot.2008.211
23. Huang DW, Sherman BT, Lempicki RA. Bioinformatics enrichment tools: paths toward the comprehensive functional analysis of large gene lists. *Nucleic Acids Res.* (2009) 37:1–3. doi: 10.1093/nar/gkn923
24. Reimand J, Kull M, Peterson H, Hansen J, Vilo J. g:Profiler–a web-based toolset for functional profiling of gene lists from large-scale experiments. *Nucleic Acids Res.* (2007) 35:W193–200. doi: 10.1093/nar/gkm226
25. Lamy J, Labas V, Harichaux G, Tsikis G, Mermillod P, Saint-Dizier M. Regulation of the bovine oviductal fluid proteome. *Reproduction.* (2016) 152:629–44. doi: 10.1530/REP-16-0397
26. Capra E, Lange-Consiglio A. The biological function of extracellular vesicles during fertilization, early embryo—maternal crosstalk and their involvement in reproduction: review and overview. *Biomolecules.* (2020) 10:1510. doi: 10.3390/biom10111510
27. Binelli M, Gonella-Diaza A, Mesquita F, Membrive C. Sex steroid-mediated control of oviductal function in cattle. *Biology.* (2018) 7:15. doi: 10.3390/biology7010015
28. Saint-Dizier M, Marnier C, Tahir MZ, Grimard B, Thoumire S, Chastant-Maillard S, et al. *OVGP1* is expressed in the canine oviduct at the time and place of oocyte maturation and fertilization: expression of oviductin in the canine oviduct. *Mol Reprod Dev.* (2014) 81:972–82. doi: 10.1002/mrd.22417
29. Van Winkle LJ. Amino acid transport regulation and early embryo development. *Biol Reprod.* (2001) 64:1–12. doi: 10.1095/biolreprod64.1.1
30. Hotamisligil GS, Bernlohr DA. Metabolic functions of FABPs—mechanisms and therapeutic implications. *Nat Rev Endocrinol.* (2015) 11:592–605. doi: 10.1038/nrendo.2015.122
31. del Collado M, da Silveira JC, Sangalli JR, Andrade GM, Sousa LR da S, Silva LA, et al. Fatty acid binding protein 3 and transzonal projections are involved in lipid accumulation during *in vitro* maturation of bovine oocytes. *Sci Rep.* (2017) 7:2645. doi: 10.1038/s41598-017-02467-9
32. Smits K, Goossens K, Van Soom A, Govaere J, Hoogewijs M, Peelman LJ. *In vivo*-derived horse blastocysts show transcriptional upregulation of developmentally important genes compared with *in vitro*-produced horse blastocysts. *Reprod Fertil Dev.* (2011) 23:364. doi: 10.1071/RD10124
33. Song GX, Shen YH, Liu YQ, Sun W, Miao LP, Zhou LJ, et al. Overexpression of *FABP3* promotes apoptosis through inducing mitochondrial impairment in embryonic cancer cells. *J Cell Biochem.* (2012) 113:3701–8. doi: 10.1002/jcb.24243
34. Budna J, Celichowski P, Knap S, Jankowski M, Magas M, Nawrocki MJ, et al. Fatty acids related genes expression undergo substantial changes in porcine oviductal epithelial cells during long-term primary culture. *Med J Cell Biol.* (2018) 6:39–47. doi: 10.2478/acb-2018-0008
35. Walter J, Huwiler F, Fortes C, Grossmann J, Roschitzki B, Hu J, et al. Analysis of the equine "cumulome" reveals major metabolic aberrations after maturation *in vitro*. *BMC Genomics.* (2019) 20:588. doi: 10.1186/s12864-019-5836-5
36. Rodriguez-Martinez H, Tienthai P, Atikuzzaman M, Vicente-Carrillo A, Rubér M, Alvarez-Rodriguez M. The ubiquitous hyaluronan: functionally implicated in the oviduct? *Theriogenology.* (2016) 86:182–6. doi: 10.1016/j.theriogenology.2015.11.025
37. Darr CR, Varner DD, Teague S, Cortopassi GA, Datta S, Meyers SA. Lactate and pyruvate are major sources of energy for stallion sperm with dose effects on mitochondrial function, motility, and ROS Production1. *Biol Reprod.* (2016) 95:1–11. doi: 10.1095/biolreprod.116.140707
38. González-Fernández L, Sánchez-Calabuig MJ, Alves MG, Oliveira PF, Macedo S, Gutiérrez-Adán A, et al. Expanded equine cumulus-oocyte complexes exhibit higher meiotic competence and lower glucose consumption than compact cumulus-oocyte complexes. *Reprod Fertil Dev.* (2018) 30:297–306. doi: 10.1071/RD16441
39. Lewis N, Hinrichs K, Leese HJ, Argo McG C, Brison DR, Sturmey R. Energy metabolism of the equine cumulus oocyte complex during *in vitro* maturation. *Sci Rep.* (2020) 10:3493. doi: 10.1038/s41598-020-60624-z
40. Steinberger B, Yu H, Brodmann T, Milovanovic D, Reichart U, Besenfelder U, et al. Semen modulated secretory activity of oviductal epithelial cells is linked to cellular proteostasis network remodeling: proteomic insights into the early phase of interaction in the oviduct *in vivo*. *J Proteomics.* (2017) 163:14–27. doi: 10.1016/j.jprot.2017.05.006
41. Yu H, Hackenbroch L, Meyer FRL, Reiser J, Razzazi-Fazeli E, Nöbauer K, et al. Identification of rabbit oviductal fluid proteins involved in pre-fertilization processes by quantitative proteomics. *Proteomics.* (2019) 19:1800319. doi: 10.1002/pmic.201800319
42. Saewu A, Kadunganattil S, Raghupathy R, Kongmanas K, Diaz-Astudillo P, Hermo L, et al. Clusterin in the mouse epididymis: possible roles in sperm maturation and capacitation. *Reproduction.* (2017) 154:867–80. doi: 10.1530/REP-17-0518
43. Smits K, Willems S, Van Steendam K, Van De Velde M, De Lange V, Ververs C, et al. Proteins involved in embryo-maternal interaction around the signalling of maternal recognition of pregnancy in the horse. *Sci Rep.* (2018) 8:5249. doi: 10.1038/s41598-018-23537-6

44. Hemachand T, Gopalakrishnan B, Salunke DM, Totey SM, Shaha C. Sperm plasma-membrane-associated glutathione S-transferases as gamete recognition molecules. *J Cell Sci.* (2002) 115:2053. doi: 10.1242/jcs.115.10.2053
45. Soleilhavoup C, Riou C, Tsikis G, Labas V, Harichaux G, Kohnke P, et al. Proteomes of the female genital tract during the oestrous cycle*. *Mol Cell Proteomics.* (2016) 15:93–108. doi: 10.1074/mcp.M115.052332
46. Liang X, Jin Y, Wang H, Meng X, Tan Z, Huang T, et al. Transgelin 2 is required for embryo implantation by promoting actin polymerization. *FASEB J.* (2019) 33:5667–75. doi: 10.1096/fj.201802158RRR
47. Breitbart H, Cohen G, Rubinstein S. Role of actin cytoskeleton in mammalian sperm capacitation and the acrosome reaction. *Reproduction.* (2005) 129:263–8. doi: 10.1530/rep.1.00269
48. Puts GS, Leonard MK, Pamidimukkala NV, Snyder DE, Kaetzel DM. Nuclear functions of NME proteins. *Lab Investig J Tech Methods Pathol.* (2018) 98:211–8. doi: 10.1038/labinvest.2017.109
49. Almiñana C, Tsikis G, Labas V, Uzbekov R, da Silveira JC, Bauersachs S, et al. Deciphering the oviductal extracellular vesicles content across the estrous cycle: implications for the gametes-oviduct interactions and the environment of the potential embryo. *BMC Genomics.* (2018) 19:622. doi: 10.1186/s12864-018-4982-5
50. Sommer A, Christensen E, Schwenger S, Seul R, Haas D, Olbrich H, et al. The molecular basis of aminoacylase 1 deficiency. *Biochim Biophys Acta BBA - Mol Basis Dis.* (2011) 1812:685–90. doi: 10.1016/j.bbadis.2011.03.005
51. Gardner DK, Wale PL. Analysis of metabolism to select viable human embryos for transfer. *Fertil Steril.* (2013) 99:1062–72. doi: 10.1016/j.fertnstert.2012.12.004
52. Hess AP, Talbi S, Hamilton AE, Baston-Buest DM, Nyegaard M, Irwin JC, et al. The human oviduct transcriptome reveals an anti-inflammatory, anti-angiogenic, secretory and matrix-stable environment during embryo transit. *Reprod Biomed Online.* (2013) 27:423–35. doi: 10.1016/j.rbmo.2013.06.013
53. Onken J, Moeckel S, Leukel P, Leidgens V, Baumann F, Bogdahn U, et al. Versican isoform V1 regulates proliferation and migration in high-grade gliomas. *J Neurooncol.* (2014) 120:73–83. doi: 10.1007/s11060-014-1545-8
54. Ricciardelli C, Russell DL, Ween MP, Mayne K, Suwiwat S, Byers S, et al. Formation of hyaluronan- and versican-rich pericellular matrix by prostate cancer cells promotes cell motility. *J Biol Chem.* (2007) 282:10814–25. doi: 10.1074/jbc.M606991200
55. Lamy J, Nogues P, Combes-Soia L, Tsikis G, Labas V, Mermillod P, et al. Identification by proteomics of oviductal sperm-interacting proteins. *Reproduction.* (2018) 155:457–66. doi: 10.1530/REP-17-0712
56. Bernabò N, Ordinelli A, Di Agostino R, Mattioli M, Barboni B. Network analyses of sperm-egg recognition and binding: ready to rethink fertility mechanisms? *Omics J Integr Biol.* (2014) 18:740–53. doi: 10.1089/omi.2014.0128
57. Bromfield EG, Nixon B. The function of chaperone proteins in the assemblage of protein complexes involved in gamete adhesion and fusion processes. *Reprod Camb Engl.* (2013) 145:R31–42. doi: 10.1530/REP-12-0316

Conflict of Interest: The authors declare that the research was conducted in the absence of any commercial or financial relationships that could be construed as a potential conflict of interest.

Publisher's Note: All claims expressed in this article are solely those of the authors and do not necessarily represent those of their affiliated organizations, or those of the publisher, the editors and the reviewers. Any product that may be evaluated in this article, or claim that may be made by its manufacturer, is not guaranteed or endorsed by the publisher.

frontiers in Veterinary Science

ORIGINAL RESEARCH
published: 25 August 2021
doi: 10.3389/fvets.2021.719319

Direct but Not Indirect Methods Correlate the Percentages of Sperm With Altered Chromatin to the Intensity of Chromatin Damage

Jordi Ribas-Maynou[1,2]*, *Marc Llavanera*[1,2], *Yentel Mateo-Otero*[1,2], *Estela Garcia-Bonavila*[1,2], *Ariadna Delgado-Bermúdez*[1,2] and *Marc Yeste*[1,2]

[1] Biotechnology of Animal and Human Reproduction (TechnoSperm), Institute of Food and Agricultural Technology, University of Girona, Girona, Spain, [2] Unit of Cell Biology, Department of Biology, Faculty of Sciences, University of Girona, Girona, Spain

OPEN ACCESS

Edited by:
Cristina Alicia Martinez, Linköping University, Sweden

Reviewed by:
Mohammad Hossein Nasr-Esfahani, Royan Institute, Iran
Marjan Sabbaghian, Royan Institute, Iran

***Correspondence:**
Jordi Ribas-Maynou
jordi.ribasmaynou@udg.edu
orcid.org/0000-0002-9101-2044

Specialty section:
This article was submitted to Animal Reproduction - Theriogenology, a section of the journal Frontiers in Veterinary Science

Received: 02 June 2021
Accepted: 29 July 2021
Published: 25 August 2021

Citation:
Ribas-Maynou J, Llavanera M, Mateo-Otero Y, Garcia-Bonavila E, Delgado-Bermúdez A and Yeste M (2021) Direct but Not Indirect Methods Correlate the Percentages of Sperm With Altered Chromatin to the Intensity of Chromatin Damage. Front. Vet. Sci. 8:719319. doi: 10.3389/fvets.2021.719319

Although sperm chromatin damage, understood as damage to DNA or affectations in sperm protamination, has been proposed as a biomarker for sperm quality in both humans and livestock, the low incidence found in some animals raises concerns about its potential value. In this context, as separate methods measure different facets of chromatin damage, their comparison is of vital importance. This work aims at analyzing eight techniques assessing chromatin damage in pig sperm. With this purpose, cryopreserved sperm samples from 16 boars were evaluated through the following assays: TUNEL, TUNEL with decondensation, SCSA, alkaline and neutral sperm chromatin dispersion (SCD) tests, alkaline and neutral Comet assays, and chromomycin A3 test (CMA3). In all cases, the extent of chromatin damage and the percentage of sperm with fragmented DNA were determined. The degree of chromatin damage and the percentage of sperm with fragmented DNA were significantly correlated ($p < 0.05$) in direct methods (TUNEL, TUNEL with decondensation, and alkaline and neutral Comet) and CMA3, but not in the indirect ones (SCD and SCSA). Percentages of sperm with fragmented DNA determined by alkaline Comet were significantly ($p < 0.05$) correlated with TUNEL following decondensation and CMA3; those determined by neutral Comet were correlated with the percentage of High DNA Stainability (SCSA); those determined by SCSA were correlated with neutral and alkaline SCD; and those determined by neutral SCD were correlated with alkaline SCD. While, in pigs, percentages of sperm with fragmented DNA are directly related to the extent of chromatin damage when direct methods are used, this is not the case for indirect techniques. Thus, the results obtained herein differ from those reported for humans in which TUNEL, SCSA, alkaline SCD, and alkaline Comet were found to be correlated. These findings may shed some light on the interpretation of these tests and provide some clues for the standardization of chromatin damage methods.

Keywords: sperm, chromatin, DNA fragmentation, TUNEL, SCSA, comet assay

INTRODUCTION

The research of biomarkers that predict sperm fertilizing ability has gained much interest in the last years and has led to the discovery of factors affecting reproductive outcomes in both humans and production animals (1–4). In humans, infertility affects millions of couples worldwide and has an incidence of ∼7–15%, being a multifactorial disease due to both male and female factors (5). As clinical treatments for infertile patients usually involve *in vitro* fertilization (IVF) and intracytoplasmic sperm injection (ICSI) and pregnancy rates using these methods are relatively low (6), research on predicting IVF/ICSI outcomes is much warranted. Contrastingly, in livestock animals, reproductive performance has been improved after many years of genetic selection of the best breeders (7). In pigs, artificial insemination is the most used method for breeding, and the quality of liquid-stored and cryopreserved sperm is evaluated to determine the potential fertility of males (8, 9). In this context, finding sperm quality biomarkers that allow the selection of the most suitable boars is crucial to increase reproductive efficiency in farms (10–12).

In the last decades, testing sperm chromatin defects has turned into a reliable biomarker of seminal quality in humans and animals (13, 14). As sperm DNA breaks are known to be important for the diagnosis of male infertility in humans (15), few reports were focused on elucidating whether or not this sperm quality parameter could predict the reproductive efficiency of production animals (16–19). DNA fragmentation can be analyzed directly, using techniques such as TUNEL and Single Cell Gel Electrophoresis (also known as Comet assay), or indirectly, through methods like Sperm Chromatin Structure Assay (SCSA) and Sperm Chromatin Dispersion test (SCD test or halo assay). These indirect techniques determine the amount of DNA damage through the differential chromatin decondensation of fragmented DNA (2, 14, 20).

The utility of chromatin fragmentation has been the source of much debate, as whereas some studies point out to the detrimental effect of DNA damage on assisted reproduction techniques (21, 22), others find opposite or inconclusive results (23–25). The reason of this controversy is related to the differences in both the methods for measuring DNA damage and the clinical outcomes used to compare these methods (26). Remarkably, while the techniques evaluating sperm DNA fragmentation in farm animals have not been compared, only four studies contrasted different DNA fragmentation methods in humans, focusing on the male infertility condition and IVF/ICSI outcomes (27–30), and one analyzed the matter in mice (31). All these reports agreed in establishing correlations between TUNEL and alkaline Comet methods, and suggested that Comet would be one of the most sensitive methods to assess sperm DNA fragmentation (32). While several efforts to obtain standardized results among laboratories have been made, controversies remain open regarding the correlation between direct (e.g., Comet and TUNEL) and indirect (e.g., SCSA and SCD) assays, as results differ between studies (27, 28). Apart from the lack of research about the correlation between techniques in livestock sperm, most studies in pigs used indirect methods, like SCD or SCSA, to assess the relationship between DNA damage and fertilizing ability (18, 19, 33, 34).

Therefore, the aim of the present study was to compare different methods (direct and indirect) that evaluate sperm DNA fragmentation in pigs, in order to establish whether these tests are correlated with each other regarding both the percentage of sperm with fragmented DNA and the incidence of chromatin damage.

MATERIALS AND METHODS

Reagents

Unless stated otherwise, all reagents were purchased from Sigma-Aldrich (St. Louis, MO, USA).

Semen Samples

Sixteen semen samples collected from sexually mature boars (18–30 months of age) were provided by a local farm that operates under standard commercial conditions (Servicios Genéticos Porcinos S.L.; Roda de Ter, Spain). Animals were not directly manipulated for the present study; thus, it did not require any specific ethical approval.

An ejaculate from each boar was obtained using the gloved-hand method, and samples were immediately diluted 1:2 (v/v) in a long-term extender (Vitasem, Magapor S.L.; Zaragoza, Spain). Just after arrival, an aliquot was intended to evaluate sperm motility and viability; the remaining volume was cryopreserved following the standard protocol utilized before in our research group (35, 36).

Sperm Cryopreservation

Semen samples were split into 50-ml aliquots, centrifuged at 2,400 × *g* and 17°C for 4 min, resuspended to a concentration of 1.5×10^9 sperm/ml in β-Lactose-egg yolk (LEY) media (80% v/v lactose, 20% v/v egg yolk), and cooled down to 5°C at a rate of −0.1°C/min. Afterwards, samples were diluted in LEYGO medium [LEY medium supplemented with 6% v/v glycerol and 1.5% Orvus ES Paste (Equex STM; Nova Chemical Sales Inc., Scituate, MA, USA)] to a final concentration of 1×10^9 sperm/ml. Finally, samples were loaded into 0.5-ml straws (MiniTüb; Tiefenbach, Germany) and submitted to the following curve: 6°C/min from 5 to −5°C (100 s); −39.82°C/min from −5 to −80°C (113 s); holding at −80°C for 30 s; −60°C/min from −80 to −150°C (70 s). At this point, samples were stored in liquid nitrogen until used.

Thawing was carried out by immersion of straws in a water bath at 38°C for 15 s, with shaking. The content of each straw was diluted with three volumes of Beltsville Thawing Solution (BTS) (0.2 M glucose, 23 mM sodium citrate, 15 mM sodium bicarbonate, 4.2 mM EDTA, 10 mM potassium chloride, and 0.1 mM kanamycin, pH 7.5).

Sperm Motility Analysis Through Computer-Assisted Sperm Analysis

A commercial computer-assisted system (Integrated Sperm Analysis System V1.0; Proiser S.L., Valencia, Spain) was used to analyze sperm motility before and after cryopreservation.

First, samples were warmed at 38°C for 15 min, and 5 μl was loaded onto a previously warmed (38°C) Makler chamber (Sefi-medical Instruments, Haifa, Israel). Different fields were captured at 100× magnification, recording 25 consecutive images at 25 images per second, until reaching 1,000 spermatozoa per assessment. At least two technical replicates per sample were evaluated, and the mean of replicates was recorded. The following parameters were assessed: percentage of total motile sperm; percentage of progressive motility; percentages of sperm with rapid, medium, and slow motility; curvilinear velocity (VCL; the instantaneously recorded sequential sperm progression along the whole trajectory; μm/s); straight-line velocity (VSL; the straight sperm trajectory per unit of time; μm/s); average path velocity (VAP; the mean sperm trajectory per unit of time; μm/s); linearity coefficient (LIN = VSL/VCL × 100; %); straightness coefficient (STR = VSL/VAP × 100; %); wobble coefficient (WOB: VAP/VCL × 100; %); mean amplitude of lateral head displacement (ALH; the mean amplitude of the lateral oscillatory movement of the sperm head around the mean trajectory; μm); and frequency of head displacement (BCF; the number of sperm head lateral oscillatory movements around the mean trajectory per unit of time; Hz).

Evaluation of Sperm Morphology

In order to assess sperm morphology, samples were incubated in 2% formaldehyde at room temperature for 5 min. Sperm cells were analyzed through SCA production Software (Sperm Class Analyzer Production, 2010; Microptic S.L., Barcelona) and classified as morphologically normal, with proximal or distal droplets, or aberrant (including head and tail anomalies). Three replicates (100 sperm each) per sample were counted.

Determination of Sperm Viability Through Flow Cytometry

Sperm viability was evaluated by assessing plasma membrane integrity with LIVE/DEAD Sperm Viability Kit (Molecular Probes, Eugene, OR, USA). Sperm diluted at a final concentration of 1×10^6 in pre-warmed PBS were first incubated with SYBR14, a membrane-permeable fluorochrome that stains sperm heads in green, for 10 min (final concentration: 32 nmol/L). Thereafter, samples were incubated with propidium iodide (PI), a membrane-impermeable fluorochrome that only penetrates membrane-damaged sperm, for 5 min (final concentration: 7.5 μmol/L).

Stained sperm were examined through a CytoFLEX cytometer (Beckman Coulter; Fullerton, CA, USA). Samples were excited with an argon-ion laser at 488 nm and 10,000 events per replicate were evaluated, using FITC (BP 525/40) and PC5.5 (690/50) filters for SYBR14 and PI, respectively. Three separate populations were identified, a membrane-intact sperm population ($SYBR14^+/PI^-$) and two subpopulations of membrane-damaged sperm with different degrees of alteration ($SYBR14^+/PI^+$ and $SYBR14^-/PI^+$). Three technical replicates per sample were examined, and data were not compensated.

Neutral and Alkaline Comet Assay

Sperm Comet assay performed in neutral pH conditions was used to determine double-strand DNA breaks, whereas alkaline Comet assay was conducted to assess the total amount of DNA damage consisting of single- and double-strand DNA breaks. The Comet assay was based on the protocol described by Ribas-Maynou et al. (37) for pig sperm, which completely decondenses DNA prior to conducting the test.

Sperm Fixation and Lysis

Sperm samples were first diluted to 5×10^5 spermatozoa/ml in PBS, and mixed 1:2 (v/v) with melted low melting point agarose at 37°C. Two 6.5-μl drops of the mixture were poured onto two agarose-pretreated slides—one for alkaline Comet and the other for neutral Comet—which were subsequently covered with an 8-mm-diameter round coverslip. Then, agarose–sample mixtures were allowed to jellify on a cold plate at 4°C, coverslips were gently removed, and both slides were incubated in three lysis solutions (all at pH 7.5): (1) 0.8 M Tris-HCl, 0.8 M DTT, and 1% SDS for 30 min; (2) 0.8 M Tris-HCl, 0.8 M DTT, and 1% SDS for 30 min; and (3) 0.4 M Tris-HCl, 0.4 M DTT, 50 mM EDTA, 2 M NaCl, 1% Tween20, and 100 μg/ml Proteinase K for 180 min.

Electrophoresis

Electrophoresis conditions differed between the two Comet variants. For slides designated to neutral Comet, electrophoresis was performed in TBE buffer (0.445 M Tris-HCl, 0.445 M Boric acid, and 0.01 M EDTA; pH 8) at 1 V/cm for 30 min; slides were subsequently washed in 0.9% NaCl solution for 2 min.

Slides designated to alkaline Comet were denatured in cold alkaline solution (0.03 M NaOH and 1 M NaCl) for 5 min and then electrophoresed at 1 V/cm for 4 min in an alkaline buffer (0.03 M NaOH; pH 13).

Neutralization, Dehydration, and Staining

After electrophoresis, both slides were incubated in neutralizing solution (0.4 M Tris-HCl; pH 7.5), dehydrated in ethanol series (70, 90, and 100%), and dried in horizontal position. Staining was conducted with 5 μl of 1× Safeview DNA stain (NBS Biologicals, Huntingdon, UK) and covered with 20 × 20 coverslips.

Imaging and Analysis

Comets were observed under an epifluorescence microscope (Zeiss Imager Z1, Carl Zeiss AG, Oberkochen, Germany). Captures of at least 100 cells per sample were performed at 100× magnification and at a resolution of 1,388 × 1,040 pixels using Axiovision 4.6 software (Carl Zeiss AG, Oberkochen, Germany). Exposure time was adjusted to avoid overexposure of Comet heads.

Analysis of both neutral and alkaline Comets was performed using the open-access CometScore v2.0 software (Rexhoover, www.rexhoover.com), which analyzes the fluorescence intensity of Comet heads and tails. After automatic analysis, a manual review of the analyzed Comets was performed to eliminate captures that did not correspond to Comets or tallied with the overlapping ones. Furthermore, incorrect interpretation of the center of Comet heads due to misanalysis was corrected during

manual revision. When the final number of correctly analyzed Comets was <50, more captures until this figure was reached were performed.

For the quantitative analysis of the amount of DNA breaks (chromatin damage intensity), Olive Tail Moment (OTM), calculated as (Tail mean intensity–Head mean intensity) × Tail DNA/100, was chosen as a reference parameter (38).

Calculation of the Percentages of Damaged Sperm

Altered and normal sperm subpopulations were determined on the basis of the percentages of sperm with fragmented DNA in all samples. Tail Length, Tail DNA, and OTM were used to run a Principal Component Analysis (PCA). These parameters were sorted into one PCA component, and the obtained data matrix was rotated through the Varimax procedure with Kaiser normalization. Variables with a loading factor higher than 0.6 and lower than 0.3 in the rotated matrix were selected. The resulting component was used to calculate regression scores that were assigned to each spermatozoon. Regression scores were used to classify each Comet through a cluster analysis, using the between-groups linkage method based on the Euclidean distance. A total of three subpopulations were identified for both neutral and alkaline Comet assays. These subpopulations corresponded to sperm with high, medium or low amount of DNA breaks, respectively.

Alkaline and Neutral Chromatin Dispersion Assay

Upon thawing, samples intended to alkaline and neutral SCD assays were washed twice in PBS (centrifugation at 600×*g* for 5 min) and diluted to 2 × 10^6 sperm/ml with PBS. Afterwards, samples were mixed (1:2) with low melting point agarose at 37°C; two drops of 6.5 μl of the mixture were allowed to jellify onto two agarose-pretreated slides at 4°C for 5 min and then covered with an 8-mm coverslip. At this point, the slide designated to alkaline variant was subjected to acid denaturation in 0.08 N HCl (39). Both slides were incubated in lysis solutions that allowed complete chromatin decondensation (37): 30 min for Lysis 1, 30 min for Lysis 2, and 180 min for Lysis 3. After lysis, slides were washed in distilled water, neutralized in neutralization solution (0.4 M Tris-HCl; pH 7.5), dehydrated in an ethanol series (70, 90, and 100%), and dried in horizontal position.

Analysis of the halo diameter was used as a quantitative parameter for DNA breaks (chromatin damage intensity), whereas the percentage of sperm with fragmented DNA was determined by classifying 400 sperm haloes using the criteria defined for sperm DNA fragmentation (40).

Conventional TUNEL Assay and TUNEL Assay With Previous DNA Decondensation

TUNEL assay was performed in two variants: with previous decondensation and without decondensation. For both variants, the standard TUNEL protocol was applied according to the *In situ* Cell Death Detection Kit (Roche Diagnostic Gmbh, Penzberg, Germany).

First, samples were thawed and washed twice in PBS (centrifugation at 600 × *g* for 5 min). For the procedure that included decondensation, samples were incubated in 2 mM DTT at room temperature for 45 min (41) and then washed twice in PBS (centrifugation at 600 × *g* for 5 min). Afterwards, and for both variants, samples were resuspended in 300 μl of permeabilization solution (0.1% sodium citrate and 0.25% Triton X-100), incubated at 4°C for 2 min, and washed twice in PBS. In the second wash, samples were split into two tubes; pellets were resuspended in (a) 50 μl of labeling solution (negative control) and (b) 50 μl of TUNEL reaction mixture (containing 45 μl of labeling solution and 5 μl of terminal deoxynucleotidyl transferase enzyme). Samples were incubated at 37°C for 60 min and subsequently washed twice in PBS. Finally, samples were diluted to a final volume of 500 μl and analyzed by flow cytometry. A positive control, which consisted of incubating the sample with 4 units/μl of DNAse I (ThermoFisher Scientific, Waltham, USA) supplemented with 10 mM $MgCl_2$ at 37°C for 1 h, was performed for setting the technique up.

A total of 10,000 spermatozoa were analyzed with a CytoFLEX flow cytometer (Beckman Coulter, Fullerton, CA, USA), using the FITC channel, with an excitation wavelength of 488 nm and a detection wavelength of 525/40 nm. Data were processed using CytExpert software (Beckman Coulter, Fullerton, CA, USA), and the respective negative control of each sample was used to set up the threshold for $TUNEL^+$ sperm (sperm with fragmented DNA). Quantitative analysis of DNA breaks was provided by the median of FITC intensity.

Sperm Chromatin Structure Assay

Sperm samples were also evaluated through the standard SCSA procedure. Briefly, thawed samples were centrifuged twice at 600 × *g* for 5 min and resuspended with TNE buffer (10 mM Tris-HCl, 150 mM NaCl, and 1 mM EDTA; pH 7.5) to a final concentration of 2 × 10^6 sperm/ml. Two hundred microliters of the sample were mixed with 400 μl of acid detergent solution (0.08 M HCl, 0.15 M NaCl, and 0.1% Triton X-100; pH 1.2). After 30 s, sperm were stained with Acridine Orange Staining solution (6 μg/ml Acridine Orange in buffer containing 0.037 M citric acid, 0.126 M Na_2HPO_4, 1.1 mM EDTA, and 0.15 M NaCl; pH 6.0) for 3 min. Five thousand sperm were analyzed through a Cell Laboratory QuantaSC cytometer (Beckman Coulter; Fullerton, CA, USA). Green and red fluorescence were collected through FL1 (BP: Dichroic/Splitter, DRLP: 550 nm, BP: 525 nm) and FL3 (LP: 670 nm), respectively. Data were not compensated.

Percentages of sperm DNA fragmentation (%SDF) were determined as the number of sperm cells with increased red fluorescence compared to the main population showing equilibrated red/green fluorescence. Percentages of high DNA stainability (%HDS) were calculated as the number of sperm cells with increased green fluorescence compared to the main population. The degree of chromatin damage was determined through the geometric mean of red fluorescence intensity (FL3).

Chromomycin A3 Test

Chromomycin A3 (CMA3) competes with protamines for the binding to the minor groove of DNA. Briefly, after thawing, sperm were washed twice in McIlvine buffer (30 mM citric acid, 140 mM Na_2HPO_4, and 10 mM $MgCl_2$) and diluted to

20×10^6 sperm/ml. Stock solution of CMA3 was prepared at 500 µg/ml. Staining was performed in 12.5 µg/ml CMA3 at room temperature for 20 min. A negative control (without the addition of CMA3) for each sample was included. Afterwards, samples were diluted 1:10 (v:v) in filtered PBS and analyzed with a CytoFLEX flow cytometer (Beckman Coulter, Fullerton, CA,

TABLE 1 | Sperm motility, viability, and morphology in fresh and frozen-thawed sperm samples.

	Fresh samples				30 min post-thaw				
	Mean	**Standard deviation**	**Median**	**Rank**	**Mean**	**Standard deviation**	**Median**	**Rank**	***P*-value**
Progressive motility (%)	69.46% ±	5.43%	69.75%	(21.95%)	51.10% ±	15%	54.14%	(50.15%)	0.001*
Non-progressive motility (%)	28.56% ±	4.43%	28.23%	(15.17%)	33.29% ±	8%	30.99%	(25.59%)	0.010*
Rapid velocity (%)	62.84% ±	20.12%	55.70%	(59.29%)	44.27% ±	16%	44.67%	(56.92%)	0.121
Medium velocity (%)	25.86% ±	12.96%	30.08%	(37.69%)	20.55% ±	5%	19.86%	(22.70%)	0.134
Slow velocity (%)	9.32% ±	7.42%	8.97%	(26.49%)	19.57% ±	7%	19.37%	(25.63%)	0.002*
Static sperm (%)	1.98% ±	2.00%	1.43%	(7.84%)	15.61% ±	12%	13.74%	(38.91%)	<0.001*
Circular tracks (*n*)	1,176.63 ±	611.67	1,080.17	(2,191.00)	1,069.67 ±	518.45	1,073.67	(1,819.00)	0.301
VCL (µm/s)	59.49 ±	17.26	51.03	(51.03)	51.60 ±	8.18	50.93	(32.30)	0.438
VSL (µm/s)	28.51 ±	5.63	26.96	(21.17)	28.05 ±	5.81	27.89	(15.96)	1.000
VAP (µm/s)	43.12 ±	10.25	38.03	(30.65)	39.33 ±	6.62	39.44	(23.90)	0.408
LIN (%)	49.70 ±	8.58	51.32	(26.72)	54.25 ±	7.23	54.59	(26.64)	0.030*
STR (%)	66.87 ±	6.23	67.95	(19.23)	70.93 ±	5.96	71.61	(19.25)	0.020*
WOB (%)	73.73 ±	6.29	76.27	(19.51)	76.14 ±	4.15	76.24	(17.50)	0.121
ALH (µm)	2.62 ±	0.62	2.42	(2.10)	2.42 ±	0.25	2.39	(0.84)	0.535
BCF (Hz)	6.38 ±	0.29	6.48	(1.03)	6.12 ±	0.65	6.41	(1.92)	0.255
Viability (% viable sperm)	89.17 ±	5.84	89.68	(24.50)	51.23 ±	12.67	53.25	(42.75)	<0.001*
Morphology (% normal morphology)	90.05 ±	6.17	91.30	(25.40)					

Asterisks indicate significant differences ($p < 0.05$) between fresh and frozen-thawed sperm (30 min post-thaw).

TABLE 2 | Sperm chromatin status analyzed through eight methods. (A) Intensity of damage. (B) Percentage of sperm with fragmented DNA or altered chromatin.

	Mean		**Standard Deviation**	**Median**	**Rank**
A					
TUNEL (FITC intensity, A.U.)	444.8	±	317.9	413.1	(958.3)
TUNEL decondensed (FITC intensity)	1,718.3	±	621.0	1,631.7	(2,142.8)
Neutral SCD (Halo area, pixels)	1,441.4	±	338.4	1,313.0	(1,049.6)
Alkaline SCD (Halo area, pixels)	1,400.3	±	455.4	1,219.6	(1,775.2)
CMA3 (Intensity 610 nm. A.U.)	333.0	±	65.6	332.1	(247.6)
SCSA (FL3 intensity, A.U.)	159.6	±	78.9	150.3	(274.3)
Alkaline comet (Olive tail moment)	14.6	±	3.2	14.6	(10.8)
Neutral comet (Olive tail moment)	4.1	±	2.0	4.2	(5.82)
B					
TUNEL (%SDF)	2.0%	±	2.0	1.9%	(6.9)
TUNEL decondensed (%SDF)	8.9%	±	5.8	9.1%	(21.7)
CMA3 (%positive cells)	11.59%	±	5.5	10.5%	(20.0)
Neutral SCD (%SDF)	2.4%	±	0.9	2.2%	(3.2)
Alkaline SCD (%SDF)	2.6%	±	2.6	2.1%	(8.3)
SCSA (%SDF)	2.6%	±	1.8	2.6%	(6.3)
SCSA (%HDS)	4.4%	±	2.8	4.81%	(9.6)
Alkaline comet (%highly damaged)	38.0%	±	20.6	33.6%	(68.3)
Alkaline comet (%medium damaged)	41.3%	±	15.9	44.3%	(59.7)
Alkaline comet (%low damaged)	20.7%	±	15.8	16.3%	(54.5)
Neutral comet (%highly damaged)	1.8%	±	2.1	1.2%	(6.9)
Neutral comet (%medium damaged)	45.5%	±	22.4	50.2%	(71.6)
Neutral comet (%low damaged)	52.7%	±	22.7	48.5%	(74.2)

USA). CMA3 was excited with a 405-nm laser and its emission was acquired through the Violet 610 channel (610/20). Data were processed using CytExpert software (Beckman Coulter, Fullerton, CA, USA), and each negative control was used to establish the threshold for $CMA3^+$ sperm. Quantification of aberrant protamination was based on the median intensity of the Violet610 channel. A positive control was performed for setting the technique up, consisting of incubating the sample in 5 mM DTT (ThermoFisher Scientific, Waltham, USA) at 37°C for 45 min.

Statistical Analyses

Data were analyzed using the Statistics Package for Social Sciences ver. 25.0 (IBM Corp.; Armonk, NY, USA). Graphs were elaborated with GraphPad Prism 8.0 Software (GraphPad, San Diego, USA).

Normal distribution was determined with Shapiro-Wilk test and homogeneity of variances was tested with Levene test. As, even after linear transformation with log(x), $\sqrt{x}$, and arcsin $\sqrt{x}$, data did not fit with parametric assumptions, differences in sperm motility and viability before and after cryopreservation were determined through the Wilcoxon test. Correlations were analyzed through the non-parametric Spearman test. For all tests, the level of significance was set at $p \leq 0.05$.

RESULTS

Sperm Motility and Viability

Sperm motility and viability measured before and after cryopreservation are shown in **Table 1**. As expected, sperm motility parameters decreased after cryopreservation; specifically, progressive motility ($p = 0.001$) was reduced, whereas non-progressive motility ($p = 0.01$) and proportions of slow and static sperm increased ($p = 0.002$ and $p < 0.001$). Similarly, sperm viability was reduced after cryopreservation ($p < 0.001$).

Sperm Chromatin Damage and Correlation Between Chromatin Damage Intensity and Percentage of Affected Cells

Table 2 shows sperm chromatin status analyzed through eight separate methods. **Table 2A** shows the intensity of DNA damage measured through TUNEL, SCD, SCSA, and Comet assays, and that of chromatin regions with abnormal protamination evaluated through the CMA3 test. **Table 2B** depicts the percentage of affected cells above the damage threshold established for each technique.

Intensity of DNA damage (FITC intensity) correlated with the percentage of sperm with fragmented DNA in both

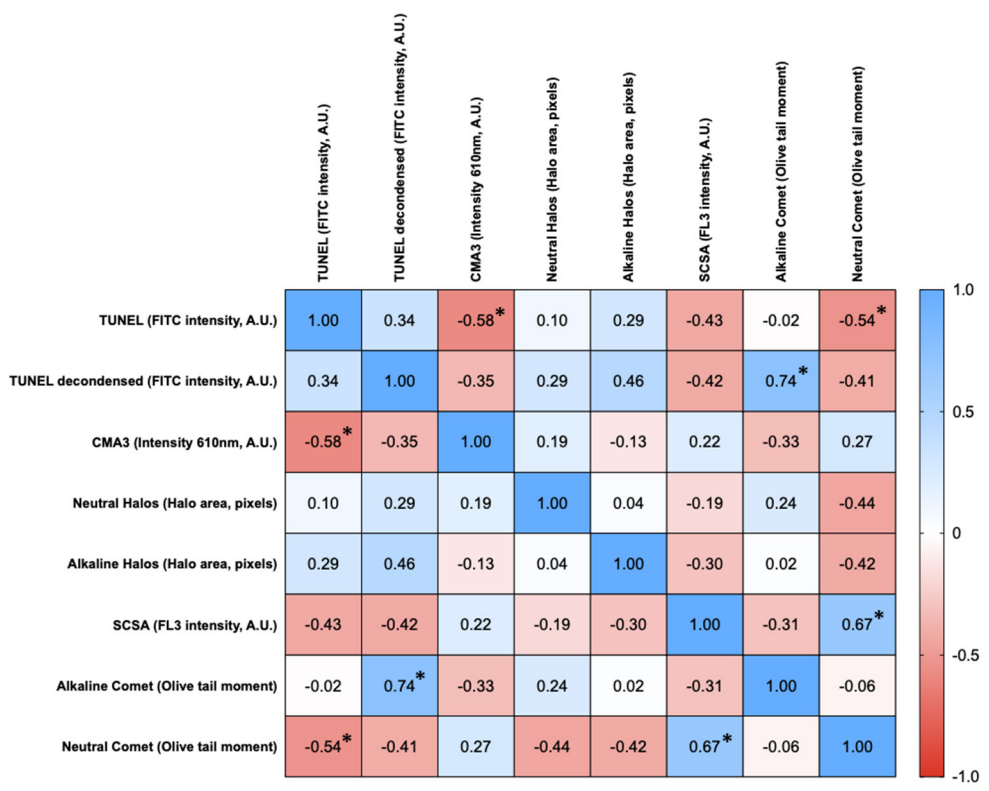

FIGURE 1 | Correlation matrix between methods regarding the degree of sperm chromatin damage. Figures in each box represent Spearman correlation coefficients. Asterisks and bold figures indicate statistically significant correlations ($p < 0.05$).

the conventional TUNEL assay ($Rs = 0.764$; $p = 0.001$) and TUNEL with DTT decondensation ($Rs = 0.659$; $p = 0.006$). For alkaline Comet, the intensity of DNA damage (measured as OTM) correlated with percentages of high ($Rs = 0.792$; $p = 0.001$) and low damage ($Rs = -0.782$ $p < 0.001$). For neutral Comet, the intensity of double-stranded DNA damage (measured as OTM) correlated with the percentage of low damage ($Rs = -0.559$; $p = 0.024$). For CMA3, the intensity of abnormal protamination also correlated with the percentage of altered sperm ($Rs = 0.779$; $p < 0.001$).

In contrast, no correlation between intensity and percentage of affected cells in alkaline SCD ($Rs = 0.263$; $p = 0.326$), neutral SCD ($Rs = 0.024$; $p = 0.931$), and SCSA ($Rs = 0.241$; $p = 0.368$) was found.

Correlations Regarding Chromatin Damage Intensity Between Tests

Figure 1 shows the matrix of correlations between different chromatin damage methods regarding damage intensity. Statistically significant correlations were found between neutral Comet OTM and SCSA ($Rs = 0.667$; $p = 0.006$), between neutral Comet OTM and TUNEL ($Rs = -0.535$; $p = 0.035$), between conventional TUNEL and CMA3 ($Rs = -0.579$; $p = 0.021$), and between alkaline Comet OTM and TUNEL after decondensation ($Rs = 0.741$; $p = 0.001$). **Figure 2** represents these statistically significant correlations.

Correlations Between Chromatin Damage Methods Regarding Percentage of Affected Cells

Percentages of affected cells for each technique were measured, and correlation coefficients between methods are summarized in **Figure 3**. Statistically significant correlations were found between percentages of high damage in alkaline Comet and TUNEL after decondensation ($Rs = 0.618$; $p = 0.013$), between percentages of low damage in alkaline Comet and CMA3 ($Rs = 0.619$; $p = 0.012$), between percentages of low damage in neutral Comet and %HDS-SCSA ($Rs = -0.509$; $p = 0.046$), between %SDF-SCSA and neutral SCD ($Rs = 0.873$; $p < 0.001$), between alkaline and neutral SCD ($Rs = 0.598$; $p = 0.016$), and between alkaline SCD and %SDF-SCSA ($Rs = 0.670$; $p = 0.006$). **Figure 4** shows these statistically significant correlations.

Correlations of Chromatin Damage With Motility, Viability, and Morphology

Both chromatin damage intensity and percentages of sperm with fragmented DNA were tested for their correlation with sperm motility and viability after cryopreservation and morphology. Correlation coefficients are summarized in **Figure 5**.

Regarding the degree of chromatin damage, statistically significant correlations between alkaline Comet OTM and VCL ($Rs = -0.514$; $p = 0.044$), between SCSA-FL3 intensity and WOB ($Rs = -0.514$; $p = 0.044$), and between SCSA-FL3 intensity and ALH ($Rs = 0.552$; $p = 0.029$) were found. Tendencies to correlation between alkaline Comet OTM and rapid velocity

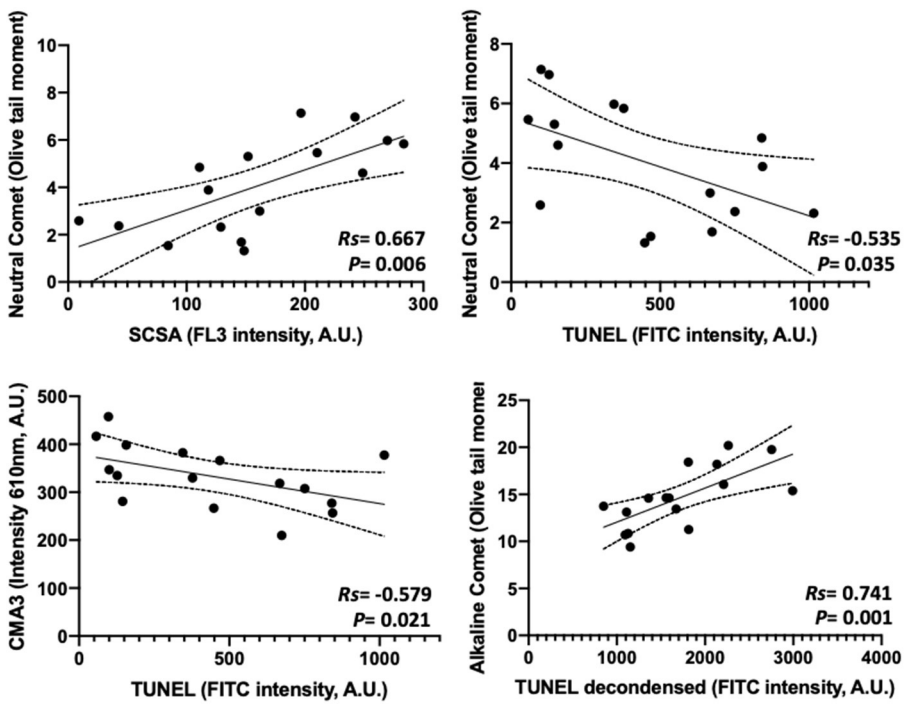

FIGURE 2 | Statistically significant correlations between parameters analyzing the degree of chromatin damage and obtained through different methods.

($Rs = -0.470$; $p = 0.068$), alkaline Comet OTM and ALH ($Rs = -0.491$; $p = 0.055$), alkaline Comet and morphology ($Rs = -0.491$; $p = 0.055$), and between SCSA and LIN ($Rs = -0.500$; $p = 0.060$) were observed.

With regard to the percentage of sperm with altered chromatin, statistically significant correlations were found between progressive motility and %SDF determined by TUNEL with DTT decondensation ($Rs = -0.568$; $p = 0.024$); progressive motility and %SDF determined by SCSA ($Rs = -0.618$; $p = 0.013$); non-progressive motility and %Highly damaged sperm in alkaline Comet ($Rs = 0.539$; $p = 0.033$); sperm with rapid velocity and %SDF determined by TUNEL with DTT decondensation ($Rs = -0.653$; $p = 0.007$); sperm with rapid velocity and %Highly damaged sperm in alkaline Comet ($Rs = -0.574$; $p = 0.022$); VCL and %SDF determined by TUNEL with DTT decondensation ($Rs = -0.582$; $p = 0.020$), %SDF determined by SCSA ($Rs = -0.544$; $p = 0.032$), and %Highly damaged sperm in alkaline Comet ($Rs = -0.674$; $p = 0.005$); VAP and %SDF determined by neutral SCD ($Rs = -0.536$; $p = 0.034$), %SDF determined by SCSA ($Rs = -0.544$; $p = 0.008$), and %Highly damaged sperm in alkaline Comet ($Rs = -0.674$; $p = 0.009$).

DISCUSSION

In the present work, we comprehensively described the correlations among eight methodological variants assessing different facets of chromatin damage, namely, DNA breaks and poor protamination. First, our results showed that the intensity of DNA damage, given by the amount of DNA breaks, is correlated with the percentages of sperm with fragmented DNA in direct (TUNEL and Comet), but not in indirect methods (SCSA and SCD assays). Second, regarding the degree of DNA damage, we mainly found significant correlations among neutral Comet, SCSA, and conventional TUNEL; and between alkaline Comet and TUNEL with DTT decondensation. Third, as far as the percentages of sperm with altered chromatin are concerned, we observed that Comet assays, especially the alkaline variant, correlated to SCD, SCSA, and the two TUNEL variants. Interestingly, correlations between low-damaged alkaline Comet and %CMA3, and between neutral Comet and %HDS (SCSA method) were also observed.

Mounting evidence supports that sperm DNA fragmentation and alterations in sperm chromatin, such as poor protamination, underlie infertility in humans and farm animals (18, 42–46).

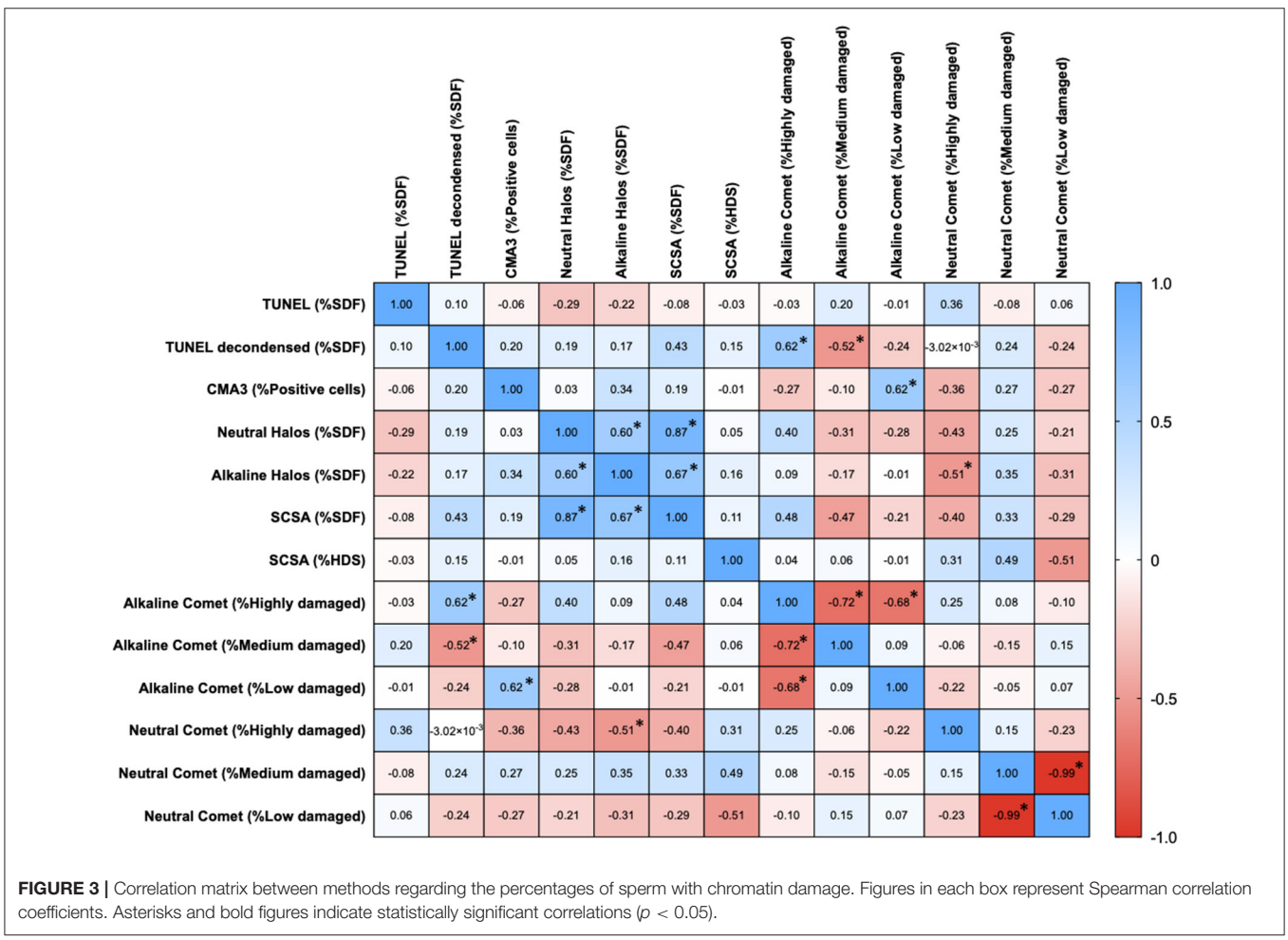

FIGURE 3 | Correlation matrix between methods regarding the percentages of sperm with chromatin damage. Figures in each box represent Spearman correlation coefficients. Asterisks and bold figures indicate statistically significant correlations ($p < 0.05$).

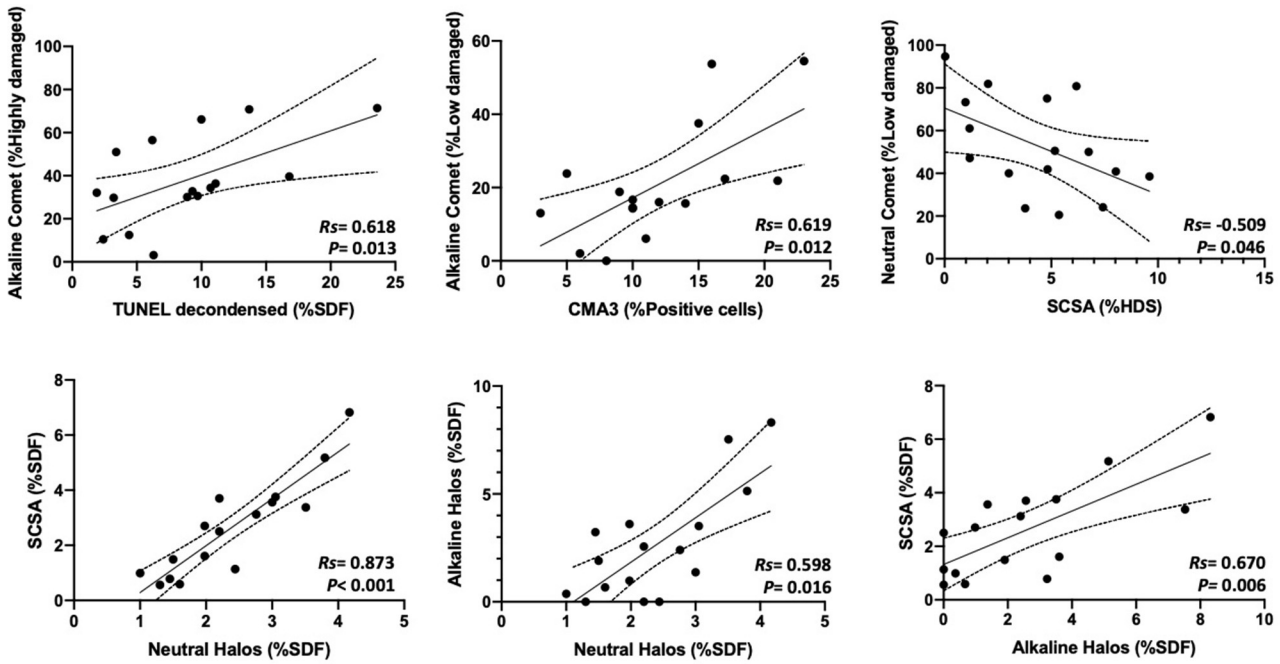

FIGURE 4 | Statistically significant correlations between parameters analyzing the percentages of sperm with chromatin damage obtained through different methods.

As the sperm cell is the vehicle that brings the paternal genetic cargo into the oocyte, it seems obvious that the disruption of that material through DNA breaks may impair embryo development and reduce pregnancy rates. Indeed, sperm chromatin damage has been reported to be higher in infertile than in fertile men (45, 47–49). However, how sperm DNA damage impairs reproductive outcomes is controversial when IVF and intracytoplasmic sperm injection are compared (50–53). In this context, establishing the role of sperm DNA damage in human infertility needs more clinical data from the most sensitive and standardized DNA damage methods (26).

In production animals such as pigs, sperm quality assessment is crucial to ensure the proper performance of semen doses. While previous research with different methods evaluating sperm DNA integrity related this parameter with cryodamage in pigs, the percentages of low DNA damage led some authors to raise concerns on its biological significance (18, 54, 55). However, a few studies aiming to establish how sperm DNA damage affects fertility outcomes following artificial insemination in pigs concurred that DNA fragmentation assessed through SCSA is related to a reduction in farrowing rate and litter size (16–19). Moreover, while previous studies evaluated the repercussion of sperm DNA damage on IVF outcomes after inducing DNA breaks *in vitro* (56–58), no data regarding the inherent sperm DNA damage in untreated pig sperm samples are available. Among other reasons, the confusing results in human infertile subjects and the concerns raised from animal studies are due to the fact that no standardized method is routinely applied, and that different chromatin damage methods analyze different aspects of chromatin impairment that lead to non-comparable results (14). In the current study, and through the parallel analysis using eight techniques, we showed that the extent of chromatin damage and the percentage of altered sperm cells were correlated in direct but not in indirect methods. These findings support previous data in human sperm, in which OTM evaluated by alkaline Comet assay was observed to be related to the percentage of sperm with fragmented DNA (53). Regarding SCD, and despite previous studies having shown that this test allows evaluating the extent of chromatin damage through the halo size, which is classified as big, medium, or small (39, 59, 60), the relationship between that size and the percentage of sperm with fragmented DNA has not been explored. Moreover, while the fluorescence intensity of TUNEL, SCSA, and CMA3 may also indicate the degree of DNA/chromatin damage (30, 61), no study has investigated whether those intensities and the percentages of sperm with fragmented DNA are correlated.

To the best of our knowledge, only five studies conducted in humans and mouse compared three or more methods of chromatin evaluation using the same sperm samples (27–31). In addition, this is the first study comparing eight methodological variants for sperm chromatin assessment in pigs. On the one hand, we surprisingly observed that percentages of sperm with fragmented DNA determined by conventional TUNEL and TUNEL after DNA decondensation were not correlated. This result is of relevant importance, as TUNEL is known to be one of the most standardized methods to assess single- and double-strand DNA breaks in cells. While pre-treating sperm with 2 mM DTT increases the sensitivity of TUNEL (41), our results suggest that this is especially important in pig sperm, as their chromatin is highly impermeable and difficult to decondense

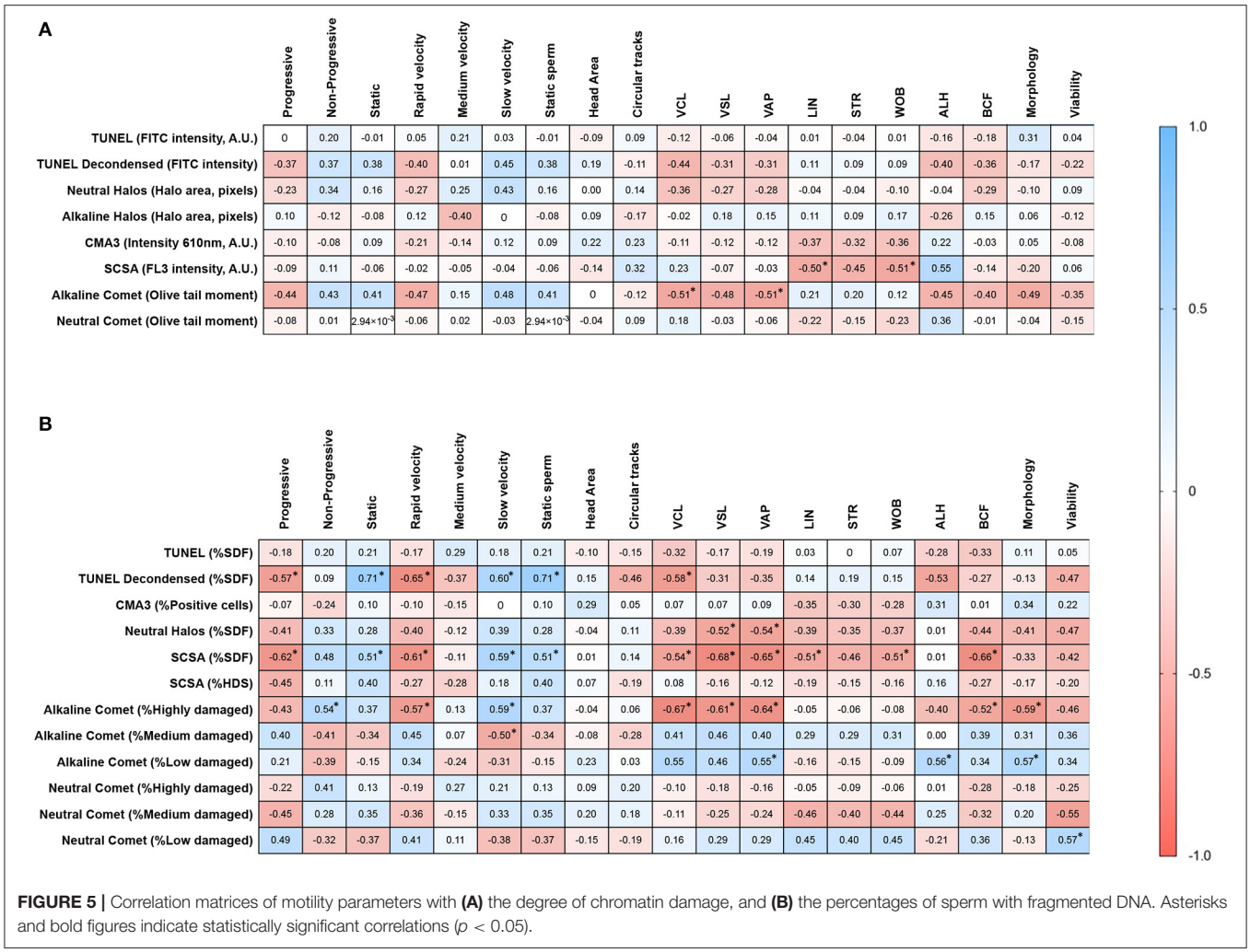

FIGURE 5 | Correlation matrices of motility parameters with **(A)** the degree of chromatin damage, and **(B)** the percentages of sperm with fragmented DNA. Asterisks and bold figures indicate statistically significant correlations ($p < 0.05$).

(37). Remarkably, and in agreement with this hypothesis, TUNEL without decondensation did not correlate to alkaline Comet, whereas TUNEL after decondensation did ($Rs = 0.618$, **Figure 4**).

On the other hand, percentages of sperm with low neutral Comet damage were found to be negatively correlated to %HDS evaluated through SCSA. This result confirmed a previous study conducted in mouse (31), in which a similar correlation between these two parameters was observed. Taken together, these findings suggest that the degree of chromatin decondensation could be related to double-strand DNA breaks. In this regard, one could hypothesize that when sperm are morphologically immature, which is linked to a higher number of histones retained and highly stainable DNA (%HDS), enzymes that like nucleases perform double-strand breaks can easily access chromatin and thus cause DNA breaks in non-protaminated regions. In fact, the presence of internal nucleases, which cause chromatin damage and have been described to exist in human, mouse, and hamster sperm, supports this hypothesis (62, 63).

Percentages of sperm with intact DNA determined by alkaline Comet were correlated with those of $CMA3^+$ sperm. At first glance, this result could seem contradictory, as CMA3 is known to be a marker of abnormal protamination (64, 65). However, it has been previously described that GC-rich sequences are preferential binding sites for CMA3 (66). This is of vital importance, since the oxidized form of guanine (8-hydroxyguanine) is the main target of oxidative DNA damage, which can also be measured through the alkaline Comet (20, 67). Therefore, this observed correlation could be explained by the presence of DNA breaks in guanine-rich sequences, which could lead to less CMA3 binding. In addition, it is worth mentioning that while the percentages of sperm with fragmented DNA correlated between indirect methods (SCD and SCSA), they did not appear to be associated to those of $CMA3^+$ sperm. This suggests that, despite SCD and SCSA relying on chromatin decondensation as a measure of DNA fragmentation, they are not related to abnormal chromatin protamination.

Finally, we investigated whether the different methods assessing DNA damage were associated to motility parameters. We observed that direct methods such as TUNEL and alkaline Comet, and indirect ones like SCSA, were correlated with progressive motility and sperm velocity. Previous studies in humans also reported that association (68–70), which may

represent a positive bias for ICSI treatments, as the most motile sperm are selected (71).

The present study is not exempt of limitations. First, despite the fact that pig sperm samples exhibit higher homogeneity than their human counterparts, thus adding robustness to our work, further research using larger sample sizes for each method is needed. Second, future studies should analyze DNA/chromatin damage in fresh and cryopreserved sperm, as freezing and thawing may affect DNA integrity (72). Finally, intra- and inter-assay variations should be determined in order to define the most robust method to assess sperm DNA damage.

In conclusion, the current study indicates that while the extent of chromatin damage is correlated with the percentage of sperm with fragmented DNA determined by direct methods (alkaline and neutral Comet, and TUNEL following decondensation), this is not the case of indirect methods (SCD and SCSA). In addition, in pig sperm, previous decondensation of 2 mM DTT is required in order for TUNEL assay to show reliable levels of sperm DNA fragmentation. Thus, direct rather than indirect methods are suggested to be more suitable to evaluate DNA fragmentation in pig sperm.

DATA AVAILABILITY STATEMENT

The raw data supporting the conclusions of this article will be made available by the authors, without undue reservation.

AUTHOR CONTRIBUTIONS

JR-M conceived the study, performed DNA damage experiments, analyzed data, conducted statistics, wrote the manuscript, revised the document, and approved the final version. ML, YM-O, and AD-B conducted CMA3 and viability experiments, discussed the results, and approved the final version. EG-B performed cryopreservation, evaluated sperm motility and morphology, and approved the final version. MY contributed to the experimental design, provided funding, coordinated the work, made a critical revision of the manuscript, and approved the final version. All authors contributed to the article and approved the submitted version.

FUNDING

The authors acknowledge the support from the Ministry of Science and Innovation, Spain (Grant No. AGL2017-88329-R), the Regional Government of Catalonia, Spain (Grant No. 2017-SGR-1229), La Marató de TV3 Foundation (Grant No. 214/857-202039), and the University of Girona (Postdoc UdG-2020, to JR-M).

SUPPLEMENTARY MATERIAL

The Supplementary Material for this article can be found online at: https://www.frontiersin.org/articles/10.3389/fvets.2021.719319/full#supplementary-material

Supplementary Figure 1 | Representative phase-contrast and epifluorescence images of negative and positive controls (incubation with 5 mM DTT at 37°C for 45 min) used to set up the CMA3 method. Scale bar = XX μm.

Supplementary Figure 2 | Representative phase-contrast and epifluorescence images of negative and positive controls (incubation with 4 IU/μL DNAse I at 37°C for 1 h) used to set up the TUNEL method. Scale bar = XX μm.

Supplementary Table 1 | Data including correlations and *P*-values for the degree of sperm chromatin damage, as depicted in **Figure 1**.

Supplementary Table 2 | Data including correlations and *P*-values for the percentages of sperm with chromatin damage, as shown in **Figure 3**.

Supplementary Table 3 | Data including correlations and *P*-values of sperm motility with **(A)** chromatin damage intensity, and **(B)** percentage of cells with chromatin damage, as depicted in **Figure 5**.

REFERENCES

1. Sutovsky P. New approaches to boar semen evaluation, processing and improvement. *Reprod Domest Anim.* (2015) 50 (Suppl. 2):11–9. doi: 10.1111/rda.12554
2. Simon L, Emery BR, Carrell DT. Review: Diagnosis and impact of sperm DNA alterations in assisted reproduction. *Best Pract Res Clin Obstet Gynaecol.* (2017) 44:38–56. doi: 10.1016/j.bpobgyn.2017.07.003
3. Long JA. The "omics" revolution: use of genomic, transcriptomic, proteomic and metabolomic tools to predict male reproductive traits that impact fertility in livestock and poultry. *Anim Reprod Sci.* (2020) 220:106354. doi: 10.1016/j.anireprosci.2020.106354
4. Panner Selvam MK, Baskaran S, Agarwal A, Henkel R. Protein profiling in unlocking the basis of varicocele-associated infertility. *Andrologia.* (2021) 53:e13645. doi: 10.1111/and.13645
5. Datta J, Palmer MJ, Tanton C, Gibson LJ, Jones KG, Macdowall W, et al. Prevalence of infertility and help seeking among 15 000 women and men. *Hum Reprod.* (2016) 31:2108–18. doi: 10.1093/humrep/dew123
6. De Geyter C, Calhaz-Jorge C, Kupka MS, Wyns C, Mocanu E, Motrenko T, et al. ART in Europe, 2015: results generated from European registries by ESHRE. *Hum Reprod Open.* (2020) 2020:hoz038. doi: 10.1093/hropen/hoaa038
7. Kemp B, Da Silva CLA, Soede NM. Recent advances in pig reproduction: focus on impact of genetic selection for female fertility. *Reprod Domest Anim.* (2018) 53 (Suppl. 2):28–36. doi: 10.1111/rda.13264
8. Yeste M, Rodríguez-Gil JE, Bonet S. Artificial insemination with frozen-thawed boar sperm. *Mol Reprod Dev.* (2017) 84:802–13. doi: 10.1002/mrd.22840
9. Schulze M, Nitsche-Melkus E, Jakop U, Jung M, Waberski D. New trends in production management in European pig AI centers. *Theriogenology.* (2019) 137:88–92. doi: 10.1016/j.theriogenology.2019.05.042
10. Parrilla I, Perez-Patiño C, Li J, Barranco I, Padilla L, Rodriguez-Martinez H, et al. Boar semen proteomics and sperm preservation. *Theriogenology.* (2019) 137:23–9. doi: 10.1016/j.theriogenology.2019.05.033
11. Recuero S, Fernandez-Fuertes B, Bonet S, Barranco I, Yeste M. Potential of seminal plasma to improve the fertility of frozen-thawed boar spermatozoa. *Theriogenology.* (2019) 137:36–42. doi: 10.1016/j.theriogenology.2019.05.035
12. De Lazari FL, Sontag ER, Schneider A, Araripe Moura AA, Vasconcelos FR, Nagano CS, et al. Proteomic identification of boar seminal plasma proteins related to sperm resistance to cooling at 17 °C. *Theriogenology.* (2020) 147:135–45. doi: 10.1016/j.theriogenology.2019.11.023
13. Kumaresan A, Das Gupta M, Datta TK, Morrell JM. Sperm DNA integrity and male fertility in farm animals: a review. *Front Vet Sci.* (2020) 7:321. doi: 10.3389/fvets.2020.00321

14. Dutta S, Henkel R, Agarwal A. Comparative analysis of tests used to assess sperm chromatin integrity and DNA fragmentation. *Andrologia.* (2021) 53:e13718. doi: 10.1111/and.13718
15. Esteves SC, Zini A, Coward RM, Evenson DP, Gosálvez J, Lewis SEM, et al. Sperm DNA fragmentation testing: summary evidence and clinical practice recommendations. *Andrologia.* (2021) 53:e13874. doi: 10.1111/and.13874
16. Evenson DP, Thompson L, Jost L. Flow cytometric evaluation of boar semen by the sperm chromatin structure assay as related to cryopreservation and fertility. *Theriogenology.* (1994) 41:637–51. doi: 10.1016/0093-691X(94)90174-H
17. Evenson DP. Loss of livestock breeding efficiency due to uncompensable sperm nuclear defects. *Reprod Fertil Dev.* (1999) 11:1–15. doi: 10.1071/RD98023
18. Boe-Hansen GB, Christensen P, Vibjerg D, Nielsen MBF, Hedeboe AM. Sperm chromatin structure integrity in liquid stored boar semen and its relationships with field fertility. *Theriogenology.* (2008) 69:728–36. doi: 10.1016/j.theriogenology.2007.12.004
19. Waberski D, Schapmann E, Henning H, Riesenbeck A, Brandt H. Sperm chromatin structural integrity in normospermic boars is not related to semen storage and fertility after routine AI. *Theriogenology.* (2011) 75:337–45. doi: 10.1016/j.theriogenology.2010.09.004
20. Ribas-Maynou J, Benet J. Single and double strand sperm dna damage: different reproductive effects on male fertility. *Genes.* (2019) 10:105. doi: 10.3390/genes10020105
21. Simon L, Zini A, Dyachenko A, Ciampi A, Carrell D. A systematic review and meta-analysis to determine the effect of sperm DNA damage on in vitro fertilization and intracytoplasmic sperm injection outcome. *Asian J Androl.* (2017) 19:80–90. doi: 10.4103/1008-682X.182822
22. Deng C, Li T, Xie Y, Guo Y, Yang Q, Liang X, et al. Sperm DNA fragmentation index influences assisted reproductive technology outcome: a systematic review and meta-analysis combined with a retrospective cohort study. *Andrologia.* (2019) 51:e13263. doi: 10.1111/and.13263
23. Evenson D, Wixon R. Meta-analysis of sperm DNA fragmentation using the sperm chromatin structure assay. *Reprod Biomed Online.* (2006) 12:466–72. doi: 10.1016/S1472-6483(10)62000-7
24. Collins JA, Barnhart KT, Schlegel PN. Do sperm DNA integrity tests predict pregnancy with in vitro fertilization? *Fertil Steril.* (2008) 89:823–31. doi: 10.1016/j.fertnstert.2007.04.055
25. Zhang Z, Zhu L, Jiang H, Chen H, Chen Y, Dai Y. Sperm DNA fragmentation index and pregnancy outcome after IVF or ICSI: a meta-analysis. *J Assist Reprod Genet.* (2015) 32:17–26. doi: 10.1007/s10815-014-0374-1
26. Ribas-Maynou J, Yeste M, Becerra-Tomás N, Aston KI, James ER, Salas-Huetos A. Clinical implications of sperm DNA damage in IVF and ICSI: updated systematic review and meta-analysis. *Biol Rev.* (2021) 96, 1284–300.
27. Ribas-Maynou J, García-Peir,ó A, Fernández-Encinas A, Abad C, Amengual MJJ, Prada E, et al. Comprehensive analysis of sperm DNA fragmentation by five different assays: TUNEL assay, SCSA, SCD test and alkaline and neutral comet assay. *Andrology.* (2013) 1:715–22. doi: 10.1111/j.2047-2927.2013.00111.x
28. Simon L, Liu L, Murphy K, Ge S, Hotaling J, Aston KI, et al. Comparative analysis of three sperm DNA damage assays and sperm nuclear protein content in couples undergoing assisted reproduction treatment. *Hum Reprod.* (2014) 29:904–17. doi: 10.1093/humrep/deu040
29. Javed A, Talkad MS, Ramaiah MK. Evaluation of sperm DNA fragmentation using multiple methods: a comparison of their predictive power for male infertility. *Clin Exp Reprod Med.* (2019) 46:14–21. doi: 10.5653/cerm.2019.46.1.14
30. Mohammadi Z, Tavalaee M, Gharagozloo P, Drevet JR, Nasr-Esfahani MH. Could high DNA stainability (HDS) be a valuable indicator of sperm nuclear integrity? *Basic Clin Androl.* (2020) 30:12. doi: 10.1186/s12610-020-00110-8
31. Pérez-Cerezales S, Miranda A, Gutiérrez-Adán A. Comparison of four methods to evaluate sperm DNA integrity between mouse caput and cauda epididymidis. *Asian J Androl.* (2012) 14:335–7. doi: 10.1038/aja.2011.119
32. Albert O, Reintsch WE, Chan P, Robaire B. HT-COMET: a novel automated approach for high throughput assessment of human sperm chromatin quality. *Hum. Reprod.* (2016) 31:938–46. doi: 10.1093/humrep/dew030
33. Alkmin DV, Martinez-Alborcia MJ, Parrilla I, Vazquez JM, Martinez EA, Roca J. The nuclear DNA longevity in cryopreserved boar spermatozoa assessed using the sperm-sus-halomax. *Theriogenology.* (2013) 79:1294–300. doi: 10.1016/j.theriogenology.2013.02.026
34. Batista C, van Lier E, Petrocelli H. Dynamics of sperm DNA fragmentation in raw boar semen and fertility. *Reprod Domest Anim.* (2016) 51:774–80. doi: 10.1111/rda.12749
35. Casas I, Sancho S, Briz M, Pinart E, Bussalleu E, Yeste M, et al. Freezability prediction of boar ejaculates assessed by functional sperm parameters and sperm proteins. *Theriogenology.* (2009) 72:930–48. doi: 10.1016/j.theriogenology.2009.07.001
36. Delgado-Bermúdez A, Llavanera M, Recuero S, Mateo-Otero Y, Bonet S, Barranco I, et al. Effect of AQP inhibition on boar sperm cryotolerance depends on the intrinsic freezability of the ejaculate. *Int J Mol Sci.* (2019) 20:6255. doi: 10.3390/ijms20246255
37. Ribas-Maynou J, Garcia-Bonavila E, Hidalgo CO, Catalán J, Miro J, Yeste M. Species-specific differences in sperm chromatin decondensation between eutherian mammals underlie distinct lysis requirements. *Front Cell Dev Biol.* (2021) 2021:669182. doi: 10.3389/fcell.2021.669182
38. Langie SAS, Azqueta A, Collins AR. The comet assay: past, present, and future. *Front Genet.* (2015) 6:266. doi: 10.3389/fgene.2015.00266
39. Fernández JL, Muriel L, Rivero MT, Goyanes V, Vazquez R, Alvarez JG. The sperm chromatin dispersion test: a simple method for the determination of sperm DNA fragmentation. *J Androl.* (2003) 24:59–66. doi: 10.1002/j.1939-4640.2003.tb02641.x
40. Tvrdá E, Arroyo F, Duračka M, López-Fernández C, Gosálvez J. Dynamic assessment of human sperm DNA damage II: the effect of sperm concentration adjustment during processing. *J Assist Reprod Genet.* (2019) 36:799–807. doi: 10.1007/s10815-019-01423-y
41. Mitchell LA, De Iuliis GN, Aitken RJ. The TUNEL assay consistently underestimates DNA damage in human spermatozoa and is influenced by DNA compaction and cell vitality: development of an improved methodology. *Int J Androl.* (2011) 34:2–13. doi: 10.1111/j.1365-2605.2009.01042.x
42. Barratt CLR, Aitken RJ, Björndahl L, Carrell DT, de Boer P, Kvist U, et al. Sperm DNA: organization, protection and vulnerability: from basic science to clinical applications–a position report. *Hum. Reprod.* (2010) 25:824–38. doi: 10.1093/humrep/dep465
43. Lewis SEM, Simon L. Clinical implications of sperm DNA damage. *Hum Fertil.* (2010) 13:201–7. doi: 10.3109/14647273.2010.528823
44. Waberski D, Henning H, Petrunkina AM. Assessment of storage effects in liquid preserved boar semen. *Reprod Domest Anim.* (2011) 46 (Suppl. 2):45–8. doi: 10.1111/j.1439-0531.2011.01836.x
45. Ribas-Maynou J, García-Peiró A, Abad C, Amengual MJ, Navarro J, Benet J. Alkaline and neutral Comet assay profiles of sperm DNA damage in clinical groups. *Hum Reprod.* (2012) 27:652–8. doi: 10.1093/humrep/der461
46. Agarwal A, Barbăro?ie C, Ambar R, Finelli R. The impact of single- and double-strand DNA breaks in human spermatozoa on assisted reproduction. *Int J Mol Sci.* (2020) 21:3882. doi: 10.3390/ijms21113882
47. Simon L, Brunborg G, Stevenson M, Lutton D, McManus J, Lewis SEM. Clinical significance of sperm DNA damage in assisted reproduction outcome. *Hum. Reprod.* (2010) 25:1594–608. doi: 10.1093/humrep/deq103
48. Esteves SC, Gosálvez J, López-Fernández C, Núñez-Calonge R, Caballero P, Agarwal A, et al. Diagnostic accuracy of sperm DNA degradation index (DDSi) as a potential noninvasive biomarker to identify men with varicocele-associated infertility. *Int Urol Nephrol.* (2015) 47:1471–7. doi: 10.1007/s11255-015-1053-6
49. Bui AD, Sharma R, Henkel R, Agarwal A. Reactive oxygen species impact on sperm DNA and its role in male infertility. *Andrologia.* (2018) 50:e13012. doi: 10.1111/and.13012
50. Zini A. Are sperm chromatin and DNA defects relevant in the clinic? *Syst Biol Reprod Med.* (2011) 57:78–85. doi: 10.3109/19396368.2010.515704
51. Zhao J, Zhang Q, Wang Y, Li Y. Whether sperm deoxyribonucleic acid fragmentation has an effect on pregnancy and miscarriage after in vitro fertilization/intracytoplasmic sperm injection: a systematic review and meta-analysis. *Fertil Steril.* (2014) 102:998–1005.e8. doi: 10.1016/j.fertnstert.2014.06.033
52. Cissen M, Wely M, van, Scholten I, Mansell S, Bruin JP, et al. Measuring sperm dna fragmentation and clinical outcomes of medically assisted reproduction: a systematic review and meta-analysis. *PLoS ONE.* (2016) 11:e0165125. doi: 10.1371/journal.pone.0165125

53. Simon L, Aston KI, Emery BR, Hotaling J, Carrell DT. Sperm DNA damage output parameters measured by the alkaline comet assay and their importance. *Andrologia.* (2017) 49:e12608. doi: 10.1111/and.12608
54. Hernández M, Roca J, Ballester J, Vázquez JM, Martínez EA, Johannisson A, et al. Differences in SCSA outcome among boars with different sperm freezability. *Int J Androl.* (2006) 29:583–91. doi: 10.1111/j.1365-2605.2006.00699.x
55. Fraser L, Strzezek J. Is there a relationship between the chromatin status and DNA fragmentation of boar spermatozoa following freezing-thawing? *Theriogenology.* (2007) 68:248–57. doi: 10.1016/j.theriogenology.2007.05.001
56. Jang HY, Kim YH, Kim BW, Park IC, Cheong HT, Kim JT, et al. Ameliorative effects of melatonin against hydrogen peroxide-induced oxidative stress on boar sperm characteristics and subsequent in vitro embryo development. *Reprod Domest Anim.* (2010) 45:943–50. doi: 10.1111/j.1439-0531.2009.01466.x
57. Yi YJ, Lee IK, Lee SM, Yun BS. An antioxidant davallialactone from *Phellinus baumii* enhances sperm penetration on in vitro fertilization of pigs. *Mycobiology.* (2016) 44:54–7. doi: 10.5941/MYCO.2016.44.1.54
58. Yi YJ, Kamala-Kannan S, Lim JM, Oh BT, Lee SM. Effects of difructose dianhydride (DFA)-IV on in vitro fertilization in pigs. *J Biomed Res.* (2017) 31:453–61. doi: 10.7555/JBR.31.20160115
59. Muriel L, Meseguer M, Fernández JL, Alvarez J, Remoh,í J, Pellicer A, et al. Value of the sperm chromatin dispersion test in predicting pregnancy outcome in intrauterine insemination: a blind prospective study. *Hum Reprod.* (2006) 21:738–44. doi: 10.1093/humrep/dei403
60. Tandara M, Bajić A, Tandara L, Bilić-Zulle L, Šunj M. Kozina V, et al. Sperm DNA integrity testing: big halo is a good predictor of embryo quality and pregnancy after conventional IVF. *Andrology.* (2014) 2:678–86. doi: 10.1111/j.2047-2927.2014.00234.x
61. Evenson DP, Wixon R. Clinical aspects of sperm DNA fragmentation detection and male infertility. *Theriogenology.* (2006) 65:979–91. doi: 10.1016/j.theriogenology.2005.09.011
62. Sotolongo B, Huang TTF, Isenberger E, Ward WS. An endogenous nuclease in hamster, mouse, and human spermatozoa cleaves DNA into loop-sized fragments. *J Androl.* (2005) 26:272–80. doi: 10.1002/j.1939-4640.2005.tb01095.x
63. Gawecka JE, Marh J, Ortega M, Yamauchi Y, Ward MA, Ward WS. Mouse zygotes respond to severe sperm DNA damage by delaying paternal DNA replication and embryonic development. *PLoS ONE.* (2013) 8:e56385. doi: 10.1371/journal.pone.0056385
64. Iranpour FG, Nasr-Esfahani MH, Valojerdi MR, Taki Al-Taraihi TM. Chromomycin A3 staining as a useful tool for evaluation of male fertility. *J Assist Reprod Genet.* (2000) 17:60–6. doi: 10.1023/A:1009406231811
65. Aitken RJ, De Iuliis GN. On the possible origins of DNA damage in human spermatozoa. *Mol Hum Reprod.* (2010) 16:3–13. doi: 10.1093/molehr/gap059
66. Murase H, Noguchi T, Sasaki S. Evaluation of simultaneous binding of chromomycin A3 to the multiple sites of DNA by the new restriction enzyme assay. *Bioorg Med Chem Lett.* (2018) 28:1832–5. doi: 10.1016/j.bmcl.2018.04.013
67. Agbaje IM, McVicar CM, Schock BC, McClure N, Atkinson AB, Rogers D, et al. Increased concentrations of the oxidative DNA adduct 7,8-dihydro-8-oxo-2-deoxyguanosine in the germ-line of men with type 1 diabetes. *Reprod Biomed Online.* (2008) 16:401–9. doi: 10.1016/S1472-6483(10)60602-5
68. Simon L, Lewis SEM. Sperm DNA damage or progressive motility: which one is the better predictor of fertilization in vitro? *Syst Biol Reprod Med.* (2011) 57:133–8. doi: 10.3109/19396368.2011.553984
69. Belloc S, Benkhalifa M, Cohen-Bacrie M, Dalleac A, Amar E, Zini A. Sperm deoxyribonucleic acid damage in normozoospermic men is related to age and sperm progressive motility. *Fertil Steril.* (2014) 101:1588–93. doi: 10.1016/j.fertnstert.2014.02.006
70. Casanovas A, Ribas-Maynou J, Lara-Cerrillo S, Jimenez-Macedo AR, Hortal O, Benet J, et al. Double-stranded sperm DNA damage is a cause of delay in embryo development and can impair implantation rates. *Fertil Steril.* (2019) 111:699–707.e1. doi: 10.1016/j.fertnstert.2018.11.035
71. Lara-Cerrillo S, Ribas-Maynou J, Rosado-Iglesias C, Lacruz-Ruiz T, Benet J, García-Peiró A. Sperm selection during ICSI treatments reduces single- but not double-strand DNA break values compared to the semen sample. *J Assist Reprod Genet.* (2021) 38:1187–96. doi: 10.1007/s10815-021-02129-w
72. Yeste M. Sperm cryopreservation update: cryodamage, markers, and factors affecting the sperm freezability in pigs. *Theriogenology.* (2016) 85:47–64. doi: 10.1016/j.theriogenology.2015.09.047

Conflict of Interest: The authors declare that the research was conducted in the absence of any commercial or financial relationships that could be construed as a potential conflict of interest.

Publisher's Note: All claims expressed in this article are solely those of the authors and do not necessarily represent those of their affiliated organizations, or those of the publisher, the editors and the reviewers. Any product that may be evaluated in this article, or claim that may be made by its manufacturer, is not guaranteed or endorsed by the publisher.

Advantages of publishing in Frontiers

OPEN ACCESS
Articles are free to read for greatest visibility and readership

FAST PUBLICATION
Around 90 days from submission to decision

HIGH QUALITY PEER-REVIEW
Rigorous, collaborative, and constructive peer-review

TRANSPARENT PEER-REVIEW
Editors and reviewers acknowledged by name on published articles

Frontiers
Avenue du Tribunal-Fédéral 34
1005 Lausanne | Switzerland

Visit us: www.frontiersin.org
Contact us: frontiersin.org/about/contact

REPRODUCIBILITY OF RESEARCH
Support open data and methods to enhance research reproducibility

DIGITAL PUBLISHING
Articles designed for optimal readership across devices

FOLLOW US
@frontiersin

IMPACT METRICS
Advanced article metrics track visibility across digital media

EXTENSIVE PROMOTION
Marketing and promotion of impactful research

LOOP RESEARCH NETWORK
Our network increases your article's readership